

Numerical Methods for Space-Time Variational Formulations of Retarded Potential Boundary Integral Equations

Von der Fakultät für Mathematik und Physik
der Gottfried Wilhelm Leibniz Universität Hannover
zur Erlangung des Grades einer
Doktorin der Naturwissenschaften
Dr. rer. nat.

genehmigte Dissertation

von

Dipl.-Math. Elke Ostermann

geboren am 02. Dezember 1980, in Barßel

2010

Referent: Prof. Dr. E. P. Stephan, Gottfried Wilhelm Leibniz Universität Hannover
Koreferent: PD Dr. M. Maischak, Brunel University, Uxbridge, United Kingdom
Koreferent: Prof. S. Sauter, Universität Zürich, Schweiz
Tag der Promotion: 21.12.2009

Abstract

This thesis discusses the numerical solution of time dependent scattering phenomena in unbounded domains using retarded potential boundary integral equations, also known as time domain boundary integral equations. We employ an unconditionally stable space-time variational formulation whose fully discrete formulation results in a marching-on-time (MOT) scheme through a history of sparse matrices and solution vectors.

The main focus of this work lies on the efficient computation of the matrix entries. We study the discrete retarded potentials evaluated on one element of a surface triangulation. We show that besides the classical corner-edge singularities on the boundary of the element additional singularities of geometrical nature exist, which we call geometrical light cone singularities. These are located on the surface of cylinders around the element's edges and parallel to the face of the element. We analyze the regularity of the discrete retarded potential using piecewise defined countably normed spaces.

Based on this analysis, we present the numerical approximation of the integrals defining the matrix entries. We derive composite quadrature schemes for the inner and outer integration. The inner integration requires the evaluation of the discrete retarded potential for which we prove exponential convergence. The outer integration involves the discrete retarded potential as an integrand and here we apply the knowledge of its regularity to construct a composite quadrature rule and prove its exponential convergence. This results in an overall exponential convergence.

We present numerical experiments underlining our theoretical investigations.

Keywords: retarded potentials, countably normed spaces, numerical quadrature

Zusammenfassung

In dieser Arbeit untersuchen wir die Lösung zeitabhängiger Streuungsprobleme in unbeschränkten Gebieten unter der Verwendung von Randintegralgleichungen mit retardierten Potentialen. Hierbei benutzen wir eine variationelle Formulierung in Raum und Zeit, die ohne weitere Bedingungen stabil ist. Das resultierende diskrete Problem entspricht einem Zeitschrittverfahren, welches die schwachbesetzten Matrizen und Lösungsvektoren aus den vorherigen Zeitschritten benötigt.

Das Hauptaugenmerk dieser Arbeit ruht auf der effizienten Berechnung der Matrixeinträge. Wir untersuchen das diskrete retardierte Potential, ausgewertet auf einem Element der Oberflächentriangulierung. Wir zeigen, dass neben den klassischen Kanten-Ecken-Singularitäten auf dem Rand des Elementes, zusätzliche Singularitäten geometrischer Natur auftreten, welche wir geometrische Lichtkegel-Singularitäten nennen. Diese befinden sich auf den Manteln der Zylinder um die Elementkanten und Elementen parallel zur Elementfläche. Wir analysieren die Regularität des diskreten retardierten Potentials mit Hilfe von stückweise definierten abzählbar normierten Räumen.

Ferner stellen wir, basierend auf den Ergebnissen dieser Analyse, eine numerische Quadratur zur Approximation der Integrale vor, welche die Matrixeinträge beschreiben. Wir leiten eine zusammengesetzte Quadraturformel für die innere und äußere Integration her. Das innere Integral erfordert die Auswertung der diskreten retardierten Potentiale. Für die vorgestellte Quadraturformel weisen wir exponentielle Konvergenz nach. Bei der äußeren Quadratur tritt das diskrete retardierte Potential als Integrand auf, so dass wir hier die Resultate bezüglich seiner Regularität anwenden müssen. Die daraus hergeleitete Quadraturformel weist ebenfalls exponentielle Konvergenz auf, so dass die gesamte Quadraturformel auch exponentiell schnell konvergiert.

Zudem stellen wir numerische Experimente vor, die unsere theoretische Ergebnisse bestätigen.

Schlagerworte: retardierte Potentiale, abzählbar normierte Räume, numerische Quadratur

Contents

1	Introduction	1
2	Retarded Potential Boundary Integral Equations and their Discretization	5
2.1	Retarded Potential Boundary Integral Equations	7
2.2	Space-Time Variational Formulations	8
2.3	Discretization of Retarded Potential Boundary Integral Equations	9
2.3.1	Discretization in Space and Time	9
2.3.2	Discrete Retarded Potentials and the MOT Algorithm	10
3	Regularity of Discrete Retarded Potentials	19
3.1	Geometrical Description of the Domains of Influence $E(x)$ and $E_R(T)$	20
3.2	Regularity of Retarded Boundary Integrals	21
3.2.1	Analysis of the Edge Integral $I_e \varphi$	25
3.2.2	Analysis of the Triangle Integral $I_T \varphi$	41
3.2.3	Singularities of the Retarded Potential	48
3.2.4	Complete Retarded Potential	51
3.3	Numerical Experiments	53
3.3.1	High Resolution Plots on a Line	53
3.3.2	Contour Plots of the Retarded Potential in Different Planes	55
3.4	Technical Results	56
4	A Composite Quadrature Rule for Retarded Potentials	61
4.1	Composite Quadrature Rule for the Inner Quadrature	63
4.1.1	Construction of a Composite Quadrature Rule	63
4.1.2	Error Analysis for the Evaluation of the Retarded Potential	67
4.2	Outer Quadrature for Discrete Retarded Potentials	76
4.2.1	Decomposition of Integration Domain $\hat{T} \cap E(T)$	76
4.2.2	Construction of the Composite Quadrature Rule	78
4.2.3	Error Analysis	80
4.3	Technical Results	81
4.4	Numerical Experiments	82
4.4.1	Accuracy of the Numerical Evaluation of Retarded Integrals	82
4.4.2	Test for the Accuracy of the Quadrature Routine	83
5	Numerical Results	87
5.1	Retarded Single Layer Potential Ansatz	87
5.2	Direct Problem using the Single Layer Potential	89
5.3	Computation Times, Memory Requirement and Performance	90
6	Conclusions	93
	Functional Framework and Notation	95
	Regularity of Discrete Retarded Potentials in \mathbb{R}^3	99

Implementation Issues	103
References	109

Nomenclature

(r, θ)	local polar coordinates
$\chi_A(x)$	indicator function for set A
$H(x)$	Heavyside function
$\delta(x)$	delta distribution
$H_\beta^{m,l}(\Omega)$	weighted Sobolev space, Definition A.1
$B_\beta^m(\Omega)$	countably normed space, Definition A.2
E_l	discrete light cone integration domain, compare (2.22)
$E(T_i, T_j)$	domain of influence of two elements, compare (4.3)
$E(x)$	domain of influence of point x
$E(T)$	domain of influence of element T , compare Lemma 3.23
$E_R(T)$	domain of influence of element T if $r_{\min} = 0$, cf. (3.3)
$C_R(e)$	domain of influence of edge e with radius R , compare (3.9)
$\Theta_R(T)$	natural decomposition of $E_R(T)$, Definition 3.19
$\Theta_{\min}^{r_{\max}}(T)$	natural decomposition of $E(T)$, cf. (3.23)
S, D, V, K, K', W	time domain boundary integral operators, compare Def. 2.2 and 2.3
$\frac{\partial}{\partial n}, \partial_n$	normal derivative
\mathcal{E}_T, n_T	triangle plane, triangle normal
p_i, ω_i, e_i, n_i	triangle label: vertex, angle, edge, edge normal (Fig. 3.3(b))
$\mathcal{P}_R(T)$	prima for triangle T with height $2R$
$B_R(x)$	sphere with center x and radius R
$\mathcal{C}_R(e)$	cylinder with axis e and radius R
$H_\sigma^s(\mathbb{R}^+, E)$	space-time Sobolev space
$Q_n^{[a,b]} f$	quadrature rule on $[a, b]$ with n quadrature points
$Q_{n,m,\sigma}^{[a,b]} f$	composite quadrature rule on $[a, b]$ with m level and a grading parameter σ

Chapter 1

Introduction

In recent years the numerical simulation of radiation and scattering phenomena in unbounded domains in three dimensions gained on importance. Here the boundary element method (BEM) [29] shows its natural strength, as it reduces the problem in the unbounded domain to an integral equation on the boundary. The solution of the integral equation then reveals the solution in every required point of the regarded domain via a cheap post-processing, whereas a finite element method (FEM) will always be restricted to some fixed mesh in a bounded neighborhood of the scatterer.

Scattering phenomena occur in very different areas e.g. in acoustics or in the propagation of elastodynamic and electromagnetic waves. In the time domain, they can be represented using retarded potential boundary integral equations, which are the topic of this work. This method has been known for a long time, but was quite unpopular as many works reported instabilities and its implementation was said to be complicated. The increasing computational power and new formulations could overcome these drawbacks. Many works have been published in this context [18, 9, 59, 19, 44, 1], although the majority of the research is concerned with the collocation method [31, 41], for which rarely a mathematical analysis exists [16]. The fully time dependent approach has the major advantage, that the complete spectrum of the solution can be rebuilt from the transient solution using e.g. the fast Fourier transform.

Bamberger and Ha-Duong propose in [4, 5] a space-time variational formulation of the underlying retarded potential integral equations for which they could prove unconditional stability. Their work is extended to electromagnetic and elastodynamic waves [57, 60, 3]. In [23, 15] an overview of the state of the art and an extensive list of references is given. In [21] numerical results are presented.

Another approach, quite popular for this type of problem, is the convolution quadrature [6, 7, 32, 34, 25]. This approach uses a time discretization scheme mapping the integral equation into the frequency domain and in a second step transforms the system back into the time domain. This scheme results in a series of dense linear equation systems. The advantage of this method is, its ability to rely on many techniques known from frequency domain problems however with their problems have to be dealt with and it does not allow a non-uniform time mesh.

The use of higher order basis functions in space and time is discussed in [46]; there B-spline fundamental solutions are computed separately for each specific geometry. Another approach using higher approximations involves the usage of global basis functions [55]. In [18] the plane wave algorithm is transferred into the time domain in order to obtain a fast method.

In this work we will apply the space-time variational method as proposed in [4, 5] and analyze the corresponding discrete system. Our main focus lies on the numerical evaluation of the integrals which describe the entries of the Galerkin matrices. The accuracy of the evaluation strongly influences the approximate solution of the linear equation system. For boundary integral equations resulting from time independent problems this was done e.g. in [49, 51]. We will discuss the regularity of the discrete retarded potential evaluated on one element and show that additional singularities exist compared to the singularities classically known for time independent potentials. We use countably normed spaces as introduced in [2] in order to describe the behavior of the discrete retarded potential. For this purpose, we introduce weight functions located on the surface of cylinders around the edges of the element and parallel to the element's face. Countably normed spaces are a well-known tool used extensively in the analysis of hp-methods e.g. [38, 26, 27, 28] in order to describe the regularity of solutions of integral equations as well as partial differential equations, but was also applied in the error analysis of quadrature schemes [49, 51]. We apply the new gained knowledge on the singularities in the construction and analysis of an appropriate quadrature scheme for the Galerkin entries occurring in the discrete space-time variational formulation. Some results of this work have already been published in [39, 40, 54].

Outline of this work

In *Chapter 2* we introduce the retarded potential boundary integral operators and the corresponding integral equations of first kind. We briefly outline the unconditionally stable space-time variational formulation originally proposed by Ha-Duong and Bamberger [4, 5] and give a detailed derivation of the fully discrete system resulting in a marching-on-time (MOT) algorithm. Here we pay special attention to the analytical evaluation of the retarded time integrals.

Chapter 3 discusses the regularity of the discrete retarded potential evaluated on one triangular element and describes its regularity in an arbitrary plane using a piecewise defined countably normed space. The discrete retarded potential is defined

$$(P\varphi)(x) := \int_{T \cap E(x)} k(x-y)\varphi(y) ds_y$$

with a kernel function $k(x-y)$, where the integration domain is the intersection of the triangle T with the domain of influence $E(x)$ of the point of observation x . This domain of influence is defined as the intersection of two concentric spheres with center x , such that we obtain an annular domain. We use the linearity of the integral to simplify the discrete retarded potential $P\varphi$ to an integral with the integration domain defined by one sphere with radius R intersected with the triangle. We analyze this simplified potential $P_R\varphi$ as follows. After verifying, that the bounded support of the simplified retarded potential is the combination of the three spheres with radius R and centers in the vertices of the triangle, the three finite cylinders around the triangle edges with radius R and the prism defined by the triangle base with height $2R$, we show in Lemma 3.2 that the gradient of the simplified potentials can be reduced to the boundary of the intersecting set. We show, that the gradient consists of a sum of integrals over the boundary of $T \cap B_R(x)$; namely of integrals over the triangle edges intersected with the sphere and of an integral over the triangle intersected with the boundary of the sphere. Before we proceed with a detailed analysis of these two types of integrals we use Lemma 3.2 in order to derive a formula for a derivative of $P_R\varphi$ of arbitrary order, which is stated in Theorem 3.4.

In Section 3.2.1 we then analyze the edge-based integral. We show, that it has bounded support defined by the union of the spheres of radius R and centers in the end points of the edges and a circular cylinder around the edge with radius R . We map the integral to an integral on a reference edge of length one (Lemma 3.5) and study the different intersection types of spheres with variable centers x and the reference edge. This defines a natural decomposition of the support of the edge-based function as proved in Lemma 3.6. In Lemma 3.8 we prove, that the edge-based function possesses one-sided singularities in the first derivative located on the surface of the cylinder (without its caps) and jumps exist on the surface of the spheres around the end points of the edge. These *geometrical light cone singularities* occur independently of the regularity of the kernel function $k(x-y)$, but dependent on the kernel function we observe the well-known classical singularity on the edge. We use these results in order to formulate the regularity on the disjoint elements of the introduced decomposition intersected with an arbitrary plane in terms of countably normed spaces. For this purpose, apart from a weight function located on the edge, we define an additional anisotropic weight function located on the surface of the cylinder and formulate Lemma 3.10. Finally we map the results back to a general edge as given in Lemma 3.11 and 3.12.

In Section 3.2.2 we analyze the second boundary integral derived in Lemma 3.2 with an integration domain defined by the intersection of the triangle and the boundary of the sphere with center x . First we discuss the bounded support of the corresponding function and show, that besides the classical singularities on the boundary of the element and the geometrical singularities on the surface of the cylinders around the edges, an additional geometrical singularity exists located on the triangles parallel to the original triangle with distance R . Here we detect jumps in the triangle function and a one-sided singularity in its first derivative as stated in Lemma 3.16. Thus, we introduce an additional weight function located on the triangles which are parallel to the original triangle and proceed with the characterization of the simplified potential $P_R\varphi$.

The natural decomposition of the support of $P_R\varphi$ is the mutual intersection of the spheres around the vertices and the cylinders around the edges of the triangle. We decompose an arbitrary plane in the natural decomposition of the support of $P_R\varphi$. Summarizing the analysis of the previous two sections, we describe the quality of the singularity set of the simplified retarded potential in Proposition 3.21. Finally we summarize the regularity of the retarded potential using the results on the subelements of the partition to obtain Theorem 3.22.

The characterization of the complete discrete retarded potential is now straight forward. All observed singularities duplicate (Proposition 3.25) and on an accordingly finer decomposition of the regarded plane we can formulate the regularity in Theorem 3.26 as a consequence of Theorem 3.22. In Lemma 3.23 we prove a specification of the support of the complete discrete retarded potential.

In Section 3.3 we present some numerical results validating the theoretical derivations. Using high resolution plots of a line and contour plots in planes parallel and perpendicular to the triangle plane, we give evidence for the geometrical position of the different types of singularities and discuss their strength.

The construction and error analysis of a composite quadrature rule for a typical Galerkin entry in a matrix of the earlier derived MOT-scheme is the topic of *Chapter 4*. We split the integral into an outer and inner integration. The outer integration evaluates the discrete retarded potential multiplied with a test function on the domain of influence of the trial element intersected with the test element, whereas the inner integration evaluates the discrete retarded potential itself on the trial element intersected with the domain of influence of a point defined by the outer integration.

In Section 4.1 we construct a composite quadrature for the discrete retarded potential. We introduce local polar coordinates (r, θ) with respect to the point of observation projected onto the triangle plane and decompose the domain of integration. On each subdomain, we perform a tensor product Gaussian quadrature which is a possibly graded quadrature in r taking into account the point singularity, if the kernel is weakly singular. We adopt the analysis of Schwab [51] to show exponential convergence of this scheme. Additionally, we estimate the error of the quadrature rule in the angle θ and show that a graded quadrature in the angle can improve the convergence if the corresponding integration domain is of a very unregular shape.

In Section 4.2 we propose a composite quadrature for the outer integral based on the results of Chapter 3. The natural decomposition of the plane, defined by the test triangle in the domain of influence of the trial element as defined in (3.23), results in an exponentially converging quadrature scheme. We take care of the different corner, edge and corner-edge singularities on the subelements intersected with the test triangle.

Numerical experiments presented in Section 4.4 validate the exponential convergence of the implemented inner quadrature scheme and give evidence, that the geometrical singularities have to be taken into account if exponential convergence of the whole quadrature scheme is desired.

In *Chapter 5* we present numerical experiments based on the MOT-algorithm derived in Chapter 2 using the quadrature schemes discussed in Chapter 4.

The Appendix is divided into three parts. In Part A we give a short overview of the weighted Sobolev spaces and countably normed spaces used throughout this work and briefly introduce the space-time Sobolev spaces as defined in [4, 5]. Part B discusses the regularity of the discrete retarded potentials on the three-dimensional subelements of the decomposition of their support rather than the restriction to the plane which was needed in the analysis of the quadrature scheme. In Part C we give some details on the implementation.

Acknowledgments

I would like to thank Prof. Dr. E. P. Stephan and PD Dr. Matthias Maischak for the suggestion of the topic and the various discussions. In particular I like to thank Prof. Stephan for the possibility to present my work at several conferences and the many critical remarks when it came to the formulation of the proofs. Matthias Maischak always took time to discuss my problems, either of mathematical or of programming nature. Moreover, I whole heartedly thank him for his hospitality during my stays at Brunel University, once he moved there. His program package MaiProgs was the basis of my work and the numerical experiments would certainly not have been possible to this extend without the foundations available in this program package. I would like my co-referee Prof. Dr. Sauter for his readiness to examine this thesis.

I also would like to give props to my colleagues at the Institute of Applied Mathematics. I thank Catalina Dominguez-Garcia for being such a good company throughout the years. For the proof-reading of this work I would like to thank Leo Neleman, Florian Leydecker and my most critical reviewer Michael Andres.

Chapter 2

Retarded Potential Boundary Integral Equations and their Discretization

Let us first give a brief summary of the underlying physical problem as e.g. pointed out in [23].

Consider the transient sound radiation of some body Ω^- , where Ω^- is a bounded open domain with a connected complement given by $\Omega := \Omega^+ = \mathbb{R}^3 \setminus \overline{\Omega^-}$. Denote by \mathbf{n} the outer normal on the boundary $\Gamma := \partial\Omega$. The scattered acoustic pressure field $u(t, x)$ induced by some incident field u^{inc} from the exterior domain fulfills the wave equation

$$\square u := \frac{1}{c^2} \frac{\partial^2 u}{\partial t^2} - \Delta u = 0, \quad (2.1)$$

where $x \in \Omega$, $t \in \mathbb{R}$ and c is the wave velocity. In the following, we set $c = 1$. We assume that the incident field has not reached Ω^- at $t = 0$ and that all functions are causal, i.e. they are vanishing for $t < 0$. Moreover, there hold initial conditions

$$u(0, x) = \frac{\partial}{\partial t} u(0, x) = 0 \quad \text{for } x \in \Omega, \quad (2.2)$$

and boundary conditions on Γ , given by an operator \mathcal{B} acting on some function f

$$\mathcal{B}u = f(t, x) \quad \text{in } \Gamma \times \mathbb{R}. \quad (2.3)$$

If $\mathcal{B}u = u$ one refers to a soft scatterer and the above described problem is called the *Dirichlet problem* and for $\mathcal{B}u = \frac{\partial u}{\partial n} - \frac{\alpha}{c} \frac{\partial u}{\partial t}$ we will refer to the *Neuman problem* and have a hard or absorbing scatterer. α is known as impedance function of the surface Γ , with $\alpha(x) \geq 0$ for all $x \in \Gamma$. For $\alpha(x) \equiv 0$ we have a hard scatterer. Moreover, it holds

$$f(t, x) = -\mathcal{B}u^{\text{inc}}(t, x).$$

The energy of the total pressure field $u^{\text{tot}} := u + u^{\text{inc}}$ is given by

$$E(t, u^{\text{tot}}) = \frac{1}{2} \int_{\Omega} |\nabla u^{\text{tot}}(t, x)|^2 + |\dot{u}^{\text{tot}}(t, x)|^2 dx.$$

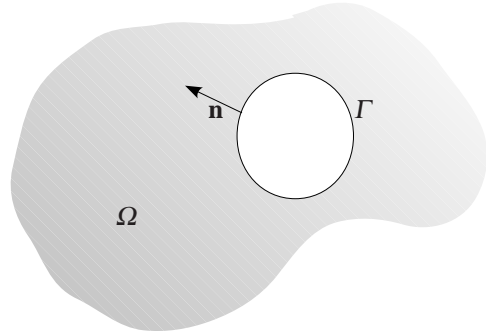
Note, that we do not have to require an explicit radiation condition, as the system describes the full physical wave behavior. The fundamental solution of the scalar wave equation (2.1) is known as

$$G(s, t, x, y) = \frac{\delta(t - s - |x - y|)}{|x - y|}.$$

Accordingly the representation formula is given [30] by

$$u(t, x) = \frac{1}{4\pi} \int_{\Gamma} \frac{\mathbf{n}_y(x - y)}{|x - y|} \left(\frac{\varphi(\tau, y)}{|x - y|^2} + \frac{\dot{\varphi}(\tau, y)}{|x - y|} \right) ds_y - \frac{1}{4\pi} \int_{\Gamma} \frac{p(\tau, y)}{|x - y|} ds_y \quad (2.4)$$

for all $(t, x) \in \Omega \times \mathbb{R}^+$ with a *retarded time* argument $\tau := t - |x - y|$, where $\varphi = u^+ - u^- = [u]$ and $p = \frac{\partial u^+}{\partial n} - \frac{\partial u^-}{\partial n} = \left[\frac{\partial u}{\partial n} \right]$.



Remark 2.1. If $c \neq 1$ the retarded time argument is $\tau = t - |x - y|/c$.

Definition 2.2. Define for $(t, x) \in \mathbb{R}^+ \times (\mathbb{R}^3 \setminus \Gamma)$ the *retarded single layer potential* by

$$Sp(t, x) = \frac{1}{4\pi} \int_{\Gamma} \frac{p(\tau, y)}{|x - y|} ds_y$$

and the *retarded double layer potential* by

$$D\varphi(t, x) = \frac{1}{4\pi} \int_{\Gamma} \frac{\mathbf{n}_y \cdot (x - y)}{|x - y|^2} \left(\frac{\varphi(\tau, y)}{|x - y|^2} + \frac{\dot{\varphi}(\tau, y)}{|x - y|} \right) ds_y.$$

Thus, (2.4) reads

$$u(t, x) = D\varphi(t, x) - Sp(t, x),$$

where $\varphi = u^+ - u^- = [u]$ and $p = \frac{\partial u^+}{\partial n} - \frac{\partial u^-}{\partial n} = \left[\frac{\partial u}{\partial n} \right]$.

Definition 2.3. Define the time domain or retarded potential boundary integral operators for $x \in \Gamma$ and $t \in \mathbb{R}^+$. The *single layer potential* reads

$$Vp(t, x) = \frac{2}{4\pi} \int_{\Gamma} \frac{p(\tau, y)}{|x - y|} ds_y$$

where its normal derivative with respect to x , the *adjoint double layer potential* is

$$\begin{aligned} K'p(t, x) &= \frac{2}{4\pi} \int_{\Gamma} \mathbf{n}_x \cdot \nabla_x \frac{p(\tau, y)}{|x - y|} d\sigma_y \\ &= \frac{2}{4\pi} \int_{\Gamma} \frac{\mathbf{n}_x \cdot (x - y)}{|x - y|^2} \left(\frac{p(\tau, y)}{|x - y|^2} + \frac{\dot{p}(\tau, y)}{|x - y|} \right) ds_y \end{aligned}$$

The *double layer potential* is given by

$$\begin{aligned} K\varphi(t, x) &= \frac{2}{4\pi} \int_{\Gamma} -\mathbf{n}_y \cdot \nabla_x \frac{\varphi(\tau, y)}{|x - y|} d\sigma_y \\ &= \frac{2}{4\pi} \int_{\Gamma} \frac{\mathbf{n}_y \cdot (x - y)}{|x - y|^2} \left(\frac{\varphi(\tau, y)}{|x - y|^2} + \frac{\dot{\varphi}(\tau, y)}{|x - y|} \right) ds_y \end{aligned}$$

and its normal derivative, the so-called *hypersingular operator* is

$$W\varphi(t, x) = - \lim_{x' \in \Omega^+ \rightarrow x} \mathbf{n}_x \cdot \nabla_{x'} \left(\frac{2}{4\pi} \int_{\Gamma} \mathbf{n}_y \cdot \nabla_{x'} \frac{\varphi(t - |x' - y|, y)}{|x' - y|} ds_y \right).$$

Remark 2.4. Formally it holds e. g. for the single layer potential

$$Sp(t, x) = \frac{1}{4\pi} \int_{\Gamma} \frac{p(\tau, y)}{|x - y|} d\sigma_y = \frac{1}{4\pi} \int_{\Gamma} \int_0^{\infty} \frac{\delta(t - s - |x - y|)}{|x - y|} p(s, y) d\sigma_y ds.$$

Denote the limits from Ω^+ and Ω^- by

$$(u)^{\pm} = \lim_{x \rightarrow \Gamma, x \in \Omega^{\pm}} u(x),$$

we can summarize the limits of the double and single layer potential and its normal derivatives by

Theorem 2.5 (Jump relations). *Let $x \in \Omega^+$ or $x \in \Omega^-$, then for $\varphi, p \in C^2(\mathbb{R} \times \Gamma)$ there holds*

$$\begin{aligned}
2(Sp)^-(t,x) &= 2(Sp)^+(t,x) = Vp(t,x) \\
2\frac{\partial(Sp)^-}{\partial n}(t,x) &= (I + K')p(t,x) \\
2\frac{\partial(Sp)^+}{\partial n}(t,x) &= (-I + K')p(t,x) \\
2(D\varphi)^-(t,x) &= (-I + K)\varphi(t,x) \\
2(D\varphi)^+(t,x) &= (I + K)\varphi(t,x) \\
2\frac{\partial(D\varphi)^-}{\partial n}(t,x) &= 2\frac{\partial(D\varphi)^+}{\partial n}(t,x) = W\varphi(t,x)
\end{aligned}$$

Proof. A proof may be found in [22] (Lemma 3 and Lemma 4a). \square

If we introduce the jump operator $[\cdot]$ across Γ defined as $[u] := u^+ - u^-$ and define the traces $\gamma_0 u = u$ and $\gamma_1 u = \frac{\partial u}{\partial n}$, we can write the above theorem in a more compact way resulting in the well known jump relations

$$\begin{aligned}
[\gamma_0 Sp] &= 0 & [\gamma_1 Sp] &= -p \\
[\gamma_0 D\varphi] &= \varphi & [\gamma_1 D\varphi] &= 0.
\end{aligned}$$

2.1 Retarded Potential Boundary Integral Equations

In this work we will focus on integral equations of first kind. See [23] and the references therein for the corresponding analysis for integral equations of second kind.

Given the boundary data $\mathcal{B}u = u = f(t,x)$ for $(t,x) \in \mathbb{R}^+ \times \Gamma$ we physically deal with a so-called *soft scatterer* and refer mathematically to a *Dirichlet problem*. Due to the Corollary of Theorem 1 (p. 116) in [22] one can represent the solution u of (2.1) using a single layer ansatz for $x \notin \Gamma$

$$u(t,x) = Sp(t,x)$$

with a density function p . The single layer operator is continuous when passing the limit onto the boundary (Theorem 2.5) such that the indirect approach yields the boundary integral equation

$$Vp(t,x) = f(t,x). \quad (2.5)$$

On the other hand, we can use the representation formula (2.4) for given boundary data $u = f$ on Γ and obtain with Theorem 2.5 and $p := \gamma_1 u$ the direct formulation

$$Vp = (K - I)f. \quad (2.6)$$

Given the boundary data $\mathcal{B}u = \partial_n u = f$, we assume the impedance function $\alpha = 0$. For this *Neuman problem* or *hard scatterer*, we can represent u using the double layer potential by some density function φ , i.e. $u = D\varphi$. Taking the normal derivative and passing the limit onto the boundary, we obtain the indirect formulation

$$W\varphi = f, \quad (2.7)$$

with some density function φ (cf. [22] Corollary of Theorem 2, p. 119). The direct approach with a given normal derivative $\partial_n u = f$ on the boundary Γ yields

$$W\varphi = (I + K')f, \quad (2.8)$$

where $\varphi = \gamma_0 u$. Besides the soft and hard scatterer, the absorbing scatterer is of practical importance. Mathematically it corresponds to the Robin problem, compare [21] for details.

2.2 Space-Time Variational Formulations

The key idea in the derivation of a space-time variational formulation is the Fourier-Laplace transformation of the time-dependent problem into frequency domain. The variational formulation in the frequency domain is then derived and analyzed. The inverse Fourier-Laplace transform maps these results back into the time domain using the theorem of Paley-Wiener and Parseval's equation and we obtain the space-time variational formulation.

Let $\omega = \eta + i\sigma$ with $\eta, \sigma \in \mathbb{R}$ and $\sigma > 0$. The Fourier-Laplace transform of (2.1) is the well-known Helmholtz equation

$$\Delta \hat{u} + \omega^2 \hat{u} = 0 \text{ in } \Omega, \quad (2.9)$$

here \hat{u} represents the Fourier-Laplace-transform of u . For more details on the functional framework compare Appendix A and the references given there. In the following, we apply the notation as introduced in [3] and define

$$\int_{-\infty}^{\infty} f(t) d_{\sigma} t := \int_{-\infty}^{\infty} f(t) e^{-2\sigma t} dt.$$

The mapping properties of the retarded potential boundary integral operators were analyzed in [22], compare also [17]. In [4] the space-time formulation of the Dirichlet problem is studied and in [5] the corresponding analysis for the Neumann problem is discussed. Compare also the overview paper [23] for more details and references. We define the bilinear forms

$$a_V(p, q) := \int_0^{\infty} \langle Vp, \partial_t q \rangle d_{\sigma} t = \int_0^{\infty} \int_{\Gamma} Vp(t, x) \partial_t q(t, x) ds_x d_{\sigma} t \quad (2.10)$$

$$a_W(\varphi, \psi) := \int_0^{\infty} \langle W\varphi, \partial_t \psi \rangle d_{\sigma} t = \int_0^{\infty} \int_{\Gamma} W\varphi(t, x) \partial_t \psi(t, x) ds_x d_{\sigma} t. \quad (2.11)$$

Both bilinear forms are continuous and coercive in appropriate space-time Sobolev spaces, compare Appendix A. Note that the spaces on which one proves the continuity and the coercivity of the bilinear forms are not the same. Moreover all estimates are dependent on σ and explicitly demand, that $\sigma > 0$.

Remark 2.6. In [4] the time derivative is taken on the trial function rather than on the test function. In [15] the time derivative is taken on the test function. Partial integration in time reveals, that both formulations only differ by a sign and the discrete formulations are equivalent.

For the Dirichlet problems (2.5) and (2.6) we define the right hand side by

$$F_1(q) := \int_0^{\infty} \int_{\Gamma} f(t, x) \partial_t q(t, x) ds_x d_{\sigma} t$$

$$F_2(q) := \int_0^{\infty} \int_{\Gamma} (K - I) f(t, x) \partial_t q(t, x) ds_x d_{\sigma} t.$$

Then we can formulate the following two variational problems for the indirect and direct Dirichlet approach (2.5) and (2.6) respectively:

$$\text{Find } p \in H_{\sigma}^s(\mathbb{R}^+, H^{-1/2}(\Gamma)) \quad a_V(p, q) = F_1(q) \quad \forall q \in H_{\sigma}^s(\mathbb{R}^+, H^{-1/2}(\Gamma)) \quad (2.12)$$

$$\text{Find } p \in H_{\sigma}^s(\mathbb{R}^+, H^{-1/2}(\Gamma)) \quad a_V(p, q) = F_2(q) \quad \forall q \in H_{\sigma}^s(\mathbb{R}^+, H^{-1/2}(\Gamma)) \quad (2.13)$$

In Theorem 2 in [4] for $f \in \mathcal{H}_{\sigma_0}^{3/2}(\mathbb{R}^+, H^{1/2}(\Gamma))$ and $\sigma_0 > 0$ it was shown that the Dirichlet problem (2.1)-(2.3) with $\mathcal{B}u = u$ possesses a unique solution with $p \in \mathcal{H}_{\sigma_0}^0(\mathbb{R}^+, H^{1/2}(\Gamma))$ and there holds the following estimate

$$\int_{-\infty}^{\infty} E(t, u) d_{\sigma} t \leq C \frac{1}{\sigma^2} \max(\sigma_0^{-1}, 1) \|f\|_{\mathcal{H}_{\sigma_0}^{3/2}(\mathbb{R}^+, H^{1/2}(\Gamma))}.$$

For the integral equations for the Neumann problem (2.7) and (2.8) we define

$$F_3(\psi) := \int_0^\infty \int_\Gamma f(t,x) \partial_t \psi(t,x) ds_x d\sigma t,$$

$$F_4(\psi) := \int_0^\infty \int_\Gamma (I + K') f(t,x) \partial_t \psi(t,x) ds_x d\sigma t.$$

Thus we formulate the following two variational problems for the indirect and direct Neuman approach (2.5) and (2.6), respectively.

$$\text{Find } \varphi \in H_\sigma^s(\mathbb{R}^+, H^{1/2}(\Gamma)) \quad a_W(\varphi, \psi) = F_3(\psi) \quad \forall \psi \in H_\sigma^s(\mathbb{R}^+, H^{1/2}(\Gamma)) \quad (2.14)$$

$$\text{Find } \varphi \in H_\sigma^s(\mathbb{R}^+, H^{1/2}(\Gamma)) \quad a_W(\varphi, \psi) = F_4(\psi) \quad \forall \psi \in H_\sigma^s(\mathbb{R}^+, H^{1/2}(\Gamma)) \quad (2.15)$$

For results on existence and uniqueness compare [5].

Note that, for the hypersingular operator partial integration gives ([22] Lemma 4b)

$$\int_0^\infty \int_\Gamma W \varphi(x,t) \eta(x,t) ds_x dt = \frac{1}{2\pi} \int_0^\infty \iint_{\Gamma \times \Gamma} \left\{ \frac{\mathbf{n}_x \cdot \mathbf{n}_y}{|x-y|} \dot{\varphi}(t-|x-y|, y) \dot{\eta}(t,x) \right. \\ \left. + \frac{\text{curl}_\Gamma \varphi(t-|x-y|, y) \cdot \text{curl}_\Gamma \eta(t,x)}{|x-y|} \right\} ds_y ds_x dt, \quad (2.16)$$

where the tangential surface curl operator curl_Γ is defined via $\text{curl}_\Gamma \varphi = n \wedge \nabla \tilde{\varphi}$, where $\tilde{\varphi} = \varphi$ in each intersection point with Γ and in a tubular neighborhood to Γ $\tilde{\varphi}$ is constant along each normal line to Γ .

2.3 Discretization of Retarded Potential Boundary Integral Equations

In this section we give the discretization of (2.12), (2.13), (2.14) and (2.15) and derive the corresponding algebraic systems.

2.3.1 Discretization in Space and Time

Choose a regular triangulation \mathcal{T}_h of Γ into a finite number of subelements Γ_j ($j \in \{1, \dots, N_s\}$) with the following properties

1. $\Gamma = \bigcup_{\Gamma_j \in \mathcal{T}_h} \Gamma_j$
2. each element Γ_j is closed a Lipschitz continuous boundary and with $\text{int} \Gamma_j \neq \emptyset$
3. for distinct $\Gamma_i, \Gamma_j \in \mathcal{T}_h$ it holds $\text{int} \Gamma_i \cap \text{int} \Gamma_j = \emptyset$

Given a reference element $T := \{(t_1, t_2) : 0 \leq t_1 \leq 1 - t_2 \leq 1\}$ and the space $S_h^{p_s}(T)$ of polynomials of degree p_s on T

$$S_h^{p_s}(T) := \left\{ v : T \rightarrow \mathbb{R} : v(t_1, t_2) = \sum_{i+j \leq p_s} \alpha_{ij} t_1^i t_2^j \right\}$$

we define for $\Gamma_j \in \mathcal{T}_h$ with

$$\Gamma_j := \{\mathbf{x} = \mathbf{x}^j + \mathbf{a}^{1,j} t_1 + \mathbf{a}^{2,j} t_2 \text{ with } (t_1, t_2) \in T \text{ and } \mathbf{a}^{1,j}, \mathbf{a}^{2,j} \in \mathbb{R}^3\},$$

the spline space of polynomials with total degree $p_s \geq 0$ by

$$S_h^{p_s}(\Gamma_j) := \{v : \Gamma_j \rightarrow \mathbb{R} : v(x) = (v \circ F)(x) \text{ with } (v \circ F) \in S_h^{p_s}(T)\}$$

where $F : T \rightarrow \Gamma_j$. Therefore, we choose the discrete spaces

$$\begin{aligned} V_h &:= \{v \in L^2(\Gamma) : v|_{\Gamma_j} \in S_h^{ps}(\Gamma_j) \text{ for every } \Gamma_j \in \mathcal{T}_h\}, \\ W_h &:= \{v \in C^0(\Gamma) : v|_{\Gamma_j} \in S_h^{ps}(\Gamma_j) \text{ for every } \Gamma_j \in \mathcal{T}_h\}. \end{aligned}$$

Note that it holds $V_h \subset H^{-1/2}(\Gamma)$ and $W_h \subset H^{1/2}(\Gamma)$.

Given a partition of the time interval $(0, \infty)$ into subintervals $I_n := (t_{n-1}, t_n]$ ($n = 1, \dots$), we choose a uniform subdivision with $|I_n| = \Delta t$, such that $t_n = n\Delta t$ ($n = 1, \dots$). Nevertheless, the presented approach also admits a nonuniform time mesh.

As the time and space variables interact in the retarded time argument $\tau = t - |x - y|$, the time discretization results in a reduction of the integration domain in space. Let us define a discrete space as an approximation of $H_\sigma^s(\mathbb{R}^+, \mathbb{R})$ by $H_\sigma^m(\Delta t, \mathbb{R})$ defined for $m \in \mathbb{N}$ and $m \geq s$ via

$$H_\sigma^m(\Delta t, \mathbb{R}) = \left\{ f \in H_\sigma^m(\mathbb{R}^+, \mathbb{R}) : f|_{I_l} \in \mathbb{P}_m \forall l \leq 1 \right\}.$$

For the discrete Dirichlet problem we can proceed as follows. Let $p_{\Delta t, h} \in H_\sigma^m(\Delta t, V_h)$ be an approximation of $p \in H_\sigma^s(\mathbb{R}^+, H^{-1/2}(\Gamma))$. Then we define the discrete problems

$$\text{Find } p_{\Delta t, h} \in H_\sigma^m(\Delta t, V_h) \quad a_V(p_{\Delta t, h}, q_{\Delta t, h}) = F_1(q_{\Delta t, h}) \quad \forall q_{\Delta t, h} \in H_\sigma^m(\Delta t, V_h), \quad (2.17)$$

$$\text{Find } p_{\Delta t, h} \in H_\sigma^m(\Delta t, V_h) \quad a_V(p_{\Delta t, h}, q_{\Delta t, h}) = F_2(q_{\Delta t, h}) \quad \forall q_{\Delta t, h} \in H_\sigma^m(\Delta t, V_h). \quad (2.18)$$

Ha-Duong investigated in [22] the a priori error of the retarded single layer ansatz (2.13), but especially for approximated surfaces Γ his results involve the quotients $\Delta t/h$ and $h/\Delta t$.

The discrete Neuman problem can then be formulated as follows. Let $\varphi_{h, \Delta t} \in H_\sigma^m(\Delta t, W_h)$ be an approximation of $\varphi \in H_\sigma^s(\mathbb{R}^+, H^{1/2}(\Gamma))$.

$$\text{Find } \varphi_{\Delta t, h} \in H_\sigma^m(\Delta t, W_h) \quad a_W(\varphi_{\Delta t, h}, \psi_{\Delta t, h}) = F_3(\psi_{\Delta t, h}) \quad \forall \psi_{\Delta t, h} \in H_\sigma^m(\Delta t, W_h), \quad (2.19)$$

$$\text{Find } \varphi_{\Delta t, h} \in H_\sigma^m(\Delta t, W_h) \quad a_W(\varphi_{\Delta t, h}, \psi_{\Delta t, h}) = F_4(\psi_{\Delta t, h}) \quad \forall \psi_{\Delta t, h} \in H_\sigma^m(\Delta t, W_h). \quad (2.20)$$

2.3.2 Discrete Retarded Potentials and the MOT Algorithm

The presented discretization scheme is known for a long time, compare e.g. [21]. In the previous sections we have discussed the discrete space-time Galerkin methods for different kinds of RPBEs. In this section we want to focus on the computation of the involved matrices. Thus, we discuss the discrete retarded potential for a general kernel $k(x - y)$ and the resulting matrix entry. Although the final results are already known from [21] we give a detailed derivation of the fully discrete system.

Analytical Evaluation of Retarded Time Integrals

Let us first discuss the analytical evaluation of time integrals with one retarded time argument, i.e. given two function f_1 and f_2 , we solve integrals of the type

$$\int_0^\infty f_1(t - |x - y|) f_2(t) dt. \quad (2.21)$$

They occur in the computation of the Galerkin entries of the discrete space-time variational formulations discussed earlier.

Remark 2.7. Note, that the analysis of the space-time variational formulation as discussed earlier explicitly demands $\sigma > 0$, as the coercivity estimate fails for $\sigma = 0$. Nevertheless, in practical computations one usually sets $\sigma = 0$, compare [21] and so do we. In [1] the integrals are also computed for $\sigma > 0$ and no significant advantage was reported. Although the stability of the schemes is only secured for $\sigma > 0$, no loss of stability is observed for $\sigma = 0$.

Before we consider the retarded time integral more generally, we discuss a simple model integral to clarify the chosen approach. Choosing piecewise constant basis functions in time represented using the Heavyside function, such that

$$\gamma^m(t) = \chi_{\mathcal{I}_m}(t) = H(t - t_{m-1}) - H(t - t_m),$$

where the indicator function $\chi_A(x)$ for a set A is defined by

$$\chi_A(x) = \begin{cases} 1 & x \in A \\ 0 & x \notin A \end{cases}.$$

We compute

$$\begin{aligned} \Upsilon_0^{n-m}(x, y) &:= \int_0^\infty \gamma^m(t - |x - y|) \dot{\gamma}^n(t) dt \\ &= \int_0^\infty (H(t - |x - y| - t_{m-1}) - H(t - |x - y| - t_m)) (\delta(t - t_{n-1}) - \delta(t - t_n)) dt \\ &= (H(t_{n-1} - |x - y| - t_{m-1}) - H(t_{n-1} - |x - y| - t_m)) \\ &\quad - (H(t_n - |x - y| - t_{m-1}) - H(t_n - |x - y| - t_m)) \\ &= [H(t_{n-m} - |x - y|) - H(t_{n-m-1} - |x - y|)] - [H(t_{n-m+1} - |x - y|) - H(t_{n-m} - |x - y|)]. \end{aligned}$$

Now, use

$$H(t_l - |x - y|) = \begin{cases} 1 & |x - y| \leq t_l \\ 0 & \text{else} \end{cases},$$

which defines the four dimensional set

$$K_l := \{(x, y) \in \Gamma \times \Gamma : |x - y| \leq t_l\}.$$

Note, that $K_{n-m-1} \subset K_{n-m} \subset K_{n-m+1}$, such that we can rewrite

$$\begin{aligned} \Upsilon_0^{n-m}(x, y) &= [\chi_{K_{n-m}}(x, y) - \chi_{K_{n-m-1}}(x, y)] - [\chi_{K_{n-m+1}}(x, y) - \chi_{K_{n-m}}(x, y)] \\ &= \chi_{E_{n-m-1}}(x, y) - \chi_{E_{n-m}}(x, y), \end{aligned}$$

where *discrete light cone integration domain* E_l is defined by

$$E_l := K_{l+1} \setminus K_l = \{(x, y) \in \Gamma \times \Gamma : t_l \leq |x - y| \leq t_{l+1}\}. \quad (2.22)$$

This integration domain is of central importance when evaluating discrete retarded Galerkin integrals. It reflects, that the evaluation of the time integrals depends only on the time difference $n - m$, which is the basis of the marching-on-time (MOT) algorithm of this method.

Denote by $S^{p,r}(\Delta t)$ the space of piecewise defined spline functions on the time mesh with time step size Δt with a degree p and let $r = 1$ indicate continuous splines, where $r = 0$ denotes discontinuous splines.

Given piecewise defined spline functions $f_1 \in S^{p_1, r_1}(\Delta t)$ and $f_2 \in S^{p_2, r_2}(\Delta t)$, where we assume, that the continuous time splines have a support of two time intervals and discontinuous time splines have a support only on one time interval. For functions defined on the discrete time interval we can evaluate the corresponding integrals of the type (2.21) always analytically and obtain

$$\Upsilon^l(x, y) = \sum_{p=0}^{n_{ring}-1} \sum_{q=0}^{p_1+p_2+1} \Upsilon_{pq} |x - y|^q \chi_{E_{l-p}}(x, y). \quad (2.23)$$

The matrix $\Upsilon = (\Upsilon_{pq})$ results from the analytic evaluation of the time integrals and n_{ring} denotes the number of light cone integration domains involved.

Remark 2.8. If $r_1 = r_2 = 0$ then always two light cone integration domains are involved, i.e. $n_{ring} = 2$. If $r_1 = 1$ and $r_2 = 0$ results in three light cone integration domains $n_{ring} = 3$. These two cases are discussed in this work, following basically the scheme presented in [21]. Nevertheless an extension to functions with $r_1 = r_2 = 1$ is possible, but then four light cone integration domains are necessary and in (2.23) $p = -1, \dots, 2$. The use of time basis functions with a bigger support is not advisable, as it requires even more light cone integration domains, which finally destroys the sparsity of the corresponding Galerkin matrices.

In the discretization of the retarded boundary integrals, the following four integrals are used

$$\begin{aligned} \Upsilon_0^{n-m}(x, y) &:= \int_0^\infty \gamma^m(t - |x - y|) \dot{\gamma}^n(t) dt, & \Upsilon_1^{n-m}(x, y) &:= \int_0^\infty \beta^m(t - |x - y|) \dot{\gamma}^n(t) dt, \\ \Upsilon_2^{n-m}(x, y) &:= \int_0^\infty \beta^m(t - |x - y|) \dot{\gamma}^n(t) dt, & \Upsilon_3^{n-m}(x, y) &:= \int_0^\infty \dot{\beta}^m(t - |x - y|) \dot{\gamma}^n(t) dt, \end{aligned}$$

where the analytical evaluation of the first integral was discussed earlier and reveals for $l = n - m$

$$\Upsilon_0^l = \begin{pmatrix} 1 \\ -1 \end{pmatrix}.$$

The remaining integrals reduce to

$$\Upsilon_1^l = \frac{1}{2\Delta t} \begin{pmatrix} t_{l+1}^2 & -2t_{l+1} & 1 \\ 2\Delta t^2 - t_l^2 - t_{l-1}^2 & 2(t_l + t_{l+1}) & -2 \\ t_{l-2}^2 & -2t_{l-2} & 1 \end{pmatrix}, \quad \Upsilon_2^l = \frac{1}{\Delta t} \begin{pmatrix} -t_{l+1} & 1 \\ t_{2l-1} & -2 \\ -t_{l-2} & 1 \end{pmatrix}, \quad \Upsilon_3^l = \frac{1}{\Delta t} \begin{pmatrix} -1 \\ 2 \\ -1 \end{pmatrix}.$$

Compare Appendix C for details on the computation of the time integrals.

Discrete Retarded Single Layer Matrices

Given the discrete problems (2.18) and (2.17), let us now discuss the derivation of linear equation system. A density $p_{\Delta t, h} \in H^0(\Delta t, V_h)$ can be approximated by

$$p_{\Delta t, h}(t, x) = \sum_{m=1}^{N_t} \sum_{i=1}^{N_s} p_i^m \gamma^m(t) \varphi_i(x) \quad \text{where } \varphi_i \in V_h$$

using piecewise constant functions $\gamma^m(t) = \chi_{I_m}(t)$.

Thus the left hand side of (2.17) and (2.18) reads for test functions $q_{\Delta t, h}(t, x) = \gamma^n(t) \varphi_j(x)$

$$a_V(p_{\Delta t, h}, q_{\Delta t, h}) = \sum_{m=1}^{N_t} \sum_{i=1}^{N_s} p_i^m \iint_{\Gamma \times \Gamma} \Upsilon_0^{n-m}(x, y) \frac{\varphi_i(y) \varphi_j(x)}{|x - y|} ds_y ds_x. \quad (2.24)$$

We have seen earlier, that $\Upsilon_0^{n-m}(x, y)$ depends only on the difference $n - m$ and thus we can rewrite (2.24) as an algebraic system in terms of matrices and vectors by

$$\sum_{m=1}^{N_t} V^{n-m} p^m,$$

where $p^m := (p_i^m)_{i=1}^{\dim(V_h)}$ and the matrix entries reduce to

$$V_{ij}^{n-m} := \sum_{p=0}^1 \Upsilon_{0, p, 1}^{n-m} \iint_{E_{n-m-p}} |x - y|^{p-1} \varphi_i(y) \varphi_j(x) ds_y ds_x$$

with $i, j = 1, \dots, \dim(V_h)$. Let us define the basic Galerkin entry.

Definition 2.9. Given a kernel function $k(x, y, x - y)$, we define the entries of the basic Galerkin matrix on one light cone integration domain E_l by

$$G_{ij}^{l,v}(k) := \iint_{E_l} k(x, y, x - y) |x - y|^v \varphi_i(y) \varphi_j(x) ds_y ds_x.$$

Thus we can rewrite (2.24)

$$V^l = G^{l-1,0}(k_V) - G^{l,0}(k_V), \quad (2.25)$$

where $k_V(x, y, x - y) = |x - y|^{-1}$ denotes the kernel of the single layer potential. In general, for a time integral with

$$Y^k(x, y) = \sum_{p=0}^{n_{ring}-1} \sum_{q=0}^{p_1+p_2+1} Y_{pq} |x - y|^q \chi_{E_{l-p}}(x, y),$$

each matrix A^l corresponding to a retarded integral $A\varphi$ with kernel $k_A(x, y, x - y)$ can be written as

$$A^l = \sum_{p=0}^{n_{ring}-1} \sum_{q=0}^{p_1+p_2+1} Y_{pq} G^{l-p,q}(k_A). \quad (2.26)$$

Example 2.10. Using linear continuous trial functions and constant test function in time the matrix entries of the matrix corresponding to the retarded single layer potential are given by

$$V_{ij}^l = \sum_{p=0}^2 \sum_{q=0}^2 Y_{1,pq}^l \iint_{E_{l-p}} |x - y|^{q-1} \varphi_i(y) \varphi_j(x) ds_y ds_x.$$

Discrete hypersingular operator matrices

Let us now focus on the discrete left hand side of (2.19) and (2.20). Then density $\varphi \in H^s(\mathbb{R}^+, H^{1/2}(\Gamma))$ ($s \leq 1$) can be approximated by piecewise linear trial functions in space and time, namely $\varphi_{\Delta t, h} \in H^1(\Delta t, W_h)$ and

$$\varphi_{\Delta t, h}(t, x) = \sum_{m=1}^{N_t} \sum_{i=1}^{N_s} \varphi_i^m \beta^m(t) \varphi_i(x) \quad \text{where } \varphi_i \in W_h$$

Choose continuous linear basis functions in space and time, i. e. $\beta^n(t) = (\Delta t)^{-1}((t - t_n)\chi_{I_n} - (t - t_{n+1})\chi_{I_{n+1}})$. Using (2.16) and choosing $\eta(t, x) = \gamma^n(t) \varphi_i(x)$ with piecewise constant basis functions $\gamma_n(t)$ in time, we can rewrite the left hand side of (2.20) and (2.19) to

$$\sum_{m=1}^{N_t} W^{n-m} \varphi^m,$$

with $\varphi^m = (\varphi_i^m)_{i=1}^{\dim(W_h)}$ and

$$\begin{aligned} W_{ij}^{n-m} &= \iint_{\Gamma \times \Gamma} \Upsilon_3^{n-m}(x, y) \frac{\mathbf{n}_x \cdot \mathbf{n}_y}{|x - y|} \varphi_i(y) \varphi_j(x) ds_y ds_x \\ &\quad + \iint_{\Gamma \times \Gamma} \Upsilon_1^{n-m}(x, y) \frac{\text{curl}_\Gamma \varphi_i(y) \cdot \text{curl}_\Gamma \varphi_j(x)}{|x - y|} ds_y ds_x, \end{aligned} \quad (2.27)$$

where $i, j = 1, \dots, \dim(W_h)$. Using (2.31) we obtain

$$\begin{aligned}
W_{ij}^l &= \sum_{p=0}^2 \Upsilon_{3,p0}^l \iint_{E_{l-p}} \frac{\mathbf{n}_x \mathbf{n}_y}{|x-y|} \varphi_i(y) \varphi_j(x) ds_y ds_x \\
&+ \sum_{p=0}^2 \sum_{q=0}^2 \Upsilon_{1,pq}^l \iint_{E_{l-p}} |x-y|^{q-1} \operatorname{curl}_\Gamma \varphi_i(y) \operatorname{curl}_\Gamma \varphi_j(x) ds_y ds_x.
\end{aligned}$$

Discrete Retarded Double Layer Matrix and its Adjoint Counterpart

In the computation of the right hand side of (2.18) and (2.20) the double layer potential and its adjoint have to be taken into account. Let us consider first the double layer potential in (2.18). We have to demand a certain regularity of the input data function f . Assume f can be approximated by piecewise linear continuous functions in space and time such that

$$f_{\Delta t, h}(t, x) = \sum_{m=1}^{N_t} \sum_{i=1}^{N_s} f_i^m \beta^m(t) \phi_i(x)$$

where $\beta^m(t) = (\Delta t)^{-1}((t - t_{m-1})\chi_{I_m}(t) - (t - t_{m+1})\chi_{I_{m+1}}(t))$ and ϕ_i is a piecewise linear function defined on element Γ_i and as before $q(t, x) = \gamma_n(t) \varphi_j(x)$, such that the right hand side of (2.18) reads in matrix vector notation

$$I(f^{n-1} - f^n) - \sum_{m=1}^n K^{n-m} f^m$$

where $f^m := (f_i^m)_{i=1, \dots, N_s} = (f(t_m, \phi_i))_{i=1, \dots, \dim(W_h)}$

$$\begin{aligned}
K_{ij}^{n-m} &:= \iint_{\Gamma \times \Gamma} \Upsilon_2^{n-m}(x, y) \frac{\mathbf{n}_y \cdot (x-y)}{|x-y|^3} \phi_i(y) \varphi_j(x) ds_y ds_x \\
&+ \iint_{\Gamma \times \Gamma} \Upsilon_3^{n-m}(x, y) \frac{\mathbf{n}_y \cdot (x-y)}{|x-y|^2} \phi_i(y) \varphi_j(x) ds_y ds_x,
\end{aligned}$$

for $i = 1, \dots, \dim(W_h)$ and $j = 1, \dots, \dim(V_h)$.

Thus the fully discrete double layer potential matrix for linear trial functions and the derivative of constant test functions in time reads

$$\begin{aligned}
K_{ij}^l &= \sum_{p=0}^2 \sum_{q=0}^1 \Upsilon_{2,pq}^l \iint_{E_{l-p}} |x-y|^{q-3} \mathbf{n}_y \cdot (x-y) \phi_i(y) \varphi_j(x) ds_y ds_y \\
&- \sum_{p=0}^2 \Upsilon_{3,p0}^l \iint_{E_{l-p}} |x-y|^{-2} \mathbf{n}_y \cdot (x-y) \phi_i(y) \varphi_j(x) ds_y ds_y,
\end{aligned}$$

and as $\Upsilon_{3,p0}^l = -\Upsilon_{2,p1}^l$ for $p = 0, 1, 2$ we obtain

$$K_{ij}^l = \sum_{p=0}^2 \Upsilon_{2,p0}^k \iint_{E_{l-p}} |x-y|^{-3} \mathbf{n}_y \cdot (x-y) \phi_i(y) \varphi_j(x) ds_y ds_y. \quad (2.28)$$

For linear trial functions and constant test function we use

$$\int_0^\infty \dot{\beta}^m(t - |x-y|) \gamma^n(t) dt = - \int_0^\infty \beta^m(t - |x-y|) \dot{\gamma}^n(t) dt = -\Upsilon_2^{n-m}(x, y)$$

which leads to

$$K_{ij}^{n-m} := \iint_{\Gamma \times \Gamma} \Upsilon_1^{n-m}(x, y) \frac{\mathbf{n}_y(x-y)}{|x-y|^3} \phi_i(y) \phi_j(x) ds_y ds_x \\ - \iint_{\Gamma \times \Gamma} \Upsilon_2^{n-m}(x, y) \frac{\mathbf{n}_y(x-y)}{|x-y|^2} \phi_i(y) \phi_j(x) ds_y ds_x$$

for $i = 1, \dots, \dim(W_h)$ and $j = 1, \dots, \dim(V_h)$. Thus the fully discrete double layer potential matrix for linear trial functions and constant test functions in time reads

$$K_{ij}^k = \sum_{p=0}^2 \sum_{q=0}^2 \Upsilon_{1,pq}^k \iint_{E_{k-p}} |x-y|^{q-3} \mathbf{n}_y(x-y) \phi_i(y) \phi_j(x) ds_y ds_x \\ - \sum_{p=0}^2 \sum_{q=0}^1 \Upsilon_{2,pq}^k \iint_{E_{k-p}} |x-y|^{q-2} \mathbf{n}_y(x-y) \phi_i(y) \phi_j(x) ds_y ds_x.$$

Using $\Upsilon_{1,p2}^k = \Upsilon_{2,p1}^k$ it reduces to

$$K_{ij}^k = \sum_{p=0}^2 \Upsilon_{1,p0}^k \iint_{E_{k-p}} |x-y|^{-3} \mathbf{n}_y(x-y) \phi_i(y) \phi_j(x) ds_y ds_x \\ - \sum_{p=0}^2 (\Upsilon_{1,p1}^k - \Upsilon_{2,p0}^k) \iint_{E_{k-p}} |x-y|^{-2} \mathbf{n}_y(x-y) \phi_i(y) \phi_j(x) ds_y ds_x. \quad (2.29)$$

The corresponding adjoint operators result in the corresponding transposed matrices.

Generalization to higher order test and trial functions in space and time

For discontinuous functions in $S^{p_i,0}(\Delta t)$ ($i = 1, 2$) with polynomial degree p_1 and p_2 for the trial and test function respectively, there holds

$$V^l = \sum_{q=0}^{p_1+p_2+1} \alpha_l^{(1)} G^{l-1,q}(k_V) + \sum_{l=0}^{p_1+p_2+1} \alpha_l^{(0)} G^{l,q}.$$

Remark 2.11. a) All retarded matrices are only sparsely populated. For a retarded matrix $A \in^{n \times n}$, the non-vanishing matrix entries are proportional to $n^2 \max(1, h/\Delta t)$. In Fig. 2.1 the typical distribution of non-vanishing matrix entries is sketched.

b) V^0 and W^0 are symmetric and positive definite, cf. Lemma 2 on page 179 and Proposition 5 on page 146 in [22]. is symmetric and positive definite.

Marching-on-in-time (MOT) Algorithm

Let us now summarize the fully discrete schemes discussed earlier in this chapter. The discrete single layer potential ansatz (2.17) using piecewise constant test and trial functions results in the following algebraic system with $n = 1, \dots$

$$\sum_{m=1}^n V^{n-m} p^m = f^{n-1} - f^n$$

which yields

$$V^0 p^n = f^{n-1} - f^n - \sum_{m=1}^{n-1} V^{n-m} p^m.$$

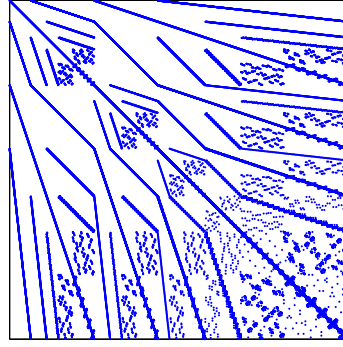


Fig. 2.1 Sparsity pattern of retarded matrix V^0 on sphere surface with 5120 elements. 0.25% non-vanishing entries.

For (2.18) we obtain

$$V^0 p^n = I(f^n - f^{n-1}) + \sum_{m=1}^n K^{n-m} f^m - \sum_{m=1}^{n-1} V^{n-m} p^m$$

where V^l is given in (2.25), K^l in (2.28) with $l := n - m$ and I denotes the corresponding mass matrix. The indirect approach for the Neuman problem (2.19) yields for linear trial and constant test functions in time

$$W^0 \phi^n = \frac{\Delta t}{2} I(f^{n-1} + f^n) - \sum_{m=1}^{n-1} W^{n-m} \phi^m$$

and for the direct formulation (2.20) there holds

$$W^0 \phi^n = \frac{\Delta t}{2} I(f^{n-1} + f^n) + \sum_{m=1}^n (K^{n-m})^T f^m - \sum_{m=1}^{n-1} W^{n-m} \phi^m$$

where W^l is defined as in (2.27) and K^l is given in (2.29).

All above described fully discrete systems are constructed in the same way. They involve the computation of a series of matrices, that are sparsely populated as the light cone integration domain E_l restricts the number of interacting element per time step. The computation of each matrix does only depend on the time difference and another remarkable property is, that for bounded surfaces Γ the matrices vanish if for the time difference $l := n - m$ there holds

$$l > \left\lceil \frac{\text{diam } \Gamma}{\Delta t} \right\rceil.$$

Thus we can describe the linear equation system for a series of non-vanishing matrices A^j with $j = 0, \dots, \hat{n}$ and a series of solution vectors x^j with $j = 1, \dots, n$ such that the MOT scheme reads

$$A^0 x^n = f^n - \sum_{m=\max(1, n-\hat{n})}^{n-1} A^{n-m} x^m =: b^n. \quad (2.30)$$

Thus for $n \leq \hat{n}$ it holds

$$b^n = f^n - \sum_{m=1}^{n-1} A^{n-m} x^m$$

and for $n > \hat{n}$ we have

$$b^n = f^n - \sum_{m=n-\hat{n}}^{n-1} A^{n-m} x^m = f^n - \sum_{m=1}^{\hat{n}} A^{\hat{n}-m+1} x^{m+(n-\hat{n})-1}.$$

One important question is, how does an error $|A_{ij}^k - \tilde{A}_{ij}^k|$ in the matrix entry (i, j) influence the error of the solution of the linear system $|x_j^n - \tilde{x}_j^n|$. To our knowledge is has not undergone a rigors analysis. Nevertheless, it is immediately clear, that the accuracy has to be high in order to avoid a pollution of the MOT scheme.

Finally, the abstract MOT scheme can be summarized as follows.

```

for  $n = 1, \dots$  do
  if  $n > \lceil \frac{\text{diam}\Gamma}{\Delta t} \rceil$  then
    Domain of influence has passed the body;
    No more matrix computation needed;
  else
    Allocate storage for basic Galerkin matrix  $G^{n-1}$  using (C.1);
    Compute  $G^{n-1}$ ;
    Compose the new retarded matrices;
    Delete basic Galerkin entries that are not needed in the next time step;
  end
  Compute right hand side by matrix vector multiplication;
  Solve solve the linear equation system;
  Store new solution vector
end

```

Algorithm 2.1: Time Stepping Algorithm

Before we close this chapter, let us briefly outline its impact on the rest of this work. The most expensive part of the MOT-scheme is the matrix computation, although the resulting matrices are sparse. The next two chapters are devoted to the analysis of the discrete retarded potential and its corresponding Galerkin entry. We have seen, that higher order basis function in time result in additional terms with multiplicative factors $|x - y|^\nu$ in the generation of the basic Galerkin entry. Thus in the following we will discuss the computation of an integral of the type

$$G_{ij}^{l,\nu} := \iint_{E_l} k_\nu(x-y) \varphi_i(y) \varphi_j(x) ds_y ds_x, \quad (2.31)$$

where $k_\nu(x-y) = |x-y|^\nu$ and $\nu \geq -1$. We can rewrite (2.31) on a triangulation Γ_h of Γ to

$$\begin{aligned} G_{ij}^{l,\nu} &= \int_{\Gamma_h} \int_{\Gamma_h \cap E(x)} k_\nu(x-y) \varphi_i(y) \varphi_j(x) ds_y ds_x \\ &= \sum_{T_i, T_j \in \Gamma_h} \int_{T_i} \int_{T_j \cap E(x)} k_\nu(x-y) \varphi_i(y) \varphi_j(x) ds_y ds_x, \end{aligned}$$

where $E(x) := B_{l+1}(x) \setminus B_l(x)$ is the so called domain of influence of the point x . The inner integral is the discrete retarded potential, which will be analyzed in the next chapter, whereas the Galerkin integral (2.31) is studied in Chapter 4.

Chapter 3

Regularity of Discrete Retarded Potentials

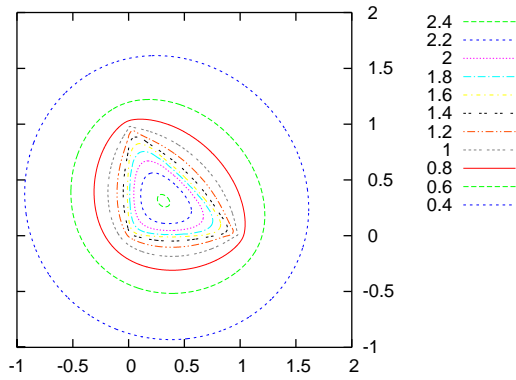


Fig. 3.1 Contour plot of Laplace single layer potential in triangle plane with triangle vertices $(0,0,0), (1,0,0), (0,1,0)$.

Discrete time independent integral equations and the corresponding potentials have been studied for years and are well understood. Singularities in the first derivatives of the discrete potentials are e.g. reported in [38]. In Fig. 3.1 we see the contour plot of the single layer potential

$$(P\varphi)(x) = \frac{1}{2\pi} \int_T \frac{1}{|x-y|} ds_y$$

of the Laplace problem evaluated for points x lying in the triangle plane. Here we use an ansatz function φ which is constant on the triangle T . The contour levels become dense close to the boundary of the triangle, which indicates a singularity in the gradient of P . In fact the potential itself is continuous, but its gradient possesses corner and corner/edge singularities on the boundary of the trial element T . If the corresponding Galerkin integrals

$$\int_{\hat{T}} \int_T \frac{1}{|x-y|} ds_y ds_x$$

are evaluated numerically, these singularities have to be taken into account. Mund [43] proposes a grading strategy towards the edges of element T in the outer integration whereas Sauter and Schwab [49] present a method using relative coordinates and the Duffy transformation that lifts the singularities. We will discuss an appropriate evaluation of the Galerkin integral of retarded potentials in Chapter 4. Note only, that the second approach is not easily generalized to retarded potentials as the use of relative coordinates also changes the usually complicated domains of integration. Moreover, as we will see in this chapter, the retarded potentials evaluated for piecewise continuous basis functions in space and time possess some additional anisotropic singularities in higher order derivatives.

We analyze the regularity of retarded potentials in terms of countably normed spaces. We show, that the potential itself is continuous and that, additionally to the classical corner/edge singularities in the first derivatives, we observe

what we call *geometrical light cone singularities* in the second derivatives. These geometrical singularities are due to the intersection of the discrete trial element with the discrete light cone integration domain. We apply these results in Chapter 4 in order to construct an accurate quadrature scheme for the Galerkin elements involved.

Note that a triangulation of the surface Γ into planar subelements planar elements enforces the evaluation of the trial function φ restricted to an element T and the discretization in time induces the integration domains E_l as defined in (2.22). Some authors rather use global basis functions [55] or B-Splines [46] in time, but so far they are only considered for collocation methods.

In Chapter 2.3 we have defined a typical Galerkin entry occurring in the discrete space-time variational formulation of retarded boundary integral equations.

Let T denote an arbitrary triangle using the notation as sketched in Fig. 3.3(b). Identify now the usually time dependent radii of the integration domain of the retarded potential with $r_{\min} := t_l$ and $r_{\max} := t_{l+1}$. Then the domain of influence of point x equals $E(x) = B_{r_{\max}}(x) \setminus B_{r_{\min}}(x)$, with $0 \leq r_{\min} < r_{\max} < \infty$ and the domain of integration of a discrete retarded boundary integral is the triangle T illuminated by $E(x)$, thus

$$T \cap E(x) = T \cap (B_{r_{\max}}(x) \setminus B_{r_{\min}}(x)) = (T \cap B_{r_{\max}}(x)) \setminus (T \cap B_{r_{\min}}(x)).$$

Using the linearity of the integral, a discrete retarded boundary integral or retarded potential can be expanded to

$$(P\varphi)(x) = \int_{T \cap B_{r_{\max}}(x)} k(x-y)\varphi(y) ds_y - \int_{T \cap B_{r_{\min}}(x)} k(x-y)\varphi(y) ds_y, \quad (3.1)$$

where $\varphi \in L^\infty(T)$ and $k(x-y)$ is a Cauchy singular kernel, i.e. the Cauchy principal value of integral (3.1) exists and is $\text{Hi}_\zeta \frac{1}{2}$ lder continuous in a neighborhood of x , compare Definition 5.1.7 in [48].

Without loss of generality, we study

$$(P_R\varphi)(x) := \int_{T \cap B_R(x)} k(x-y)\varphi(y) dy. \quad (3.2)$$

for $x \in \mathbb{R}^3$ and $R \geq 0$.

3.1 Geometrical Description of the Domains of Influence $E(x)$ and $E_R(T)$

Throughout this chapter, we fix the notation of a triangle T as sketched in Fig. 3.3(b). Denote the vertices of the triangle by p_i , the edges by e_i and the planar edge normals n_i ($i = 1, 2, 3$). The triangle plane is defined by

$$\mathcal{E}_T := \{y \in \mathbb{R}^3 : (p - y, n_T) = 0\},$$

for $p \in T$, where n_T denotes the triangle normal.

The function $(P_R\varphi)(x)$ vanishes, if the intersection $T \cap B_R(x)$ is empty, i.e. if $\text{dist}(x, T) > R$. The sphere $B_R(x)$ intersects a triangle vertex p_i only if $x \in B_R(p_i)$. A triangle edge e_i with end points p_j ($j \in \{1, 2, 3\} \setminus \{i\}$) is intersected by $B_R(x)$, if

$$x \in \bigcup_{j \neq i} B_R(p_j) \cup \mathcal{C}_R(e_i),$$

where $\mathcal{C}_R(e_i)$ denotes a circular cylinder with axis e_i and radius R .

The triangle interior is intersected by $B_R(x)$ if $x \in \mathcal{P}_R(T) \cup \bigcup_i (B_R(p_i) \cup \mathcal{C}_R(e_i))$, where the triangular prism $\mathcal{P}_R(T)$ is defined via

$$\mathcal{P}_R(T) := \{y \in \mathbb{R}^3 : y = y_T + \gamma n_T, \text{ where } y_T \in T, \gamma \in (-R, R)\}.$$

Thus, the support of $(P_R\varphi)(x)$ is

$$E_R(T) := \text{supp}(P_R\varphi) = \mathcal{P}_R(T) \cup \bigcup_{i=1}^3 (B_R(p_i) \cup \mathcal{C}_R(e_i)). \quad (3.3)$$

Remark 3.1. The above described geometrical object is also known as trianguloid and can be written as the Minkowski sum of a sphere $B_R(0)$ and a triangle T , i.e. $T + B_R(0) := \{a + b : a \in T, b \in B_R(0)\}$. Especially in computer graphics domains like this are studied in the context of convolution surfaces [8] or sphere-swept volumes. We will refer to $E_R(T)$ as the domain of influence of element T . A sketch of $E_R(T)$ may be found in Fig. 3.2.

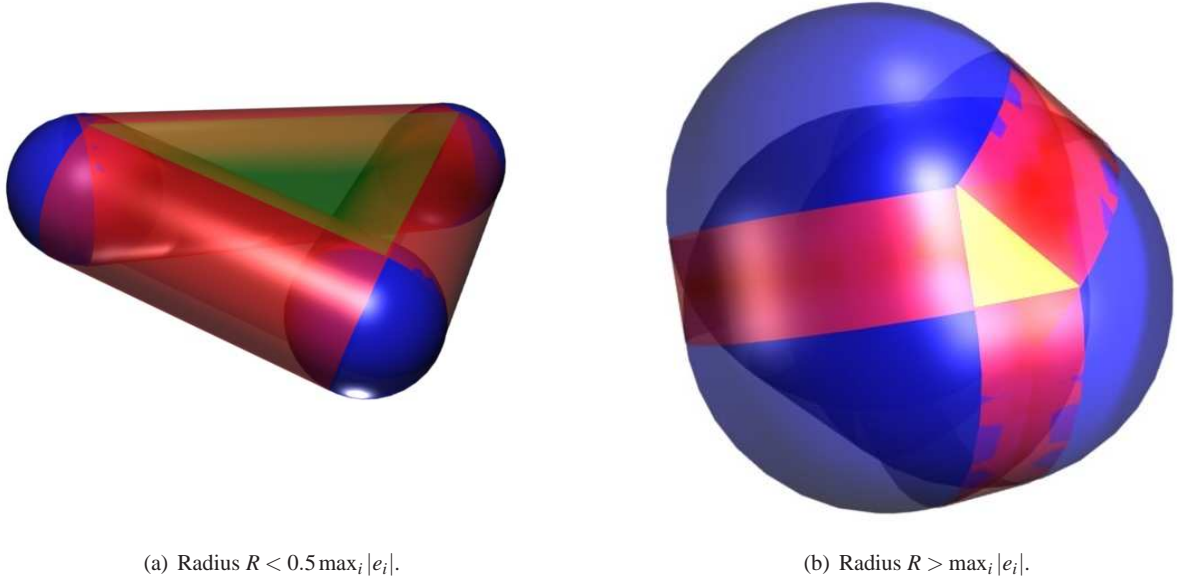


Fig. 3.2 Three-dimensional plot of the domain of influence $E_R(T)$.

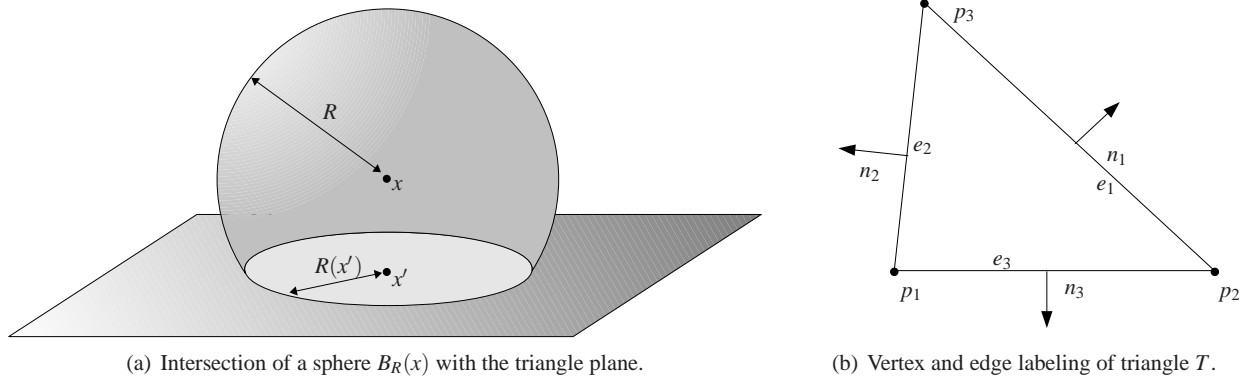


Fig. 3.3

3.2 Regularity of Retarded Boundary Integrals

In the following lemma we explicitly compute the gradient of the discrete retarded potential (3.2). We decompose the integral into integrals over the triangle edges, circle segments and the original integration domain. Within the proof we use a direct functional representation of the indicator functions of the intersecting domains via one-dimensional Heaviside functions H .

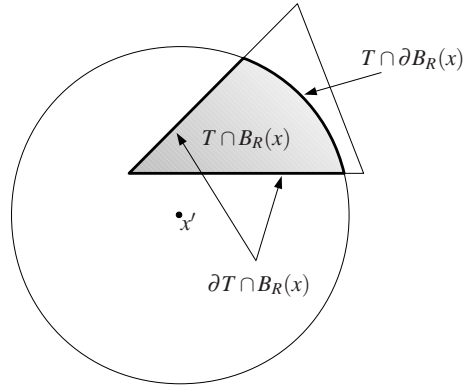


Fig. 3.4 Decomposition of the domain of integration.

Lemma 3.2. Given a triangle T with vertices p_i and edges e_i with corresponding outer normals n_i ($i = 1, 2, 3$) as sketched in Fig. 3.3(b). n_T denotes the triangle normal. The orthogonal projection of $x \in \mathbb{R}^3$ onto the triangle plane \mathcal{E}_T is given by $x' = x + (p - x, n_T)n_T$, where $p \in \mathcal{E}_T$. For $\varphi \in C^1(T) \cap L^\infty(T)$ and $x \in E_R(T)$ it holds

$$\begin{aligned} \nabla(P_R\varphi)(x) &= n_T \frac{(x - p, n_T)}{R'(x)} \int_{T \cap \partial B_R(x)} k(x - y)\varphi(y) ds_y - \sum_{i=1}^3 n_i \int_{e_i \cap B_R(x)} k(x - y)\varphi(y) ds_y \\ &+ \int_{T \cap B_R(x)} k(x - y)\nabla\varphi(y) ds_y, \end{aligned} \quad (3.4)$$

where $R'(x) = (R^2 - (p - x, n_T)^2)^{1/2}$ and $\nabla(P_R\varphi) = 0$ for $x \notin E_R(T)$.

Before we continue with the proof of the above lemma, let us consider its impact on the following analysis. In Chapter 3.2.1 we study the integrals in the sum of the second term in (3.4) and define

$$(I_{e_i}\varphi)(x) := \int_{e_i \cap B_R(x)} k(x - y)\varphi(y) ds_y. \quad (3.5)$$

We will prove, that this function is continuous in \mathbb{R}^3 , but exhibits anisotropic singularities in its first derivatives, which results in anisotropic singularities in the second derivatives of (3.2). In Chapter 3.2.2 we will study the first term in (3.4) and therefore introduce

$$(I_T\varphi)(x) := \frac{(x - p, n_T)}{R'(x)} \int_{T \cap \partial B_R(x)} k(x - y)\varphi(y) ds_y. \quad (3.6)$$

We will see, that this function possesses jumps parallel to the triangle plane, i.e. the discrete potential (3.2) exhibits a jump in its first derivatives.

Proof (of Lemma 3.2). For $x \notin E_R(T)$ $(P_R\varphi)$ vanishes and thus do its higher derivatives. Let $x \in E_R(T)$, then we rewrite the potential (3.2) using indicator functions and $B_R(x) \cap \mathcal{E}_T = B_{R'}(x') \cap \mathcal{E}_T$ (cf. Fig. 3.3(a)) and for $y \in \mathcal{E}_T$ it holds $\chi_{B_R(x)}(y) = \chi_{B_{R'}(x')}(y) = H(R'(x) - |y - x'|)$.

Denote by p'_i the projection of p_i onto the line through the edge e_i . Given a plane with normal n_i and point p'_i , the indicator function of the left half space can be represented by $H(-n_i(y - p'_i))$. Now a triangle is the intersection of the three left half spaces corresponding to the edges of the triangle intersected with the triangle plane \mathcal{E}_T , such that

$$\chi_T(y) = \chi_{\mathcal{E}_T}(y) \prod_{i=1}^3 H(-n_i(y - p'_i)),$$

which then yields

$$\begin{aligned}
(P_R\varphi)(x) &= \int_{\mathbb{R}^3} \chi_{B_R(x)}(y) \chi_T(y) k(x-y) \varphi(y) dy \\
&= \int_{\mathbb{R}^3} \underbrace{\chi_{B_R(x)}(y) \chi_{\mathcal{E}_T}(y)}_{=\chi_{B_{R'}(x')}(y) \chi_{\mathcal{E}_T}(y)} \prod_{i=1}^3 H(-n_i(y-p'_i)) k(x-y) \varphi(y) dy \\
&= \int_{\mathcal{E}_T} H(R'(x) - |y-x'|) \prod_{i=1}^3 H(-n_i(y-p'_i)) k(x-y) \varphi(y) dy.
\end{aligned}$$

Thus

$$\nabla(P_R\varphi)(x) = \int_{\mathcal{E}_T} \nabla_x [H(R'(x) - |y-x'|) k(x-y)] \varphi(y) \prod_{i=1}^3 H(-n_i(y-p'_i)) dy.$$

One easily verifies

$$\begin{aligned}
\nabla_x(y, x') &= \nabla_x [(y, x) + (p-x, n_T)(y, n_T)] = y - (y, n_T) n_T, \\
\nabla_x(x', x') &= \nabla_x [(x, x) + 2(p-x, n_T)(x, n_T) + (p-x, n_T)^2] = 2(x - (x, n_T) n_T),
\end{aligned}$$

such that as $y \in \mathcal{E}_T$

$$\nabla_x |y-x'| = -\frac{1}{|y-x'|} (y-x - (y-x, n_T) n_T) = -\frac{y-x'}{|y-x'|}.$$

We can compute

$$\begin{aligned}
\nabla_x H(R'(x) - |y-x'|) &= \delta(R'(x) - |y-x'|) \left(\frac{(p-x, n_T)}{R'(x)} n_T + \frac{y-x'}{|y-x'|} \right) \\
&= \delta(R'(x) - |y-x'|) \frac{(p-x, n_T)}{R'(x)} n_T - \nabla_y H(R'(x) - |y-x'|).
\end{aligned}$$

Moreover, $\nabla_x k(x-y) = -\nabla_y k(x-y)$ and thus using the product rule

$$\begin{aligned}
\nabla_x [H(R'(x) - |y-x'|) k(x-y)] &= \delta(R'(x) - |y-x'|) \frac{(p-x, n_T)}{R'(x)} n_T k(x-y) \\
&\quad - \nabla_y [H(R'(x) - |y-x'|) k(x-y)].
\end{aligned}$$

Now, we have

$$\begin{aligned}
\nabla(P_R\varphi)(x) &= \frac{(p-x, n_T)}{R'(x)} n_T \int_{\mathcal{E}_T} \delta(R'(x) - |y-x'|) \prod_{i=1}^3 H(-n_i(y-p'_i)) k(x-y) \varphi(y) dy \\
&\quad - \int_{\mathcal{E}_T} \nabla_y [H(R'(x) - |y-x'|) k(x-y)] \prod_{i=1}^3 H(-n_i(y-p'_i)) \varphi(y) dy.
\end{aligned} \tag{3.7}$$

We apply the product rule $(\nabla_y f)g = \nabla_y(f \cdot g) - f \nabla_y g$ for $f(x, y) = H(R'(x) - |y-x'|) k(x-y)$ and $g(x, y) = \prod_{i=1}^3 H(-n_i(y-p'_i)) \varphi(y)$. Now, since g has bounded support, we can rewrite the second term in (3.7) using that $\int_{\mathcal{E}_T} \nabla_y(f \cdot g) dy$ vanishes. Note that we evaluate the integrals in the sense of distributions.

We compute explicitly

$$\begin{aligned} \nabla_y \left[\prod_{i=1}^3 H(-n_i(y-p'_i)) \varphi(y) \right] &= - \sum_{i=1}^3 n_i \delta(-n_i(y-p'_i)) \prod_{j \neq i} H(-n_j(y-p'_j)) \varphi(y) \\ &\quad + \prod_{i=1}^3 H(-n_i(y-p'_i)) \nabla_y \varphi(y). \end{aligned}$$

As mentioned earlier in this proof for $y \in \mathcal{E}_T$ it holds $\chi_{B_R(x)}(y) = \chi_{B_{R'}(x')}(y) = H(R'(x) - |y - x'|)$ and $\chi_{e_i}(y) = \delta(-n_i(y-p'_i)) \prod_{j \neq i} H(-n_j(y-p'_j))$. Thus the second term in (3.7) reduces to

$$- \sum_{i=1}^3 n_i \int_{e_i \cap B_R(x)} k(x-y) \varphi(y) ds_y + \int_{T \cap B_R(x)} k(x-y) \nabla_y \varphi(y) ds_y.$$

Rewriting for $x \in \mathcal{E}_T$

$$\delta(R'(x) - |y - x'|) \prod_{i=1}^3 H(-n_i(y-p'_i)) = \delta(R - |y - x|) \prod_{i=1}^3 H(-n_i(y-p'_i)) = \chi_{T \cap \partial B_R(x)}(y),$$

the first term in (3.7) reduces to

$$\frac{(p-x, n_T)}{R'(x)} n_T \int_{T \cap \partial B_R(x)} k(x-y) \varphi(y) ds_y,$$

which yields the assertion. \square

Remark 3.3. A generalization to quadrilateral elements is straight forward, as we only have to regard one additional edge. Thus the support of the corresponding potential is the sphere-swept volume of a quadrilateral (compare Remark 3.1) and the below discussed singularities have one additional contribution to the edge based singularities.

Using Lemma 3.2 we can show recursively

Theorem 3.4. *For $\varphi \in C^{|\alpha|}(\mathbb{R}^3)$ there holds*

$$\begin{aligned} D^\alpha(P_R \varphi)(x) &= n_T \cdot \left(\sum_{l=1}^{\alpha_1} \partial_1^{\alpha_1-l} (I_T \partial_1^{l-1} \partial_2^{\alpha_2} \partial_3^{\alpha_3} \varphi)(x) \right) - \sum_{i=1}^3 n_i \cdot \left(\sum_{l=1}^{\alpha_1} \partial_1^{\alpha_1-l} (I_{e_i} \partial_1^{l-1} \partial_2^{\alpha_2} \partial_3^{\alpha_3} \varphi)(x) \right) \\ &\quad - \sum_{l=1}^{\alpha_2} \partial_1^{\alpha_1} \partial_2^{\alpha_2-l} (I_T \partial_2^{l-1} \partial_3^{\alpha_3} \varphi)(x) - \sum_{l=1}^{\alpha_3} \partial_1^{\alpha_1} \partial_2^{\alpha_2} \partial_3^{\alpha_3-l} (I_T \partial_3^{l-1} \varphi)(x) \\ &\quad + (P_R(D^\alpha \varphi))(x), \end{aligned}$$

where the operators $I_{e_i} \varphi$ and $I_T \varphi$ are defined in (3.5) and (3.6), respectively.

Proof. Show first by induction for $n \in \mathbb{N}$

$$\begin{aligned} \partial_j^n (P_R \varphi)(x) &= (n_T)_j \sum_{l=1}^n \partial_j^{n-l} (I_T \partial_j^{l-1} \varphi)(x) - \sum_{i=1}^3 (n_i)_j \sum_{l=1}^n \partial_j^{n-l} (I_{e_i} \partial_j^{l-1} \varphi)(x) \\ &\quad + \int_{T \cap B_R(x)} k(x-y) \partial_j^n \varphi(y) ds_y. \end{aligned} \tag{3.8}$$

For $n = 0$ the first two terms vanish and only the function $(P_R \varphi)(x)$ remains. For $n = 1$ the result follows directly from Lemma 3.2 and finally for $n + 1$ we conclude with (3.8) by applying Lemma 3.2 to its last term

$$\begin{aligned}
\partial_j^{n+1}(P_R\varphi)(x) &= \partial_j(\partial_j^n(P_R\varphi)(x)) \\
&= (n_T)_j \sum_{l=1}^n \partial_j^{n+1-l}(I_T \partial_j^{l-1}\varphi)(x) - \sum_{i=1}^3 (n_i)_j \sum_{l=1}^n \partial_j^{n+1-l}(I_{e_i} \partial_j^{l-1}\varphi)(x) \\
&\quad + (n_T)_j (I_T \partial_j^n \varphi)(x) - \sum_{i=1}^3 (n_i)_j (I_{e_i} \partial_j^n \varphi)(x) + \int_{T \cap B_R(x)} k(x-y) \partial_j^{n+1} \varphi(y) ds_y \\
&= (n_T)_j \sum_{l=1}^{n+1} \partial_j^{n+1-l}(I_T \partial_j^{l-1}\varphi)(x) - \sum_{i=1}^3 (n_i)_j \sum_{l=1}^{n+1} \partial_j^{n+1-l}(I_{e_i} \partial_j^{l-1}\varphi)(x) \\
&\quad + \int_{T \cap B_R(x)} k(x-y) \partial_j^{n+1} \varphi(y) ds_y.
\end{aligned}$$

If we now successively apply (3.8), there directly follows

$$\begin{aligned}
D^\alpha(P_R\varphi)(x) &= \partial_1^{\alpha_1} \partial_2^{\alpha_2} \partial_3^{\alpha_3}(P_R\varphi)(x) \\
&= \partial_1^{\alpha_1} \partial_2^{\alpha_2} \left((n_T)_3 \sum_{l=1}^{\alpha_3} \partial_3^{\alpha_3-l}(I_T \partial_3^{l-1}\varphi)(x) - \sum_{i=1}^3 (n_i)_3 \sum_{l=1}^{\alpha_3} \partial_3^{\alpha_3-l}(I_{e_i} \partial_3^{l-1}\varphi)(x) \right. \\
&\quad \left. + \int_{T \cap B_R(x)} k(x-y) \partial_3^{\alpha_3} \varphi(y) ds_y \right) \\
&= (n_T)_3 \sum_{l=1}^{\alpha_3} \partial_1^{\alpha_1} \partial_2^{\alpha_2} \partial_3^{\alpha_3-l}(I_T \partial_3^{l-1}\varphi)(x) - \sum_{i=1}^3 (n_i)_3 \sum_{l=1}^{\alpha_3} \partial_1^{\alpha_1} \partial_2^{\alpha_2} \partial_3^{\alpha_3-l}(I_{e_i} \partial_3^{l-1}\varphi)(x) \\
&\quad + \partial_1^{\alpha_1} \left((n_T)_2 \sum_{l=1}^{\alpha_2} \partial_2^{\alpha_2-l}(I_T \partial_2^{l-1} \partial_3^{\alpha_3} \varphi)(x) - \sum_{i=1}^3 (n_i)_2 \sum_{l=1}^{\alpha_2} \partial_2^{\alpha_2-l}(I_{e_i} \partial_2^{l-1} \partial_3^{\alpha_3} \varphi)(x) \right. \\
&\quad \left. + \int_{T \cap B_R(x)} k(x-y) \partial_2^{\alpha_2} \partial_3^{\alpha_3} \varphi(y) ds_y \right) \\
&= (n_T)_3 \sum_{l=1}^{\alpha_3} \partial_1^{\alpha_1} \partial_2^{\alpha_2} \partial_3^{\alpha_3-l}(I_T \partial_3^{l-1}\varphi)(x) - \sum_{i=1}^3 (n_i)_3 \sum_{l=1}^{\alpha_3} \partial_1^{\alpha_1} \partial_2^{\alpha_2} \partial_3^{\alpha_3-l}(I_{e_i} \partial_3^{l-1}\varphi)(x) \\
&\quad + (n_T)_2 \sum_{l=1}^{\alpha_2} \partial_1^{\alpha_1} \partial_2^{\alpha_2-l}(I_T \partial_2^{l-1} \partial_3^{\alpha_3} \varphi)(x) - \sum_{i=1}^3 (n_i)_2 \sum_{l=1}^{\alpha_2} \partial_1^{\alpha_1} \partial_2^{\alpha_2-l}(I_{e_i} \partial_2^{l-1} \partial_3^{\alpha_3} \varphi)(x) \\
&\quad + (n_T)_1 \sum_{l=1}^{\alpha_1} \partial_1^{\alpha_1-l}(I_T \partial_1^{l-1} \partial_2^{\alpha_2} \partial_3^{\alpha_3} \varphi)(x) - \sum_{i=1}^3 (n_i)_1 \sum_{l=1}^{\alpha_1} \partial_1^{\alpha_1-l}(I_{e_i} \partial_1^{l-1} \partial_2^{\alpha_2} \partial_3^{\alpha_3} \varphi)(x) \\
&\quad + \int_{T \cap B_R(x)} k(x-y) \partial_1^{\alpha_1} \partial_2^{\alpha_2} \partial_3^{\alpha_3} \varphi(y) ds_y.
\end{aligned}$$

□

3.2.1 Analysis of the Edge Integral $I_{e_i}\varphi$

In this section we study the function (3.5). We restrict the analysis to kernels of the form $k_\nu(x-y) = |x-y|^\nu$ with $\nu \geq -1$ and define

$$(I_{e_i}^\nu \varphi)(x) := \int_{e_i \cap B_R(x)} k_\nu(x-y) \varphi(y) ds_y.$$

The support of (3.5) is given by

$$C_R(e_i) := \mathcal{C}_R(e_i) \cup \bigcup_{j \neq i} B_R(p_j). \quad (3.9)$$

Note, that $C_R(e_i)$ is a subset of $E_R(T)$. We sketched some interesting cases in Fig. 3.5.

First, we map the edge e_i of the triangle to a reference edge e of length one, i.e. by translating, rotating and scaling the original edge e_i . This reference situation shall be studied in detail, in order to analyze the edge based integrals as derived in Lemma 3.2 in detail. In the following, we denote by e the reference edge with end points $m_1 := (0, 0, 0)^T$ and $m_2 := (0, 1, 0)^T$. Let \hat{e} denote an arbitrary edge of an triangle with end points \hat{m}_1 and \hat{m}_2 and an edge normal $n_{\hat{e}}$ lying in the triangle plane.

Lemma 3.5. *Given an arbitrary edge \hat{e} of the triangle T with end points \hat{m}_1 and \hat{m}_2 and the unit triangle normal n_T . Let $\varphi \in L^\infty(\hat{e})$ and $\hat{R} \in \mathbb{R}$. Then there exists a scaled rotation including a translation $\mathcal{F} : \mathbb{R}^3 \mapsto \mathbb{R}^3$ with $\mathcal{F}(e) = \hat{e}$ such that*

$$(I_{\hat{e}}^v \varphi)(\hat{x}) = |\hat{e}|^{v+1} \int_{e \cap B_R(x)} k_v(x-y) \tilde{\varphi}(y) ds_y,$$

where $R = |\hat{e}|^{-1} \hat{R}$, $y = \mathcal{F}^{-1}(\hat{y})$, $x = \mathcal{F}^{-1}(\hat{x})$, $\tilde{\varphi}(y) = (\varphi \circ \mathcal{F})(y)$ and $k_v(x-y) = |x-y|^v$ with $v \geq -1$.

Proof. Define the affine transformation, such that $\mathcal{F}(e) = \hat{e}$. We consider the basis

$$\langle (1, 0, 0)^T, (0, 1, 0)^T, (0, 0, 1)^T \rangle$$

in the reference situation. With $d_{\hat{e}} := \hat{m}_2 - \hat{m}_1$ we define the basis $\langle n_{\hat{e}}, d_{\hat{e}}/|\hat{e}|, n_T \rangle$ where $n_{\hat{e}} = |\hat{e}|^{-1}(d_{\hat{e}} \times n_T)$ corresponds to the planar normal of the triangle edge. Thus, we can define the mapping by

$$\mathcal{F}(x) = Ax + \hat{m}_1 = \hat{x},$$

where the transformation matrix is $A := (|\hat{e}|n_{\hat{e}}, d_{\hat{e}}, |\hat{e}|n_T)$. Moreover it holds

$$\mathcal{F}^{-1}(\hat{e} \cap B_{\hat{R}}(\hat{x})) = \mathcal{F}^{-1}(\hat{e}) \cap \mathcal{F}^{-1}(B_{\hat{R}}(\hat{x})) = e \cap B_R(\mathcal{F}^{-1}(\hat{x})).$$

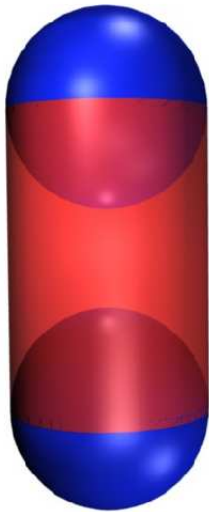
Thus, we can substitute

$$\begin{aligned} (I_{\hat{e}}^v \varphi)(\hat{x}) &= \int_{\mathcal{F}^{-1}(\hat{e} \cap B_{\hat{R}}(\hat{x}))} k_v(\mathcal{F}(x) - \mathcal{F}(y)) \varphi(\mathcal{F}(y)) |\det(A)| ds_y \\ &= |\det(A)| \int_{e \cap B_R(x)} k_v(A(x-y)) \varphi(\mathcal{F}(y)) ds_y \\ &= |\det(A)| |\hat{e}|^v \int_{e \cap B_R(x)} k_v(x-y) \varphi(\mathcal{F}(y)) ds_y \\ &= |\hat{e}|^{v+1} \int_{e \cap B_R(x)} k_v(x-y) \varphi(\mathcal{F}(y)) ds_y. \end{aligned}$$

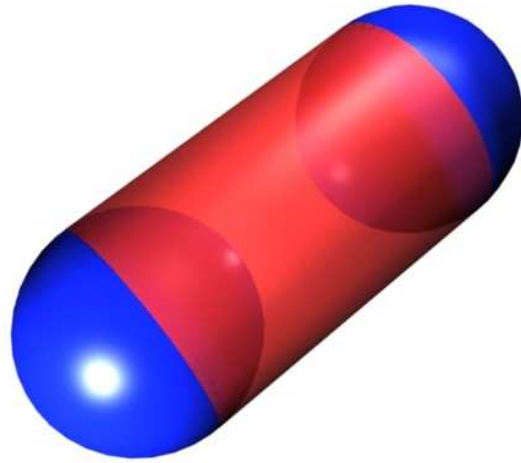
In the last steps we used $|A(x-y)| = |\hat{e}||x-y|$ and $\det(A) = |\hat{e}|$ as A is a rotation matrix scaled with $|\hat{e}|$. \square

In the following we will analyze the reference edge function defined by

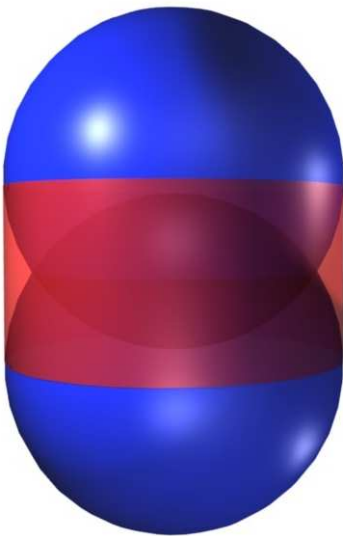
$$(I^v \varphi)(x) := \int_{e \cap B_R(x)} k_v(x-y) \varphi(y) ds_y. \quad (3.10)$$



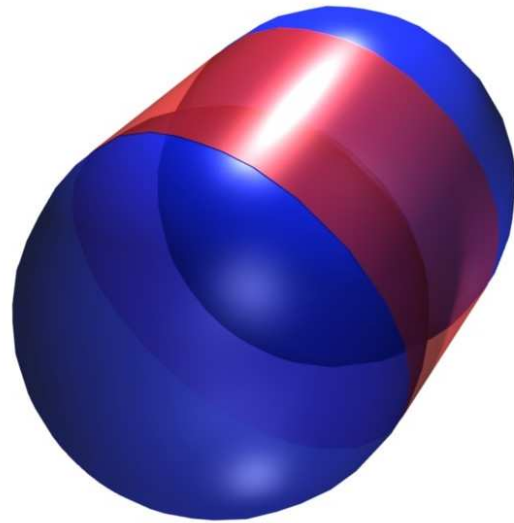
(a) $|e| > 2R$.



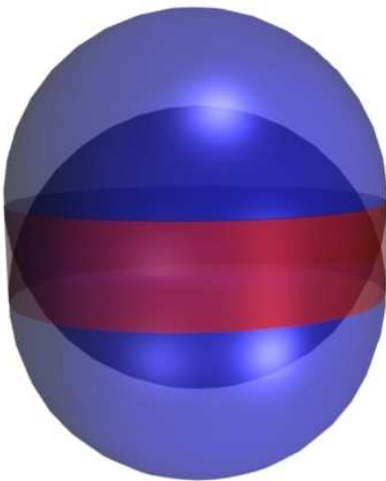
(b) $|e| > 2R$.



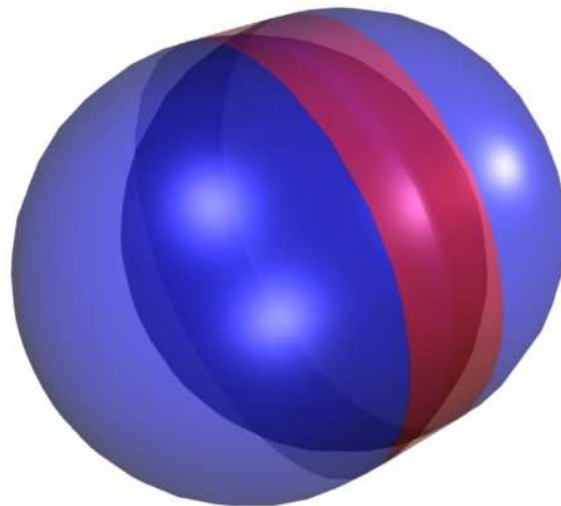
(c) $2R > |e| > R$.



(d) $2R > |e| > R$.



(e) $|e| < R$.



(f) $|e| < R$.

Fig. 3.5 Three-dimensional visualization of $C_R(e)$.

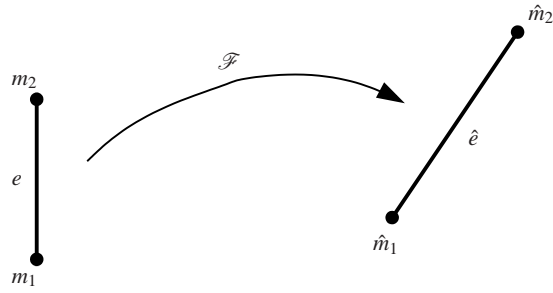


Fig. 3.6 Mapping of reference edge e to edge \hat{e} .

Let us first study the intersection of the sphere $B_R(x)$ and the edge e . The different types of intersection define a natural decomposition of $C_R(e)$. In Fig. 3.5 several three-dimensional visualizations of this partition are plotted. In Fig. 3.8(a) and 3.8(b) the below introduced decomposition of \mathbb{R}^3 is sketched in the triangle plane.

Lemma 3.6. *Let $x \in \mathbb{R}^3$. There exists a decomposition of \mathbb{R}^3 in at most five disjoint subsets given by*

$$\begin{aligned}
 S_1 &:= B_R(m_1) \setminus \overline{B_R(m_2)}, \\
 S_2 &:= B_R(m_2) \setminus \overline{B_R(m_1)}, \\
 S_3 &:= B_R(m_1) \cap B_R(m_2), \\
 S_4 &:= C_R(e) \setminus (\overline{B_R(m_1)} \cup \overline{B_R(m_2)}), \\
 S_5 &:= \mathbb{R}^3 \setminus (\overline{S_1} \cup \overline{S_2} \cup \overline{S_3} \cup \overline{S_4})
 \end{aligned} \tag{3.11}$$

and we can compute explicitly

$$e \cap B_R(x) = \begin{cases} \left\{ y \in \mathbb{R}^3 : y = m_1 + \gamma(x_s^{(2)} - m_1); \gamma \in [0, 1] \right\} & x \in S_1 \\ \left\{ y \in \mathbb{R}^3 : y = x_s^{(1)} + \gamma(m_2 - x_s^{(1)}); \gamma \in [0, 1] \right\} & x \in S_2 \\ e & x \in S_3 \\ \left\{ y \in \mathbb{R}^3 : y = x_s^{(1)} + \gamma(x_s^{(2)} - x_s^{(1)}); \gamma \in [0, 1] \right\} & x \in S_4 \\ \emptyset & x \in S_5, \end{cases}$$

where $x_s^{(1)}$ and $x_s^{(2)}$ denote the intersection points of the sphere $B_R(x)$ and the edge e given by

$$x_s^{(1)} := \left(0, x_2 - \sqrt{R^2 - x_1^2 - x_3^2}, 0 \right)^T \quad \text{and} \quad x_s^{(2)} := \left(0, x_2 + \sqrt{R^2 - x_1^2 - x_3^2}, 0 \right)^T.$$

Proof. The intersection of a sphere and an edge in the (x_1, x_2) -plane can be rewritten as the intersection of the edge and the circle corresponding to the intersection of the sphere and the (x_1, x_2) -plane. Thus using the notation introduced in Lemma 3.2 we can write $e \cap B_R(x) = e \cap B_{R'}(x')$, where $x' = (x_1, x_2, 0)^T$ and $R'(x) = (R^2 - x_3^2)^{1/2}$. The intersection $e \cap B_{R'}(x')$ where $e : x = \gamma(0, 1, 0)^T$ with $\gamma \in [0, 1]$ results in the following equation

$$x_1^2 + (x_2 - \gamma)^2 + x_3^2 = R^2,$$

with roots $\gamma_{1,2} = x_2 \pm \sqrt{R^2 - x_1^2 - x_3^2}$. A case distinction yields the subdomains S_i with $i = 1, \dots, 5$. \square

Remark 3.7. a) Note that, $S_3 = \emptyset$ if $R \leq \frac{1}{2}$.

b) In Fig. 3.7 a sketch of the geometrical intersection cases is given. For $x \in S_1$ or $x \in S_2$ the edge is intersected once and twice for $x \in S_4$. For $x \in S_3$ the whole edge e is illuminated, i.e. the edge lies in the sphere $B_R(x)$ and for $x \in S_5$ the intersection is the empty set.

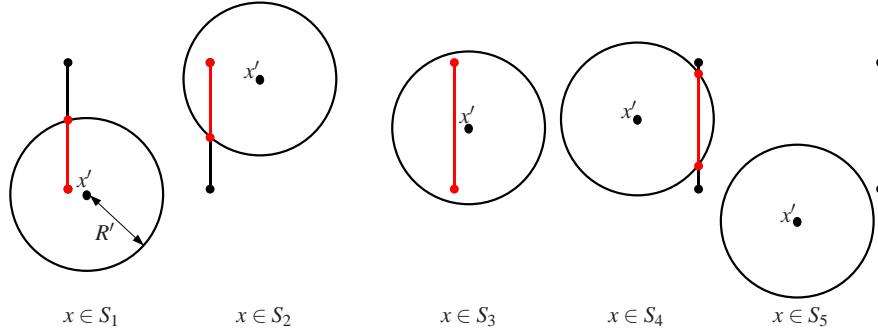


Fig. 3.7 Five different cases for the intersection of $B_{R'}(x')$ and e .

Lemma 3.6 verifies, that the support of $(I_e^V \varphi)(x)$ is a so-called capsule, a sphere-swept volume of a segment as sketched in Fig. 3.5. This support $C_R(e)$ is a composition of the spheres $B_R(m_1)$ and $B_R(m_2)$ and the cylinder $\mathcal{C}_R(e)$ with radius R and axis e .

The following analysis shows, that the reference edge function (3.10) has anisotropic singularities in its gradient. The position of these singularities is determined on the boundaries of the subdomains S_i as defined in (3.11), i.e. the surface of the spheres $\partial B_R(m_i)$ ($i = 1, 2$), corresponding to the dashed blue circles in Fig. 3.8 and the surface of the cylinder $\mathcal{C}_R(e)$ (without the caps) indicated by the red lines and denoted by Γ_{45} .

The boundaries Γ_{ij} are defined as interfaces between the domains S_i and S_j , where $i < j$. The following boundaries are of special interest, see also Fig. 3.8(c).

1. Case $S_3 = \emptyset$.

$$\begin{aligned} \bar{S}_1 \cap \bar{S}_4 &= \Gamma_{14} & \bar{S}_2 \cap \bar{S}_4 &= \Gamma_{24} \\ \bar{S}_1 \cap \bar{S}_5 &= \Gamma_{15} & \bar{S}_2 \cap \bar{S}_5 &= \Gamma_{25} & \bar{S}_4 \cap \bar{S}_5 &= \Gamma_{45} \end{aligned}$$

2. Case $S_3 \neq \emptyset$.

$$\begin{aligned} \bar{S}_1 \cap \bar{S}_2 &= \Gamma_{12} = \Gamma_c \\ \bar{S}_1 \cap \bar{S}_3 &= \Gamma_{13} & \bar{S}_2 \cap \bar{S}_3 &= \Gamma_{23} \\ \bar{S}_1 \cap \bar{S}_4 &= \Gamma_{14} & \bar{S}_2 \cap \bar{S}_4 &= \Gamma_{24} & \bar{S}_3 \cap \bar{S}_4 &= \Gamma_{34} = \Gamma_c \\ \bar{S}_1 \cap \bar{S}_5 &= \Gamma_{15} & \bar{S}_2 \cap \bar{S}_5 &= \Gamma_{25} & \bar{S}_3 \cap \bar{S}_5 &= \emptyset & \bar{S}_4 \cap \bar{S}_5 &= \Gamma_{45} \end{aligned}$$

An explicit parameterization of the above defined boundaries, if not vanishing, is

$$\begin{aligned} \Gamma_c &:= \left\{ x \in \mathbb{R}^3 : x_2 = \frac{1}{2} \text{ and } x_1^2 + x_3^2 = R^2 - \frac{1}{4} \right\}, \\ \Gamma_{13} &:= \left\{ x \in \mathbb{R}^3 : x_2 = 1 - \sqrt{R^2 - x_1^2 - x_3^2} \text{ and } x_1^2 + x_3^2 \leq R^2 - \frac{1}{4} \right\}, \\ \Gamma_{14} &:= \left\{ x \in \mathbb{R}^3 : x_2 = \sqrt{R^2 - x_1^2 - x_3^2} \text{ and } \max\left(0, R^2 - \frac{1}{4}\right) \leq x_1^2 + x_3^2 \leq R^2 \right\}, \\ \Gamma_{15} &:= \left\{ x \in \mathbb{R}^3 : x_2 = -\sqrt{R^2 - x_1^2 - x_3^2} \text{ and } x_1^2 + x_3^2 \leq R^2 \right\}, \\ \Gamma_{23} &:= \left\{ x \in \mathbb{R}^3 : x_2 = \sqrt{R^2 - x_1^2 - x_3^2} \text{ and } x_1^2 + x_3^2 \leq R^2 - \frac{1}{4} \right\}, \\ \Gamma_{24} &:= \left\{ x \in \mathbb{R}^3 : x_2 = 1 - \sqrt{R^2 - x_1^2 - x_3^2} \text{ and } \max\left(0, R^2 - \frac{1}{4}\right) \leq x_1^2 + x_3^2 \leq R^2 \right\}, \\ \Gamma_{25} &:= \left\{ x \in \mathbb{R}^3 : x_2 = 1 + \sqrt{R^2 - x_1^2 - x_3^2} \text{ and } x_1^2 + x_3^2 \leq R^2 \right\}, \\ \Gamma_{45} &:= \left\{ x \in \mathbb{R}^3 : 0 \leq x_2 \leq 1 \text{ and } x_1^2 + x_3^2 = R^2 \right\}. \end{aligned} \tag{3.12}$$

Note that $\partial B_R(m_1) = \Gamma_{14} \cup \Gamma_{15} \cup \Gamma_{23}$, $\partial B_R(m_2) = \Gamma_{13} \cup \Gamma_{24} \cup \Gamma_{25}$ and $\partial \mathcal{C}_R(e) = \Gamma_{45}$. Moreover, we define the jump of a function f over a boundary Γ_{ij} by

$$[f]_{\Gamma_{ij}} := \lim_{\substack{x \in S_i \\ x \rightarrow \Gamma_{ij}}} f(x) - \lim_{\substack{x \in S_j \\ x \rightarrow \Gamma_{ij}}} f(x).$$

Whereas, if there is a singularity in a domain ε , we interpret the jump in the following way

$$[f]_{\Gamma_{ij}} := \lim_{\substack{x \in S_i \setminus \varepsilon \\ x \rightarrow \Gamma_{ij}}} f(x) - \lim_{\substack{x \in S_j \setminus \varepsilon \\ x \rightarrow \Gamma_{ij}}} f(x).$$

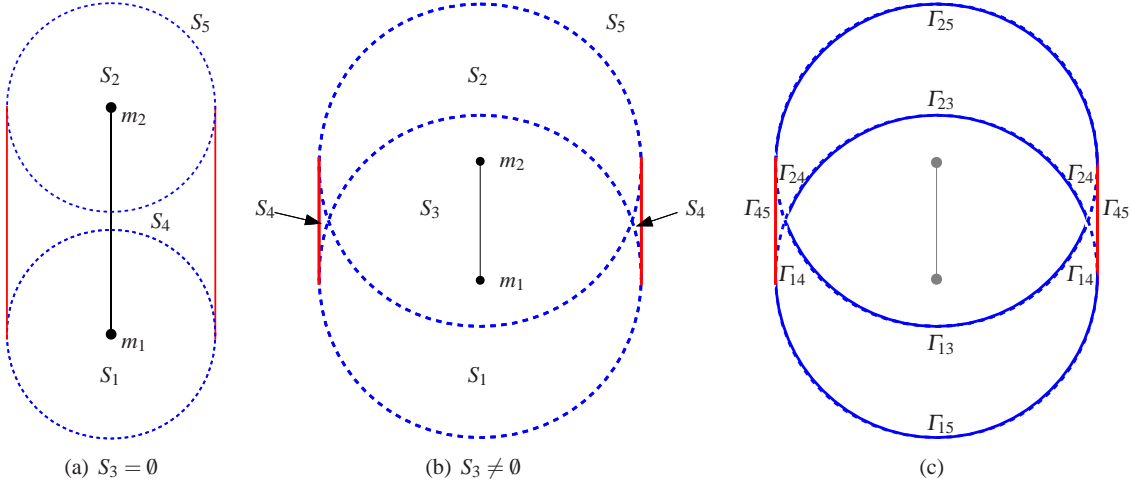


Fig. 3.8 Domain and boundary definitions on $C_R(e)$.

We define the jump of a function f on the surface of a sphere $B_R(m)$ by

$$[f]_{\partial B_R(m)} = \lim_{\substack{x \rightarrow \partial B_R(m) \\ x \in \mathbb{R}^3 \setminus \overline{B_R(m)}}} f - \lim_{\substack{x \rightarrow \partial B_R(m) \\ x \in B_R(m)}} f.$$

We observe different regularities of $(I_e^v \varphi)$ on the subdomains S_i .

Lemma 3.8. Given $k_v(x-y) := |x-y|^v$ for $v \in \mathbb{Z}$ with $v \geq -1$ and $\varphi \in L^\infty(e)$.

The first derivatives of $I_e^v \varphi$ possess anisotropic jumps on $\partial B_R(m_1)$, $\partial B_R(m_2)$ and a one sided pole on $\partial \mathcal{C}_R(e)$ without the caps. Perpendicular to the edge e there holds for $j = 1$ or $j = 3$

$$\begin{aligned} \left| [\partial_j (I_e^v \varphi)]_{\partial B_R(m_2)} \right| &= R^v |x_j| (R^2 - x_1^2 - x_3^2)^{-1/2} |\varphi(m_2)|, \\ \left| [\partial_j (I_e^v \varphi)]_{\partial B_R(m_1)} \right| &= R^v |x_j| (R^2 - x_1^2 - x_3^2)^{-1/2} |\varphi(m_1)|, \\ \left| [\partial_j (I_e^v \varphi)]_{\partial \mathcal{C}_R(e)} \right| &= 2R^v \lim_{x \rightarrow \partial \mathcal{C}_R(e)} \frac{|\varphi(0, x_2, 0)| |x_j|}{(R^2 - x_1^2 - x_3^2)^{1/2}}, \end{aligned}$$

and parallel to the edge the derivative with respect to x_2 exhibits a constant jump of size

$$\begin{aligned} \left| [\partial_2(I_e^v \varphi)]_{\partial B_R(m_2)} \right| &= R^v |\varphi(m_1)|, \\ \left| [\partial_2(I_e^v \varphi)]_{\partial B_R(m_1)} \right| &= R^v |\varphi(m_2)|, \\ \left| [\partial_2(I_e^v \varphi)]_{\partial \mathcal{C}_R(e)} \right| &= 0. \end{aligned}$$

$I_e^v \varphi$ has a singularity on the edge e for $v = -1$ and for $v \geq 0$ the integral is continuous.

Proof. Due to Lemma 3.6 $(I_e^v \varphi)$ vanishes in S_5 whereas in $C_R(e) = \bigcup_{i=1}^4 S_i$ it holds

$$(I_e^v \varphi)(x) = \int_{e \cap B_R(x)} k_v(x-y) \varphi(y) ds_y = \int_{a(x)}^{b(x)} k_v(x-y) \varphi(y) dy_2,$$

where $y_1 = y_3 = 0$ and

$$\begin{aligned} a(x) &= \begin{cases} 0 & x \in S_1 \cup S_3 \\ x_2 - \sqrt{R^2 - x_1^2 - x_3^2} & x \in S_2 \cup S_4, \end{cases} \\ b(x) &= \begin{cases} 1 & x \in S_2 \cup S_3 \\ x_2 + \sqrt{R^2 - x_1^2 - x_3^2} & x \in S_1 \cup S_4. \end{cases} \end{aligned}$$

Clearly, $a, b \in C^0(C_R(e))$ and on the boundary $\partial C_R(e) = \Gamma_{15} \cup \Gamma_{25} \cup \Gamma_{45}$ the domain of integration and thus the integral vanishes as

$$\lim_{x \rightarrow \partial C_R(e)} a(x) = \lim_{x \rightarrow \partial C_R(e)} b(x) \quad (x \in C_R(x)).$$

As the integration domain changes continuously in $C_R(e)$, $I_e^v \varphi$ is continuous for $v \geq 0$, whereas $I_e^v \varphi$ possesses a singularity on the edge for $v = -1$ which corresponds to the classical singularity.

Consider now $\nabla(I_e^v \varphi)$. Define $\mathbf{a} := (0, a(x), 0)^T$ and $\mathbf{b} := (0, b(x), 0)^T$ and compute

$$\nabla(I_e^v \varphi)(x) = (\nabla b(x)) k_v(x - \mathbf{b}) \varphi(\mathbf{b}) - (\nabla a(x)) k_v(x - \mathbf{a}) \varphi(\mathbf{a}) + \int_{a(x)}^{b(x)} \nabla_x k_v(x-y) \varphi(y) dy_2.$$

Here we use the similar structure of $\nabla a(x)$ and $\nabla b(x)$ and define the functions $g(x) := \sqrt{R^2 - x_1^2 - x_3^2}$ and

$$G(x) := \left(\frac{x_1}{\sqrt{R^2 - x_1^2 - x_3^2}}, 1, \frac{x_3}{\sqrt{R^2 - x_1^2 - x_3^2}} \right)^T = (\partial_1 g(x), 1, \partial_3 g(x))^T.$$

Then we obtain on the different subdomains

$$\begin{aligned} \partial_j(I_e^v \varphi)(x)|_{S_1} &= R^v (-1)^j G_j(x) \varphi(\mathbf{b}) + \int_0^{b(x)} \partial_{x_j} k_v(x-y) \varphi(y) dy_2, \\ \partial_j(I_e^v \varphi)(x)|_{S_2} &= -R^v G_j(x) \varphi(\mathbf{a}) + \int_{a(x)}^1 \partial_{x_j} k_v(x-y) \varphi(y) dy_2, \\ \nabla(I_e^v \varphi)(x)|_{S_3} &= \int_0^1 \nabla_x k_v(x-y) \varphi(y) dy_2, \\ \partial_j(I_e^v \varphi)(x)|_{S_4} &= R^v G_j(x) ((-1)^j \varphi(\mathbf{b}) - \varphi(\mathbf{a})) + \int_{a(x)}^{b(x)} \partial_{x_j} k_v(x-y) \varphi(y) dy_2, \\ \nabla(I_e^v \varphi)(x)|_{S_5} &= 0, \end{aligned} \tag{3.13}$$

with $k_v(x - \mathbf{a}) = k_v(x - \mathbf{b}) = R^v$ for all $x \in S_1 \cup S_2 \cup S_4$.

Again, we are interested in the continuity properties. G is continuous in $C_R(e)$, but one observes a singularity on Γ_{45} . Using a similar argumentation as for $I_e^v \varphi$, it follows, that $\partial_j(I_e^v \varphi)|_{S_i}$ is continuous (excluding the edge e) and vanishes on $\partial C_R(e)$. On $\Gamma \in \{\Gamma_c, \Gamma_{13}, \Gamma_{14}, \Gamma_{15}, \Gamma_{23}\}$ there holds

$$\lim_{x \rightarrow \Gamma} a(x) = 0,$$

and thus $\mathbf{a} = m_1$, whereas on Γ_{25} it holds $a(x) = 1$ thus $\mathbf{a} = m_2$. On $\Gamma \in \{\Gamma_c, \Gamma_{13}, \Gamma_{23}, \Gamma_{24}, \Gamma_{25}\}$ there holds

$$\lim_{x \rightarrow \Gamma} b(x) = 1,$$

therefore $\mathbf{b} = m_2$. For $x \in \Gamma_{15}$ we obtain $\mathbf{b} = m_1$ and on Γ_{45} it holds $a(x) = b(x) = x_2$. On Γ_{24} we have $a(x) = 2x_2 - 1$ and for $x \in \Gamma_{14}$ it yields $b(x) = 2x_2$. In (3.13) one observes, that in S_1, S_2 and S_4 we have an additional terms connected to G . Therefore, we have to analyze $G_j : C_R(e) \rightarrow \mathbb{R}$ for $j = 1, 3$ as defined above.

Using the boundary definition as given in (3.12) one concludes, that G_j is continuous on Γ_{13}, Γ_{23} . On the boundaries Γ_{14} and Γ_{15} we observe a pole of type $\lim_{\alpha \rightarrow R} (R^2 - \alpha^2)^{-1/2}$ on the circle given by $x_1^2 + x_3^2 = R^2$ and $x_2 = 0$. Similarly, on Γ_{24} and Γ_{25} we observe a pole of type $\lim_{\alpha \rightarrow R} (R^2 - \alpha^2)^{-1/2}$ on the circle given by $x_1^2 + x_3^2 = R^2$ and $x_2 = 1$. Whereas, on the whole boundary Γ_{45} it holds

$$\lim_{x \rightarrow \Gamma_{45}} G_j(x) = x_j \lim_{\alpha \rightarrow R} (R^2 - \alpha^2)^{-1/2} \quad x_j \in [-R, R].$$

Thus one computes for $j = 1$ and $j = 3$

$$\begin{aligned} [\partial_j(I_e^v \varphi)]_{\Gamma_{12}} &= -R^v x_j (\varphi(m_2) - \varphi(m_1)) \\ [\partial_j(I_e^v \varphi)]_{\Gamma_{13}} &= [\partial_j(I_e^v \varphi)]_{\Gamma_{25}} = -[\partial_j(I_e^v \varphi)]_{\Gamma_{24}} = -R^v x_j (R^2 - x_1^2 - x_3^2)^{-1/2} \varphi(m_2) \\ [\partial_j(I_e^v \varphi)]_{\Gamma_{15}} &= [\partial_j(I_e^v \varphi)]_{\Gamma_{23}} = -[\partial_j(I_e^v \varphi)]_{\Gamma_{14}} = -R^v x_j (R^2 - x_1^2 - x_3^2)^{-1/2} \varphi(m_1) \\ [\partial_j(I_e^v \varphi)]_{\Gamma_{34}} &= R^v x_j (\varphi(m_1) + \varphi(m_2)) \\ [\partial_j(I_e^v \varphi)]_{\Gamma_{45}} &= -2R^v \varphi(0, x_2, 0) \lim_{x_1^2 + x_3^2 \rightarrow R^2} \frac{x_j}{(R^2 - x_1^2 - x_3^2)^{1/2}} \end{aligned}$$

We observe a jump of constant size parallel to the edge.

$$\begin{aligned} [\partial_2(I_e^v \varphi)]_{\Gamma_{12}} &= R^v (\varphi(m_1) + \varphi(m_2)) \\ [\partial_2(I_e^v \varphi)]_{\Gamma_{14}} &= [\partial_2(I_e^v \varphi)]_{\Gamma_{15}} = -[\partial_2(I_e^v \varphi)]_{\Gamma_{23}} = R^v \varphi(m_1) \\ [\partial_2(I_e^v \varphi)]_{\Gamma_{24}} &= [\partial_2(I_e^v \varphi)]_{\Gamma_{25}} = -[\partial_2(I_e^v \varphi)]_{\Gamma_{13}} = -R^v \varphi(m_2) \\ [\partial_2(I_e^v \varphi)]_{\Gamma_{34}} &= -R^v (\varphi(m_2) - \varphi(m_1)) \\ [\partial_2(I_e^v \varphi)]_{\Gamma_{45}} &= 0 \end{aligned}$$

□

In the following lemma, we describe the regularity of the reference integral $I_e^v \varphi$ using piecewise defined countably normed spaces. Next to a classical singularity due to the kernel function, there exist geometrical light cone singularities corresponding to the intersection of the sphere and the edge. We show, that these anisotropic singularities have different strength on the regarded subdomains. We observe poles on the surface of the cylinder with axis e and jumps on the surface of the spheres.

These geometrical singularities influence the regularity in the subdomains S_1, S_2 and S_4 , where the effect on S_4 is stronger than on S_1 and S_2 . Moreover, the discontinuities result in a decomposition of $C_R(e)$, on which we define countably normed spaces.

We want to apply our knowledge of the singularities of discrete retarded potentials in Chapter 4 in order to discuss the quadrature error of the corresponding Galerkin integrals. In this context the retarded potential is multiplied by a

test function and integrated over the boundary Γ . As we use a triangulation of the boundary, we evaluate the integral element-wise. Each element \hat{T} defines a triangle plane $\mathcal{E}_{\hat{T}}$ with normal $n_{\hat{T}}$ and we have to describe the behavior of the discrete retarded potential in this plane. Thus we have to intersect the three-dimensional elements of the natural decomposition of $C_R(e)$ with the triangle plane $\mathcal{E}_{\hat{T}}$. In the following, we will consider its regularity within a certain plane, where we aim to apply the obtained results in the error analysis of the outer quadrature in Chapter 4. Given a plane \mathcal{E} with normal n defined by

$$(x - p, n) = 0$$

where $p \in \mathcal{E}$ and its distance to the origin is $d = p \cdot n$.

In the following two lemmata, we consider two functions in terms of their regularity in countably normed spaces. Let us first describe the edge function on a fixed integration domain.

There exist detailed analysis on the classically known kernel singularities of boundary integrals [49, 51]. Here we will consider kernel functions $k(x - y)$ holding the Calderon-Zygmund type inequality [13]

$$|D^\alpha k(x - y)| \leq C_0 C_1^{|\alpha|} \alpha! \|x - y\|^{\min(l - \alpha, 0)} \quad (3.14)$$

with $l > -1$. Furthermore, we assume, that on a bounded subset $A \subset \mathbb{R}^3$ there holds

$$(\hat{I}\varphi)(x) := \int_e k(x - y)\varphi(y) ds_y \in B_\beta^{l_{ker}-1}(A)$$

with a weight function $\Phi_{\beta, \alpha, l_{ker}-1}(x)$ located on the edge e . For the new singularities of geometrical type has to be analysed separately. From (3.13) we know, that a description of an edge function on the subdomains involves the analysis of a function $g(x_1, x_3) := (R^2 - x_1^2 - x_3^2)^{1/2}$.

Lemma 3.9. *Given a function $g(x) := (R^2 - x_1^2 - x_3^2)^{1/2}$ and a plane \mathcal{E} . Let A denote a planar subset of \mathcal{E} and*

a) *If the plane \mathcal{E} is parallel to e , we have singularities on the two intersection lines of the cylinder wall of $C_R(e)$. We introduce local coordinates ξ_1, ξ_2 in the plane \mathcal{E} , such that ξ_1 and ξ_2 are perpendicular and parallel to e , resp. The origin of the local coordinate system is the projection of the vertex m_1 of e onto \mathcal{E} . Then it holds $g \in B_\beta^1(S_4 \cap \mathcal{E})$ for $\beta \in (0, 1)$ and $g \in B_\beta^2(S_i \cap \mathcal{E})$ for $\beta \in (\frac{3}{4}, 1)$ with $i = 1, 2$, where R' denotes the distance to the cylindrical singularity in the plane and*

$$B_\beta^l(A) := \left\{ u \in H^{l-1}(A) : \left\| (R'^2 - \xi_1^2)^{\alpha_1 - l + \beta} \partial_{\xi_1}^{\alpha_1} \partial_{\xi_2}^{\alpha_2} u \right\|_{L^2(A)} \leq C d^{k-l} (k-l)! \text{ for } |\alpha| = k \geq l, C \geq 0, d \geq 1 \right\}$$

b) *If the plane \mathcal{E} is perpendicular to e , we have singularities on the intersection circle of the cylinder wall of $C_R(e)$. We introduce local polar coordinates ξ_1, ξ_2 in the plane \mathcal{E} , such that ξ_1 is the radial variable and ξ_2 denotes the angular variable. The origin of the local coordinate system is the projection of the vertex m_1 of e onto \mathcal{E} . Then it holds $g \in B_\beta^1(S_4 \cap \mathcal{E})$ for $\beta \in (0, 1)$ and $g \in B_\beta^1(S_i \cap \mathcal{E})$ for $\beta \in (\frac{3}{4}, 1)$ with $i = 1, 2$, where R' denotes the distance to the cylindrical singularity in the plane and*

$$B_\beta^l(A) := \left\{ u \in H^{l-1}(A) : \left\| (R'^2 - \xi_1^2)^{\alpha_1 - l + \beta} \partial_{\xi_1}^{\alpha_1} \partial_{\xi_2}^{\alpha_2} u \right\|_{L^2(A)} \leq C d^{k-l} (k-l)! \text{ for } |\alpha| = k \geq l, C \geq 0, d \geq 1 \right\}$$

c) *In $S_4 \cap \mathcal{E}$ we choose a local elliptic coordinate coordinate system defined on the semi-axes of the intersecting ellipse. Then $g \in B_\beta^1(S_4 \cap \mathcal{E})$ with*

$$B_\beta^l(A) := \left\{ u \in H^{l-1}(A) : \left\| (\sin^{-2} \theta - \cosh^2 \xi_1 \cos^2 \xi_2 - \cos^{-2} \theta \sinh^2 \xi_1 \sin^2 \xi_2)^{\alpha_1 - l + \beta} \partial_{\xi_1}^{\alpha_1} \partial_{\xi_2}^{\alpha_2} u \right\|_{L^2(A)} \leq C d^{k-l} (k-l)! \right. \\ \left. \text{for } |\alpha| = k \geq l, C \geq 0, d \geq 1 \right\}.$$

In S_1 and S_2 we observe maximally two point singularities, thus we can further subdivide the domain, such that only on point singularity per subelement is present and define on such an element a local polar coordinate system with origin located the singularity and radial variable ξ_1 and angular variable ξ_2 . Then there holds $g \in B_\beta^2(S_i \cap \mathcal{E})$ for

$i = 1, 2$ with

$$B_\beta^l(A) := \left\{ u \in H^{l-1}(A) : \left\| \xi_1^{\alpha_1 - l + \beta} \partial_{\xi_1}^{\alpha_1} \partial_{\xi_2}^{\alpha_2} u \right\|_{L^2(A)} \leq C d^{k-l} (k-l)! \text{ for } |\alpha| = k \geq l, C \geq 0, d \geq 1 \right\}.$$

Proof. Within this proof we use the following recursion formula several times. Given a function $g(\xi_1) := (R^2 - \xi_1^2)^{\frac{1}{2}}$ it holds $\partial_{\xi_1}^n g = (R^2 - \xi_1^2)^{-\frac{2n-1}{2}} p_n(\xi_1)$, where p_n is a polynomial in ξ_1 of degree n . Proof by induction. Clearly, this is true for $n = 1$. Now,

$$\begin{aligned} \partial_{\xi_1}^{n+1} g &= \partial_1 (R^2 - \xi_1^2)^{-\frac{2n-1}{2}} p_n(\xi_1) \\ &= (R^2 - \xi_1^2)^{-\frac{2n+1}{2}} \left((2n-1) \xi_1 p_n(\xi_1) + (R^2 - \xi_1^2) \partial_1 p_n(\xi_1^2) \right) \\ &= (R^2 - \xi_1^2)^{-\frac{2n+1}{2}} p_{n+1}(\xi_1). \end{aligned}$$

In the following we analyze the intersection of the partition elements S_i ($i = 1, \dots, 5$) as defined in (3.11) with the plane \mathcal{E} . We intersect the two spheres $B_R(m_1)$ and $B_R(m_2)$ and the cylinder $\mathcal{C}_R(e)$ with the plane. The intersection of a sphere and a plane is either a circle or vanishes. If the plane is tangential to the sphere, the intersection is a point. The intersection of a cylinder wall and a plane is more involved. Therefore, we split the analysis into three basic cases

- a) $\mathcal{E} \parallel e$ The intersection of the cylinder and the plane results in two parallel lines, one line or is empty.
- b) $\mathcal{E} \perp e$ The intersection of the cylinder $\mathcal{C}_R(e)$ is either empty or a circle.
- c) $\mathcal{E} \nparallel e$ and $\mathcal{E} \not\perp e$ The intersection of the cylinder without its caps and the plane results in an ellipse, the arc of an ellipse or the empty set. Compare Fig. 3.9 for some examples of the resulting intersections.

For case (a), i.e. the edge and the plane are parallel, we can restrict the analysis to planes parallel to the (x_1, x_2) -plane. Due to the symmetry of the regarded spheres and the cylinder there is no loss of generality. The plane normal is then $n = (0, 0, 1)^T$. There is only a non-empty intersection, if the distance of the plane to the origin holds $d \in (-R, R)$. Now the radius of the circles is $R' = \sqrt{R^2 - d^2}$ and $m'_1 = (0, 0, d)^T$, $m'_2 = (0, 1, d)$. In local coordinates ξ_1, ξ_2 parallel and perpendicular to e , resp., the light cone function reduces to $g(\xi_1) = \sqrt{R^2 - \xi_1^2}$ and for higher derivatives there exists a polynomial p_n of degree n , such that

$$\partial_{\xi_1}^n g(\xi_1) = (R^2 - \xi_1^2)^{-\frac{2n-1}{2}} p_n(\xi_1).$$

The derivatives with respect to ξ_2 vanish and it remains to study the derivatives with respect to ξ_1 . We first verify, that $g \in H^1(S_1 \cap \mathcal{E})$

$$\begin{aligned} \left\| \partial_{\xi_1} g \right\|_{L^2(S_1 \cap \mathcal{E})}^2 &\leq \int_{-R'}^{R'} \xi_1^2 \int_{-\sqrt{R'^2 - \xi_1^2}}^{\sqrt{R'^2 - \xi_1^2}} (R'^2 - \xi_1^2)^{-1} d\xi_2 d\xi_1 \\ &\leq R'^2 \int_{-R'}^{R'} (R'^2 - \xi_1^2)^{-1/2} d\xi_1 = R'^2 \arcsin \frac{\xi_1}{R'} \Big|_{-R'}^{R'} = R'^2 \pi \end{aligned}$$

In order to show, that $g \in H_\beta^{m,2}(S_1 \cap \mathcal{E})$ for $m \geq 2$, we need to estimate the weighted norms of the higher derivatives $\partial_1^k g$ for $2 \leq k \leq m$

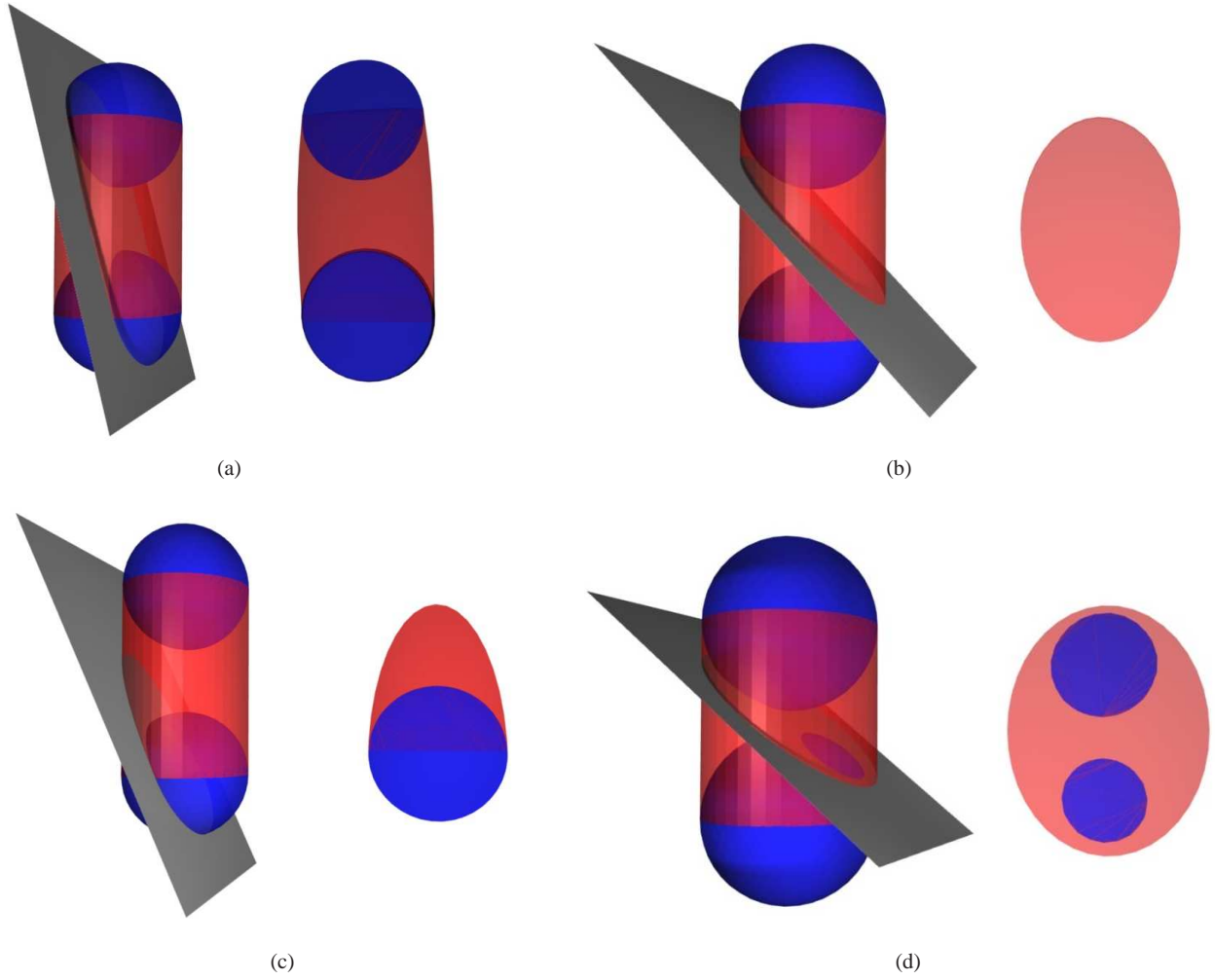


Fig. 3.9 $C_R(e)$ intersected with different planes and the resulting intersection.

$$\begin{aligned}
 \left\| \partial_1^k g(R'^2 - \xi_1^2)^{k-2+\beta} \right\|_{L^2(S_1 \cap \mathcal{E})}^2 &= \int_{-R'}^{R'} (\partial_1^k g)^2 (R'^2 - \xi_1^2)^{2(k-2+\beta)} (R'^2 - \xi_1^2)^{\frac{1}{2}} d\xi_1 \\
 &= \int_{-R'}^{R'} (R'^2 - \xi_1^2)^{-\frac{5}{2}+2\beta} p_k^2(\xi_1) d\xi_1 \\
 &\leq C \max_{\xi \in S_1 \cap \mathcal{E}} |p_k(\xi)|^2 \int_{-R'}^{R'} (R'^2 - \xi_1^2)^{-\frac{5}{2}+2\beta} d\xi_1 < \infty \quad \text{if } \beta \in \left(\frac{3}{4}, 1\right)
 \end{aligned}$$

Note that, the integral $\int_0^R (R^2 - \xi_1^2)^\alpha d\xi_1$ exists for $\alpha > -1$ as the following limit exists for $s < 1$

$$\lim_{\xi_1 \rightarrow R} (R - \xi_1)^s (R^2 - \xi_1^2)^\alpha = \lim_{\xi_1 \rightarrow R} (R - \xi_1)^{s+\alpha} (R + \xi_1)^\alpha.$$

It remains to show

$$\max_{\xi \in (S_1 \cap \mathcal{E})} |p_k(\xi)| \leq Cd^{k-2}(k-2)! \tag{3.15}$$

Estimation of $p_n(\xi_1)$:

It holds $|p_2(\xi_1)| \leq 2R^2$. Assume now, that for $p_n(\xi_1) = \sum_{j \leq n} \alpha_j^{(n)} \xi_1^j$ it holds $|p_n(\xi_1)| \leq Cd^{n-2}(n-2)!$, where $d = \max(1, R^2)$. Then one deduces the following recursion formula

$$\begin{aligned} p_{n+1}(\xi_1) &= (2n-1)x_1 p_n(\xi_1) + (R^2 - \xi_1^2) p_n'(\xi_1) \\ &= \sum_{j \leq n} (2n-1-j) \alpha_j^{(n)} \xi_1^{j+1} + R^2 \sum_{j \leq n} \alpha_j^{(n)} j \xi_1^{j-1} \\ &= \sum_{j \leq n+1} (2n-j) \alpha_{j-1}^{(n)} \xi_1^j + R^2 \sum_{j \leq n-1} \alpha_{j+1}^{(n)} (j+1) \xi_1^j \end{aligned}$$

such that

$$\alpha_j^{(n+1)} = (2n-j) \alpha_{j-1}^{(n)} + (j+1) R^2 \alpha_{j+1}^{(n)}.$$

Use this relation and (3.15), to estimate

$$\begin{aligned} |p_{n+1}(\xi_1)| &= \left| \sum_{j \leq n+1} ((2n-j) \alpha_{j-1}^{(n)} + (j+1) R^2 \alpha_{j+1}^{(n)}) \xi_1^j \right| \\ &\leq (2n-1) |p_n(\xi_1)| + n R^2 |p_n(\xi_1)| \\ &\leq (3n-1) (R')^{n+1} \sum_{i+j \leq n} |\alpha_j^{(n)}| \end{aligned}$$

Estimate the sum of the absolute value of the coefficients via

$$\begin{aligned} \sum_{j \leq n} |\alpha_j^{(n)}| &\leq \sum_{j \leq n} (2n-2-j) |\alpha_j^{(n-1)}| + (R')^2 \sum_{j \leq n} (j+1) |\alpha_j^{(n-1)}| \\ &\leq ((2n-2) + (R')^2 n) \sum_{j \leq n} |\alpha_j^{(n-1)}| \\ &\leq (2 + R^2) n \sum_{j \leq n} |\alpha_j^{(n-1)}| \\ &\leq (2 + R^2)^n n!. \end{aligned}$$

Now, $n = e^{\ln n} \leq e^n$ and there follows

$$\begin{aligned} |p_{n+1}(\xi_1)| &\leq 3n (R')^{n+1} (2 + R^2)^n n! \\ &\leq C e^2 (R' (2 + R^2) e^2)^{n-1} (n-1)!. \end{aligned}$$

On S_2 we can proceed in the same manner, where on S_4 there holds $g \in L^2(S_4 \cap \mathcal{E})$ but $g \notin H^1(S_4 \cap \mathcal{E})$. $g \in H^{m,1}(S_4 \cap \mathcal{E})$ for $m \geq 1$ as it holds for $1 \leq k \leq m$

$$\begin{aligned} \left\| \partial_{\xi_1}^k g (R^2 - \xi_1^2)^{k-1+\beta} \right\|_{L^2(S_4 \cap \mathcal{E})}^2 &= \int_{-R'}^{R'} g^{(k)}(\xi_1)^2 (R^2 - \xi_1^2)^{2(k-1+\beta)} d\xi_1 \\ &= C \max_{\xi \in (S_4 \cap \mathcal{E})} |p_k^2(\xi_1)| \int_{-R'}^{R'} (R^2 - \xi_1^2)^{2\beta-1} d\xi_1 < \infty \text{ for } \beta \in (0, 1). \end{aligned}$$

From (3.15) it immediately follows

$$\max_{\xi \in (S_4 \cap \mathcal{E})} |p_k^2(\xi_1)| \leq Cd^{2(k-1)} (k-1)!$$

and thus $g \in B_\beta^1(S_4 \cap \mathcal{E})$.

Let us now consider case (b), i.e. planes \mathcal{E} perpendicular to the edge e . Due to the symmetry of the regarded objects it is again sufficient to reduce the analysis to planes perpendicular to the (x_1, x_2) -plane with $n = (1, 0, 0)$ and $d \in \mathbb{R}$. Here the radius of the intersected circles, if not vanishing, is $R' = \sqrt{R^2 - x_1^2}$. The cylinder intersected with the plane is either a circle with Radius R for $d \in [0, 1]$ or the empty set. All circles have the common center $m_c = (0, d, 0)$. If $d \neq 0$ and $d \neq 1$ the intersection with the spheres always results in circles with a finite distance to the singularity on the surface of the cylinder. Therefore, we regard the case $d = [0, 1]$ in more detail. We introduce a local polar coordinate system in \mathcal{E} with origin m_c and radial and angular variable ξ_1 and ξ_2 , resp. As g is only dependent to ξ_1 , we have to estimate the derivatives with respect to ξ_1 and it holds $g \in B_\beta^1(S_1 \cap \mathcal{E})$ for $\beta \in (0, 1)$ as

$$\begin{aligned} \left\| \partial_{\xi_1}^k g (R'^2 - \xi_1^2)^{2(k-1+\beta)} \right\|_{L^2(S_1 \cap \mathcal{E})}^2 &\leq \int_0^{2\pi} \int_0^{R'} (\partial_{\xi_1}^k g)^2 (R'^2 - \xi_1^2)^{2(k-1+\beta)} \xi_1 d\xi_1 d\xi_2 \\ &= \int_0^{2\pi} \int_0^{R'} (R'^2 - \xi_1^2)^{2\beta-1} p_k^2(\xi_1) \xi_1 d\xi_1 d\xi_2 \\ &\leq C \max_{\xi \in S_1 \cap \mathcal{E}} 2\pi |p_k(\xi)|^2 \int_0^{R'} (R'^2 - \xi_1^2)^{2\beta-1} \xi_1 d\xi_1 \\ &\leq C \max_{\xi \in S_1 \cap \mathcal{E}} 2\pi |p_k(\xi_1)|^2 \left(\int_0^{R'} (R - \xi_1)^{2(2\beta-1)} \xi_1 d\xi_1 \right)^{\frac{1}{2}} \left(\int_0^R (R + \xi_1)^{2(2\beta-1)} \xi_1 d\xi_1 \right)^{\frac{1}{2}} \\ &\leq C d^{k-1} (k-1)! \quad \text{if } \beta \in (0, 1) \end{aligned}$$

Here we used, that we can apply the same estimation for p_k as before. Now $S_4 \cap \mathcal{E}$ is a circle and $g \in B_\beta^1(S_4 \cap \mathcal{E})$ using the polar local coordinates with the argumentation above. Note, that this result is not optimal, if R is big and the distance to $d = 0$ or $d = 1$ is big enough, the function is regular.

In case (c), where the plane is neither parallel nor perpendicular to the edge, we can restrict the analysis to planes with a normal $n = (\sin \theta, \cos \theta, 0)$ with $\theta \in (0, \pi/2)$ and a distance d to the origin. We introduce a local elliptic coordinate system whose center m is the center of the ellipse. In a rotated coordinate system defined by the two semi-axes e_a and e_b with variables z_1 and z_2 of the intersecting ellipse the local coordinates ξ_1, ξ_2 are defined by

$$\begin{aligned} z_1 &= e \cosh \xi_1 \cos \xi_2 \\ z_2 &= e \sinh \xi_1 \sin \xi_2 \end{aligned}$$

where e is fixed as the linear eccentricity of the intersecting ellipse. Before we continue, let us shortly summarize the main properties of the intersecting ellipse. The lengths of the two semi-axes are $a = R'/\cos \theta$ and $b = R'$. Thus the linear eccentricity $e = \sqrt{a^2 - b^2} = 1/\sin \theta$. Therefore, g reads in the local elliptic coordinate system

$$\tilde{g}(\xi_1, \xi_2) = \left(\frac{a^2 b^2}{a^2 - b^2} - b^2 \cosh^2 \xi_1 \cos^2 \xi_2 - a^2 \sinh^2 \xi_1 \sin^2 \xi_2 \right)^{\frac{1}{2}}$$

where $\frac{a^2 b^2}{e^2} = R'^2 \sin^{-2} \theta$. For the intersecting ellipse $\xi_1 = \kappa$ is fixed and it holds $\cosh \kappa = \frac{a}{e} = \sin^{-1} \theta$ and $\sinh \kappa = \frac{b}{e} = \tan^{-1} \theta$. Now,

$$\begin{aligned}\partial_{\xi_1} \tilde{g} &= - \left(\frac{a^2 b^2}{a^2 - b^2} - b^2 \cosh^2 \xi_1 \cos^2 \xi_2 - a^2 \sinh^2 \xi_1 \sin^2 \xi_2 \right)^{-\frac{1}{2}} [b^2 \cos^2 \xi_2 + a^2 \sin^2 \xi_2] \cosh \xi_1 \sinh \xi_1 \\ \partial_{\xi_2} \tilde{g} &= \left(\frac{a^2 b^2}{a^2 - b^2} - b^2 \cosh^2 \xi_1 \cos^2 \xi_2 - a^2 \sinh^2 \xi_1 \sin^2 \xi_2 \right)^{-\frac{1}{2}} [b^2 \cosh^2 \xi_1 - a^2 \sinh^2 \xi_1] \cos \xi_2 \sin \xi_2\end{aligned}$$

Now, $b^2 \cosh^2 \xi_1 - a^2 \sinh^2 \xi_1 = 0$ for $\xi_1 = \kappa$ and thus the derivative with respect to ξ_2 vanishes due to l'Hospital on the intersecting ellipse and we identify the leading singularity of derivatives $\partial_{\xi_1}^{\alpha_1} \partial_{\xi_2}^{\alpha_2} \tilde{g}$ as

$$\left(\frac{a^2 b^2}{a^2 - b^2} - b^2 \cosh^2 \xi_1 \cos^2 \xi_2 - a^2 \sinh^2 \xi_1 \sin^2 \xi_2 \right)^{-\frac{2\alpha_1+1}{2}}.$$

The remaining part is a polynomial in $\cosh \xi_1$, $\sinh \xi_1$, $\cos \xi_2$ and $\sin \xi_2$, which can be easily estimated, such that it holds

$$\left\| (\sin^{-2} \theta - \cosh^2 \xi_1 \cos^2 \xi_2 - \cos^{-2} \theta \sinh^2 \xi_1 \sin^2 \xi_2)^{\alpha_1-1+\beta} \partial_{\xi_1}^{\alpha_1} \partial_{\xi_2}^{\alpha_2} u \right\|_{L^2(S_4 \cap \mathcal{E})} \leq C d^{k-1} (k-1)!$$

The radii of the intersected circles, if not vanishing, are for $B_R(m_1)$ and $B_R(m_2)$ given by $R_1 = \sqrt{R^2 - d^2}$ and $R_2 = \sqrt{R^2 - (d - \cos \theta)^2}$, respectively. We can at most observe two point singularities and they can be treated by the classical theory as originally introduced in [20]. $g \in B_\beta^2(S_1)$ and $g \in B_\beta^2(S_2)$ for $\beta \in (0, 1)$ in the corresponding local coordinates. \square

We have described the singularity on the cylinder wall and as this singularity is of significant importance for the regularity description of retarded potentials, we will refer to this type of singularity in the following as *cylindrical singularity*.

Now, we have analyzed all necessary components in order to formulate the regularity of the edge function $I_e^V \varphi$ in an arbitrary plane \mathcal{E} .

Lemma 3.10 (Regularity of $I_e^V \varphi$ restricted to a plane \mathcal{E}). *Given a plane \mathcal{E} . Subdivide the disjoint elements S_i ($i = 1, \dots, 5$) as defined in (3.11) of the decomposition of $C_R(e) \cap \mathcal{E}$ such that on each new subelement $S' \cap \mathcal{E}$ there exists only one type of singularity.*

- For a cylindrical singularity w.r.t. edge e there holds in a local coordinate system (ξ_1, ξ_2) as defined in Lemma 3.9 depending on the orientation of \mathcal{E}

$$I_e^V \varphi(x) \in B_\beta^1(S' \cap \mathcal{E})$$

with a weight function located on the cylinder wall of $C_R(e)$ and $\beta \in (0, 1)$. The intersection of S' with the plane \mathcal{E} refers to exactly one of the cases in Lemma 3.9.

- If on $S' \cap \mathcal{E}$ a classically known kernel singularity w.r.t. edge e is observed, we can describe the regularity as follows.

$$I_e^V \varphi(x) \in B_\beta^{l_{ker}-1}(S' \cap \mathcal{E})$$

with a weight function located on the edge e and $\beta \in (0, 1)$.

Proof. In Lemma 3.8 we have seen, that on the interfaces of the partition of $C_R(e)$ there exist jumps. Because of these jumps, we have to study the regularity of $I_e^V \varphi$ on each subdomain $S_i \cap \mathcal{E}$ separately. Moreover, depending on the kernel function $k_V(x-y)$ apart from the geometrical singularities classically known kernel singularities located on the edge e can occur, compare (3.13). Thus it is necessary to further subdivide a regarded subelement $S_i \cap \mathcal{E}$ if $e \subset S_i \cap \mathcal{E}$. In Lemma 3.9 the influence of the geometrical singularities was analysed which is now combined with the classically known singularities located on the edge e and we obtain the following discussion on the different subelements. Let $S'_i \cap \mathcal{E}$ denote such a decomposition element of $S_i \cap \mathcal{E}$.

1. *Analysis in $S_3 \cap \mathcal{E}$.* Due to (3.13) here the geometrical singularities have no influence and thus no further subdivision is necessary, as only the classically known kernel singularity has an impact on the regularity of $I_e^v \varphi$ in $S_3 \cap \mathcal{E}$. Thus we can directly apply the classically known regularity results.
2. *Analysis in $S_1 \cap \mathcal{E}$ and $S_2 \cap \mathcal{E}$.* Without loss of generality, we can restrict the analysis to S_1 . Here we have to deal with an additional boundary term as given in (3.13). Nevertheless, the classically known kernel singularity can also influence the regularity of $I_e^v \varphi$. Thus we have to further subdivide the $S_1 \cap \mathcal{E}$ such that on each resulting subelement we either have the influence of the classically known kernel singularity or the geometrical singularity. As these singularities are located on curves with a finite distance such a decomposition always exists.
If such a subelement S'_1 now involves the classically known kernel singularity, we can apply the same arguments as given on S_3 . If the subelement S'_1 involves the geometrical singularity, we can apply Lemma 3.9 and obtain in the appropriate local coordinate system (ξ_1, ξ_2)

$$I_e^v \varphi(x) \in B_\beta^1(S' \cap \mathcal{E}).$$

Note, that for general planes, we can only conclude $I_e^v \varphi \in B_\beta^1(S_i \cap \mathcal{E})$ ($i = 1, 2$), although for planes parallel to e , we obtain the better result $I_e^v \varphi \in B_\beta^2(S_i \cap \mathcal{E})$, compare Lemma 3.9 a.

3. *Analysis in $S_4 \cap \mathcal{E}$.* We apply the same arguments as for S_1 and S_2 . With an appropriate decomposition due to the edge e we obtain the same results for the elements with classically known kernel singularities or cylindrical singularities, respectively. But in contrast to S_1 and S_2 there exists no improved regularity for planes parallel to e .
4. *Analysis in $S_5 \cap \mathcal{E}$.* $I_e^v \varphi$ vanishes in S_5 .

□

Back transformation to a general edge

Now, we want to map the result on the reference edge e to a general edge \hat{e} . First, we can transfer the results of Lemma 3.8 to a general edge function and obtain

Lemma 3.11. *Let $k_v(x-y) := |x-y|^v$ for $v \geq -1$ and $\varphi \in L^\infty(\hat{e})$.*

$I_{\hat{e}}^v \varphi$ is continuous in \mathbb{R}^3 , whereas the first derivatives possess jumps on $\partial B_{\hat{R}}(\hat{m}_i)$ ($i = 1, 2$) and poles on $\partial \mathcal{C}_R(\hat{e})$ (without the caps). As $I_{\hat{e}}^v \varphi$ vanishes in $\mathbb{R}^3 \setminus \mathcal{C}_R(\hat{e})$ this pole is one-sided in $\mathcal{C}_R(\hat{e})$.

$$\begin{aligned} \left| [\partial_{n_{\hat{e}}}(I_{\hat{e}}^v \varphi)]_{\partial B_{\hat{R}}(\hat{m}_1)} \right| &= |\hat{e} \hat{R}^v |n_{\hat{e}}(\hat{x} - \hat{m}_1)| (\hat{R}^2 - (n_{\hat{e}}(\hat{x} - \hat{m}_1))^2 - (n_T(\hat{x} - \hat{m}_1))^2)^{-1/2} |\varphi(\hat{m}_1)|, \\ \left| [\partial_{n_{\hat{e}}}(I_{\hat{e}}^v \varphi)]_{\partial B_{\hat{R}}(\hat{m}_2)} \right| &= |\hat{e} \hat{R}^v |n_{\hat{e}}(\hat{x} - \hat{m}_1)| (\hat{R}^2 - (n_{\hat{e}}(\hat{x} - \hat{m}_1))^2 - (n_T(\hat{x} - \hat{m}_1))^2)^{-1/2} |\varphi(\hat{m}_2)|, \\ \left| [\partial_{n_{\hat{e}}}(I_{\hat{e}}^v \varphi)]_{\partial \mathcal{C}_R(\hat{e})} \right| &= 2|\hat{e} \hat{R}^v \lim_{\hat{x} \rightarrow \partial \mathcal{C}_R(\hat{e})} \frac{|\varphi(|\hat{e}|^{-3}(\hat{e}(\hat{x} - \hat{m}_1))\hat{e})| |n_{\hat{e}}(\hat{x} - \hat{m}_1)|}{(\hat{R}^2 - (n_{\hat{e}}(\hat{x} - \hat{m}_1))^2 - (n_T(\hat{x} - \hat{m}_1))^2)^{1/2}}, \\ \left| [\partial_{n_T}(I_{\hat{e}}^v \varphi)]_{\partial B_{\hat{R}}(\hat{m}_1)} \right| &= |\hat{e} \hat{R}^v |n_T(\hat{x} - \hat{m}_1)| (\hat{R}^2 - (n_{\hat{e}}(\hat{x} - \hat{m}_1))^2 - (n_T(\hat{x} - \hat{m}_1))^2)^{-1/2} |\varphi(\hat{m}_1)|, \\ \left| [\partial_{n_T}(I_{\hat{e}}^v \varphi)]_{\partial B_{\hat{R}}(\hat{m}_2)} \right| &= |\hat{e} \hat{R}^v |n_T(\hat{x} - \hat{m}_1)| (\hat{R}^2 - (n_{\hat{e}}(\hat{x} - \hat{m}_1))^2 - (n_T(\hat{x} - \hat{m}_1))^2)^{-1/2} |\varphi(\hat{m}_2)|, \\ \left| [\partial_{n_T}(I_{\hat{e}}^v \varphi)]_{\partial \mathcal{C}_R(\hat{e})} \right| &= 2|\hat{e} \hat{R}^v \lim_{\hat{x} \rightarrow \partial \mathcal{C}_R(\hat{e})} \frac{|\varphi(|\hat{e}|^{-3}(\hat{e}(\hat{x} - \hat{m}_1))\hat{e})| |n_T(\hat{x} - \hat{m}_1)|}{(\hat{R}^2 - (n_{\hat{e}}(\hat{x} - \hat{m}_1))^2 - (n_T(\hat{x} - \hat{m}_1))^2)^{1/2}}. \end{aligned}$$

We observe a jump of constant size parallel to the edge

$$\begin{aligned} \left| [\partial_{\hat{e}}(I_{\hat{e}}^V \varphi)]_{\partial B_{\hat{R}}(\hat{m}_1)} \right| &= |\hat{e}| \hat{R}^V |\varphi(\hat{m}_2)|, \\ \left| [\partial_{\hat{e}}(I_{\hat{e}}^V \varphi)]_{\partial B_{\hat{R}}(\hat{m}_2)} \right| &= |\hat{e}| \hat{R}^V |\varphi(\hat{m}_1)|, \\ \left| [\partial_{\hat{e}}(I_{\hat{e}}^V \varphi)]_{\partial \mathcal{C}_R(\hat{e})} \right| &= 0. \end{aligned}$$

Proof. Due to Lemma 3.5 it holds $(I_{\hat{e}}^V \varphi)(\hat{x}) = |\hat{e}|^{v+1} I^V(x)$ with $R = \hat{R}/|\hat{e}|$ and $x = \mathcal{F}^{-1}(\hat{x})$. It immediately follows $|\hat{e}| \partial_{x_1} = \partial_{n_{\hat{e}}}$, $\partial_{x_2} = \partial_{\hat{e}}$ and $|\hat{e}| \partial_{x_3} = \partial_{n_T}$ as it holds $x = \frac{1}{|\hat{e}|^2} A^T(\hat{x} - b)$. Now

$$\begin{aligned} \partial_{n_{\hat{e}}}(I_{\hat{e}}^V \varphi)(\hat{x}) &= |\hat{e}|^v \partial_{x_1} I^V(x) \\ \partial_{\hat{e}}(I_{\hat{e}}^V \varphi)(\hat{x}) &= |\hat{e}|^{v+1} \partial_{x_2} I^V(x) \\ \partial_{n_T}(I_{\hat{e}}^V \varphi)(\hat{x}) &= |\hat{e}|^v \partial_{x_3} I^V(x) \end{aligned}$$

and therefore using Lemma 3.8

$$\left| [\partial_{\hat{e}}(I_{\hat{e}}^V \varphi)]_{\partial B_{\hat{R}}(\hat{m}_2)} \right| = |\hat{e}|^{v+1} \left| [\partial_{x_2} I^V]_{\partial B_R(m_2)} \right| = |\hat{e}|^{v+1} R^V |\tilde{\varphi}(m_1)| = |\hat{e}| \hat{R}^V |\varphi(\hat{m}_1)|$$

As

$$R^2 - x_1^2 - x_3^2 = \frac{1}{|\hat{e}|^2} (\hat{R}^2 - (n_{\hat{e}}(\hat{x} - \hat{m}_1))^2 - (n_T(\hat{x} - \hat{m}_1))^2)$$

and we obtain using Lemma 3.8

$$\begin{aligned} \left| [\partial_{n_{\hat{e}}}(I_{\hat{e}}^V \varphi)]_{\partial B_{\hat{R}}(\hat{m}_2)} \right| &= |\hat{e}|^{v+1} \left| [\partial_1 I^V]_{\partial B_R(m_2)} \right| \\ &= \hat{R}^V |\hat{e}| \frac{|n_{\hat{e}}(\hat{x} - \hat{m}_1)|}{|\hat{e}|} |\hat{e}| (\hat{R}^2 - (n_{\hat{e}}(\hat{x} - \hat{m}_1))^2 - (n_T(\hat{x} - \hat{m}_1))^2)^{-1/2} |\varphi(\hat{m}_2)| \end{aligned}$$

The remaining jumps are obtained in a similar manner. \square

Finally we transform the regularity description in terms of countably normed spaces to a general triangle edge \hat{e} by introducing local coordinates in appropriate local coordinate systems.

Lemma 3.12. [Regularity of $I_{\hat{e}}^V \varphi$ restricted to a plane \mathcal{E}] Given a plane \mathcal{E} . We can decompose $C_{\hat{R}}(\hat{e}) \cap \mathcal{E}$ into

$$S \in \{C_{\hat{R}}(\hat{e}) \setminus (B_{\hat{R}}(\hat{m}_1) \cup B_{\hat{R}}(\hat{m}_2)); B_{\hat{R}}(\hat{m}_1) \cap B_{\hat{R}}(\hat{m}_2); B_{\hat{R}}(\hat{m}_1) \setminus B_{\hat{R}}(\hat{m}_2); B_{\hat{R}}(\hat{m}_2) \setminus B_{\hat{R}}(\hat{m}_1)\}.$$

If there exist multiple singularities in $A \cap \mathcal{E}$ we further subdivide the planar element until only one type of singularity exists per regarded subelement $S' \cap \mathcal{E}$.

- For a cylindrical singularity w.r.t. edge \hat{e} there holds in a local coordinate system (ξ_1, ξ_2) defined as in Lemma 3.9 depending on the orientation of \mathcal{E}

$$I_{\hat{e}}^V \varphi(x) \in B_{\beta}^1(S' \cap \mathcal{E})$$

with a weight function located on the cylinder wall. and $\beta \in (0, 1)$. The intersection of S' with the plane \mathcal{E} refers to exactly one of the cases in Lemma 3.9.

- If on $S' \cap \mathcal{E}$ a classically known kernel singularity w.r.t. edge \hat{e} is observed, we can describe the regularity as follows.

$$I^n u_{\hat{e}} \varphi(\xi) \in B_{\beta}^{l_{ker}-1}(S' \cap \mathcal{E})$$

with a weight function located on the edge \hat{e} and $\beta \in (0, 1)$.

Proof. Follows directly from the analysis of the edge function on the reference edge e . The local coordinates as introduced in Lemma 3.9 are defined independently of the orientation of the reference edge and therefore apply also to

the general situation. Note that the elements of the natural decomposition $C_R(e)$ are transformed to the spheres and the cylinder given above. This is a direct consequence of Lemma 3.5. \square

3.2.2 Analysis of the Triangle Integral $I_T \varphi$

So far, we have analyzed the edge based integral $I_e^V \varphi$ and it remains to study the second boundary integral of Lemma 3.2. In this section we consider the function

$$(I_T \varphi)(x) := \frac{(x-p, n_T)}{R'(x)} \int_{T \cap \partial B_R(x)} k_V(x-y) \varphi(y) ds_y.$$

Note, that we do not restrict to kernels like $k_V(x-y) = |x-y|^V$ but allow general kernels.

Let us first regard the domain of integration $T \cap \partial B_R(x)$. For $x \in \mathbb{R}^3$ the set $T \cap \partial B_R(x)$ is not empty if $\text{dist}(x, T) \leq R$ and $\text{dist}(x, p_i) \geq R$ for at least one vertex p_i ($i = 1, 2, 3$) of T , such that

$$T \cap \partial B_R(x) \neq \emptyset \Leftrightarrow x \in E_R(T) \setminus \bigcap_{i=1}^3 B_R(p_i).$$

Therefore,

$$(I_T \varphi)(x) = \begin{cases} \frac{(x-p, n_T)}{R'(x)} \int_{T \cap \partial B_R(x)} k_V(x-y) \varphi(y) ds_y & x \in E_R(T) \setminus \bigcap_{i=1}^3 B_R(p_i) \\ 0 & \text{else.} \end{cases} \quad (3.16)$$

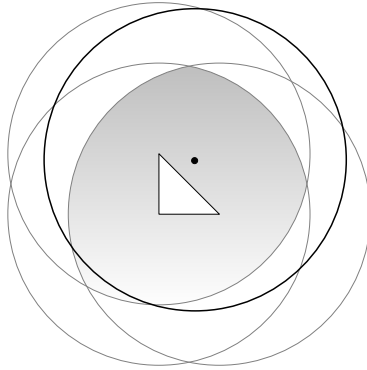


Fig. 3.10 Visualization of $T \cap \partial B_R(x) = \emptyset$ for $x \in \bigcap_{i=1}^3 B_R(p_i)$.

In order to discuss the regularity of the triangle integral $(I_T \varphi)(x)$ as defined in (3.6), see Lemma 3.2, we will regard the auxiliary problem replacing the triangle T by the whole triangle plane \mathcal{E}_T .

Auxiliary Problem: $\mathcal{E}_{\text{ref}} \cap \partial B_R(x)$

Here we focus on the reference situation $\mathcal{E}_{\text{ref}} = \{x : x_3 = 0\}$, i.e. $n_T = (0, 0, 1)$, such that $R'(x) = (R^2 - x_3^2)^{1/2}$ and choosing $p_{\text{ref}} = 0 \in \mathcal{E}_{\text{ref}}$ it holds $(x - p_{\text{ref}}, n_T) = x_3$ and $x' = (x_1, x_2, 0)$. We define

$$(I_{\mathcal{E}_{\text{ref}}} \varphi)(x) := \begin{cases} \frac{x_3}{R'(x)} \int_{\mathcal{E}_{\text{ref}} \cap \partial B_R(x)} k_V(x-y) \varphi(y) ds_y & |x_3| < R \\ 0 & |x_3| \geq R, \end{cases} \quad (3.17)$$

where $y_3 = 0$. Again, we use that $\mathcal{E}_{\text{ref}} \cap \partial B_R(x) = \mathcal{E}_{\text{ref}} \cap \partial B_{R'}(x')$, i.e. we integrate over the boundary of a circle with radius $R'(x)$ and center x' in the (x_1, x_2) -plane. Introducing polar coordinates (r, θ) with respect to x' , namely with $r_\theta := (\cos \theta, \sin \theta, 0)$ there holds $y = R'(x)r_\theta + x'$. This reveals for $|x_3| < R$

$$(I_{\mathcal{E}_{\text{ref}}}\varphi)(x) = x_3 \int_0^{2\pi} k(x_3 n_T - R'(x)r_\theta) \varphi(R'(x)r_\theta + x') d\theta. \quad (3.18)$$

Now, $I_{\mathcal{E}_{\text{ref}}}(x)$ is continuous for $|x_3| < R$ but possesses a jump at $x_3 = \pm R$ as

$$\lim_{x_3 \rightarrow \pm R} (I_{\mathcal{E}_{\text{ref}}}\varphi)(x) = \pm R k(\pm R n_T) \int_0^{2\pi} \varphi(x') d\theta = \pm 2\pi R k(\pm R n_T) \varphi(x') \neq 0.$$

Let us now consider the first derivatives of $I_{\mathcal{E}_{\text{ref}}}(x)$. For $|x_3| < R$ we obtain

$$\partial_{x_j} (I_{\mathcal{E}_{\text{ref}}}\varphi)(x) = x_3 \int_0^{2\pi} k(x_3 n_T - R'(x)r_\theta) \partial_{y_1} \varphi(y) \Big|_{y=R'(x)r_\theta+x'} d\theta \quad (j = 1, 2).$$

This integral is of the same type as (3.18), thus for φ sufficiently smooth, we again observe a jump for $x_3 = \pm R$. Clearly this works for higher order derivatives, too.

For the derivative with respect to x_3 we use

$$\begin{aligned} \partial_{x_3} (k(x_3 n_T - R'(x)r_\theta) \varphi(R'(x)r_\theta + x')) &= \left[n_T + \frac{x_3}{R'(x)} r_\theta \right] \nabla_z k(z) \Big|_{z=x_3 n_T - R'(x)r_\theta} \varphi(R'(x)r_\theta + x') \\ &\quad - k(x_3 n_T - R'(x)r_\theta) \frac{x_3}{R'(x)} r_\theta \nabla_z \varphi(z) \Big|_{z=R'(x)r_\theta+x'} \end{aligned}$$

such that

$$\begin{aligned} \partial_{x_3} (I_{\mathcal{E}_{\text{ref}}}\varphi)(x) &= \int_0^{2\pi} k(x_3 n_T - R'(x)r_\theta) \varphi(R'(x)r_\theta + x') d\theta \\ &\quad + x_3 \left(n_T + \frac{x_3}{R'(x)} r_\theta \right) \int_0^{2\pi} \nabla_z k(z) \Big|_{z=x_3 n_T - R'(x)r_\theta} \varphi(R'(x)r_\theta + x') d\theta \\ &\quad - x_3^2 \frac{1}{R'(x)} r_\theta \int_0^{2\pi} k(x_3 n_T - R'(x)r_\theta) \nabla_z \varphi(z) \Big|_{z=R'(x)r_\theta+x'} d\theta \end{aligned}$$

which is singular for $x_3 \rightarrow \pm R$. We can formulate its regularity in countably normed spaces, which yields the following lemma.

Lemma 3.13. *Given an arbitrary plane \mathcal{E} with normal n and distance d to the origin. Denote by Q a bounded subset of \mathcal{E}_{ref} and define $Q_R := \{x : |x_3| < R \text{ and } (x_1, x_2, 0) \in Q\}$. Given the function $g(x) = (R^2 - x_3^2)^{1/2}$.*

- *If \mathcal{E} and \mathcal{E}_{ref} are parallel the function g is regular in local coordinates in the plane \mathcal{E} .*
- *If \mathcal{E} and \mathcal{E}_{ref} are not parallel, the singularity is if present located on a line. We define a local cartesian coordinate system in \mathcal{E} with directions e_{\parallel} and e_{\perp} parallel or perpendicular to the line singularity. ξ_1 and ξ_2 are the variables corresponding to e_{\perp} and e_{\parallel} respectively. Then*

$$\begin{aligned} g &\in B_{\beta}^1(Q_R \cap \mathcal{E}) \\ &= \left\{ u \in H^{l-1}(Q_R \cap \mathcal{E}) : \left\| (R^2 - \xi_1^2)^{\alpha_1 - l + \beta} \partial_{\xi_1}^{\alpha_1} \partial_{\xi_2}^{\alpha_2} u \right\|_{L^2(Q_R \cap \mathcal{E})} \leq C d^{k-l} (k-l)! \text{ for } |\alpha| = k \geq l, C \geq 0, d \geq 1 \right\} \end{aligned}$$

Proof. We have to show that for a function $g(x) = (R^2 - x_3^2)^{1/2}$ and $\beta \in (0, 1)$, it holds $g \in B_{\beta}^1(Q_R \cap \mathcal{E})$ with a weight function in the local coordinate system. The proof follows the argumentation of the proof of Lemma 3.9. Note, that it is necessary to bound the integration domain to Q_R if the second plane is parallel to the plane \mathcal{E}_{ref} , but it is no loss of generality as we seek to study the integral $I_T \varphi$ on its naturally bounded support. As in Lemma 3.9 we regard the following three cases: the planes \mathcal{E} and \mathcal{E}_{ref} are parallel, perpendicular or neither of them.

If the planes are parallel, i.e. $n = \pm n_T$ all regarded derivatives in a local coordinate system are regular. If the planes are perpendicular, we can regard planes with normal $n = (1, 0, 0)$. Here the local cartesian coordinate system is defined in the direction of the triangle normal e_\perp and perpendicular to this direction e_\parallel denoted by ξ_1 and ξ_2 respectively. We thus have to analyze the derivatives with respect to ξ_1 and ξ_2 . As the function is singular in ξ_1 , we can only conclude $I_{\mathcal{E}_{\text{ref}}}\varphi \in B_\beta^1(Q_R \cap \mathcal{E})$. If the planes are neither parallel nor perpendicular, we can only conclude $I_{\mathcal{E}_{\text{ref}}}\varphi \in B_\beta^1(Q_R \cap \mathcal{E})$ as the planes can be close to perpendicular, compare also the argumentation in the proof of Lemma 3.9. For planes neither parallel nor perpendicular, we either have no singularity at all (if the singular parallelly shifted triangles are not intersected) or we have a line and can define a local coordinate system similar to the parallel case using the directions e_\parallel and e_\perp parallel and perpendicular to the line singularity respectively. \square

As the above introduced local coordinate system is independent of the orientation of \mathcal{E}_{ref} , we can rephrase the above lemma to

Lemma 3.14. *Given an arbitrary plane \mathcal{E} with normal n and distance d to the origin. Denote by Q a bounded subset of \mathcal{E}_{ref} and define $Q_R := \{x : |(x - p, n_T)| < R \text{ and } x' = x - (p - x, n_T) \in Q\}$.*

- If \mathcal{E} and \mathcal{E}_{ref} are parallel the function g is regular in local coordinates in the plane \mathcal{E} .
- If \mathcal{E} and \mathcal{E}_{ref} are not parallel, the singularity is if present located on a line. We define a local cartesian coordinate system in \mathcal{E} with directions e_\parallel and e_\perp parallel or perpendicular to the line singularity. ξ_1 and ξ_2 are the variables corresponding to e_\perp and e_\parallel respectively. Then

$$I_{\mathcal{E}_T} \in B_\beta^1(Q_R \cap \mathcal{E}) = \left\{ u \in H^{l-1}(Q_R \cap \mathcal{E}) : \left\| (R^2 - \xi_1^2)^{\alpha_1 - l + \beta} \partial_{\xi_1}^{\alpha_1} \partial_{\xi_2}^{\alpha_2} u \right\|_{L^2(Q_R \cap \mathcal{E})} \leq C d^{k-l} (k-l)! \text{ for } |\alpha| = k \geq l, C \geq 0, d \geq 1 \right\}$$

Proof. Here we can directly apply Lemma 3.13. The local coordinate systems are defined with respect to the possible singularity and thus independent of the orientation of \mathcal{E}_T . \square

Due to the importance of this second geometrical singularity, we refer to this singularity in the following as *planar singularity*, as the singularity is located in a plane or subsets of it.

Let us finally summarize the quality of the observed singularity in the following proposition.

Proposition 3.15. *Given a triangle plane \mathcal{E}_T and $\varphi \in C^1(\mathcal{E}_T) \cap L^\infty(\mathcal{E}_T)$. The function*

$$(I_{\mathcal{E}_T}\varphi)(x) := \begin{cases} \frac{(x-p, n_T)}{R'(x)} \int_{\mathcal{E}_T \cap \partial B_R(x)} k_\nu(x-y)\varphi(y) ds_y & |(x-p, n_T)| < R \\ 0 & \text{else} \end{cases}$$

is continuous for $|(x-p, n_T)| < R$ and possesses a jump of size R at $|(x-p, n_T)| = R$ and a singularity in the first derivative.

The above problem focuses on what is happening, perpendicular to the triangle. The next auxiliary problem tries to answer the question on what is happening, when the sphere meets an edge of the triangle. For this purpose, we regard the case of a half plane intersected with a sphere.

Auxiliary Problem: Half Plane

In order to study the situation, when the sphere meets a triangle edge, we regard the half plane

$$\mathcal{H}_{\text{ref}} := \{x : x_3 = 0 \text{ and } x_1 \geq 0\}.$$

Thus we define

$$(I_{\mathcal{H}_{\text{ref}}}\varphi)(x) := \begin{cases} \frac{x_3}{R'(x)} \int_{\mathcal{H}_{\text{ref}} \cap \partial B_R(x)} k_V(x-y)\varphi(y) ds_y & |x_3| < R \text{ and } x \in \mathcal{C}_R(\partial \mathcal{H}_{\text{ref}}) \\ 0 & \text{else} \end{cases} \quad (3.19)$$

where $\partial \mathcal{H}_{\text{ref}} := \{x : x_1 = x_3 = 0\}$ such that $\mathcal{C}_R(\partial \mathcal{H}_{\text{ref}})$ is the infinite cylinder with radius R around the x_2 -axis. If $|x_3| < R$ and $x \in \mathcal{C}_R(\partial \mathcal{H}_{\text{ref}})$, we use polar coordinates with respect to x' and obtain

$$(I_{\mathcal{H}_{\text{ref}}}\varphi)(x) = x_3 \int_{-\theta(x)}^{\theta(x)} k(x_3 n_T - R'(x)r_\theta)\varphi(R'(x)r_\theta + x') d\theta, \quad (3.20)$$

where $\cos \theta(x) = x_1/R'(x)$. Such that for $|x_3| \leq R$

$$\theta(x_1, x_3) = \begin{cases} \arccos\left(\frac{-x_1}{\sqrt{R^2 - x_3^2}}\right) & x_1 \in (-R, 0) \\ \frac{\pi}{2} & x_1 = 0 \\ \pi - \arccos\left(\frac{x_1}{\sqrt{R^2 - x_3^2}}\right) & x_1 \in (0, R) \\ 0 & x_1 \leq -R \\ \pi & x_1 \geq R \end{cases}$$

defines a continuous function. Later on, we will need the partial derivatives of $\theta(x)$ given by

$$\partial_{x_1} \theta(x_1, x_3) = \begin{cases} \frac{1}{\sqrt{R^2 - x_1^2 - x_3^2}} & x_1 \in (-R, R) \\ 0 & \text{else} \end{cases} \quad \partial_{x_3} \theta(x_1, x_3) = \begin{cases} \frac{x_1 x_3 (R^2 - x_3^2)^{-1}}{\sqrt{R^2 - x_1^2 - x_3^2}} & x_1 \in (-R, R) \\ 0 & \text{else} \end{cases}$$

and clearly $\partial_{x_2} \theta(x_1, x_3) = 0$.

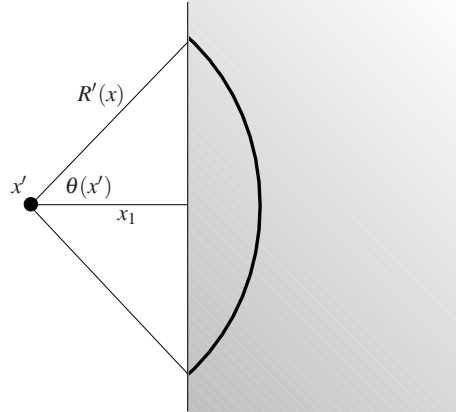


Fig. 3.11 Visualization of the intersection $B_R(x) \cap \mathcal{H}_{\text{ref}}$.

Let us first study the continuity of $(I_{\mathcal{H}_{\text{ref}}}\varphi)(x)$. This function is clearly continuous for $x \in \{x : x_1^2 + x_3^2 < R^2\}$. Thus it remains to regard the limits onto the boundary of this domain. For $x_1 = 0$ and $|x_3| \rightarrow R$ there directly applies the analysis of the reference plane. If we regard these limits for $x_1 = 0$ it holds $x' \in \partial \mathcal{H}_{\text{ref}}$ and $\theta(x) = \frac{\pi}{2}$, such that we obtain

$$\lim_{x_3 \rightarrow \pm R} (I_{\mathcal{H}_{\text{ref}}}\varphi)(x) = \pm R k(\pm R n_T) \int_{-\frac{\pi}{2}}^{\frac{\pi}{2}} \varphi(x') d\theta = \pm \pi R k(\pm R n_T) \varphi(x') \neq 0, \quad (3.21)$$

i.e. we observe a jump with a scaling factor π rather than 2π corresponding the opening angle on the boundary of the half plane. Transferring this observation to the triangle, it follows, that if $x' \in e_i$ for some edge e_i , there exists a jump of size π .

It remains to study the limit onto the boundary of the cylinder $\mathcal{C}_R(\partial\mathcal{H}_{\text{ref}})$

$$\lim_{x_1^2+x_3^2 \rightarrow R^2} (I_{\mathcal{H}_{\text{ref}}}\varphi)(x) = \lim_{x_1^2+x_3^2 \rightarrow R^2} x_3 \int_{-\theta(x)}^{\theta(x)} k(x_3 n_T - R'(x)r_\theta) \varphi(R'(x)r_\theta + x') d\theta,$$

where

$$\lim_{x_1^2+x_3^2 \rightarrow R^2} \theta(x) = \lim_{x_1^2+x_3^2 \rightarrow R^2} \arccos\left(\frac{-x_1}{\sqrt{R^2 - x_3^2}}\right) = \arccos(\pm 1) = 0.$$

Thus the integral vanishes and the function is continuous on this part of the boundary.

Therefore, we have shown that $(I_{\mathcal{H}_{\text{ref}}}\varphi)(x)$ is a continuous function except for $x_1 = 0$ and $|x_3| = R$ where the function exhibits a jump.

In the next step, we aim to study the first and later on the general higher derivatives of $(I_{\mathcal{H}_{\text{ref}}}\varphi)(x)$. Compute the first derivatives of (3.20).

$$\begin{aligned} \partial_{x_1}(I_{\mathcal{H}_{\text{ref}}}\varphi)(x) &= x_3 \partial_{x_1} \theta(x) \left[k(x_3 n_T - R'(x)r_{\theta(x)}) \varphi(R'(x)r_{\theta(x)} + x') \right. \\ &\quad \left. - k(x_3 n_T - R'(x)r_{-\theta(x)}) \varphi(R'(x)r_{-\theta(x)} + x') \right] \\ &\quad + x_3 \int_{-\theta(x)}^{\theta(x)} k(x_3 n_T - R'(x)r_\theta) \partial_{x_1} \varphi(R'(x)r_\theta + x') d\theta \\ \partial_{x_2}(I_{\mathcal{H}_{\text{ref}}}\varphi)(x) &= x_3 \int_{-\theta(x)}^{\theta(x)} k(x_3 n_T - R'(x)r_\theta) \partial_{x_2} \varphi(R'(x)r_\theta + x') d\theta \\ \partial_{x_3}(I_{\mathcal{H}_{\text{ref}}}\varphi)(x) &= \int_{-\theta(x)}^{\theta(x)} k(x_3 n_T - R'(x)r_\theta) \varphi(R'(x)r_\theta + x') d\theta \\ &\quad + x_3 \partial_{x_3} \theta(x) \left[k(x_3 n_T - R'(x)r_{\theta(x)}) \varphi(R'(x)r_{\theta(x)} + x') \right. \\ &\quad \left. - k(x_3 n_T - R'(x)r_{-\theta(x)}) \varphi(R'(x)r_{-\theta(x)} + x') \right] \\ &\quad + x_3 \int_{-\theta(x)}^{\theta(x)} \partial_{x_3} (k(x_3 n_T - R'(x)r_\theta) \varphi(R'(x)r_\theta + x')) d\theta \end{aligned}$$

Here we meet some of the effects as discussed earlier in Section 3.2.1. The derivative with respect to x_2 shows the same behavior as for the auxiliary problem on the plane and is continuous. The third term in $\partial_{x_3} I_{\mathcal{H}_{\text{ref}}}\varphi$ reflects the same behavior as for the auxiliary problem on the plane. Whereas the second term in $\partial_{x_3} I_{\mathcal{H}_{\text{ref}}}\varphi$ is far more interesting. Here the geometrical singularity situated on the surface of a cylinder around the boundary of the half plane is of exactly the same quality as discussed in Lemma 3.11. There we have already discussed its regularity and we again observe the one-sided singularity on the surface of the cylinder. Moreover, we can observe very nicely the interaction of these singularities in $\partial_{x_3} \theta(x_1, x_3)$, where both singularities, the singularity around the boundary of the half plane and the singularity perpendicular to the triangle face are combined.

Clearly, one can formulate the regularity in terms of countably normed spaces on the presented partition, but we want to delay this analysis and discuss the problem evaluated on a sector first. Note, that the analysis of a half plane also involves the regularity of the kernel $k_V(x-y)$, compare Section 3.2.1.

Auxiliary Problem: Sector

In order to study the effects, when the sphere meets a triangle edge in more detail, we restrict the analysis to a planar sector \mathcal{S}_{ref} with opening angle ω .

Assume, that the sector is the intersection of two half planes, such that the vertex of the sector lies in the origin.

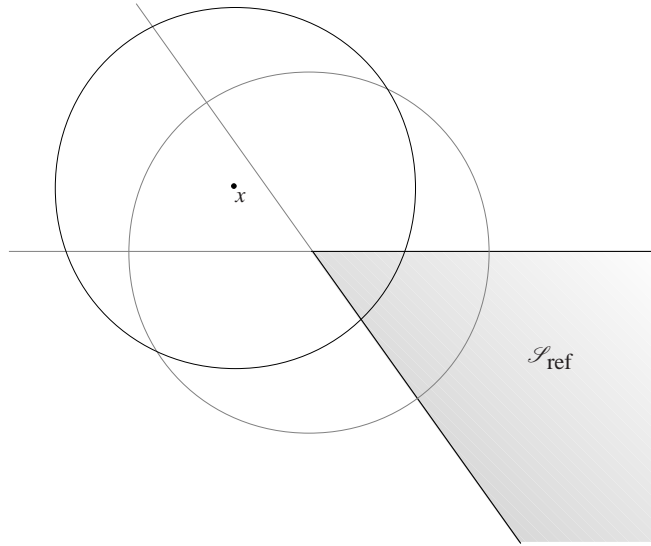


Fig. 3.12 Visualization of the intersection $\partial B_R(x) \cap \mathcal{S}_{\text{ref}}$.

Now the support of the regarded integral is the combination of two cylinders around the boundary of the half plane, a strip with height $2R$ with center-base \mathcal{S}_{ref} and a sphere around the origin. The behavior of the regarded integral within the cylinders and the strip follows directly from the two previous auxiliary problems and within the sphere, each ray of the sector is intersected only once, which again draws a strong connection to the behavior of $I_e^V \varphi$ as discussed in the last section.

We can construct the angular integration domain using the angles derived in the auxiliary problem of the half plane. We again observe the edge-vertex singularity known from Section 3.2.1 and additionally, the singularity parallel to the face of the sector. Thus the regularity has to be regarded in the decomposition induced by the intersection of the sphere around the sector origin, the cylinders around its edges and the unbounded prism with base \mathcal{S}_{ref} and height $2R$.

The behavior of the function is the same as discussed before, but one additional effect on the sector origin has to be regarded, namely in polar coordinates we obtain for $x = (0, 0, x_3)$

$$\lim_{x_3 \rightarrow \pm R} (I_{\mathcal{S}_{\text{ref}}} \varphi)(x) = \pm R k(\pm R n_T) \int_0^\omega \varphi(x') d\theta = \pm \omega R k(\pm R n_T) \varphi(x') \neq 0$$

which reflects the behavior parallel to the triangle edges with distance R .

Reference Triangle

Denote by T_{ref} the triangle with vertices $p_1 = (0, 0, 0)$, $p_2 = (1, 0, 0)$ and $p_3 = (0, 1, 0)$. Replacing the triangle plane by the triangle T_{ref} yields

$$(I_{T_{\text{ref}}} \varphi)(x) := \begin{cases} \frac{x_3}{R'(x)} \int_{T_{\text{ref}} \cap \partial B_R(x)} k_V(x-y) \varphi(y) ds_y & x \in E_R(T_{\text{ref}}) \setminus \bigcap_{i=1}^3 B_R(p_i) \\ 0 & \text{else} \end{cases}.$$

Again we introduce polar coordinates with respect to x' . In order to study the continuity of $(I_{T_{\text{ref}}} \varphi)(x)$ we have to consider the limits $(I_{T_{\text{ref}}} \varphi)(x)$ onto the boundary of its support $E_R(T_{\text{ref}}) \setminus \bigcap_{i=1}^3 B_R(p_i)$. First we analyze $(I_{T_{\text{ref}}} \varphi)(x)$ on $\partial E_R(T_{\text{ref}})$ and distinguish the following cases:

1. If $x \rightarrow \overline{T}_{\text{ref}} \pm Rn_T$ we can proceed as follows.

For $x' \in \text{int } T_{\text{ref}}$ there always exists a neighborhood of x' such that the intersecting circle lies within the triangle and thus we can directly apply the above results of Prop. 3.15 to obtain

$$\lim_{x_3 \rightarrow \pm R} (I_{T_{\text{ref}}} \varphi)(x) = \pm 2\pi R k(\pm Rn_T) \varphi(x')$$

2. If $x' = p_i$ for $i = 1, 2, 3$ there holds with the corresponding inner triangle angle ω_i

$$\lim_{x_3 \rightarrow \pm R} (I_{T_{\text{ref}}} \varphi)(x) = \pm R k(\pm Rn_T) \int_0^{\omega_i} \varphi(x') d\theta = \pm \omega_i R k(\pm Rn_T) \varphi(x') \neq 0$$

3. For $x' \in e_i$ we obtain

$$\lim_{x_3 \rightarrow \pm R} (I_{T_{\text{ref}}} \varphi)(x) = \pm R k(\pm Rn_T) \int_0^\pi \varphi(x') d\theta = \pm \pi R k(\pm Rn_T) \varphi(x') \neq 0$$

This behavior is also displayed in the numerical experiments in Chapter 3.3, compare Fig. 3.19.

If $x \rightarrow \partial E_R(T_{\text{ref}}) \setminus \{x : x \in \overline{T}_{\text{ref}} \pm R\}$ we take the limit onto the spheres and the surfaces of the cylinders without its caps building the boundary of $E_R(T_{\text{ref}})$ as discussed in Section 3.1. Consequently $x' \notin \overline{T}_{\text{ref}}$.

Studying now the interior boundary $\partial(\bigcap_{i=1}^3 B_R(p_i))$ of $\text{supp}(I_{T_{\text{ref}}} \varphi)$ one immediately verifies, that $(I_{T_{\text{ref}}} \varphi)(x) \rightarrow 0$ for $x \in \text{supp}(I_{T_{\text{ref}}} \varphi)$ and $x \rightarrow \partial(\bigcap_{i=1}^3 B_R(p_i))$, as the angular integration domain vanishes for all x .

Mapping the above results into a general triangle plane, we can formulate the following lemma

Lemma 3.16. *For $(I_T \varphi)(x)$ as specified in (3.16) on the exterior boundary of the support $\partial E_R(T)$ there holds for $x \in E_R(T) \setminus \bigcap_{i=1}^3 B_R(p_i)$*

$$\lim_{x \rightarrow \partial E_R(T)} (I_T \varphi)(x) = \pm \alpha(x') R k(\pm Rn_T) \varphi(x')$$

where

$$\alpha(x') = \begin{cases} 2\pi & x' \in \text{int } T \\ \pi & x' \in \{e_1, e_2, e_3\} \setminus \{p_1, p_2, p_3\} \\ \omega_i & x' = p_i (i = 1, 2, 3) \\ 0 & x' \notin \overline{T} \end{cases}$$

On the interior boundary $\partial(\bigcap_{i=1}^3 B_R(p_i))$ there holds for $x \in \text{supp}(I_T \varphi)$

$$\lim_{x \rightarrow \partial(\bigcap_{i=1}^3 B_R(p_i))} (I_T \varphi)(x) = 0.$$

Moreover, the gradient of $I_T \varphi$ has one-sided poles on the surface of the cylinders without its caps with axis e_i and jumps on the surfaces of the spheres with centers p_i .

Proof. Mapping the before discussed results on the reference triangle T_{ref} onto a general triangle T . □

Remark 3.17. If we now reduce the analysis to kernels $k_\nu(x-y) = |x-y|^\nu$ with $\nu \geq -1$, as it occurs for the discrete retarded single layer potential, it holds in Lemma 3.16 $k(\pm Rn_T) = R^\nu$.

At this point, we want to delay the analysis of the regularity of $I_T \varphi$ in terms of countably normed spaces in \mathbb{R}^3 and restricted to a plane \mathcal{E} to the next section. As some effects are similar to the results for $I_e^\nu \varphi$ discussed in the previous section, we need a partition of the regarded domains with respect to the spheres around the vertices and cylinders around the edges, which is introduced in the next section. Note that the critical domain corresponds to the yellow shaded triangles in Fig. 3.2.

3.2.3 Singularities of the Retarded Potential

Now, we are able to describe the singularity distribution of retarded potentials in the discrete light cone. Let us again consider the simplified potential (3.2). As we have seen in Section 3.2.1 and 3.2.2 a retarded potential possesses anisotropic singularities generated by the edge/vertex or the face of the triangle. These singularities are induced by the intersection of the triangle with the sphere $B_R(x)$, therefore, we call them in the following *geometrical light cone singularities*. They occur additional to the classical corner-edge singularities on the boundary of the element induced by the regularity of the integral kernel. Before we continue with the discussion of (3.2) let us summarize these different singularities.

Definition 3.18. Singularities on the boundary of a triangle T are called *classical corner/edge singularities*. We distinguish the geometrical light cone singularities in the following way. Singularities located on the wall of the cylinder of $\mathcal{C}_R(e)$ are called *cylindrical light cone singularities* and singularities located parallel to the triangle face with a distance R are called *plane light cone singularities*.

We have analyzed the triangle integral (3.6) and the edge function (3.5). Both cases result in a decomposition of the support of the integrals. Using Lemma 3.2 we conclude, that on the regarded decomposition elements all these regularities interfere. Thus we have a complicated structure of the overall decomposition of $E_R(T)$. In Fig. 3.2 two basic cases of the three-dimensional objects are plotted. One clearly observes the decomposition of the domain of influence $E_R(T)$ into the capsulars $C_R(e_i)$ of the triangle edges which include the spheres $B_R(p_i)$ around the triangle vertices p_i and its complement $E_R(T) \setminus \bigcup_{i=1}^3 C_R(e_i)$. We will not give the explicit decomposition of $E_R(T)$ as it has a very complicated structure and can have different numbers of subelements depending on the radius R as sketched in Fig. 3.14 and Fig. 3.13. We rather use the following abstract definition of the decomposition of $E_R(T)$.

Definition 3.19 (Partition of $E_R(T)$). Given a triangle T , define a disjoint decomposition of \mathbb{R}^3 through the (minimal) partition given by

$$\Theta_R(T) := \{A \subset \mathbb{R}^3 : A \cap B = A \text{ or } A \cap B = \emptyset \forall B \in \{E_R(T), C_R(e_i), B_R(p_i) : i = 1, 2, 3\}\} \quad (3.22)$$

where $C_R(e_i)$ is defined in (3.9) and $E_R(T)$ is given by (3.3).

Remark 3.20. (i) Note that, for $A_1, A_2 \in \Theta_R(T)$ it holds $A_1 \cap A_2 = \emptyset$ or $A_1 = A_2$.

(ii) Let us construct one explicit example of the decomposition $E_R(T)$. Assume $R > \text{diam} T$. Denote $B_i := B_R(p_i)$ and $C_i = C_R(e_i) \setminus \bigcup_{j \neq i} B_R(p_j)$. Then

$$\begin{aligned} E_R(T) &= E_R(T) \setminus \bigcup_{i=1}^3 C_R(e_i) \\ &\oplus B_1 \cap B_2 \cap B_3 \oplus C_1 \cap C_2 \cap C_3 \\ &\oplus B_1 \setminus C_R(e_1) \oplus B_2 \setminus C_R(e_2) \oplus B_3 \setminus C_R(e_3) \\ &\oplus C_1 \setminus B_1 \oplus C_2 \setminus B_2 \oplus C_3 \setminus B_3 \\ &\oplus (B_1 \cap B_2) \setminus B_3 \oplus (B_1 \cap B_3) \setminus B_2 \oplus (B_2 \cap B_3) \setminus B_1 \\ &\oplus C_1 \cap B_1 \oplus C_2 \cap B_2 \oplus C_3 \cap B_3 \end{aligned}$$

Let us first consider the behavior of $P_R \varphi$. In Fig. 3.2 the singularity distribution of $P_R \varphi$ is sketched in a three-dimensional plot. The cylindrical singularities are marked in red. The spheres are blue and the plane light cone singularities are shaded in yellow.

Proposition 3.21. Let $\varphi \in L^\infty(T)$.

- The integral (3.2) exists and defines a continuous function in \mathbb{R}^3 . Moreover, $P_R \varphi \in L^2(\mathbb{R}^3)$.
- The gradient of $P_R \varphi$ is singular on the edges and vertices of the triangle T and possesses a jump parallel to the triangle face with distance R . In its second derivatives P_R exhibits jumps on the surface of the spheres with centers in the vertices and radius R and one-sided singularities from the interior on the surface of the cylinders (without the caps) where the edges are the axis and the radius is R .

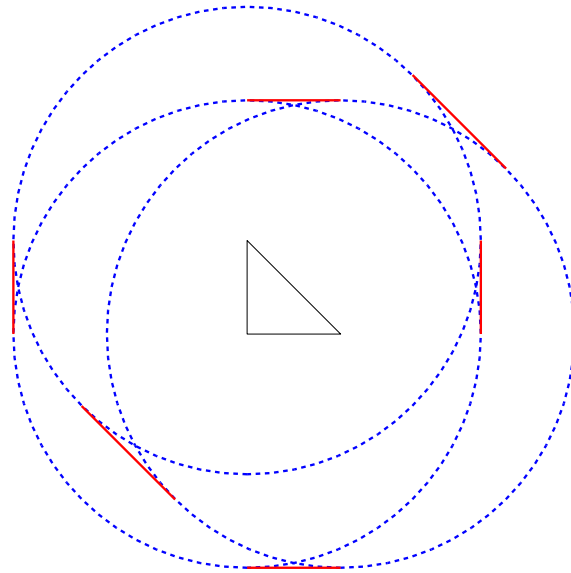
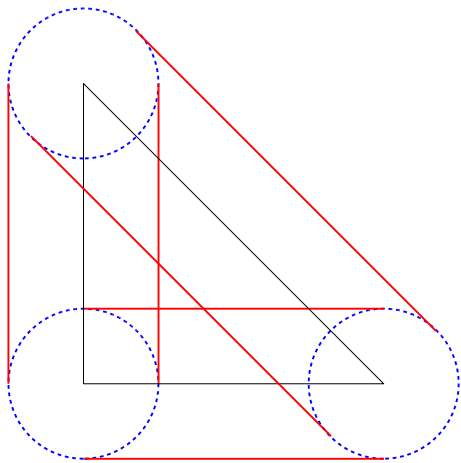
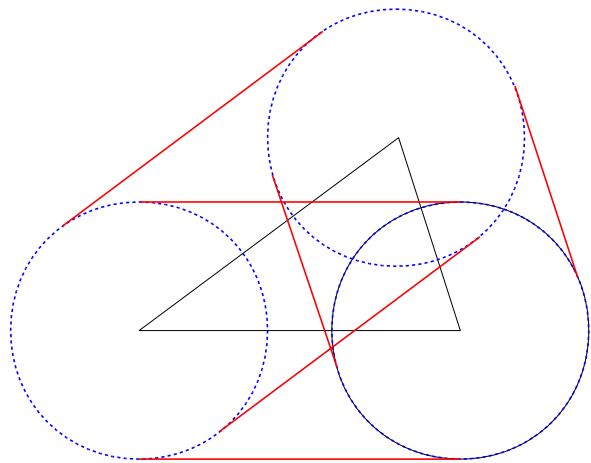


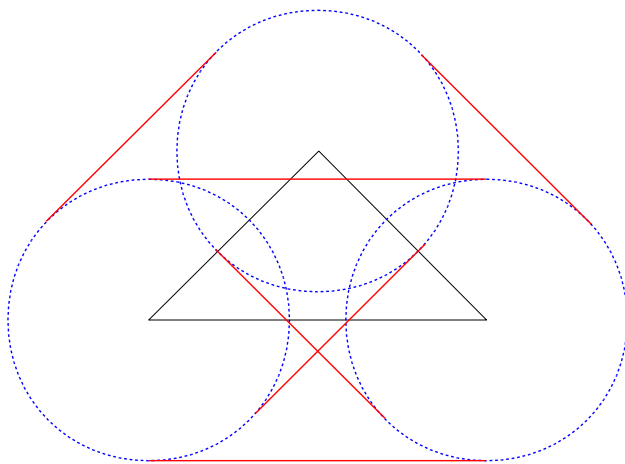
Fig. 3.13 Cross section of the domain of influence $E_R(T)$



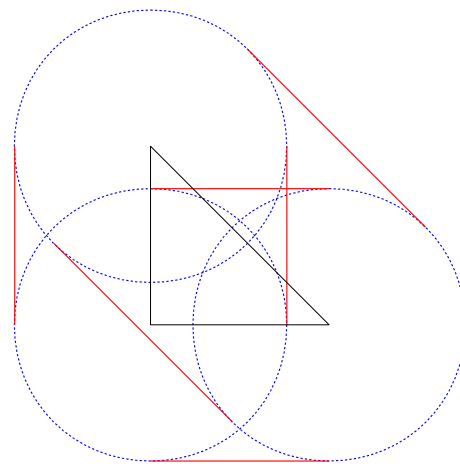
(a) $R < \text{diam}(T)$, Partition of $E_R(T)$ into 10 subelements.



(b) $R < \text{diam}(T)$, $|e_1| < R$, $|e_2| \geq R$ and $|e_3| \geq R$, Partition of $E_R(T)$ into 14 subelements.



(c) $R < \text{diam}(T)$, $|e_1| < R$, $|e_2| < R$ and $|e_3| \geq R$, Partition of $E_R(T)$ into 15 subelements.



(d) $R \geq \text{diam}(T)$, Partition of $E_R(T)$ into 14 subelements.

Fig. 3.14 Cross section of the domain of influence $E_R(T)$ with the triangle plane for different radii R .

Proof. The proof of part (a) results directly from the classical boundary integral.

For weakly singular kernels, we can apply the results of the classical single layer potential

$$\tilde{P}\varphi(x) := \int_T k_V(x-y)\varphi(y) ds_y.$$

Theorem 3.35 in [48] states the existence and the continuity of $\tilde{P}(x)$. In the proof the domain of integration is split into a neighborhood of x and its complement. Now $B_R(x)$ is such a neighborhood and thus, as the integral exists and is shown to be continuous on Lipschitz continuous surfaces, we can transfer the result to $(P_R\varphi)(x)$.

Note, $P_R\varphi$ has a bounded support $E_R(T)$, whose closure is compact and thus

$$\|P_R\varphi\|_{L^2(\mathbb{R}^3)}^2 = \|P_R\varphi\|_{L^2(E_R(T))}^2$$

Part (b) is a consequence of Lemma 3.2 and the behavior of $I_T\varphi$ and $I_{e_i}\varphi$ as discussed in Lemma 3.16 and 3.11, respectively. \square

Let us now formulate the regularity of the simplified retarded potential (3.2).

Theorem 3.22. *Given a triangle T and a plane \mathcal{E} . For each $A \in \Theta_R(T)$ there exists a decomposition of $A \cap \mathcal{E}$ such that there exists only one type of singularity per subelement $A' \cap \mathcal{E}$.*

- *For a cylindrical singularity w.r.t. edge e_i there holds in a local coordinate system (ξ_1, ξ_2) defined according to Lemma 3.9*

$$P_R\varphi \in B_\beta^2(A' \cap \mathcal{E}),$$

where $\beta \in (0, 1)$ and the weight function is located on the cylinder wall of $C_R(e_i)$. The orientation of plane \mathcal{E} defines exactly one of the three cases discussed in Lemma 3.9.

- *For a planar singularity there holds in a local cartesian coordinate system (ξ_1, ξ_2) defined according to Lemma 3.13*

$$P_R\varphi \in B_\beta^2(A' \cap \mathcal{E}),$$

where $\beta \in (0, 1)$ and the weight function is located in the planes parallelly shifted to the triangle plane \mathcal{E}_T by R . The singularities if present are located on line segments.

- *for a classically known kernel singularity w.r.t. edge e_i in a local coordinate system (ξ_1, ξ_2) with*

$$P_R\varphi \in B_\beta^{l_{ker}}(A' \cap \mathcal{E}),$$

where $\beta \in (0, 1)$ and the weight function is located on the edge e_i .

Proof (of Theorem 3.22). Due to Lemma 3.2 and Theorem 3.4 we know that by analyzing the corresponding functions $I_{e_i}\varphi$ and $I_T\varphi$, we fully describe the regularity of $P_R\varphi$. Das $I_{e_i}\varphi$ and $I_T\varphi$ describe the derivatives of $P_R\varphi$, we win one order of regularity if we regard $P_R\varphi$. We combine the results of Lemma 3.10 and 3.13 for $I_e^V\varphi$ and $I_T\varphi$ to a regularity result for $P_R\varphi$ as due to Lemma 3.2 both of the functions influence the gradient of $P_R\varphi$. Due to the jumps in the first and second derivatives of $P_R\varphi$ on the interfaces between the elements of the decomposition $\Theta_R(T)$, we again can only locally describe its regularity on the elements $A \in \Theta_R(T)$. As already discussed in Lemma 3.10 we have the additional influence of the classically known kernel singularities. Here they are based on the edges of the triangle T . The edge of T not only define such a classically known kernel singularity, but each of these edges e_i moreover define a (cylindrical) geometrical singularity located on a the wall of the cylinder with radius R and axis e_i . Thus we have three times the effects of the analysis of the edge integral $I_e^V\varphi$. We can adopt the arguments used in Lemma 3.10, but the regularity can only be described in local coordinate systems (ξ_1, ξ_2) depending on the edge generating the specific type of singularity and the orientation of the plane \mathcal{E} , compare Lemma 3.9 and 3.13.

Let $A \subset A' \in \Theta_R(T)$. Subdivide $A \cap \mathcal{E}$ until there exists only one kind of singularity per element corresponding to a cylindrical, a planar or a classically known singularity. Thus we have elements with possibly circular, elliptic or straight edges, that possess either a point singularity in one of the corners of the element or a singularity located on one part of the boundary edges or no singularity at all. Note that all geometrical singularities have a cut-off behavior, i.e. the singularity based on a line segment is only one-sided.

□

3.2.4 Complete Retarded Potential

Let us finally comment on the full retarded potential (3.1) for $r_{\min} > 0$. In Fig. 3.15 we sketch its singularity distribution in the triangle plane. Clearly, this is again a three-dimensional object. Its support is the gray shaded domain in Fig. 4.1(a) and also referred to as domain of influence of the triangle T . In the following lemma, we analyze the geometrical description of this domain of influence.

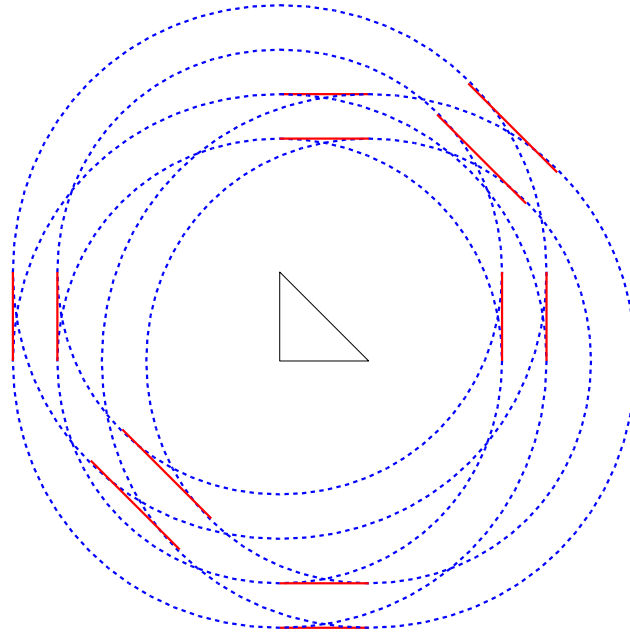


Fig. 3.15 Singularity distribution of (3.1) for $r_{\min} > 0$ in the triangle plane.

Lemma 3.23. *Let $r_{\max} > r_{\min} \geq 0$. There holds*

$$E(T) = E_{r_{\max}}(T) \setminus \bigcap_{i=1}^3 B_{r_{\min}}(p_i),$$

where $E_{r_{\max}}(T) := \{y \in \mathbb{R}^3 : |x - y| \leq r_{\max} \text{ and } x \in T\}$.

Proof. It holds

$$\begin{aligned} E_{r_{\max}}(T) &:= \{y \in \mathbb{R}^3 : |x - y| \leq r_{\max} \text{ and } x \in T\} = \bigcup_{x \in T} \overline{B_{r_{\max}}(x)} \\ E(T) &:= \{y \in \mathbb{R}^3 : r_{\min} \leq |x - y| \leq r_{\max} \text{ and } x \in T\} = \bigcup_{x \in T} (\overline{B_{r_{\max}}(x)} \setminus B_{r_{\min}}(x)). \end{aligned}$$

Now, as $E(T) \subseteq E_{r_{\max}}(T)$ we can write $E(T) = E_{r_{\max}}(T) \setminus (E_{r_{\max}}(T) \setminus E(T))$ and compute

$$\begin{aligned}
y \in E_{r_{\max}}(T) \setminus E(T) &\Leftrightarrow y \in \bigcup_{x \in T} \overline{B_{r_{\max}}(x)} \wedge y \notin \bigcup_{x \in T} (\overline{B_{r_{\max}}(x)} \setminus B_{r_{\min}}(x)) \\
&\Leftrightarrow \left(\exists x \in T : y \in \overline{B_{r_{\max}}(x)} \right) \wedge \neg \left(\exists x \in T : y \in (\overline{B_{r_{\max}}(x)} \setminus B_{r_{\min}}(x)) \right) \\
&\Leftrightarrow \left(\exists x \in T : y \in \overline{B_{r_{\max}}(x)} \right) \wedge \left(\forall x \in T : y \notin (\overline{B_{r_{\max}}(x)} \setminus B_{r_{\min}}(x)) \right) \\
&\Leftrightarrow \left(\exists x \in T : y \in \overline{B_{r_{\max}}(x)} \right) \wedge \left([\forall x \in T : y \in B_{r_{\max}}^c(x)] \vee [\forall x \in T : y \in B_{r_{\min}}(x)] \right) \\
&\Leftrightarrow \left(\left(\exists x \in T : y \in \overline{B_{r_{\max}}(x)} \right) \wedge (\forall x \in T : y \in B_{r_{\min}}(x)) \right) \\
&\Leftrightarrow (\forall x \in T : y \in B_{r_{\min}}(x)) \\
&\Leftrightarrow y \in \bigcap_{x \in T} B_{r_{\min}}(x),
\end{aligned}$$

where we used $B_{r_{\min}}(x) \subset B_{r_{\max}}(x)$. Thus it follows $E(T) = E_{r_{\max}}(T) \setminus \bigcap_{x \in T} B_{r_{\min}}(x)$.

As T is convex, the intersection of all spheres with center $x \in T$ and radius r_{\min} equals the intersection of the spheres whose centers are the vertices p_i of T , such that

$$\bigcap_{x \in T} B_{r_{\min}}(x) = \bigcap_{i=1}^3 B_{r_{\min}}(p_i).$$

□

Remark 3.24. Note that for $r_{\min} < \frac{1}{2} \max_i |e_i|$ we have $E(T) = E_{r_{\max}}(T)$, i.e. T fully illuminates itself.

Next, we describe the quality of the singularities of (3.1). Note, that all singularities duplicate as sketched in Fig. 3.15.

Proposition 3.25. *Let $\varphi \in L^\infty(T)$.*

- a) *The integral (3.1) exists and defines a continuous function in \mathbb{R}^3 .*
- b) *The gradient of $P\varphi$ is singular on the edges and vertices of the triangle T and possesses jumps parallel to the triangle face with distance r_{\min} and r_{\max} . In its second derivatives P exhibits jumps on the surface of the spheres with centers in the vertices and radii r_{\min} and r_{\max} and one-sided singularities from the interior on the surface of the cylinders (without the caps) where the edges are the axis and the radii are r_{\min} and r_{\max} .*

Proof. Due to (3.1) it holds

$$(P\varphi)(x) = (P_{r_{\max}}\varphi)(x) - (P_{r_{\min}}\varphi)(x)$$

and thus the assertions is a consequence of proposition 3.21 applied to $P_{r_{\max}}\varphi$ and $P_{r_{\min}}\varphi$. □

In order to give a regularity result of the retarded potential reduced to a plane \mathcal{E} , let us first define the natural decomposition of \mathbb{R}^3

$$\Theta_{r_{\min}}^{r_{\max}}(T) := \{A \subset \mathbb{R}^3 : A \cap B = A \text{ or } A \cap B = \emptyset \forall B \in \{\Theta_{r_{\min}}(T), \Theta_{r_{\max}}(T)\}\}. \quad (3.23)$$

An example of this decomposition intersected with the triangle plane is sketched in Fig. 3.15. We describe the regularity of the retarded potential $P\varphi$ as defined in (3.1) in the following theorem.

Theorem 3.26. *Given a triangle T and a plane \mathcal{E} . For each $A \in \Theta_{r_{\min}}^{r_{\max}}(T)$ there exists a decomposition of $A \cap \mathcal{E}$ such that there exists only one type of singularity per subelement $A' \cap \mathcal{E}$.*

- *For a cylindrical singularity w.r.t. edge e_i and radius R there holds in a local coordinate system (ξ_1, ξ_2) defined according to Lemma 3.9*

$$P\varphi \in B_\beta^2(A' \cap \mathcal{E}),$$

where $\beta \in (0, 1)$ and the weight function is located on the cylinder wall of $C_R(e_i)$. The orientation of plane \mathcal{E} defines exactly one of the three cases discussed in Lemma 3.9 and either $R = r_{\min}$ or $R = r_{\max}$.

- For a planar singularity there holds in a local cartesian coordinate system (ξ_1, ξ_2) defined according to Lemma 3.13

$$P\varphi \in B_\beta^2(A' \cap \mathcal{E}),$$

where $\beta \in (0, 1)$ and the weight function is located in the planes parallelly shifted to the triangle plane \mathcal{E}_T by R . The singularities if present are located on line segments and either $R = r_{\min}$ or $R = r_{\max}$.

- for a classically known kernel singularity w.r.t. edge e_i in a local coordinate system (ξ_1, ξ_2) with

$$P\varphi \in B_\beta^{l_{ker}}(A' \cap \mathcal{E}),$$

where $\beta \in (0, 1)$ and the weight function is located on the edge e_i .

Proof. As we have seen in the very beginning of this chapter in (3.1) it holds

$$(P\varphi)(x) = (P_{r_{\max}}\varphi)(x) - (P_{r_{\min}}\varphi)(x)$$

such that we can apply Theorem 3.22 and on the induced decomposition of the regarded plane, we obtain the piecewise defined regularity description. On the composition of all spheres $B_{r_{\min}}(p_i)$ the retarded potential behaves like the classical time independent potential and thus, the two terms cancel out, which is also confirmed by Lemma 3.23. \square

3.3 Numerical Experiments

In this section, we use the numerical evaluation of retarded potentials as discussed in Chapter 4.1. Given a reference triangle T with vertices $p_1 = (0, 0, 0)^T$, $p_2 = (1, 0, 0)^T$ and $p_3 = (0, 1, 0)^T$.

3.3.1 High Resolution Plots on a Line

Let $R > 0$. We analyze the simplified retarded potential (3.2) with piecewise constant trial functions, i.e. $\varphi(y) = 1$ on T . In the following, high resolution plots along different lines for different kernel functions $k_\nu(x - y) = |x - y|^\nu$ of the potential and its directional derivative are presented. We observe the behavior discussed earlier in this section.

In the Triangle Plane

Consider first the bisecting line $\mathbf{d} = \gamma(1, 1, 0)^T$ with $\gamma \in \mathbb{R}$ in the triangle plane \mathcal{E}_T . In Fig. 3.16 the singularity distribution in \mathcal{E}_T is sketched. Using a high resolution we aim to compute the potential and the directional derivative of the simplified potential (3.2) for different kernel functions $k_\nu(x - y) = |x - y|^\nu$ with $\nu = -1$ and $\nu = 0$. Choose $R = 0.2$. In Fig. 3.17(a) and 3.17(b) the potential and the directional derivative are plotted for $\nu = -1$ and in Fig. 3.17(c) and 3.17(d) one finds the corresponding data for $\nu = 0$, both plotted over the signed distance $d(\mathbf{x}) := \mathbf{x} \cdot \mathbf{d}/|d|$ to the origin. In \mathbf{x}_1 the domain of influence $E_R(x_1)$ first meets the triangle T . Here the potential and its directional derivative are continuous for $\nu = 0$ and $\nu = -1$ as expected (cf. Fig. 3.17(a) and 3.17(c)). Fig. 3.17(b) clearly displays the classical singularities on the triangle edges and vertices due to the weakly singular kernel in \mathbf{x}_2 and \mathbf{x}_6 . The singularity in \mathbf{x}_3 can not be observed separately as it is superposed by the stronger singularities in \mathbf{x}_4 . For all points on \mathbf{d} between \mathbf{x}_4 and \mathbf{x}_5 the domain of integration is T and thus constant. For \mathbf{x}_5 and \mathbf{x}_7 we again observe a bend in the directional derivative, which indicates the singularity in the second derivative.

The singularities in \mathbf{x}_1 , \mathbf{x}_3 , \mathbf{x}_4 , \mathbf{x}_5 and \mathbf{x}_7 are indeed of geometrical nature which becomes clear, as we observe a similar behavior for k_0 and k_{-1} . Thus they are independent of the regularity of the kernel function k .

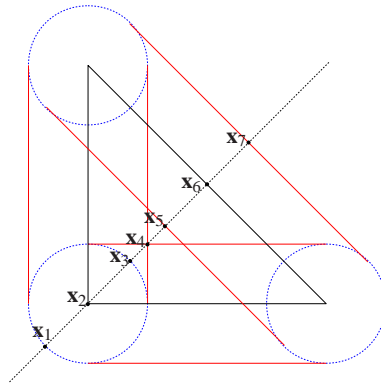


Fig. 3.16 High resolution plot on dashed black line of simplified retarded potential (3.2).

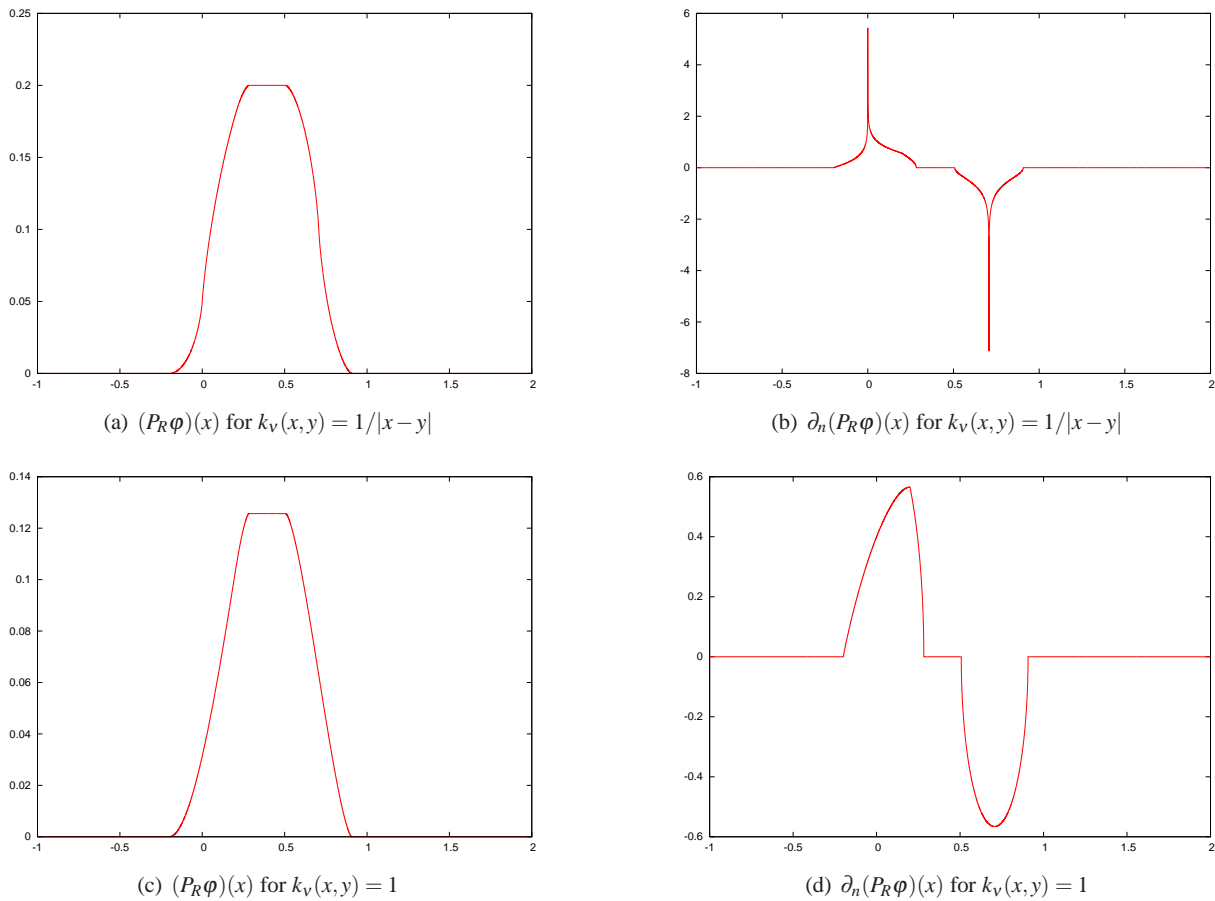


Fig. 3.17 High resolution plots on the line along $(1, 1, 0)^T$.

Perpendicular to the Triangle Plane

If we plot the discrete retarded potential (3.2) and its directional derivative along a line perpendicular to the triangle plane, we can nicely observe the jumps in the first derivatives of $(P_R\varphi)(x)$ as they were predicted in Lemma 3.16. In Fig. 3.18 we compare the size of the jumps for different kernel functions k_ν and in Fig. 3.19 we study the case of a line intersecting a vertex and edge of the triangle.

Let $R = 0.2$. $(P_R\varphi)(x)$ is continuous for $\nu = -1$ and $\nu = 0$, compare Fig. 3.18(a) and Fig. 3.18(c). In Fig. 3.18(b) we observe a jump of size 1 in $x_3 = \pm R$, which corresponds to the results of Lemma 3.16. Note that the kernel is multiplied by $1/2\pi$ and $\nu = -1$. For $\nu = 0$ we observe a jump of size $2\pi R$ in $x_3 = \pm R$.

Choose now $R = 0.5$. We regard the directional derivative perpendicular to the triangle plane for a kernel function with $\nu = 0$. Fig. 3.19(a) verifies that the directional derivative of $(P_R\varphi)(x)$ possesses a jump of size $\omega_1 R$ in $x_3 = \pm R$ on a line perpendicular to the triangle plane through p_1 with angle $\omega_1 = \pi/2$. On a line passing perpendicular through an edge as displayed in Fig. 3.19(b) we observe the expected jump of size πR .

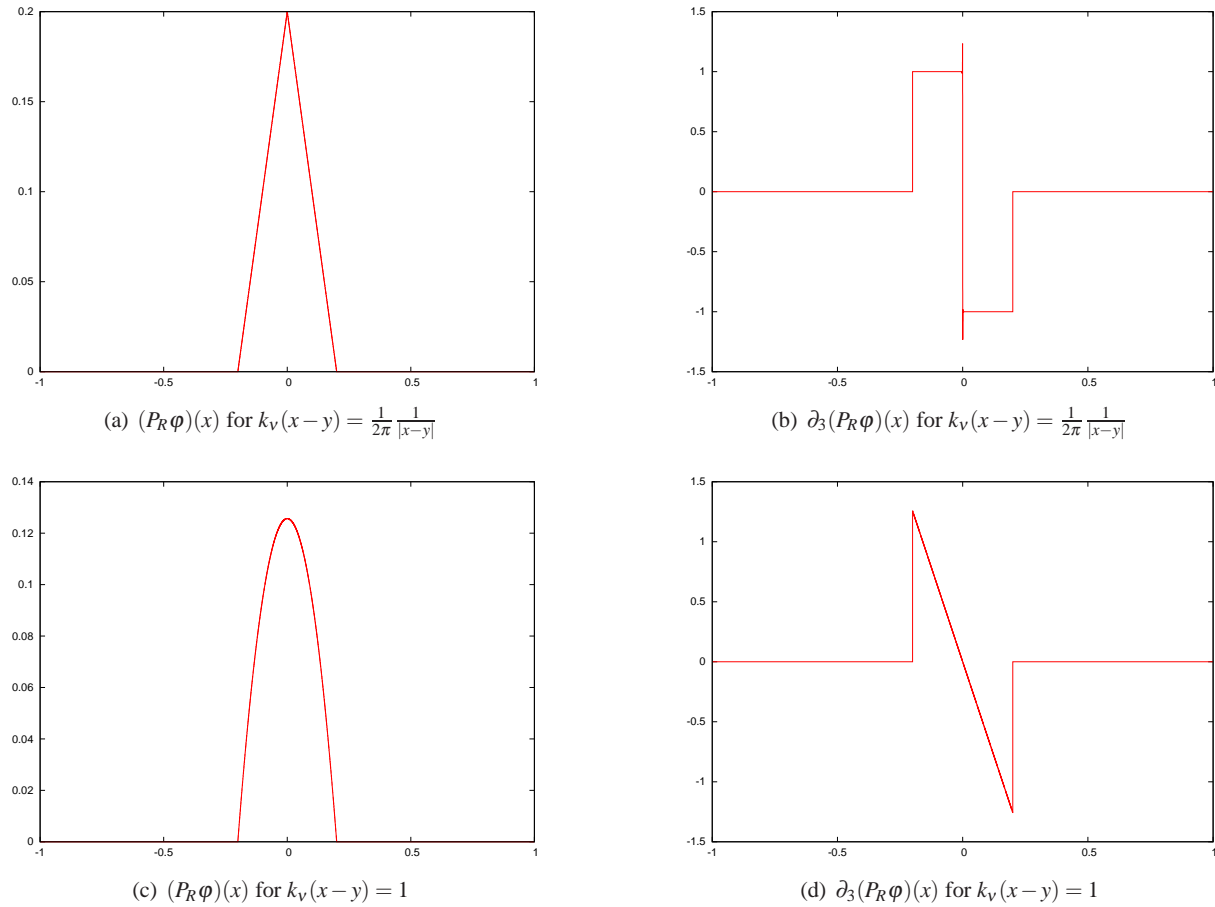


Fig. 3.18 High resolution plots on the line $x = (0.25, 0.25, 0) + s(0, 0, 1)$ ($s \in [-1, 1]$), $r_{\min} = 0$ and $r_{\max} = 0.2$. We plot $(P_R\varphi)$ and $\partial_3(P_R\varphi)$ over x_3 for different kernels k and constant basis functions on the reference triangle T .

3.3.2 Contour Plots of the Retarded Potential in Different Planes

In this subsection we focus on the weakly singular kernel $k_\nu(x - y) = |x - y|^{-1}$. We analyze the discrete retarded potential (3.1) and its gradient within different planes parallel and perpendicular to the triangle plane \mathcal{E}_T . In contrast to the high resolution plots on different lines we will focus also on the case $r_{\min} > 0$ and the change of the minimal and maximal radius, where we fix $r_{\max} - r_{\min} = \Delta t$.

In Fig. 3.20 and 3.21 we focus on the evaluation of the discrete retarded potential (3.1) with $\Delta t = 0.3$ in the triangle plane \mathcal{E}_T . The potential itself is continuous, but we clearly observe the expected singularities. In the right picture of Fig. 3.20(a) we note the classical corner and edge singularities on the boundary of the triangle due to the singular kernel function.

In the gradient plots of $P(x)$ for $r_{\min} > 0$ the contour levels become dense parallel to the triangle edges with distance r_{\min} and r_{\max} as sketched in Fig. 3.15 indicating the geometrical light cone singularities as discussed in Theorem 3.26. Moreover we clearly observe, how the discrete retarded potential moves over the triangle plane for increasing radii. In Fig. 3.22 an additional surface plot of the absolute gradient of $P(x)$ finally draws the attention to the steep growth close to the geometrical light cone singularities.

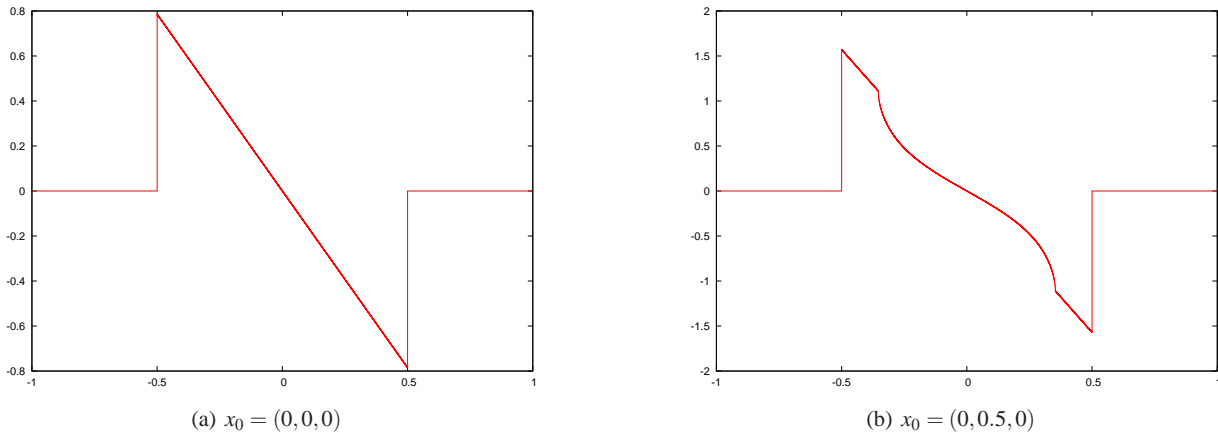


Fig. 3.19 High resolution plots on the line $x = x_0 + s(0, 0, 1)$ ($s \in [-1, 1]$), $r_{\min} = 0$ and $r_{\max} = 0.5$. We plot $\partial_3(P_R\varphi)$ over x_3 for $k_V(x-y) = 1$ and constant basis functions on the reference triangle T .

As we have discussed earlier in this chapter and sketched in Fig. 3.2 the support of $P(x)$ is a three-dimensional object, namely the domain of influence $E(T)$. In order to underline this fact, in Fig. 3.23 we plot the absolute gradient of the potential in four planes parallel to \mathcal{E}_T with different distances x_3 to \mathcal{E}_T .

We see how for increasing x_3 the singularities squeeze together and how for $x_3 = 2.0$ the singularities due to r_{\min} vanish as they have smaller support.

Finally, we want to focus on the strongest geometrical light cone singularity, the jump parallel to the triangle. Fix $r_{\min} = 1.9$ and $r_{\max} = 2.1$. In Fig. 3.24 contour plots of the potential and its derivative $\partial_3 P$ in the plane perpendicular to the triangle plane \mathcal{E}_T with $x_1 = 0.25$ are plotted and we clearly observe the singularities due to the first term in Lemma 3.2 as analyzed in Lemma 3.16. The jumps occur in the first derivatives and are therefore stronger as the singularities due to the second term in 3.2, this is the reason, why they do not show so clearly as in the figures before.

3.4 Technical Results

Lemma 3.27. Let $f_n(t) = \int (t^2 + a^2)^{n/2} dt$ for $n \geq -1$. It holds

$$f_{2j+1}(t) = \frac{(2j+1)!!}{(2j+2)!!} \left(\sum_{k=0}^j \frac{(2(j-k))!!}{2(j-k+1)!!} a^{2k} g_{2(j-k)+1}(t) + a^{2j+2} f_{-1}(t) \right) \quad (3.24)$$

$$f_{2j+2}(t) = \frac{(2j+2)!!}{(2j+3)!!} \sum_{k=0}^{j+1} \frac{(2(j-k)+1)!!}{(2(j-k)+2)!!} a^{2k} g_{2(j-k)+2}(t) \quad (3.25)$$

for $j \geq 0$, where $g_n(t) := t(t^2 + a^2)^{n/2}$ and

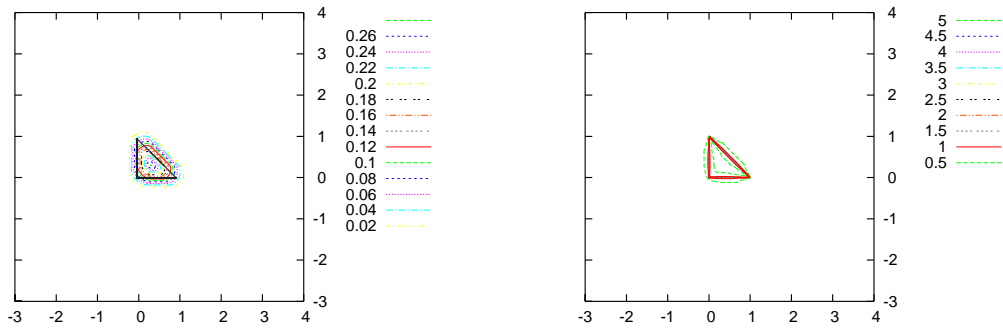
$$f_{-1}(t) = \operatorname{arsinh} \frac{t}{a} = \ln(t + \sqrt{t^2 + a^2}).$$

Proof. Let us first prove the following recurrence formulas

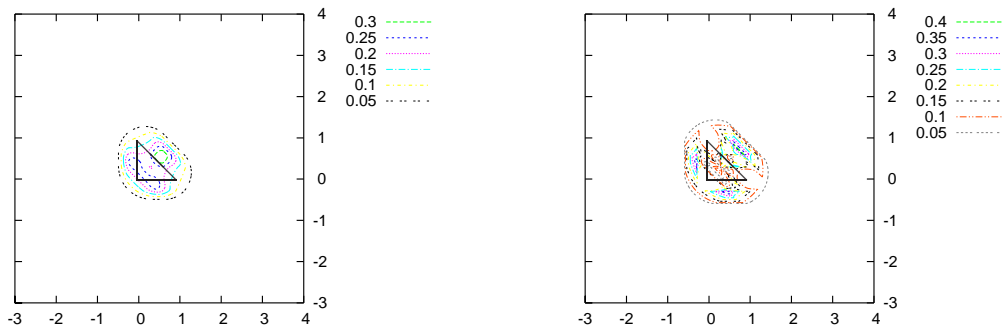
$$f_{2j+1}(t) = \frac{1}{2j+2} \left[t(t^2 + a^2)^{\frac{2j+1}{2}} + (2j+1)a^2 f_{2j-1}(t) \right], \quad (3.26)$$

$$f_{2j+2}(t) = \frac{1}{2j+3} \left[t(t^2 + a^2)^{j+1} + 2(j+1)a^2 f_{2j}(t) \right]. \quad (3.27)$$

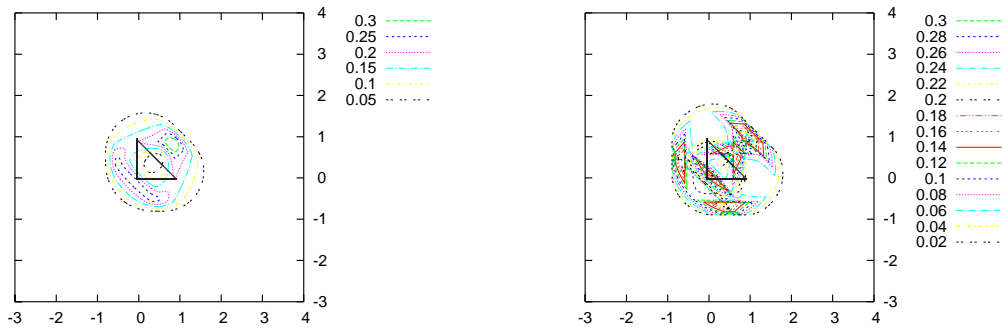
If $n = 2j - 1$, there holds



(a) $r_{\min} = 0, r_{\max} = 0.3$



(b) $r_{\min} = 0.3, r_{\max} = 0.6$



(c) $r_{\min} = 0.6, r_{\max} = 0.9$

Fig. 3.20 $P(x)$ (left) and $|\nabla P(x)|$ (right) are plotted for increasing radii r_{\min} and r_{\max} for points x in the triangle plane \mathcal{E}_T . All computations were done on the reference triangle T .

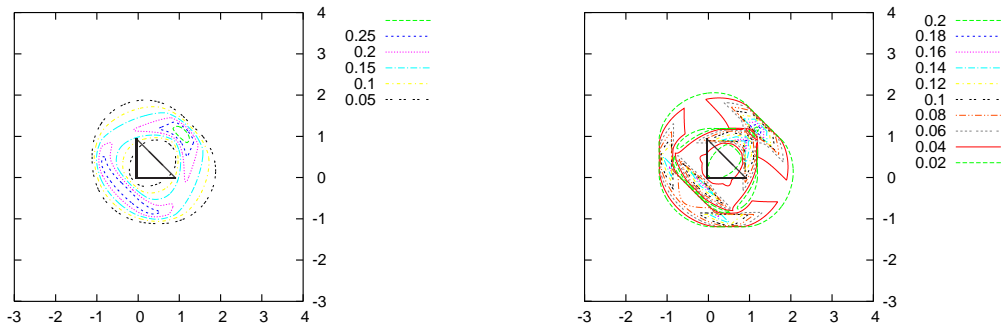
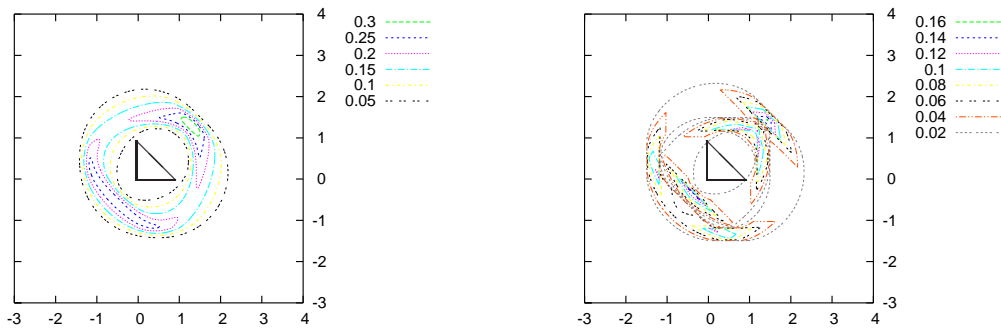
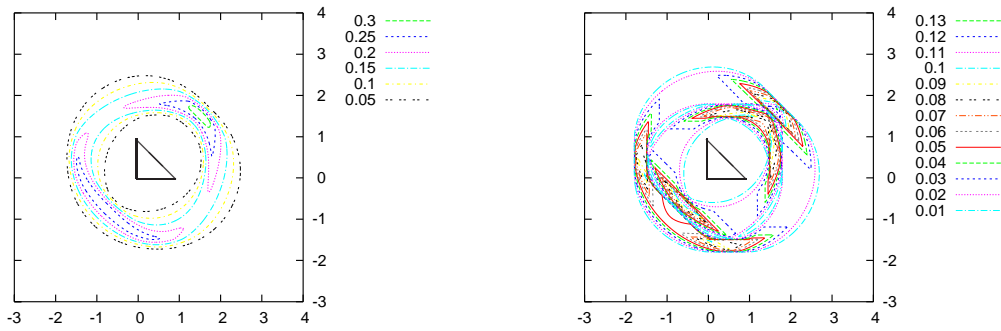
(a) $r_{\min} = 0.9, r_{\max} = 1.2$ (b) $r_{\min} = 1.2, r_{\max} = 1.5$ (c) $r_{\min} = 1.5, r_{\max} = 1.8$

Fig. 3.21 $P(x)$ (left) and $|\nabla P(x)|$ (right) are plotted for increasing radii r_{\min} and r_{\max} for points x in the triangle plane \mathcal{E}_T . All computations were done on the reference triangle T . Continuation of Fig. 3.20.

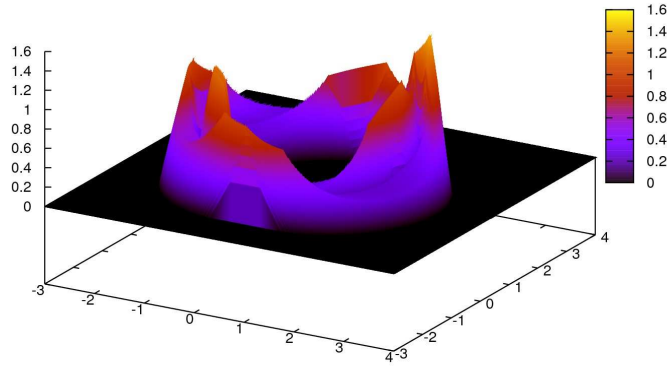


Fig. 3.22 Surface plot of the absolute value of the retarded potential on the reference triangle T .

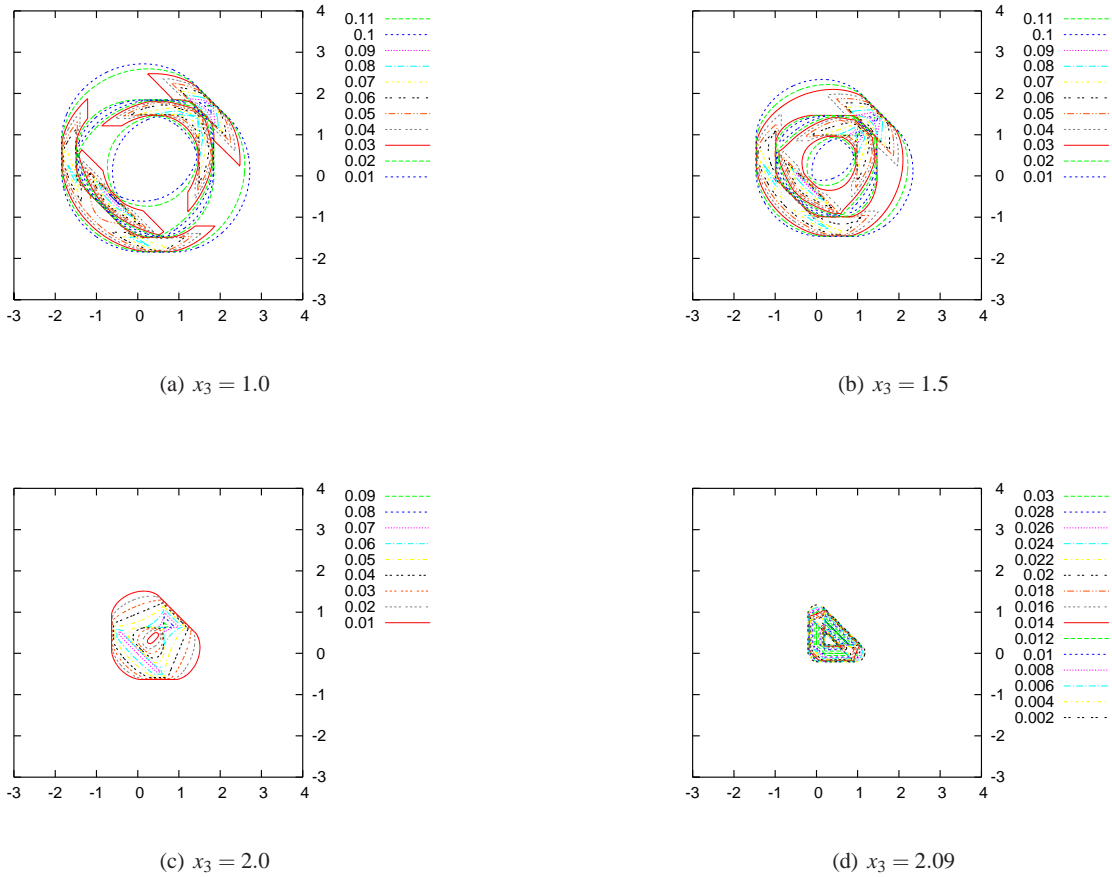


Fig. 3.23 Contour plots of $|\nabla P(x)|$ with fixed $r_{\min} = 1.8$, $r_{\max} = 2.1$ for points in a plane with distance x_3 to the triangle plane.

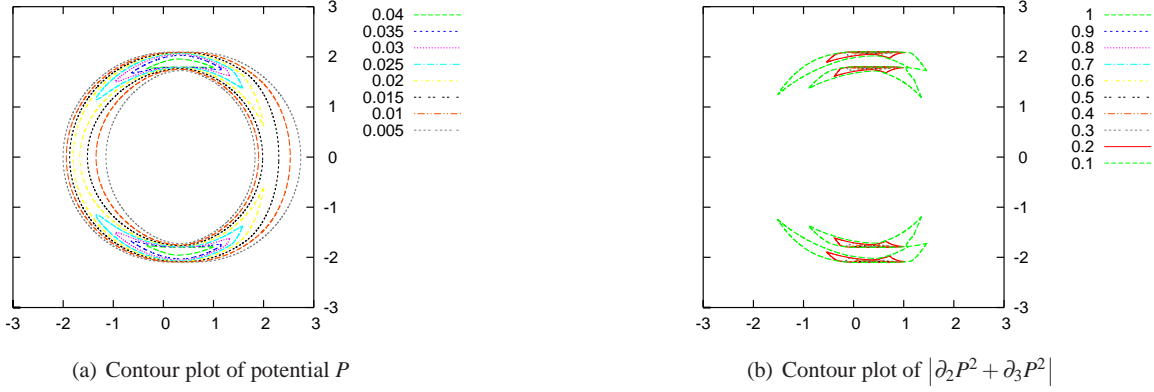


Fig. 3.24 $r_{\min} = 1.9$ and $r_{\max} = 2.1$. Contour plots for $x_1 = 0.25$

$$\begin{aligned} \partial_t(t^2 + a^2)^{\frac{2j+1}{2}} &= (t^2 + a^2)^{\frac{2j+1}{2}} + (2j+1)t^2(t^2 + a^2)^{\frac{2j-1}{2}} \\ &= (2j+2)(t^2 + a^2)^{\frac{2j+1}{2}} - (2j+1)a^2(t^2 + a^2)^{\frac{2j-1}{2}}. \end{aligned}$$

Integration with respect to t yields (3.26). For $n = 2j$ we obtain (3.27) with

$$\begin{aligned} \partial_t(t^2 + a^2)^{j+1} &= (t^2 + a^2)^{j+1} + 2(j+1)t^2(t^2 + a^2)^j \\ &= (2j+3)(t^2 + a^2)^{j+1} - 2(j+1)a^2(t^2 + a^2)^j. \end{aligned}$$

Summarizing for arbitrary $n \geq 1$ it holds

$$f_n(t) = \frac{1}{n+1} (g_n(t) + na^2 f_{n-2}(t))$$

Now, we can prove the desired relations by induction. First for odd indices for $j = 0$ (3.24) immediately follows from (3.26) and

$$\begin{aligned} f_{2j+3}(t) &= \frac{1}{2j+4} [g_{2j+3}(t) + (2j+3)a^2 f_{2j+1}(t)] \\ &= \frac{1}{2j+4} \left[g_{2j+3}(t) + \frac{2j+3}{2j+2} \left(\frac{(2j+1)!!}{(2j)!!} \sum_{k=0}^j \frac{(2(j-k))!!}{(2(j-k)+1)!!} a^{2k+2} g_{2(j-k)+1}(t) \right) \right. \\ &\quad \left. + \frac{(2j+3)!!}{(2j+2)!!} a^{2j+4} f_{-1}(t) \right] \\ &= \frac{1}{2j+4} \left[\frac{(2j+3)!!}{(2j+2)!!} \sum_{k=0}^{j+1} \frac{(2(j-k)+2)!!}{(2(j-k)+3)!!} a^{2k} g_{2(j-k)+3}(t) + \frac{(2j+3)!!}{(2j+2)!!} a^{2j+4} f_{-1}(t) \right], \end{aligned}$$

which finishes the proof for (3.24). For even indices it works quite similar. For $j = 0$ (3.27) validates the result and

$$\begin{aligned} f_{2j+4}(t) &= \frac{1}{2j+5} [g_{2j+4}(t) + (2j+4)a^2 f_{2j+2}(t)] \\ &= \frac{1}{2j+5} \left[g_{2j+4}(t) + (2j+4) \left(\frac{(2j+2)!!}{(2j+3)!!} \sum_{k=0}^{j+1} \frac{(2(j-k)+1)!!}{(2(j-k)+2)!!} a^{2k} g_{2(j-k)+2}(t) \right) \right] \\ &= \frac{1}{2j+5} \left[\frac{(2j+4)!!}{(2j+3)!!} \sum_{k=0}^{j+2} \frac{(2(j-k)+3)!!}{(2(j-k)+4)!!} a^{2k} g_{2(j-k)+4}(t) \right] \end{aligned}$$

yield (3.25). Note that $g_0(t) = f_0(t)$. □

Chapter 4

A Composite Quadrature Rule for Retarded Potentials

Quadrature rules for time independent boundary integrals and the corresponding Galerkin entries have been studied intensively, see e.g. [47, 49, 48, 51, 43]. The authors follow different approaches for the numerical computation of the weakly singular integrals. A quadrature scheme for the boundary integral or potential is presented in [51] and analyzed using countably normed spaces. A graded quadrature towards the point singularity of the potential is introduced. In [43] Mund adopts this scheme by separating the inner and the outer integration and applying a grading in the outer integral towards the edges of the elements. Schwab and Sauter [49] employ relative coordinates in order to lift the singularity of the kernel function using a Duffy trick, which results in a stable and reliable quadrature scheme. They do not evaluate the inner and the outer integral separately, but solve the problem in one step applying a four dimensional tensor product quadrature rule. In [13] the idea of relative coordinates is adopted to an analysis using Gevrey classes. There also exist many approaches for the fast numerical evaluation of boundary integrals, e.g. in the context of hierarchical matrices [24]. These methods use the decay of the kernel function and the separation in near and far field. This is not easily adopted for retarded potentials because, as we have seen in Chapter 3 there exist geometrically distributed singularities that also occur in the far field.

To our knowledge, the numerical evaluation of retarded potentials and their discrete space-time Galerkin entries have not undergone a rigorous error analysis. In [53] the analytical evaluation of the discrete retarded potentials is discussed, but not the corresponding matrix entry.

In this chapter, we apply the results of Chapter 3 and construct a quadrature rule for the numerical computation of the entries of a matrices resulting the discrete bilinear forms. This construction proceeds in two steps, separating the outer and the inner integration. As discussed in Chapter 2.3 the time integrals are evaluated analytically and result in a light cone integration domain E_l as defined in (2.22), such that we have to evaluate terms like

$$G_{ij}^{l,v} = \iint_{E_l} k_v(x-y) \varphi_i(y) \varphi_j(x) ds_y ds_x, \quad (4.1)$$

where $k_v(x-y) = |x-y|^v$ denotes a weakly singular kernel function and φ_i and φ_j are piecewise defined polynomial trial and test functions with bounded support. Identify $r_{\min} := t_l$ and $r_{\max} := t_{l+1}$ and regard the prototype integral

$$G_{ij}^v := \iint_E k_v(x-y) \varphi_i(y) \varphi_j(x) ds_y ds_x, \quad (4.2)$$

with

$$E := \{(x,y) \in \Gamma \times \Gamma \text{ s.t. } r_{\min} \leq |x-y| \leq r_{\max}\}.$$

Moreover, define the point light cone or the domain of influence of point $x \in \mathbb{R}^3$ sketched in Fig. 4.1(b) by

$$E(x) := B_{r_{\max}}(x) \setminus B_{r_{\min}}(x) = \{y \in \mathbb{R}^3 \text{ s.t. } r_{\min} \leq |x-y| \leq r_{\max}\},$$

and the element light cone or the domain of influence of a triangle $T \in \mathbb{R}^3$ sketched in Fig. 4.1(a) by

$$E(T) := \bigcup_{x \in T} E(x) = \{y \in \mathbb{R}^3 : r_{\min} \leq |x-y| \leq r_{\max}, x \in T\}.$$

As we have seen in Section 3.2.4 $E(T)$ is the support of a discrete retarded potential evaluated on $T \cap E(x)$. Defining

$$E(T_j, T_i) := E \cap (T_j \times T_i), \quad (4.3)$$

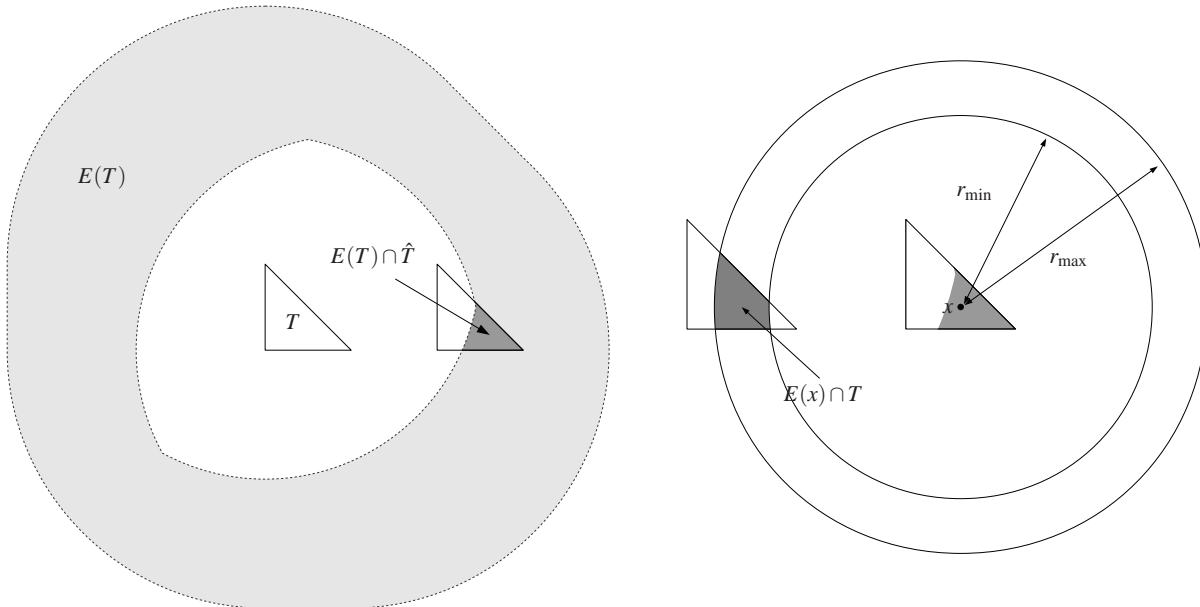
we rewrite (4.2) to

$$\begin{aligned} G_{ij}^v &= \sum_{\substack{T_{i'} \subset \text{supp } \varphi_i \\ T_{j'} \subset \text{supp } \varphi_j}} \iint_{E(T_{i'}, T_{j'})} k_v(|x-y|) \varphi_i(y) \varphi_j(x) ds_y ds_x \\ &= \sum_{\substack{T_{i'} \subset \text{supp } \varphi_i \\ T_{j'} \subset \text{supp } \varphi_j}} \int_{E(T_{i'} \cap T_{j'})} \varphi_j(x) P_{i,j'}(x) ds_x, \end{aligned} \quad (4.4)$$

with a retarded potential $P_{i,j'}$ given by

$$P_{i,j'}(x) := \int_{E(x) \cap T_{i'}} k_v(|x-y|) \varphi_i(y) ds_y. \quad (4.5)$$

We implement a quadrature rule for the integration with respect to x (outer quadrature) and depending on this we



(a) Outer integral: Domain of influence of triangle \hat{T} intersected with triangle T .

(b) Inner integral: Domain of influence $E(x)$ of point $x \in E(T) \cap \hat{T}$.

Fig. 4.1 Domains of influence and the illumination of test and trial element \hat{T} and T during the evaluation of the inner and outer integral of the Galerkin entry.

evaluate the retarded potential (inner quadrature). We present appropriate decomposition strategies for both parts of the quadrature scheme and discuss grading strategies. In order to keep the notation as plain as possible, we will study the following simplified integral. Given the *trial element* T and the *test element* \hat{T} and test and trial functions φ and $\hat{\varphi}$ defined on T and \hat{T} , respectively, a typical entry in the Galerkin matrix reads

$$G(\varphi, \hat{\varphi}) := (P\varphi, \hat{\varphi}) = \int_{E(T) \cap \hat{T}} (P\varphi)(x) \hat{\varphi}(x) ds_x, \quad (4.6)$$

where we evaluate the retarded integral

$$(P\varphi)(x) := \int_{E(x) \cap T} k(x-y)\varphi(y) ds_y. \quad (4.7)$$

Before we continue with the construction and analysis of a quadrature rule for $G(\varphi, \widehat{\varphi})$, let us briefly describe the structure of the integral $G(\varphi, \widehat{\varphi})$. In Fig. 4.1 the main idea of the integration is sketched. Let us first consider the outer integral. In Chapter 3 we have discussed the regularity of the integrand P in detail. We evaluate $\widehat{\varphi}$ only in the element \widehat{T} , such that the integration domain reduces to $E(T) \cap \widehat{T}$, compare Fig. 4.1(a). Thus element T illuminates a part of element \widehat{T} through its domain of influence $E(T)$. For the inner integral, each point $x \in E(T) \cap \widehat{T}$ illuminates the element T through its domain of influence $E(x)$ and we integrate over $E(x) \cap T$. Thus the illuminated part of \widehat{T} illuminates a part of element T in the inner integration, as sketched in Fig. 4.1(b).

Following the ideas in [43] we evaluate the outer and the inner integral step by step decomposing the integration domain and using a grading strategy for the different singularities. To our knowledge this was not done up to now in this extend. Especially in engineering circles also an adaptive quadrature is used for the computation of the discrete potential [42]. But even here, a rigorous error analysis is still missing and it raises the question how the cut-off behavior due to the different domains of influence affects its accuracy.

4.1 Composite Quadrature Rule for the Inner Quadrature

In this section we will construct and analyze a composite quadrature rule for $P\varphi$ as defined in (4.7). We will present a specified composite quadrature rule and an error analysis.

4.1.1 Construction of a Composite Quadrature Rule

Decomposition of the integration domain $E(x) \cap T$

We seek a parametric representation of the integration domain $E(x) \cap T$. The domain of influence $E(x)$ of point x is an annular domain with center x and radii r_{\min} and r_{\max} . Therefore, we have to find the intersection of triangle T and two concentric spheres. This three-dimensional intersection problem can be rewritten to a two-dimensional intersection in a three-dimensional space. Let x' denote the orthogonal projection of x onto the triangle plane \mathcal{E}_T and define $d := |x - x'|$, cf. Fig. 4.2(b)). Then

$$E(x) \cap \mathcal{E}_T = (B_{r'_{\min}}(x') \setminus B_{r'_{\max}}(x')) \cap \mathcal{E}_T = \{y \in \mathcal{E}_T : r'_{\min} \leq |x' - y| \leq r'_{\max}\},$$

where $r'_{\min/\max} := (r_{\min/\max}^2 - d^2)^{1/2}$ and thus

$$E(x) \cap T = (B_{r'_{\min}}(x') \setminus B_{r'_{\max}}(x')) \cap T.$$

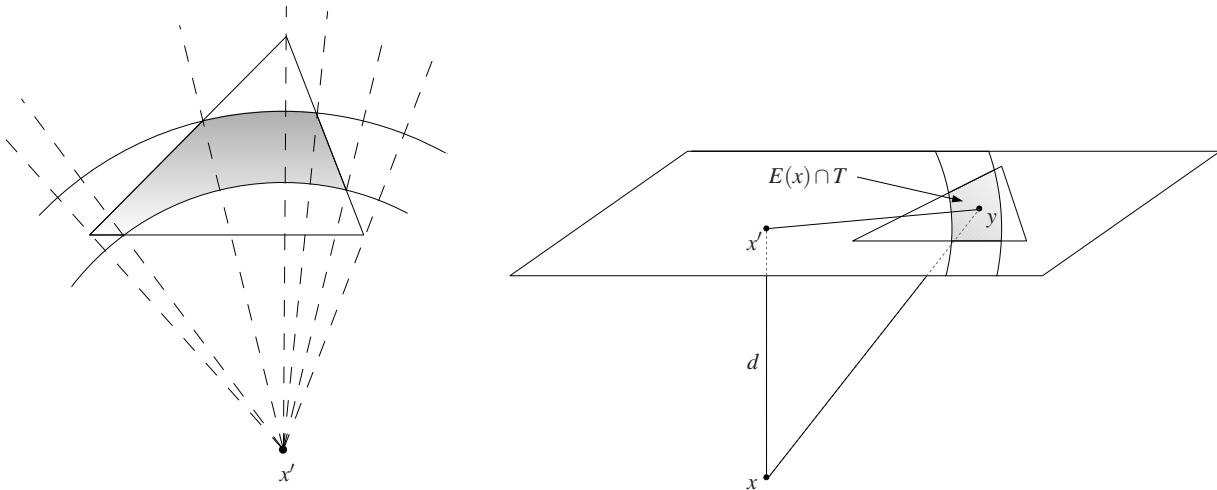
Now, we introduce polar coordinates (r, θ) with respect to x' and decompose $E(x) \cap T = \bigcup_{l=1}^{n_d} D_l$, where the subdomains D_l are defined on a sector (θ_l, θ_{l+1}) with a lower bound $r_{1,l}(\theta)$ and an upper bound $r_{2,l}(\theta)$ in radial direction, such that

$$D_l := \{(r, \theta) : \theta \in (\theta_l, \theta_{l+1}) \text{ and } r \in (r_{1,l}(\theta), r_{2,l}(\theta))\}.$$

The radial bounds direction are characterized by the position of the intersected edge e compared to the concentric circles,

$$r_{1,l} := \begin{cases} r'_{\min} & e \in B_{r'_{\min}}(x) \\ r_e(\theta) & \text{else} \end{cases} \quad r_{2,l} := \begin{cases} r'_{\max} & e \notin B_{r'_{\max}}(x) \\ r_e(\theta) & \text{else} \end{cases},$$

where $r_e(\theta)$ is the representation of the intersected triangle edge e in polar coordinates with respect to x' , which reads



(a) Example for a decomposition of $E(x) \cap T$ with respect to x' into $n_d = 5$ subelements.

(b) Projection of x onto the triangle plane.

Fig. 4.2

$$r_e(\theta) = \frac{v \cdot n}{n_1 \cos \theta + n_2 \sin \theta}, \quad (4.8)$$

where $n = (n_1, n_2, n_3)^T$ denotes the normal of the edge and v is the end point of e .

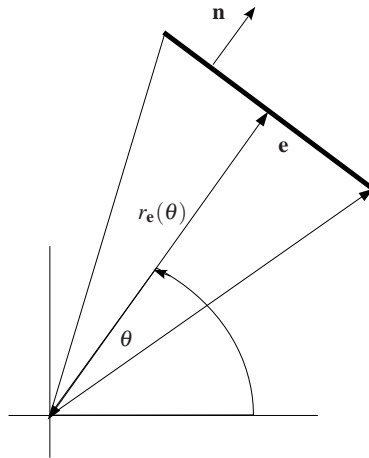


Fig. 4.3 Representation of an edge e in polar coordinates (r, θ) .

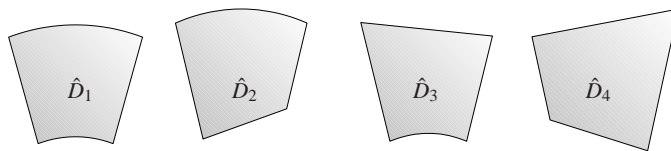


Fig. 4.4 Generic integration domains

Remark 4.1. a) The above definition of the domain D_l for $l = 2, 3, 4$ are still valid, if one side of the element vanishes.

For example, if the decomposition element includes a vertex of the triangle. Given a triangle T and let $r_{\max} > r_{\min} >$

0. In Fig. 4.2(a) we sketch a typical decomposition of the illuminated triangle domain $T \cap E(x)$ into five subdomains.

b) The number of subelements D_l is bounded by 12.

c) It holds $r_{i,l} \in C^\infty(\theta_l, \theta_{l+1})$ for $i = 1, 2$.

Thus the representation of (4.7) in polar coordinates reads

$$(P\varphi)(x) = \sum_{l=1}^{n_d} \int_{D_l} (d^2 + r^2)^{\frac{\nu}{2}} \varphi(r, \theta) r dr d\theta, \quad (4.9)$$

where $d > 0$ and φ denotes a sufficiently regular function. Note by e_1 and e_2 the upper and lower line segment in a decomposition element, with edge normals n_1, n_2 and vertices v_1 and v_2 , respectively. We identify four generic cases of decomposition types as sketched in Fig. 4.4 and thus define \hat{D}_l for $l = 1, \dots, 4$ via

$$\begin{aligned} \hat{D}_1 &:= \{(r, \theta) : \theta \in (\theta_1, \theta_2) \text{ and } r \in (r_{\min}, r_{\max})\}, \\ \hat{D}_2 &:= \{(r, \theta) : \theta \in (\theta_1, \theta_2) \text{ and } r \in (r_{e_1}(\theta), r_{\max})\}, \\ \hat{D}_3 &:= \{(r, \theta) : \theta \in (\theta_1, \theta_2) \text{ and } r \in (r_{\min}, r_{e_2}(\theta))\}, \\ \hat{D}_4 &:= \{(r, \theta) : \theta \in (\theta_1, \theta_2) \text{ and } r \in (r_{e_1}(\theta), r_{e_2}(\theta))\}, \end{aligned} \quad (4.10)$$

and thus it is sufficient to regard

$$(\hat{P}_l \varphi)(r, \theta) := \int_{\hat{D}_l} (d^2 + r^2)^{\frac{\nu}{2}} \varphi(r, \theta) r dr d\theta \quad l = 1, \dots, 4. \quad (4.11)$$

Before we continue with the construction of a quadrature rule for (4.11) let us fix some notation. We basically use the notation of [13]

Geometric mesh and composite quadrature

Given some function f on an interval $[a, b]$ and define an integral

$$\mathcal{I}f = \int_a^b f dx,$$

we denote by $Q_n^{[a,b]}$ the Gauß- $\frac{1}{2}$ -Legendre quadrature rule with n quadrature points on the interval $[a, b]$ given by

$$Q_n^{[a,b]} f := \sum_{i=1}^n w_i f(x_i)$$

with quadrature nodes x_i and quadrature weights w_i . Note that a Gauß- $\frac{1}{2}$ -Legendre quadrature rule of order n is exact for polynomials of degree $2n - 1$. If the integration domain is clear from the context we simply refer to Q_n . For $f \in C^{2n}(a, b)$ there holds the well known error estimate [33]

$$E^{[a,b]} f := Q_n^{[a,b]} f - \mathcal{I}f = \frac{(b-a)^{2n+1} (n!)^4}{(2n+1) [(2n)!]^3} \frac{d^{2n}}{d\xi^{2n}} f(\xi) \quad \text{where } \xi \in (a, b). \quad (4.12)$$

Given a subdivision of $[0, 1]$ into m subintervals I_j ($j = 1, \dots, m$), a *variable order composite Gauß- $\frac{1}{2}$ rule* on $[0, 1]$ with degree vector $\mathbf{n} = (n_1, \dots, n_m)$ is defined by

$$Q_{n,m,\sigma} g := \sum_{j=1}^m Q_{n_j}^{I_j} g.$$

For $n_1 = \dots = n_m$ we refer to a *constant order composite quadrature* and otherwise to a *variable order composite quadrature*. If the underlying composition is a geometric subdivision, one also refers to a *graded quadrature*. A geometric subdivision of $[0, 1]$ with m levels and a grading parameter $\sigma \in (0, 1)$ is defined by

$$[0, 1] = \bigcup_{j=1}^m I_j, \text{ where } I_j := [x_{j-1}, x_j],$$

where

$$x_0 := 0, \quad x_j := \sigma^{m-j} \quad (j = 1, \dots, m).$$

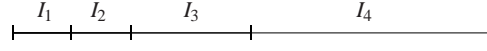


Fig. 4.5 A geometric subdivision of $[0, 1]$ with $\sigma = 0.5$ and $m = 4$.

A generalization to an arbitrary interval $[a, b]$ is straight forward applying a linear mapping

$$x_0 := a, \quad x_j := a + (b - a)\sigma^{m-j} \quad (j = 1, \dots, m).$$

Construction of a composite quadrature rule for (4.11)

The construction of a quadrature rule for (4.11) involves the integration domains \hat{D}_l with $l = 2, 3, 4$ which have θ -depending integration bounds in r and can be of regular shape. Although the initial triangle is regular, its intersection with the domain of influence $E(x)$ easily results in unregular subelements.

Each domain D_l ($l = 1, \dots, 4$) can be described in polar coordinates with respect to x' and we can rewrite (4.11) to

$$\hat{P}_l(r, \theta) = \int_{\theta_1}^{\theta_2} \int_{r_1(\theta)}^{r_2(\theta)} f(r, \theta) dr d\theta,$$

where

$$f(r, \theta) := (d^2 + r^2)^{\frac{\nu}{2}} \varphi(r, \theta)r$$

and

$$r_1(\theta) = \begin{cases} r_{\min} & \text{on } \hat{D}_1, \hat{D}_3 \\ r_{e_1}(\theta) & \text{on } \hat{D}_2, \hat{D}_4 \end{cases} \quad r_2(\theta) = \begin{cases} r_{\max} & \text{on } \hat{D}_1, \hat{D}_2 \\ r_{e_2}(\theta) & \text{on } \hat{D}_3, \hat{D}_4 \end{cases}.$$

The composite quadrature rule on the ray $(r_1(\theta), r_2(\theta))$ is defined by

$$Q^{[r_1(\theta), r_2(\theta)]} f := Q_{n_r, m_r, \sigma_r}^{[r_1(\theta), r_2(\theta)]} f$$

where $n_r = (n_1^{(r)}, \dots, n_m^{(r)})$, $m_r \geq 1$ and $\sigma_r \in (0, 1]$ and denote by $Q_{n_\theta}^{[\theta_1, \theta_2]} f$ the quadrature rule of order n_θ , such that

$$Q^{\hat{D}_l} f := Q_{n_\theta}^{[\theta_1, \theta_2]} (Q_{n_r, m_r, \sigma_r}^{[r_1(\theta), r_2(\theta)]} f)$$

Remark 4.2. On \hat{D}_1 the classical tensor product Gaussian quadrature rule applies as the radial integration domain is independent of the angle θ and we obtain

$$Q^{\hat{D}_1} f = Q_{n_\theta, m_\theta, \sigma_\theta}^{[\theta_1, \theta_2]} \otimes Q_{n_r, m_r, \sigma_r}^{[r_{\min}, r_{\max}]} f.$$

4.1.2 Error Analysis for the Evaluation of the Retarded Potential

In this subsection we seek to study the integral

$$I^{(D_l)} f := \int_{\theta_1}^{\theta_2} \int_{r_1(\theta)}^{r_2(\theta)} f(r, \theta) dr d\theta, \quad (4.13)$$

where we define the quadrature rule

$$Q^{(D_l)} f := Q_{n_\theta}^{[\theta_1, \theta_2]} \left(Q_{n_r, m_r, \sigma_r}^{[r_1(\theta), r_2(\theta)]} f \right)$$

for $n_r = (n_1, \dots, n_m)$ denoting the number of quadrature points on each subinterval of the geometric mesh with m_r level and grading factor σ_r . n_θ denotes the number of quadrature points in θ and is chosen proportional to m_r .

Theorem 4.3. *Given a function $f \in B_\beta^0(T)$ with a weight function $\Phi_{\beta, \alpha, 0}(r) = r^{|\alpha| + \beta}$ and let $\max(1, \sqrt{r_{\max}})(\theta_2 - \theta_1) < eC_\theta$, then there holds for D_l as defined in (4.10)*

$$\left| I^{(D_l)} f - Q^{(D_l)} f \right| \leq C e^{-b \sqrt[3]{N}}$$

for $l = 1, \dots, 4$ and where N denotes the total number of quadrature points and C and b are positive constants independently of N , but depending on the grading factor σ_r the number of levels m_r and on f . C_θ is defined in Lemma 4.6.

Proof. We can split the error into an error depending on the angle and one depending on the radius and obtain

$$\begin{aligned} \left| \mathcal{I} f - Q^{(D_l)} f \right| &\leq \int_{\theta_1}^{\theta_2} \underbrace{\left| \int_{r_1(\theta)}^{r_2(\theta)} f(r, \theta) dr - Q^{[r_1(\theta), r_2(\theta)]} f \right|}_{=: |E^{[r_1(\theta), r_2(\theta)]} f|} d\theta \\ &\quad + \underbrace{\left| \int_{\theta_1}^{\theta_2} Q^{[r_1(\theta), r_2(\theta)]} f d\theta - Q^{[\theta_1, \theta_2]} \otimes Q^{[r_1(\theta), r_2(\theta)]} f \right|}_{=: |E^{[\theta_1, \theta_2]} Q^{[r_1(\theta), r_2(\theta)]} f|} \\ &\leq (\theta_2 - \theta_1) \max_{\theta \in (\theta_1, \theta_2)} \left| E^{[r_1(\theta), r_2(\theta)]} f \right| + \left| E^{[\theta_1, \theta_2]} Q^{[r_1(\theta), r_2(\theta)]} f \right| \end{aligned}$$

As $f \in B_\beta^0(T)$, on each ray there holds $f \in B_\beta^0(0, \sqrt{2})$ for $\beta \in (0, \frac{1}{2})$ and thus Lemma 4.4 yields

$$\left| E^{[r_1(\theta), r_2(\theta)]} f \right| \leq C_1 e^{-b_1 \sqrt{N_r}}$$

where we know from the proof of Lemma 4.4, that $m_r^2 \sim N_r$.

From Lemma 4.6 with $Q^{[r_1(\theta), r_2(\theta)]} f \in C^{2n_\theta}(\theta_1, \theta_2)$ we obtain for $\max(1, \sqrt{r_{\max}})(\theta_2 - \theta_1) < eC_\theta$

$$\left| E^{[\theta_1, \theta_2]} Q^{[r_1(\theta), r_2(\theta)]} f \right| \leq C_2 (\theta_2 - \theta_1) e^{-b_2 n_\theta},$$

where N_r denotes the total number of quadrature points on one ray and C_θ is defined as in Lemma 4.6.

The total number of quadrature points N on the domain D_l is $N = N_r n_\theta \sim m^3$, such that $m \sim \sqrt[3]{N}$ and as $n_\theta \sim m$ we finally obtain

$$\begin{aligned} \left| \mathcal{I} f - Q^{(D_l)} f \right| &\leq (\theta_2 - \theta_1) C_1 e^{-b_1 \sqrt{N_r}} + (\theta_2 - \theta_1) C_2 e^{-b_2 n_\theta} \\ &\leq (\theta_2 - \theta_1) C e^{-bn_\theta} \\ &\leq (\theta_2 - \theta_1) C e^{-b \sqrt[3]{N}}. \end{aligned}$$

□

For a fixed angle θ the error on a ray $[0, r(\theta)]$ can be estimated as follows.

Lemma 4.4 (Error analysis on ray). *Given $f \in B_\beta^0([0, r(\theta)])$ and $\beta \in (0, \frac{1}{2})$. Then for every $\sigma \in (0, 1)$ and a linear degree vector p with*

$$p_j = \max\{1, \lfloor \mu j \rfloor\} \quad \text{and} \quad \mu > \frac{(\frac{3}{2} - \beta) \ln \sigma}{\ln F_{\min}},$$

where F_{\min} is defined within the proof, there exists a constant $b > 0$ independently of N such that there holds

$$\left| E^{[r_1(\theta), r_2(\theta)]} f \right| \leq C \exp(-b\sqrt{N_r}).$$

where C is a constant depending on f .

Proof. In this proof, we will follow the lines of the proof of Theorem 4.1 in [51]. We restrict the analysis to $r_1(\theta) = 0$, i.e. the singularity is approached, if $r_1(\theta) > 0$ the following analysis can be adopted. In the following, we will suppress the index r and rather write σ , m and n as there is no confusion possible. It holds

$$\left| E^{[r_1(\theta), r_2(\theta)]} f \right| \leq \left| \int_{I_1} f(r, \theta) dr \right| + \sum_{j=2}^m \left| \int_{I_j} f(r, \theta) dr - Q_j f \right|, \quad (4.14)$$

where $r_0 = 0$, $r_j = r_2(\theta) \sigma^{m-j}$ for $j = 1, \dots, m$ and thus $I_j = (r_{j-1}, r_j)$. Let us now estimate the first term. Here we use $f \in B_\beta^0(I_1)$ for $\beta \in (0, \frac{1}{2})$ and we obtain

$$\begin{aligned} \left| \int_{I_1} f(r, \theta) dr \right| &\leq \int_{I_1} |f| r^\beta r^{-\beta} dr \\ &\leq \left(\int_0^{r_1} r^{-2\beta} dr \right)^{\frac{1}{2}} \left(\int_{I_1} |f|^2 r^{2\beta} dr \right)^{\frac{1}{2}} \\ &= \frac{[r_2(\theta) \sigma^{m-1}]^{\frac{1}{2}-\beta}}{\sqrt{1-2\beta}} |f|_{H_\beta^{0,0}(I_1)}. \end{aligned}$$

Each summand in the second term of (4.14) can be estimated using Lemma 4.12 by the infimum over all polynomials π of total degree $p_j := 2n_j - 1$ and we obtain

$$\left| E_{r(\theta), f} \right| \leq \frac{[r_2(\theta) \sigma^n]^{\frac{1}{2}-\beta}}{\sqrt{1-2\beta}} C_f + \sum_{j=2}^m 2|I_j| \inf_{\pi} \|f - \pi\|_{L^\infty(I_j)}$$

and by Lemma 4.13 we obtain together with Lem. 4.16 and as $h_j = \frac{1-\sigma}{\sigma} r_{j-1} =: \lambda r_{j-1}$

$$\begin{aligned} \inf_{\pi} \|f - \pi\|_{L^\infty(I_j)}^2 &\leq C \sum_{k=0}^1 h_j^{2k-1} \inf_{\pi} |f - \pi|_{H^k(I_j)}^2 \\ &\leq C \sum_{k=0}^1 h_j^{2k-1} r_{j-1}^{-2(\beta+k)} \frac{\Gamma(p_j - s_j + 1)}{\Gamma(p_j + s_j + 3 - 2k)} \left(\frac{\lambda}{2}\right)^{2s_j} |f|_{H_\beta^{s_j+1,0}(J)}^2 \\ &\leq C r_{j-1}^{1-2\beta} \frac{\Gamma(p_j - s_j + 1)}{\Gamma(p_j + s_j + 1)} \left(\frac{\lambda}{2}\right)^{2s_j} |f|_{H_\beta^{s_j+1,0}(J)}^2 \\ &= C r_2(\theta)^{1-2\beta} \sigma^{(m-j+1)(1-2\beta)} \frac{\Gamma(p_j - s_j + 1)}{\Gamma(p_j + s_j + 1)} \left(\frac{\lambda}{2}\right)^{2s_j} |f|_{H_\beta^{s_j+1,0}(J)}^2 \end{aligned}$$

As $f \in B_\beta^0(0, r_2(\theta))$ it yields

$$\begin{aligned} \inf_{\pi} \|f - \pi\|_{L^\infty(I_j)}^2 &\leq CC_f^2 (d_f)^{2s_j+2} r_2(\theta)^{1-2\beta} \sigma^{(m-j+1)(1-2\beta)} \frac{\Gamma(p_j - s_j + 1)}{\Gamma(p_j + s_j + 1)} (\Gamma(s_j + 2))^2 \left(\frac{\lambda}{2}\right)^{2s_j} \\ &\leq CC_f^2 (d_f)^2 r_2(\theta)^{1-2\beta} \sigma^{(m-j+1)(1-2\beta)} \frac{\Gamma(p_j - s_j + 1)}{\Gamma(p_j + s_j + 1)} (\Gamma(s_j + 2))^2 \left(\frac{\rho d_f}{2}\right)^{2s_j}, \end{aligned}$$

where $\rho = \max(1, \lambda)$. Following the proof of Theorem 3.36 in [52], select $s_j = \alpha_j p_j$ with $\alpha_j \in (0, 1)$ for $j = 2, \dots, n_r$ and we can estimate using Stirling's Formula

$$\begin{aligned} \frac{\Gamma((1-\alpha)p+1)}{\Gamma((1+\alpha)p+1)} (\Gamma(2+\alpha p))^2 &\sim \frac{(p-s)!}{(p+s)!} ((s+1)!)^2 \\ &\sim \left[\frac{(1-\alpha)^{(1-\alpha)}}{(1+\alpha)^{(1+\alpha)}} \right]^p \left(\frac{1-\alpha}{1+\alpha} \right)^{\frac{1}{2}} p^{-2\alpha p} e^{-3} (1+\alpha p)^{3+2\alpha p} \end{aligned}$$

Now,

$$(1+\alpha p)^{2\alpha p} = (\alpha p)^{2\alpha p} \left(1 + \frac{1}{\alpha p}\right)^{2\alpha p} \rightarrow (\alpha p)^{2\alpha p} e^2 \quad (p \rightarrow \infty)$$

and thus

$$\frac{\Gamma((1-\alpha)p+1)}{\Gamma((1+\alpha)p+1)} (\Gamma(2+\alpha p))^2 \leq Cp^3 \left[\frac{(1-\alpha)^{(1-\alpha)}}{(1+\alpha)^{(1+\alpha)}} \right]^p \alpha^{2\alpha p}$$

Inserting the definition of function F as given in Lemma 4.18 we can obtain

$$\inf_{\pi} \|f - \pi\|_{L^\infty(I_j)}^2 \leq CC_f^2 d_f^2 r_2(\theta)^{2(\frac{1}{2}-\beta)} \sigma^{2(m-j+1)(\frac{1}{2}-\beta)} p_j^3 (F(\rho d_f, \alpha))^{2p_j}$$

such that

$$|I_j| \inf_{\pi} \|f - \pi\|_{L^\infty(I_j)} \leq CC_f d_f \frac{(1-\sigma)}{\sigma} r_2(\theta)^{(\frac{3}{2}-\beta)} \sigma^{(m-j+1)(\frac{3}{2}-\beta)} p_j^{3/2} (F(\rho d_f, \alpha))^{p_j}$$

Now, Lemma 4.18 yields

$$F_{\min} = \min_{\alpha \in (0,1)} F(\rho d_f, \alpha) = F(\rho d_f, \alpha_{\min}) < 1 \quad \text{with} \quad \alpha_{\min} = \left(1 + \left(\frac{\rho d_f}{2}\right)^2\right)^{-1/2} < 1.$$

Thus the estimation results in

$$\begin{aligned} |E_{r(\theta)f}| &\leq CC_f \left[\frac{r_2(\theta)^{(\frac{1}{2}-\beta)} \sigma^{m(\frac{1}{2}-\beta)}}{\sqrt{1-2\beta}} + \sum_{j=2}^m d_f r_2(\theta)^{\frac{3}{2}-\beta} \sigma^{(m+1-j)(\frac{3}{2}-\beta)} p_j^{3/2} F_{\min}^{p_j} \right] \\ &\leq CC_f d_f \sigma^{(m+1)(\frac{3}{2}-\beta)} r_2(\theta)^{\frac{2}{3}-\beta} \max(1, r_2(\theta)) \left[1 + \sum_{j=2}^m p_j^{3/2} F_{\min}^{p_j} \right] \end{aligned}$$

Select $p_j = \lfloor \mu j \rfloor$ ($j = 2, \dots, m$) and a slope μ that will be determined later, where $\lfloor x \rfloor := \max_{k \in \mathbb{Z}, k \leq x} k$. Define the index

$$j_0 := \max_{2 \leq j \leq m} (j : \lfloor j\mu \rfloor \leq 1),$$

such that the term in squared brackets can be estimated independently of m by

$$1 + \sum_{j=2}^m p_j^{3/2} F_{\min}^{p_j} \leq 1 + \sum_{j=2}^{j_0} \frac{F_{\min}}{\sigma^{j(\frac{3}{2}-\beta)}} + \sum_{j=j_0+1}^m (j\mu)^{3/2} \left(\frac{F_{\min}^\mu}{\sigma^{\frac{3}{2}-\beta}} \right)^j.$$

Here the last term can be estimated for $m \rightarrow \infty$ by a constant C if

$$\frac{F_{\min}^{\mu}}{\sigma^{\frac{3}{2}-\beta}} < 1 \quad \Leftrightarrow \quad \mu > \frac{(\frac{3}{2}-\beta) \ln \sigma}{\ln F_{\min}}.$$

Thus we obtain

$$|E_{r(\theta)f}| \leq CC_f d_f r_2(\theta)^{\frac{2}{3}-\beta} \max(1, r_2(\theta)) \sigma^{(m+1)(\frac{3}{2}-\beta)}$$

If we estimate the number of quadrature points $N_{r(\theta)}$ on each ray, we obtain with $p_j = 2n_j - 1$

$$N_{r(\theta)} \leq \sum_{j=1}^m n_j \leq \frac{1}{2} \sum_{j=1}^m (p_j + 1) \leq \frac{\mu}{2} m^2.$$

and we can estimate $r_2(\theta) \leq r_{\max}$, such that

$$|E_{r(\theta)f}| \leq CC_f d_f \max(1, r_{\max}^2) \exp(-bN_r^{1/2}).$$

□

The estimation of $|E^{[\theta_1, \theta_2]} Q_{p_r}^{[r_1(\theta), r_2(\theta)]} f|$ uses a different technique. Due to the structure of integral (4.13), each angular integration point results in a ray in the radial integration. In domain \hat{D}_1 this is obviously no problem, as the shape is always regular, but for \hat{D}_2 and \hat{D}_3 and worst for \hat{D}_4 the shape can be very anisotropic and we can no longer rely on any regular structure of the integration domain, although the original triangulation surely was shape regular.

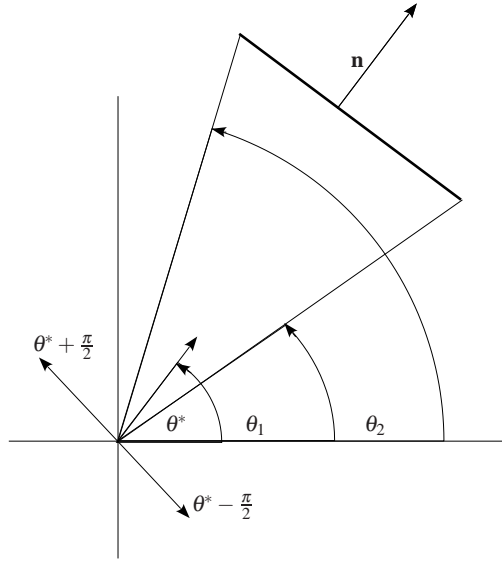


Fig. 4.6 Sketch of edge function $r_e(\theta)$ and its visualization.

On the domains \hat{D}_l for $l = 2, 3, 4$, the integration bounds in r depend on θ . Thus, the estimation of the error in the angle involves the computation of the higher derivatives of $r_{\mathbf{n}}(\theta)$ which is analyzed in the following lemma.

Lemma 4.5. Given a function $r_{\mathbf{n}}(\theta) = (n_1 \cos \theta + n_2 \sin \theta)^{-1}$ with $n_1 = \cos \theta^*$ and $n_2 = \sin \theta^*$, compare Fig. 4.6 then

$$\left| \partial_{\theta}^k r_{\mathbf{n}}(\theta) \right| \leq 2^k k! |\cos(\theta - \theta^*)|^{-(k+1)}$$

Proof. The addition theorem yields $r_{\mathbf{n}}(\theta) = \cos^{-1}(\theta - \theta^*)$ and one immediately verifies, that

$$\partial_{\theta}^k r_{\mathbf{n}}(\theta) = \begin{cases} \cos^{-1}(\theta - \theta^*) \sum_{j=0}^l \alpha_j^{(2l)} \tan^{2j}(\theta - \theta^*) & k = 2l \\ \cos^{-1}(\theta - \theta^*) \sum_{j=0}^l \alpha_j^{(2l+1)} \tan^{2j+1}(\theta - \theta^*) & k = 2l + 1 \end{cases}$$

as one proves by induction for odd and even orders of derivative

$$\begin{aligned} \partial_{\theta}^{2l+1} r_{\mathbf{n}}(\theta) &= \partial_{\theta} \partial_{\theta}^{2l} r_{\mathbf{n}}(\theta) \\ &= \frac{1}{\cos(\theta - \theta^*)} \sum_{j=0}^l \alpha_j^{(2l)} \tan^{2j+1}(\theta - \theta^*) + 2j \alpha_j^{(2l)} (1 + \tan^2(\theta - \theta^*)) \tan^{2j-1}(\theta - \theta^*) \\ &= \frac{1}{\cos(\theta - \theta^*)} \sum_{j=0}^l \left(\alpha_j^{(2l)} + 2j \alpha_j^{(2l)} + 2(j+1) \alpha_{j+1}^{(2l)} \right) \tan^{2j+1}(\theta - \theta^*) \\ \partial_{\theta}^{2l} r_{\mathbf{n}}(\theta) &= \frac{1}{\cos(\theta - \theta^*)} \sum_{j=0}^{l-1} \alpha_j^{(2l-1)} \tan^{2j+2}(\theta - \theta^*) + \alpha_j^{(2l-1)} (2j+1) (1 + \tan^2(\theta - \theta^*)) \tan^{2j}(\theta - \theta^*) \\ &= \frac{1}{\cos(\theta - \theta^*)} \sum_{j=0}^l \left(\alpha_{j-1}^{(2l-1)} + (2j+1) \alpha_j^{(2l-1)} \right) \tan^{2j}(\theta - \theta^*) \\ &\quad + \frac{1}{\cos(\theta - \theta^*)} \sum_{j=1}^l (2j-1) \alpha_{j-1}^{(2l-1)} \tan^{2j}(\theta - \theta^*) \end{aligned} \tag{4.15}$$

Thus we can estimate

$$\left| \partial_{\theta}^k r_{\mathbf{n}}(\theta) \right| \leq |\cos(\theta - \theta^*)|^{-(k+1)} \sum_{j=1}^l \left| \alpha_j^{(k)} \right| \tag{4.16}$$

and by comparing the coefficients in (4.15), we can derive a recursion formula for the coefficients

$$\begin{aligned} \alpha_j^{(2l)} &= \alpha_{j-1}^{(2l-1)} + (2j+1) \alpha_j^{(2l-1)} + (2j-1) \alpha_{j+1}^{(2l-1)} \quad (j = 0, \dots, l) \\ \alpha_j^{(2l+1)} &= \alpha_j^{(2l)} + (2j) \alpha_j^{(2l)} + (2j+2) \alpha_{j-1}^{(2l)} \quad (j = 0, \dots, l), \end{aligned}$$

where $\alpha_{-1}^{(2l)} = \alpha_{-1}^{(2l-1)} = \alpha_l^{(2l-1)} = \alpha_{l+1}^{(2l)} = 0$. This results for even orders of derivative in

$$\begin{aligned} \sum_{j=0}^l \left| \alpha_j^{(2l+1)} \right| &\leq \sum_{j=0}^l \left| \alpha_j^{(2l)} + 2j \alpha_j^{(2l)} + 2(j+1) \alpha_{j+1}^{(2l)} \right| \\ &\leq \sum_{j=0}^l \left| \alpha_j^{(2l)} \right| + 2l \sum_{j=0}^l \left| \alpha_j^{(2l)} \right| + 2l \sum_{j=0}^l \left| \alpha_j^{(2l)} \right| \\ &\leq (4l+1) \sum_{j=0}^l \left| \alpha_j^{(2l)} \right|. \end{aligned}$$

For odd derivatives this yields

$$\begin{aligned} \sum_{j=0}^l \left| \alpha_j^{(2l)} \right| &\leq \sum_{j=0}^l \left| \alpha_{j-1}^{(2l-1)} + (2j+1) \alpha_j^{(2l-1)} + (2j-1) \alpha_{j+1}^{(2l-1)} \right| \\ &\leq (1 + (2(l-1) + 1) + 2l - 1) \sum_{j=0}^{l-1} \left| \alpha_j^{(2l-1)} \right| \\ &\leq (4l-1) \sum_{j=0}^{l-1} \left| \alpha_j^{(2l-1)} \right|, \end{aligned}$$

and thus the successive application of this estimate gives

$$\sum_j |\alpha_j^{(k)}| \leq 2(k+1) \sum_j |\alpha_j^{(k-1)}| \leq 2^k k!$$

and (4.16) yields the desired estimate. \square

Let us now consider the error analysis in the angle.

Lemma 4.6. *Given the assumptions as in Theorem 4.3 and let $\max(1, \sqrt{r_{\max}})(\theta_2 - \theta_1) < eC_\theta$ on D_2, D_3 and D_4 , with*

$$C_\theta := \begin{cases} \min_{\theta \in (\theta_1, \theta_2)} |\cos(\theta - \theta_1^*)| & \text{in } \hat{D}_2 \\ \min_{\theta \in (\theta_1, \theta_2)} |\cos(\theta - \theta_2^*)| & \text{in } \hat{D}_3 \\ \min_{\theta \in (\theta_1, \theta_2)} (|\cos(\theta - \theta_1^*)|, |\cos(\theta - \theta_2^*)|) & \text{in } \hat{D}_4 \end{cases}$$

where θ_i^* denotes the angle corresponding to the edge normal \mathbf{n}_i ($i = 1, 2$); then there exist positive constants b and C independently of n_θ such that

$$\left| E^{[\theta_1, \theta_2]} \mathcal{Q}_{n_\theta}^{[r_1(\theta), r_2(\theta)]} f \right| \leq C(\theta_2 - \theta_1) e^{-bn_\theta}. \quad (4.17)$$

Proof. We estimate the higher derivatives of

$$g(\theta) := \mathcal{Q}^{[r_1(\theta), r_2(\theta)]} f(r(\theta), \theta) = \mathcal{Q}_i^{[0,1]} f((r_2(\theta) - r_1(\theta))t + r_1(\theta), \theta) \quad (4.18)$$

on subdomain \hat{D}_i , as defined in (4.10), where

$$r(\theta) = \begin{cases} (r_{\max} - r_{\min})t + r_{\min} & \text{in } \hat{D}_1 \\ (r_{\max} - r_{\mathbf{e}_1}(\theta))t + r_{\mathbf{e}_1}(\theta) & \text{in } \hat{D}_2 \\ (r_{\mathbf{e}_2}(\theta) - r_{\min})t + r_{\min} & \text{in } \hat{D}_3 \\ (r_{\mathbf{e}_2}(\theta) - r_{\mathbf{e}_1}(\theta))t + r_{\mathbf{e}_1}(\theta) & \text{in } \hat{D}_4 \end{cases}$$

where $r_{\mathbf{e}_i}(\theta)$ is defined as in (4.8) and $\mathbf{n}_i, \mathbf{v}_i$ are the normal vector and right vertex vector of an edge e_i .

Although (4.18) is clearly regular in θ on all regarded subdomains, we have to estimate the error with great care. We are interested in the error due to the quadrature rule corresponding to the integration with respect to the angle θ . For a Gauß- $\frac{1}{2}$ -Legendre quadrature rule of order n , we use the classical error estimate (4.12).

Thus we have to estimate higher order derivatives with respect to θ of $\mathcal{Q}^{[r_1(\theta), r_2(\theta)]}(f(r(\theta), \theta))$. We first analyze the higher order derivatives of $f(r(\theta), \theta)$ on the subdomains.

In Corollary 2.11 in [14] we find a simplified version of the multivariate formula of Faà di Bruno yielding for (4.18)

$$\partial_\theta^n f(r(\theta), \theta) = \sum_{1 \leq |\alpha| \leq n} D^\alpha f \sum_{\mathbf{k} \in p(n, \alpha)} n! \prod_{j=1}^n \frac{(\partial_\theta^j r(\theta))^{k_{j,1}} (\partial_\theta^j \theta)^{k_{j,2}}}{k_{j,1}! k_{j,2}! [j!]^{|\mathbf{k}_j|}},$$

where $\alpha = (\alpha_1, \alpha_2)$, $\mathbf{k}_j = (k_{j,1}, k_{j,2})$ and

$$p(n, \alpha) = \left\{ (\mathbf{k}_1, \dots, \mathbf{k}_n) : \mathbf{k}_j \geq 0, \sum_{j=1}^n \mathbf{k}_j = \alpha, \sum_{j=1}^n j |\mathbf{k}_j| = n \right\}.$$

In our specific case, we can further simplify the formula and obtain, using the convention $0^0 = 1$ and writing $k_j := k_{j,1}$

$$\partial_\theta^n f(r(\theta), \theta) = \sum_{1 \leq |\alpha| \leq n} D^\alpha f \sum_{\mathbf{k} \in p(n, \alpha)} \frac{n!}{\alpha_2!} \prod_{j=1}^n \frac{(\partial_\theta^j r(\theta))^{k_j}}{k_j! [j!]^{k_j}}, \quad (4.19)$$

where now $k_{1,2} = \alpha_2$ and $k_{j,2} = 0$ for $j \geq 2$ and we rewrite

$$p(n, \alpha) = \left\{ (k_1, \dots, k_n) : k_j \geq 0, \sum_{j=1}^n k_j = \alpha_1, \sum_{j=1}^n jk_j = n - \alpha_2 \right\}.$$

Denote by θ_i^* the angle corresponding to the unit normal vector \mathbf{n}_i for $i = 1, 2$, then there holds on the different domains

1. On \hat{D}_1 we have $\partial_\theta^n r(\theta) = 0$ for all $j \geq 1$ and thus

$$\partial_\theta^n f(r(\theta), \theta) = \sum_{1 \leq |\alpha| \leq n} D^\alpha f$$

2. On \hat{D}_2 there holds $\partial_\theta^j r(\theta) = (1-t)\partial_\theta^j r_{\mathbf{e}_1}(\theta)$ and with Lemma 4.5 we obtain

$$\begin{aligned} \left| \partial_\theta^j r(\theta) \right| &\leq 2^j j! |\mathbf{v}_1| |\cos(\theta - \theta_1^*)|^{-(j+1)} \\ &\leq 2^j j! r_{\max} |\cos(\theta - \theta_1^*)|^{-(j+1)}, \end{aligned}$$

where we can estimate without loss of generality, that $|\mathbf{v}_1| \leq r'_{\max}$, as \mathbf{v}_1 can be chosen, such that it is located in the ring $B_{r'_{\max}}(x') \setminus B_{r'_{\min}}(x')$ and $r'_{\max} \leq r_{\max}$. Now we can estimate (4.19) such that

$$\left| \partial_\theta^n f(r(\theta), \theta) \right| \leq \sum_{1 \leq |\alpha| \leq n} \|D^\alpha f\|_\infty \sum_{\mathbf{k} \in p(n, \alpha)} \frac{n!}{\alpha_2! k_1! \dots k_n!} \prod_{j=1}^n \left(2^j r_{\max} |\cos(\theta - \theta_1^*)|^{-(j+1)} \right)^{k_j}.$$

Now, for $\mathbf{k} = (k_1, \dots, k_n) \in p(n, \alpha)$ it holds

$$\begin{aligned} \prod_{j=1}^n \left(2^j r_{\max} |\cos(\theta - \theta_1^*)|^{-(j+1)} \right)^{k_j} &= 2^{\sum_{j=1}^n j k_j} r_{\max}^{\sum_{j=0}^n k_j} |\cos(\theta - \theta_1^*)|^{-\sum_{j=1}^n j k_j - \sum_{j=0}^n k_j} \\ &= 2^{n - \alpha_2} r_{\max}^{\alpha_1} |\cos(\theta - \theta_1^*)|^{\alpha_2 - n - \alpha_1}, \end{aligned}$$

such that

$$\begin{aligned} \left| \partial_\theta^n f(r(\theta), \theta) \right| &\leq C_f \sum_{1 \leq |\alpha| \leq n} \frac{n!}{\alpha_2!} 2^{n - \alpha_2} r_{\max}^{\alpha_1} |\cos(\theta - \theta_1^*)|^{\alpha_2 - n - \alpha_1} \sum_{\mathbf{k} \in p(n, \alpha)} \prod_{j=1}^n \frac{1}{k_j!} \\ &\leq C_f n! 2^n r_{\max}^n |\cos(\theta - \theta_1^*)|^{-2n} \sum_{1 \leq |\alpha| \leq n} \frac{1}{\alpha_2!} \sum_{\mathbf{k} \in p(n, \alpha)} \prod_{j=1}^n \frac{1}{k_j!}. \end{aligned}$$

Let us now show, that

$$\sum_{\mathbf{k} \in p(n, \alpha)} \prod_{j=1}^n \frac{1}{k_j!} \leq \frac{1}{\alpha_1!} \binom{n-1}{\alpha_1-1}.$$

Here we use the following formula [14]

$$r! \sum_{\mathbf{k} \in \hat{p}(n, r)} \prod_{j=1}^n \frac{1}{k_j!} = \binom{n-1}{r-1} \quad (4.20)$$

for

$$\hat{p}(n, r) := \left\{ (k_1, \dots, k_n) : \sum_{j=1}^n k_j = r, \sum_{j=1}^n j k_j = n \right\}.$$

As $|p(n, \alpha)| \leq |\hat{p}(n, \alpha_1)|$ we conclude the desired estimate with (4.20) and

$$\sum_{\mathbf{k} \in p(n, \alpha)} \prod_{j=1}^n \frac{1}{k_j!} \leq \sum_{\mathbf{k} \in \hat{p}(n, \alpha_1)} \prod_{j=1}^n \frac{1}{k_j!}.$$

Therefore,

$$|\partial_{\theta}^n f(r(\theta), \theta)| \leq C_f n! 2^n r_{\max}^n |\cos(\theta - \theta_1^*)|^{-2n} \sum_{1 \leq |\alpha| \leq n} \frac{1}{\alpha_1! \alpha_2!} \binom{n-1}{\alpha_1-1},$$

and if we now use $\sum_{\alpha_2=0}^{n-\alpha_1} \frac{1}{\alpha_2!} \leq e$ and

$$\sum_{\alpha_1=0}^n \frac{1}{(\alpha_1-1)!} \frac{1}{\alpha_1} \binom{n-1}{\alpha_1-1} \leq \sum_{\alpha_1=0}^n \binom{n}{\alpha_1} = 2^n,$$

it finally yields

$$\|\partial_{\theta}^n f(r(\theta), \theta)\|_{\infty} \leq C_f |\cos(\theta - \theta_1^*)|^{-2n} \max(1, r_{\max})^n n! 2^{2n}.$$

With the classical error estimate (4.12) we obtain

$$\begin{aligned} Ef &= \mathcal{Q}_n^{[\theta_1, \theta_2]} - \mathcal{I}f \\ &\leq \frac{(\theta_2 - \theta_1)^{2n+1}}{2n+1} \frac{(n!)^4}{(2n!)^3} \|\partial_{\theta}^n f(r(\theta), \theta)\|_{\infty} \\ &\leq \frac{(\theta_2 - \theta_1)^{2n+1}}{2n+1} \frac{(n!)^5}{(2n!)^3} C_f \max(1, r_{\max}^n) \max_{\theta \in (\theta_1, \theta_2)} |\cos(\theta - \theta_1^*)|^{-2n} 2^{2n}. \end{aligned}$$

Stirling's formula yields

$$\frac{(n!)^5}{(2n!)^3} \sim \frac{\pi}{\sqrt{2}} \left(\frac{e}{64}\right)^n \frac{1}{n^{n-1}}$$

and obtain

$$\frac{(n!)^5}{(2n+1)(2n!)^3} 4^n \sim \frac{\pi}{3\sqrt{2}} \left(\frac{e}{16}\right)^n \frac{1}{n^{n-1}} = \frac{\pi}{3\sqrt{2}} e^{-n(\ln(16)-1)-(n-1)\ln n} \leq C e^{-2n}.$$

Thus it yields

$$\begin{aligned} E^{D_1} f &\leq C(\theta_2 - \theta_1)^{2n+1} \max(1, r_{\max}^n) \max_{\theta \in (\theta_1, \theta_2)} |\cos(\theta - \theta_1^*)|^{-2n} e^{-2n} \\ &\leq C(\theta_2 - \theta_1) e^{2n \ln(\theta_2 - \theta_1)} e^{-2n \ln(C_{\theta})} e^{-2n} \max(1, r_{\max}^n), \end{aligned}$$

where

$$C_{\theta} := \min_{\theta \in (\theta_1, \theta_2)} |\cos(\theta - \theta_1^*)|$$

such that

$$E^{D_1} f \leq C(\theta_2 - \theta_1) e^{-2n(-\ln(\theta_2 - \theta_1) + \ln(C_{\theta}) + 1)} \max(1, r_{\max}^n)$$

Now for $r_{\max} \leq 1$

$$-\ln(\theta_2 - \theta_1) + \ln(C_{\theta}) + 1 > 0$$

which yields the condition

$$\theta_2 - \theta_1 < e C_{\theta}$$

and for $r_{\max} > 1$

$$-\frac{1}{2} \ln(r_{\max}) - \ln(\theta_2 - \theta_1) + \ln(C_\theta) + 1 > 0$$

such that

$$\sqrt{r_{\max}}(\theta_2 - \theta_1) < eC_\theta$$

and we finally obtain

$$E^{D_2} f \leq C(\theta_2 - \theta_1)e^{-bn}$$

for positive constants C and b independent of n .

3. On \hat{D}_3 there holds $\partial_\theta^j r(\theta) = t \partial_\theta^j r_{\mathbf{e}_2}(\theta)$ and with Lemma 4.5 we obtain

$$\left| \partial_\theta^j r(\theta) \right| \leq 2^j j! r_{\max} |\cos(\theta - \theta_2^*)|^{-(j+1)}$$

the same argumentation as on \hat{D}_2 yields for $\max(1, \sqrt{r_{\max}})\theta_2 - \theta_1 < eC_\theta$ where

$C_\theta := \min_{\theta \in (\theta_1, \theta_2)} |\cos(\theta - \theta_2^*)|$ the following estimate

$$E^{D_3} f \leq C(\theta_2 - \theta_1)e^{-bn}$$

4. On \hat{D}_4 there holds $\partial_\theta^j r(\theta) = t \partial_\theta^j r_{\mathbf{e}_2}(\theta) + (1-t) \partial_\theta^j r_{\mathbf{e}_1}(\theta)$ and Lemma 4.5 yields

$$\left| \partial_\theta^j r(\theta) \right| \leq 2^j j! r_{\max} |\cos(\theta - \theta_2^*)|^{-(j+1)} + 2^n n! r_{\max} |\cos(\theta - \theta_1^*)|^{-(n+1)}$$

Now define

$$C_\theta := \min_{\theta \in (\theta_1, \theta_2)} (|\cos(\theta - \theta_1^*)|, |\cos(\theta - \theta_2^*)|)$$

which for $\max(1, \sqrt{r_{\max}})\theta_2 - \theta_1 < eC_\theta$ results in

$$Ef \leq C(\theta_2 - \theta_1)e^{-bn}$$

□

Numerical experiments have shown, that the proposed quadrature converges exponentially fast even, when the condition $\max(1, \sqrt{r_{\max}})(\theta_2 - \theta_1) < eC_\theta$ is violated, but then the pre-asymptotical interval is relatively big.

We observe, that the constant in (4.17) depending on θ blows up for θ approaching $\theta_i^* \pm \frac{k\pi}{2}$ ($i = 1, 2, k \in \mathbb{N}$). This singularity is never reached, as the normal vector of the line segment would be perpendicular to ray direction and the decomposition strategy ensures, that this case is not possible. Nevertheless, θ can get close to this point and thus we investigate a grading in direction of the critical point. Let us consider domain \hat{D}_2 with a graded quadrature $Q_{n,m,\sigma}^{[\theta_1, \theta_2]}$ towards $\theta_1^* \pm \frac{k\pi}{2}$. Without loss of generality, we can assume, that $\theta_1^* \pm \frac{k\pi}{2} < \theta_1$ and thus we apply a constant order composite quadrature with a geometric mesh towards θ_1 with $\theta_0 = \theta_1$, $\theta_j := \theta_1 + \sigma_\theta^{m_\theta+1-j}(\theta_2 - \theta_1)$ and $\mathbf{n}_\theta := (n_0, n_0, \dots, n_0)$ given by

$$Q_{n_\theta, m_\theta, \sigma_\theta}^{[\theta_1, \theta_2]} f = \sum_{j=0}^{m_\theta} Q_{n_0}^j f.$$

The constant C_θ can be controlled by scaling the integration domain down, when C_θ becomes small. Then the exponential convergence can be guaranteed without claiming conditions on the size of the integration domain in θ and we can formulate the following lemma.

Lemma 4.7. *For the constant order composite quadrature $Q_{n_\theta, m_\theta, \sigma_\theta}^{[\theta_1, \theta_2]} f$ there holds*

$$E^{[\theta_1, \theta_2]} Q_{n_\theta, m_\theta, \sigma_\theta} f \leq C e^{-bn_\theta}$$

where the total number of quadrature points is given by $N_\theta = m_\theta n_\theta$. b and C are constants independent of N_θ .

Proof. Construct the composition such that on each subinterval there holds

$$\max(1, \sqrt{r_{\max}}) |I_j| < eC_\theta,$$

which can be achieved by a grading towards the critical values $\theta_1^* \pm \frac{\pi}{2}$. Thus Lemma 4.6 yields

$$E^{[\theta_1, \theta_2]} Q_{n_\theta, m_\theta, \sigma_\theta} f \leq \sum_{j=1}^m E^{[I_j]} Q_{n_\theta} f \leq \sum_{j=1}^m C e^{-bn_\theta} \leq m_\theta C e^{-bn_\theta} = C e^{-bn_\theta \ln(m_\theta)} \leq C e^{-bn_\theta}.$$

□

We can use this result to obtain the following theorem.

Theorem 4.8. *Given a function $f \in B_\beta^0(T)$ with a weight function $\Phi_{\beta, \alpha, 0}(r) = r^{|\alpha| + \beta}$, then there holds for D_l as defined in (4.10)*

$$\left| I^{(D_l)} f - Q^{(D_l)} f \right| \leq C e^{-b \sqrt[3]{N}}$$

for $l = 1, \dots, 4$ and where N denotes the total number of quadrature points and C and b are positive constants independently of N , but depending on the grading factor σ_r , the number of levels m_r and on f .

Proof. The proof is similar to the proof of Theorem 4.3, but it uses Lemma 4.7 to achieve unconditional exponential convergence in the angle. □

If we now return to the retarded potential $(P\varphi)(x)$ as defined in (4.7), we can construct the inner quadrature rule by

$$Q^{(\text{in})} f = \sum_{l=1}^{n_d} Q^{(D_l)} f$$

and apply the convergence results on the subdomains. Theorem 4.3.

Theorem 4.9 (Error on $E(x) \cap T$). *Given the retarded potential $P\varphi$ as defined in (4.9), it holds*

$$\left| P\varphi - Q^{(\text{in})} f \right| \leq C e^{-b \sqrt[3]{N}}$$

where $f(r, \theta) = (d^2 + r^2)^{\frac{\nu}{2}} \varphi(r, \theta) r$ and $Q^{(\text{in})} f$ defines the composite quadrature rule on the subdomains D_l and uses a total number of quadrature points N , b , C are positive constants independent of N .

Proof. Due to [51] $f \in B_\beta^0(T)$ and we apply Theorem 4.3 and obtain

$$\left| P - Q^{(\text{in})} f \right| \leq \sum_{l=1}^{n_d} \left| I^{(D_l)} - Q^{(D_l)} P \right| \leq C e^{-b \sqrt[3]{N}}.$$

□

4.2 Outer Quadrature for Discrete Retarded Potentials

4.2.1 Decomposition of Integration Domain $\widehat{T} \cap E(T)$

In Chapter 3 the regularity of the discrete retarded potential evaluated on an element T was discussed. We have proven, that the function corresponding to the discrete retarded potential possesses besides the classical singularities several

singularities of geometrical nature. The classical singularities have the strongest influence on the continuity of higher order derivatives, if we deal with weakly singular kernel functions as known from the time independent case, cf. [43]. Nevertheless, the geometrical singularities have also a significant influence on the regularity of higher order derivatives of $P\phi$. In Fig. 3.2 the distribution of the geometrical singularities in \mathbb{R}^3 is sketched for $r_{\min} = 0$. For $r_{\min} > 0$ we obtain an additional set of geometrical singularities, as discussed in Section 3.2.4.

A numerical integration of $P\phi$ over the domain $\hat{T} \cap E(T)$ has to pay attention to these different singularities. In order to achieve an exponential convergence, we have to incorporate these singularities into a composite quadrature rule including an appropriate grading strategy. Thus let us first describe an appropriate decomposition of the integration domain. Regard first the simplified domain of influence $E_R(T)$ as defined in (3.3) with $R > 0$.

Intersect the domain of influence $E_R(T)$ including the spheres $B_R(p_i)$ and the cylinders $\mathcal{C}_R(e_i)$ with the plane $\mathcal{E}_{\hat{T}}$ corresponding to the test element \hat{T} . These intersections can result in quite complicated shapes. In Chapter 3 we have already discussed some of these intersections in the triangle plane \mathcal{E}_T , compare e.g. Fig. 3.15 and some results perpendicular and parallel to this plane, cf. Fig. 3.23 and 3.24. But how do these intersections look like, if the triangle planes \mathcal{E}_T and $\mathcal{E}_{\hat{T}}$ are neither parallel nor perpendicular?

The intersection of a sphere $B_R(p_i)$ and a plane $\mathcal{E}_{\hat{T}}$ always results in a circle $B_{R'}(p'_i)$. Given the normal $n_{\hat{T}}$ of the plane $\mathcal{E}_{\hat{T}}$ and a point $\hat{p} \in \mathcal{E}_{\hat{T}}$ we can describe such a circle in the following way. First project its center p_i into the triangle plane $\mathcal{E}_{\hat{T}}$ which results in $p'_i = p_i - (p_i - \hat{p}, n_{\hat{T}})n_{\hat{T}}$. If the sphere is actually intersecting the plane, the radius of the projected circle is due to Pythagoras' theorem

$$R'(p_i) = \begin{cases} \sqrt{R^2 - (p_i - \hat{p}, n_{\hat{T}})^2}, & |(p_i - \hat{p}, n_{\hat{T}})| < R \\ 0, & \text{else} \end{cases}.$$

If the circles touch a cylinder in a point, there exists a point singularity. If the circle coincides with the surface of the cylinder touching its caps, there exists a one-sided singularity on the whole boundary of the circle. If the circle does not touch the cylinders, the potential is regular.

Therefore, on the three circles $B_{R'}(p'_i)$ with $(i = 1, 2, 3)$ the potential $P(x)$ possesses one-sided singularities from the interior of the circle.

Coming now to the intersection set of a cylinder $\mathcal{C}_R(e)$ with the plane $\mathcal{E}_{\hat{T}}$ the situation is a bit more complicated. Here e denotes the axis of $\mathcal{C}_R(e)$ and m_1 and m_2 are the end points of e . The intersection can result in circles, ellipses or in either one line or two parallel lines and as we regard a finite cylinder, also in subsets of these elements. In Chapter 11.7.3 in [50] a detailed case study for intersection of plane and cylinder is presented. Note that in contrast the analysis of [50], our cylinder has open caps. Denote the axis direction of the cylinder $d = e/|e|$ and its center point $c = (m_1 + m_2)/2$. The half-height of the cylinder is $h = |e|/2$. There three basic cases are distinguished

1. $\mathcal{E}_{\hat{T}} \parallel e$, i.e. $|d \cdot n_{\hat{T}}| = 1$: The intersection is either one or two line segments for a distance $\text{dist}(e, \mathcal{E}_{\hat{T}}) = R$ or $\text{dist}(e, \mathcal{E}_{\hat{T}}) < R$. If $\text{dist}(e, \mathcal{E}_{\hat{T}}) > R$, then the intersecting set is empty.
2. $\mathcal{E}_{\hat{T}} \perp e$, i.e. $|d \cdot n_{\hat{T}}| = 0$: If $\text{dist}(c, \mathcal{E}_{\hat{T}}) < h$ the intersection is a circle; for $\text{dist}(c, \mathcal{E}_{\hat{T}}) \geq h$ the intersection is empty.
3. $\mathcal{E}_{\hat{T}}$ and e_i are neither parallel nor perpendicular. Compute the intersection point I_a of $\mathcal{E}_{\hat{T}}$ with the axis of the cylinder and compute its distance to the center point c
 - a. $\text{dist}(I_a, c) < h$: There always exists an intersection.
 - b. $\text{dist}(I_a, c) \geq h$: There might exist an intersection depending on the relative position of the plane compared to the cylinder.

In both cases the intersection will be an ellipse, an elliptical arc or two elliptical arcs. For an infinite cylinder the ellipse can be represented [50] by

$$\begin{aligned} c_e &= m_1 + \frac{(p - m_1) \cdot n_{\hat{T}}}{a \cdot n_{\hat{T}}} a \\ r_u &= \frac{R}{|a \cdot n_{\hat{T}}|} & u &= \frac{a - (a \cdot n_{\hat{T}})n_{\hat{T}}}{|a - (a \cdot n_{\hat{T}})n_{\hat{T}}|} \\ r_v &= R & v &= n_{\hat{T}} \times u, \end{aligned}$$

where c_e is the origin of the ellipse with axis direction u and v and radii r_u and r_v .

On the boundary of the intersected domains (without the caps) there exists a one-sided edge singularity.

These three spheres and cylinders are a subset of the domain of influence $E_R(T)$. The only remaining part is the prism $\mathcal{P}_R(T)$, i.e. we have to intersect the plane $\mathcal{E}_{\hat{T}}$ with the shifted trial elements $T_{R^\pm} := T \pm R$. This intersection is either

a line, a point, the whole triangle or empty, depending on the relative position of the plane $\mathcal{E}_{\hat{T}}$ to the triangle T . In Chapter 11.5.3 [50] a detailed analysis of the different cases and its detection may be found. Note that for the general case with $r_{\min} > 0$ all these singularities duplicate as pointed out in Proposition 3.25.

4.2.2 Construction of the Composite Quadrature Rule

The discrete retarded potential (4.7) was analyzed in for Theorem 3.26. We have to decompose the plane $\mathcal{E}_{\hat{T}}$ induced by the test element with respect to the singularity field of the retarded potential given by $\Theta_{r_{\min}}^{r_{\max}}(T)$ as defined in (3.23). This partition intersected with the test element \hat{T} defines the the composition of the integration domain $E(T) \cap \hat{T}$ of the outer integral and thus

$$G(\varphi, \hat{\varphi}) = \sum_{A=A' \cap \mathcal{E}_{\hat{T}}, A' \in \Theta_{r_{\min}}^{r_{\max}}(T)} \int_{A \cap \hat{T}} f(x) dx.$$

The elements $A \in \Theta_{r_{\min}}^{r_{\max}}(T)$ can have a complicated structure, but they all can be described as a polygon with κ edges, where each edge is a line segment, the arc of a circle or the arc of an ellipse. It is also possible, that the partition elements result in complete circles and ellipses. In Fig. 4.7 a typical decomposition for the example discussed in the beginning, compare Fig. 4.1(a), is sketched. In this specific example the test element \hat{T} is decomposed into 5 elements illuminated by $E(T)$. The remaining part of the element is not part of the integration domain. We define the outer quadrature rule via

$$\mathcal{Q}^{(\text{out})} f := \sum_{A=A' \cap \mathcal{E}_{\hat{T}}, A' \in \Theta_{r_{\min}}^{r_{\max}}(T)} \mathcal{Q}^{(A \cap \hat{T})} f.$$

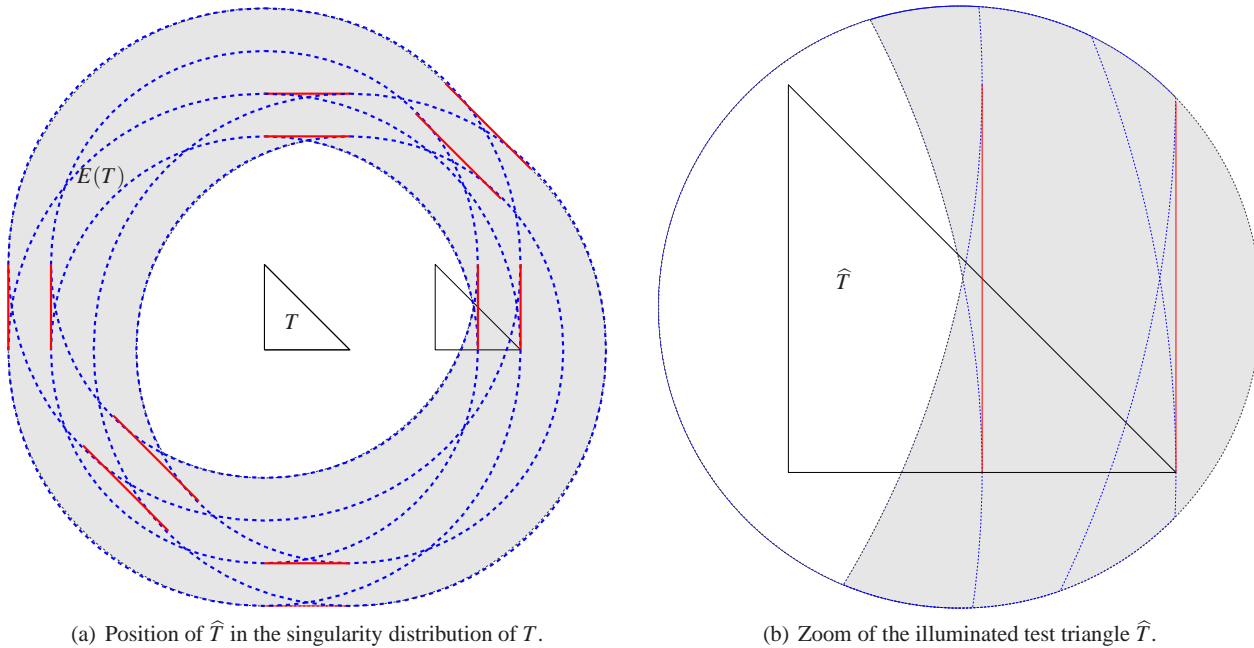


Fig. 4.7 Example of the decomposition of \hat{T} in the natural decomposition as induced by T if both elements lie in the same plane.

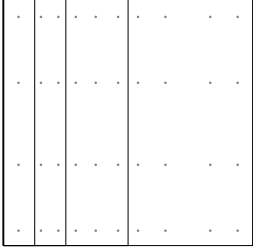
Before we continue, we collect some definitions of geometric meshes for corner, edge and corner edge singularities. Denote by $K := [0, 1] \times [0, 1]$ the unit square. We define $x_0 = 0$ and $x_k = \sigma^{m-k}$ for $k = 1, \dots, m$, such that $I_k := [x_{k-1}, x_k]$, where $m \in \mathbb{N}$ is the grading level and $\sigma \in (0, 1)$ the grading parameter. The geometric mesh K_m^σ is defined in the following ways, depending on the type of singularity..

Geometric mesh for a corner singularity: In [51] we find the following suggestion of a geometric mesh for a point with $m \in \mathbb{N}$ level and grading parameter $\sigma \in (0, 1)$. The decomposition K_m^σ of K into $3(m-1) + 1$ elements K_{ij} is

$$\begin{aligned} K_{jj} &= I_j \times I_j \quad (j = 1, \dots, m), \\ K_{1j} &= \left(\bigcup_{l=1}^{j-1} I_l \right) \times I_j \quad (j = 2, \dots, m) & K_{j1} &= I_j \times \left(\bigcup_{l=1}^{j-1} I_l \right) \quad (j = 2, \dots, m). \end{aligned}$$

Compare also Fig. 4.8(a). The degree vector is given by $p = (p_1, \dots, p_m)$, such that on the elements K_{1j} , K_{j1} and K_{jj} a quadrature rule of degree p_j is used.

Geometric mesh for an edge singularity:



The decomposition K_m^σ of K into m elements K_j is

$$K_j = I_j \times [0, 1] \quad (j = 1, \dots, m).$$

Compare also Fig. 4.8(b). The degree vector is given by $p = (p_1, \dots, p_m)$. We define a spline space $S^p(K_m^\sigma)$ of piecewise defined polynomials $p(x, y)$ with a polynomial degree p_j in x_1 and p in x_2 on K_j , i.e. $v|_{I_j \times I_j} \in P_{p_j, p}(K_j)$, where we demand $p \sim m$. On the right hand side, an example with quadrature points is sketched.

We will prove the exponential convergence of a composite quadrature rule for an anisotropic quadrature rule.

Proposition 4.10. *Let $f \in B_\beta^l(K)$, with an anisotropic weight function like $\Phi_{\beta, \alpha, l}(x_1, x_2) = x_1^{|\alpha| - l + \beta}$. Then the variable order composite quadrature rule as described above yields exponential convergence, i.e.*

$$|I^K f - Q^K f| \leq C e^{-b \sqrt[3]{N}},$$

where b and C are constants independent of the total number of quadrature points N .

Proof. By construction it holds, $Q^K f := (Q^{[0,1]} \otimes Q^{I_j})f$ and thus

$$\begin{aligned} |I^K f - Q^K f| &\leq \sum_{j=1}^m |I^{K_j} f - Q^{K_j} f| \\ &\leq \sum_{j=1}^m \left| \int_{K_j} f - Q^{[0,1]} \int_{I_j} f \right| + \left| Q^{[0,1]} \int_{I_j} f - Q^{K_j} f \right| \\ &= \sum_{j=1}^m \left| I^{I_j} (I^{[0,1]} - Q^{[0,1]}) f \right| + \left| Q^{[0,1]} (I^{I_j} - Q^{I_j}) f \right| \\ &\leq \sum_{j=1}^m |I_j| \max_{x_1 \in I_j} \left| (I^{[0,1]} - Q^{[0,1]}) f(x_1, \cdot) \right| + \sum_{j=1}^m \max_{x_2 \in [0,1]} \left| (I^{I_j} - Q^{I_j}) f(\cdot, x_2) \right| \end{aligned}$$

Now, the function is analytic parallel to the edge and perpendicular to the edge, we can apply the usual B_β -analysis in one-dimension as already discussed in Lemma 4.4, such that

$$|I^K f - Q^K f| \leq C_2 e^{-b_2 n_2} + C_1 e^{-b_1 \sqrt{N_1}},$$

where n_2 denotes the number of quadrature point for the evaluation in x_2 and $N_1 \sim m^2$ denotes the total number of quadrature points for the evaluation in x_1 . C_1, C_2, b_1 and b_2 are positive constants independent of n_2 and N_1 . As $n_2 \sim m$ we further estimate

$$|I^K f - Q^K f| \leq C e^{-b \sqrt[3]{N}}.$$

□

Geometric mesh for an corner-edge singularity: In [38] the following geometric mesh is proposed. The decomposition consists of m^2 elements defined via

$$K_{ij} = I_i \times I_j \quad (i, j = 1, \dots, m) \quad (4.21)$$

Moreover, for a degree vector $p = p_1, \dots, p_m$ we define a spline space $S^p(K_\sigma^m)$ of piecewise defined polynomials $p(x, y)$ with a polynomial degree p_i in x_1 and p_j in x_2 on $I_i \times I_j$, i.e. $v|_{I_i \times I_j} \in P_{p_i, p_j}(K_{ij})$. Compare also Fig. 4.8(c).

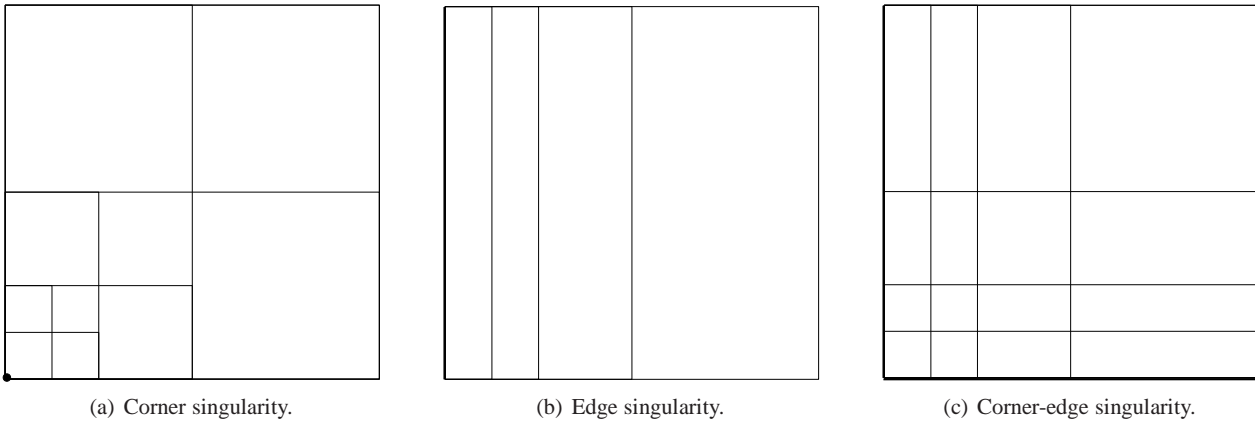


Fig. 4.8 Grading strategy for the different types of singularities for $m = 4$ and $\sigma = 0.5$.

4.2.3 Error Analysis

Theorem 4.11. Given a function $f(x, y) := k(x - y)\varphi(y)\widehat{\varphi}(x)$ it holds

$$\left| G(\varphi, \widehat{\varphi}) - Q^{(\text{out})} Q^{(\text{in})} f \right| \leq C e^{-b \sqrt[4]{N}}$$

where b and C denote positive constants independent of the number of quadrature points N .

Proof. Define $f(x, y) := k(x - y)\varphi(y)\widehat{\varphi}(x)$ and estimate

$$\left| G(\varphi, \widehat{\varphi}) - Q^{(\text{out})} Q^{(\text{in})} f \right| \leq \left| G(\varphi, \widehat{\varphi}) - Q^{(\text{out})}(P\varphi)(x) \right| - \left| Q^{(\text{out})}(P\varphi)(x) - Q^{(\text{out})} Q^{(\text{in})} f \right|$$

The second term can be estimated by Theorem 4.9, whereas for the estimation of the first term, we have to apply the knowledge of the regularity of $P\varphi$ as formulated in Theorem 3.26. Each partition element can involve corner, edge and corner-edge singularities. Corner or point singularities have been analyzed in Theorem 4.1 [51]. Corner and corner-edge singularities have been analyzed in the context of the hp-method, compare [27] for the exponential convergence on geometric meshes with edge singularities and [38] the corresponding corner-edge singular case. These

techniques can also be applied in the construction of a quadrature on a domain with edge or corner-edge singularities. In Proposition 4.10 we give a short proof for the exponential convergence of the graded quadrature for an edge singularity. The regularity the retarded potential on each partition element $A \in \Theta_{r_{\min}, \ell_T}^{r_{\max}}(T)$ intersected with the test triangle \widehat{T} is described by a countably normed space $B_\beta^l(A \cap \widehat{T})$, where the weight function and the order are given in Theorem 3.26. Therefore, we can always divide the regarded subelement, such that a conform mapping of the above described model situation yields, that there exist positive constants b and C independent of the number of quadrature points N such that

$$\left| \int_{A \cap \widehat{T}} P\varphi(x) \widehat{\varphi}(x) ds_x - Q^{(A \cap \widehat{T})}((P\varphi)(x) \widehat{\varphi}(x)) \right| \leq Ce^{-b\sqrt[4]{N}}$$

and thus the assertion follows. \square

4.3 Technical Results

In this section we collect some of the auxiliary results used throughout this chapter. Some of the presented results are quoted from other works or slightly modified and only stated for the sake of completeness, whereas some where delayed, as the estimation is straight forward, but lengthy. The next lemmata were used in the proof of Lemma 4.4.

Lemma 4.12 (Lemma 4.1 in [51]). *Let $f \in C^0(\overline{\Omega})$, $\Omega \subset \mathbb{R}^r$, and let Q be a PI quadrature rule on Ω which is exact of total degree $p \geq 0$. Then*

$$\left| \int_{\Omega} f dx - Qf \right| \leq 2|\Omega| \inf_{\pi} \|f - \pi\|_{L^\infty(\Omega)}$$

where the infimum is taken over all polynomials π of total degree p .

Lemma 4.13 (Lemma 4.3 in [51]). *Let $\Omega = (-h/2, h/2)^r \subset \mathbb{R}^r$ with $h \in (0, 1)$ and $l > r/2$ a natural number. Then we have for every $\psi \in H^l(\Omega)$*

$$\|\psi\|_{L^\infty(\Omega)}^2 \leq C \sum_{m=0}^l h^{2m-r} |\psi|_{H^m(\Omega)}^2$$

where the constant C depends on r , but is independent of h .

Lemma 4.14 (Lemma 3.38 in [52]). *Let $J = (a, b) \subset \mathbb{R}$, $h = b - a$ and $u \in H^{p+1}(J)$ for some $p \geq 1$. Then there exists a polynomial ϕ of degree p on J , such that for $m = 0, 1$*

$$\left\| (u - \phi)^{(m)} \right\|_{L^2(J)}^2 \leq Ch^{-2m} \left(\frac{h}{2} \right)^{2(s+1)} \frac{(p-s)!}{(p+s+2-2m)!} \left\| u^{(s+1)} \right\|_{L^2(J)}^2$$

where $C > 0$ is independent of h , p and u and $s \in \mathbb{N}_0$, $s \leq p$, $m = 0, 1$ if $p \geq 1$ and $s = m = 0$ if $p = 0$. Moreover, $u(a) = \phi(a)$ and $u(b) = \phi(b)$ for $p \geq 1$.

Remark 4.15. Again, we do not need an exact interpolation on the boundary and a more general version of Lem. 4.14 would do the job.

The next Lemma is a modification of Lemma 3.39 in [52] for B_β^0 -functions.

Lemma 4.16. *Let $J = (a, b) \subset (0, 1)$, $0 < \lambda < C_J$ and $h = b - a = \lambda a$. For each $u \in H_\beta^{s+1}(J)$ there exists a polynomial ϕ of degree $p \geq 1$, such that*

$$\left\| (u - \phi)^{(m)} \right\|_{L^2(J)}^2 \leq Ca^{-2(\beta+m)} \frac{\Gamma(p-s+1)}{\Gamma(p+s+3-2m)} \left(\frac{\lambda}{2} \right)^{2s} |u|_{H_\beta^{s+1,0}(J)}^2$$

for $s \leq p$, $s \in \mathbb{R}$ and $m = 0, 1$.

Proof. It holds

$$\left\| u^{(s+1)} \right\|_{L^2(J)} = \left\| u^{(s+1)} r^{\beta+s+1} r^{-(\beta+s+1)} \right\|_{L^2(J)} \leq a^{-(\beta+s+1)} |u|_{H_\beta^{s+1,0}(J)}$$

Using this and Lem. 4.14 it yields

$$\begin{aligned} \left\| (u - \phi)^{(m)} \right\|_{L^2(J)}^2 &\leq Ch^{-2m} \left(\frac{h}{2} \right)^{2(s+1)} \frac{(p-s)!}{(p+s+2-2m)!} a^{-2(\beta+s+1)} |u|_{H_\beta^{s+1,0}(J)}^2 \\ &\leq CC_J a^{-2(\beta+m)} \left(\frac{\lambda}{2} \right)^{2(s+1-m)} \frac{(p-s)!}{(p+s+2-2m)!} |u|_{H_\beta^{s+1,0}(J)}^2 \\ &\leq Ca^{-2(\beta+m)} \left(\frac{\lambda}{2} \right)^{2s} \frac{(p-s)!}{(p+s+2-2m)!} |u|_{H_\beta^{s+1,0}(J)}^2 \end{aligned} \quad (4.22)$$

whereas the last step uses that λ is bounded, which is the case for geometrical meshes, cf. remark 4.17. Applying the real method of interpolation as stated e.g. in [52] Theorem B.3. we define $\sigma := s + \theta - 1$ for $\theta \in (0, 1)$ and

$$H_\beta^{\sigma+1,0}(J) := (H_\beta^{s,0}(J), H_\beta^{s+1,0}(J))_{\theta, \infty}$$

Thus the error operator $T : H_\beta^{s+1,0}(J) \rightarrow L^2(J)$ with $Tu := (u - \phi)^{(m)}$ is linear and bounded due to (4.22). Thus interpolation yields (here we can apply an argumentation similar to Schwab in [52] p. 92)

$$\begin{aligned} \|T\|_{H_\beta^{\sigma+1,0}(J) \rightarrow L^2(J)}^2 &\leq \|T\|_{H_\beta^{s,0}(J) \rightarrow L^2(J)}^{2(1-\theta)} \|T\|_{H_\beta^{s+1,0}(J) \rightarrow L^2(J)}^{2\theta} \\ &\leq Ca^{-2(\beta+m)} \left(\frac{\lambda}{2} \right)^{2\sigma} \frac{\Gamma(p+1-\sigma)}{\Gamma(p+1+\sigma+2-2m)}. \end{aligned}$$

Inserting the definition of σ and using that $\Gamma(x)$ is a monotone increasing function for $x \geq 1$ the assertion follows. \square

Remark 4.17. For the proposed geometrical subdivision of the ray, we have $\lambda = (1 - \sigma)/\sigma$ which is bounded for $\sigma > 0$, but can become arbitrary large for $\sigma \rightarrow 0$. Nevertheless, for practical purposes σ wouldn't be chosen too close to zero.

Lemma 4.18. Define $F : (1, \infty) \times (0, 1) \rightarrow \mathbb{R}$ via

$$F(d, \alpha) := \left(\frac{\alpha d}{2} \right)^\alpha \left(\frac{(1-\alpha)^{1-\alpha}}{(1+\alpha)^{1+\alpha}} \right)^{1/2}$$

then it holds

$$\inf_{\alpha \in (0,1)} F(d, \alpha) = F(d, \alpha_{\min}) < 1, \quad \alpha_{\min} = \frac{2}{\sqrt{4+d^2}}.$$

4.4 Numerical Experiments

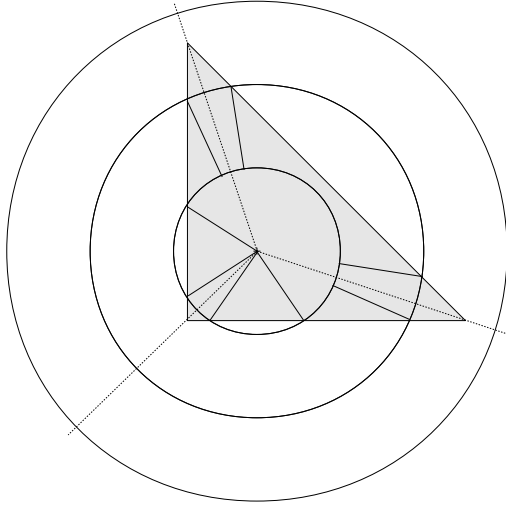
4.4.1 Accuracy of the Numerical Evaluation of Retarded Integrals

Let us discuss the evaluation of retarded potentials following the quadrature schemes introduced in Section 4.1. We will choose $r_{\min} = t_l$ and $r_{\max} = t_{l+1}$, where $t_l = l\Delta t$ and evaluate

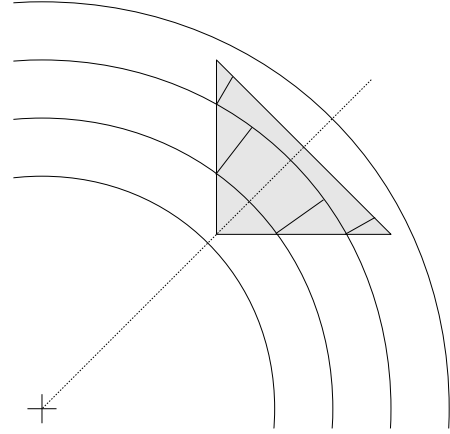
$$P(x) = \int_{T \cap B_{t_{l+1}}(x) \setminus B_{t_l}(x)} \frac{1}{|x-y|} ds_y \quad (l = 0, 1, \dots)$$

where we fix the triangle $T = \{(0, 0, 0), (1, 0, 0), (0, 1, 0)\}$.

Fix $\Delta t = 1/3$. As we have already discussed the composite quadrature for this type of integral in some detail, we only want to underline the composition of the integration domain for some of the chosen points x as sketched in Fig. 4.9. We observe, that for $x = (0.25, 0.25, 0)$ the intersection $T \cap B_{l+1}(x) \setminus B_l(x)$ vanishes for $l \geq 3$, such that we regard the potential evaluation on the first three rings. Each ring corresponds to one time step in the final MOT scheme. In Fig. 4.9(a) the decomposition on each ring is sketched.



(a) Example: Point in triangle, $x = (0.25, 0.25, 0)^T$.



(b) Example: Point outside triangle, $x = (-1, -1, 0)^T$.

Fig. 4.9 Examples for the decomposition of the integration domain for $\Delta t = 0.3$.

The first ring is decomposed into 7 subelements, the second into 9 and the third into four subelements. One immediately notices the different size of these subelements, such that a uniform distribution of quadrature points is a difficult task. A grading in the angle is not necessary for this example, as the use of polar coordinates lifts the point singularity. For integrals with a stronger singularity on the kernel, as e.g. occurring for the double layer potential, this is naturally not true.

In Fig. 4.10(a) and 4.10(b) we observe the exponential convergence for $x = (0.25, 0.25, 0)$ and $x = (-1, -1, 0)$ on all rings. In Fig. 4.9(b) the decomposition of the integration domain for $x = (-1, -1, 0)$ is sketched.

As analyzed in Lemma 4.6 the exponential convergence of the Gaussian quadrature over the angle can possess a big pre-asymptotic interval. Thus we apply an additional grading in the angle, depending on the distance of the angular integration domain to the critical values as identified in Lemma 4.6. In the practical implementation, we activate the angular grading if the direction of the angular integration x_θ and the normal n of the edge representation $r_e(\theta)$ as defined in (4.8) are almost perpendicular. We choose $|x_\theta \cdot n| < 0.2$. If $x = (0.1, 0.85, 0)$ we can observe the effect of the grading. In Fig. 4.10(c) we have exponential convergence on all four rings. Using a grading in the angle in Fig. 4.10(d) and Fig. 4.10(e) the convergence on ring 1 for $l = 1$ is significantly improved compared with Fig. 4.10(c), where a grading with $\sigma = 0.17$ seems to be the better choice.

Remark 4.19. (i) Note, that this quadrature scheme was used to compute the figures in Section 3.3.

(ii) As we use polar coordinates for the kernel function $|x - y|^{-1}$ no grading in the radius is necessary.

4.4.2 Test for the Accuracy of the Quadrature Routine

Given the matrix V corresponding to the classical single layer potential

$$V_{ij} := \frac{1}{2\pi} \int_{\Gamma} \int_{\Gamma} \frac{\varphi_i(x)\varphi_j(y)}{|x-y|} ds_y ds_x$$

and the basic Galerkin matrix

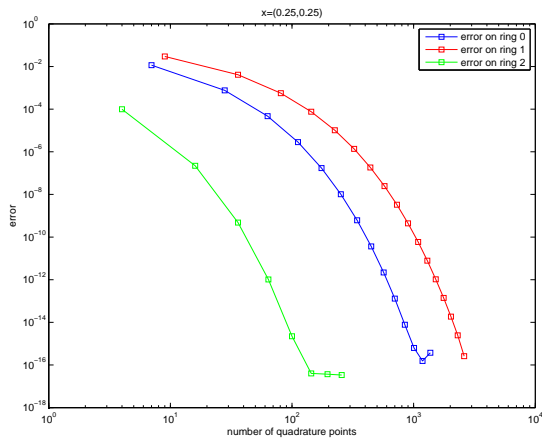
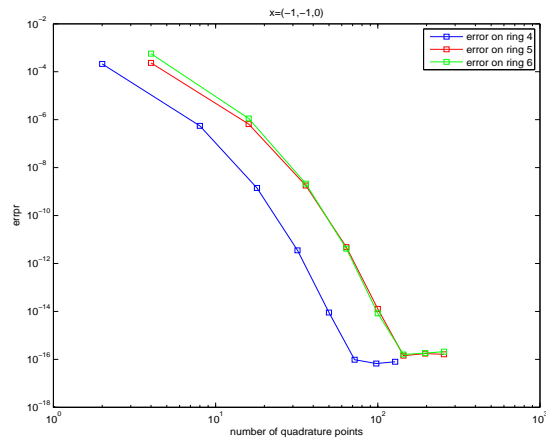
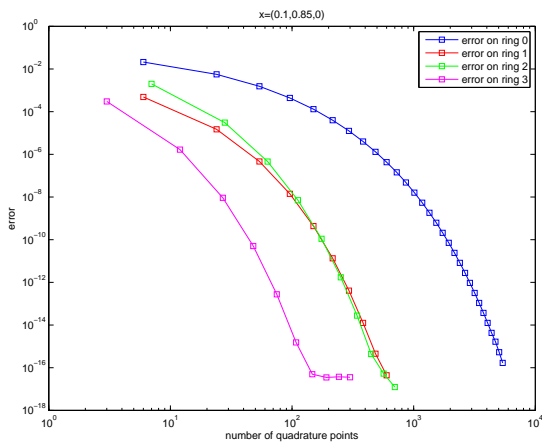
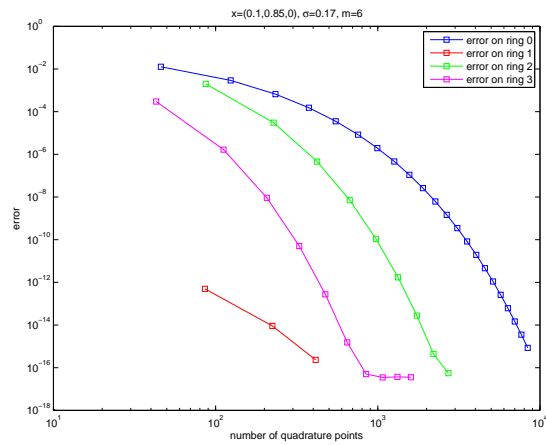
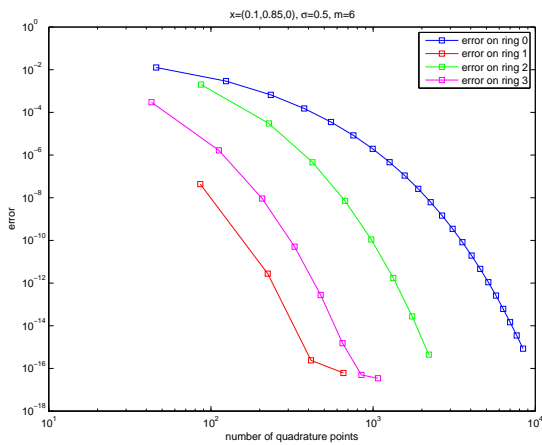
(a) $x = (0.25, 0.25, 0)^T$, without grading.(b) $x = (-1, -1, 0)^T$, without grading.(c) $x = (0.1, 0.85, 0)^T$, without grading.(d) $x = (0.1, 0.85, 0)^T$, $\sigma = 0.17$, $m = 6$.(e) $x = (0.1, 0.85, 0)^T$, $\sigma = 0.5$, $m = 6$.

Fig. 4.10 Error of the retarded potential $P(x) = \int_{B_{l+1}(x) \setminus B_l(x)} |x-y|^{-1} ds_y$ with $\Delta t = 1/3$ in different points x .

$$G_{ij}^k := \frac{1}{2\pi} \iint_{E_k} \frac{\varphi_i(x)\varphi_j(y)}{|x-y|} ds_y ds_x,$$

for $i, j = 1, \dots, \dim(V_h)$. Due to the additivity of the integral it holds for a bounded boundary Γ

$$V = \sum_{k=0}^{\infty} G^k = \sum_{k=0}^{\hat{n}} G^k, \quad (4.23)$$

with $\hat{n} + 1$ non-vanishing matrices.

For this numerical experiment we use the recursively refined icosahedron as an approximation of the sphere. Two refinement steps correspond to 320 triangles on the surface mesh. We use the analytical evaluation of the time independent single layer matrix as proposed in [38] and realized within the program package MaiProgs [37]. We compare the maximal error in the matrix entries of the sum of the retarded matrices and the analytical version of the time independent matrix, as pointed out in (4.23). We contrast different quadrature strategies for the retarded matrices and analyze their behavior for different polynomial degrees in space and different time step sizes.

Numerical experiments have shown, that a quadrature scheme with a cut-off function on the kernel function does not yield the desired accuracy.

In Table 4.1 we the standard outer quadrature for weakly singular integrals as provided in MaiProgs [37], compare also [38]. Here grading towards the singular edges and vertices of the corresponding trial element is used as e.g. sketched in [43]. The inner quadrature implements the decomposition of the integration domain as described in Section 4.1.1. We do not gain an exponential convergence as we did not implement the full decomposition scheme as discussed in Section 4.2.2. Nevertheless, we achieve already an accuracy that lead to a stable MOT-scheme as we will see in the next chapter.

p/N	Δt	\hat{n}	$\max(V - \sum_{i=0}^{\hat{n}} G^k)$				
			24 quad. points	12 quad. points	8 quad. points	4 quad. points	2 quad. points
0/320	3.0	0	2.9778e-08	2.9647e-08	8.5263e-09	4.7401e-06	1.0468e-04
	1.0	1	2.9778e-08	2.9647e-08	8.5263e-09	4.7401e-06	1.0468e-04
	0.5	3	2.9778e-08	2.9647e-08	8.5263e-09	4.7401e-06	1.0468e-04
	0.25	7	2.9778e-08	2.9652e-08	9.0388e-09	4.6643e-06	1.0174e-04
	0.125	15	2.9778e-08	2.9684e-08	1.6393e-08	2.6057e-06	6.3145e-05
	0.0625	31	2.9778e-08	2.9752e-08	2.5795e-08	9.0869e-07	2.8050e-05
1/960	3.0	0	1.8828e-08	1.9044e-08	4.6762e-08	5.2965e-06	1.0917e-04
	1.0	1	1.8828e-08	1.9044e-08	4.6762e-08	5.2965e-06	1.0917e-04
	0.5	3	1.8828e-08	1.9044e-08	4.6762e-08	5.2965e-06	1.0917e-04
	0.25	7	1.8828e-08	1.9050e-08	4.7177e-08	5.2488e-06	1.0601e-04
	0.125	15	1.8828e-08	1.8979e-08	3.6390e-08	2.9440e-06	6.5484e-05
	0.0625	31	1.8828e-08	1.8914e-08	2.7276e-08	1.2705e-06	3.3426e-05
2/1920	3.	0	2.4462e-08	2.4638e-08	4.9144e-08	5.0653e-06	1.0744e-04
	1.	1	2.4462e-08	2.4638e-08	4.9144e-08	5.0653e-06	1.0744e-04
	0.5	3	2.4462e-08	2.4638e-08	4.9144e-08	5.0653e-06	1.0744e-04
	0.25	7	2.4462e-08	2.4638e-08	4.8080e-08	4.8564e-06	1.0266e-04
	0.125	15	2.4462e-08	2.4633e-08	3.8654e-08	2.7042e-06	6.2303e-05
	0.0625	31	2.4462e-08	2.4510e-08	3.0234e-08	1.0976e-06	3.0921e-05

Table 4.1 Analysis of the polar quadrature for retarded potentials for different polynomial degrees p of the test and trial functions in space and different time steps Δt on sphere with 320 triangles and $G^k(f) \in \mathbb{R}^{N \times N}$ ($k = 0, \dots, \hat{n}$) with $f(x, y, x - y) = |x - y|^{-1}$. Equal distribution of quadrature points in subelements using polar quadrature without grading in r for potential evaluation.

In Table 4.2 we performed the same experiment for the kernel of the double layer potential and observe, that the influence of the geometrical light cone singularities is even worse.

$p/N_1 \times N_2$	Δt	\hat{n}	$\max(K - \sum_{i=0}^{\hat{n}} G^k)$				
			24 quad. points	12 quad. points	8 quad. points	4 quad. points	2 quad. points
0/320×162	3.0	0	1.5655e-11	4.6712e-11	2.7278e-09	2.6086e-07	5.9782e-06
	1.0	1	1.5194e-07	1.5194e-07	1.5200e-07	2.3555e-07	5.2483e-06
	0.5	3	1.5194e-07	1.5194e-07	1.5200e-07	2.3555e-07	5.2483e-06
	0.25	7	1.5194e-07	1.5194e-07	1.5200e-07	2.3555e-07	5.2483e-06
	0.125	15	1.5194e-07	1.5194e-07	1.5194e-07	2.3555e-07	5.2483e-06
	0.0625	31	1.5194e-07	1.5194e-07	1.5194e-07	2.3367e-07	4.3491e-06

Table 4.2 Analysis of the polar quadrature for retarded potentials for different polynomial degrees p of the test and trial functions in space and different time steps Δt on sphere with 320 triangles and $G^k(f) \in \mathbb{R}^{N_1 \times N_2}$ ($k = 0, \dots, \hat{n}$) with $f(x, y, x - y) = n_y \cdot (x - y) |x - y|^{-3}$. Equal distribution of quadrature points in subelements using polar quadrature with grading in r for potential evaluation.

Chapter 5

Numerical Results

Never in the history of mankind has it been possible to produce so many wrong answers so quickly.
Carl-Erik Fröber

In this Chapter we present numerical experiments validating our code and underlying the efficiency of the method. All computations were done as an extension of the software package MaiProgs [37]. The presented results were computed on a cluster with 5 nodes à 8 cores with 2.93 GHz and 48 Gbyte, where each core uses two Intel Nehalem X5570 processors.

5.1 Retarded Single Layer Potential Ansatz

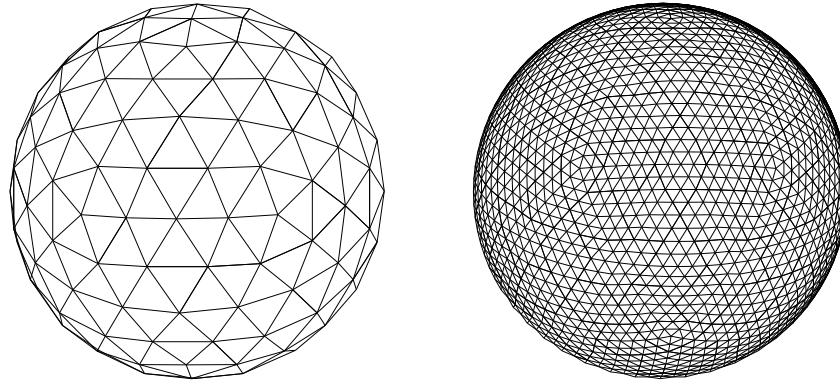


Fig. 5.1 Mesh of the surface of the sphere with 320 and 5120 elements.

We solve the single layer ansatz $V\varphi = f$. The corresponding space-time variational formulation (2.12) and its discretization (2.17) have been discussed earlier. In [7] for $\Gamma = B_1(0)$ an exact solution of the problem is given. The surface mesh of $\Gamma := \partial B_1(0)$ is generated by a recursive refinement of the icosahedron, compare Figure 5.1. For $f(t, x) = \sin^5(t)$ it is known, that the exact solution is given by $\varphi(t, x) = \partial_t f(t, x) = 10 \sin^4(t) \cos(t)$ for $t \in [0, 2]$ and thus

$$\|\varphi(t, \cdot)\|_{L^2(\partial B_1(0))} = 20\sqrt{\pi} \sin^4(t) \cos(t) \quad t \in [0, 2].$$

Although the presented schemes are unconditionally stable, we give the ratio between space and time discretization and define

$$\beta := \frac{\Delta t}{h} c,$$

where we set $c = 1$. This corresponds to the Courant-Friedrichs-Levy coefficient known for finite difference methods and sometimes abbreviated by *CFL*. Nevertheless, in our case it is only a factor that reflects the relation between space and time resolution commonly used for these kind of MOT schemes [21].

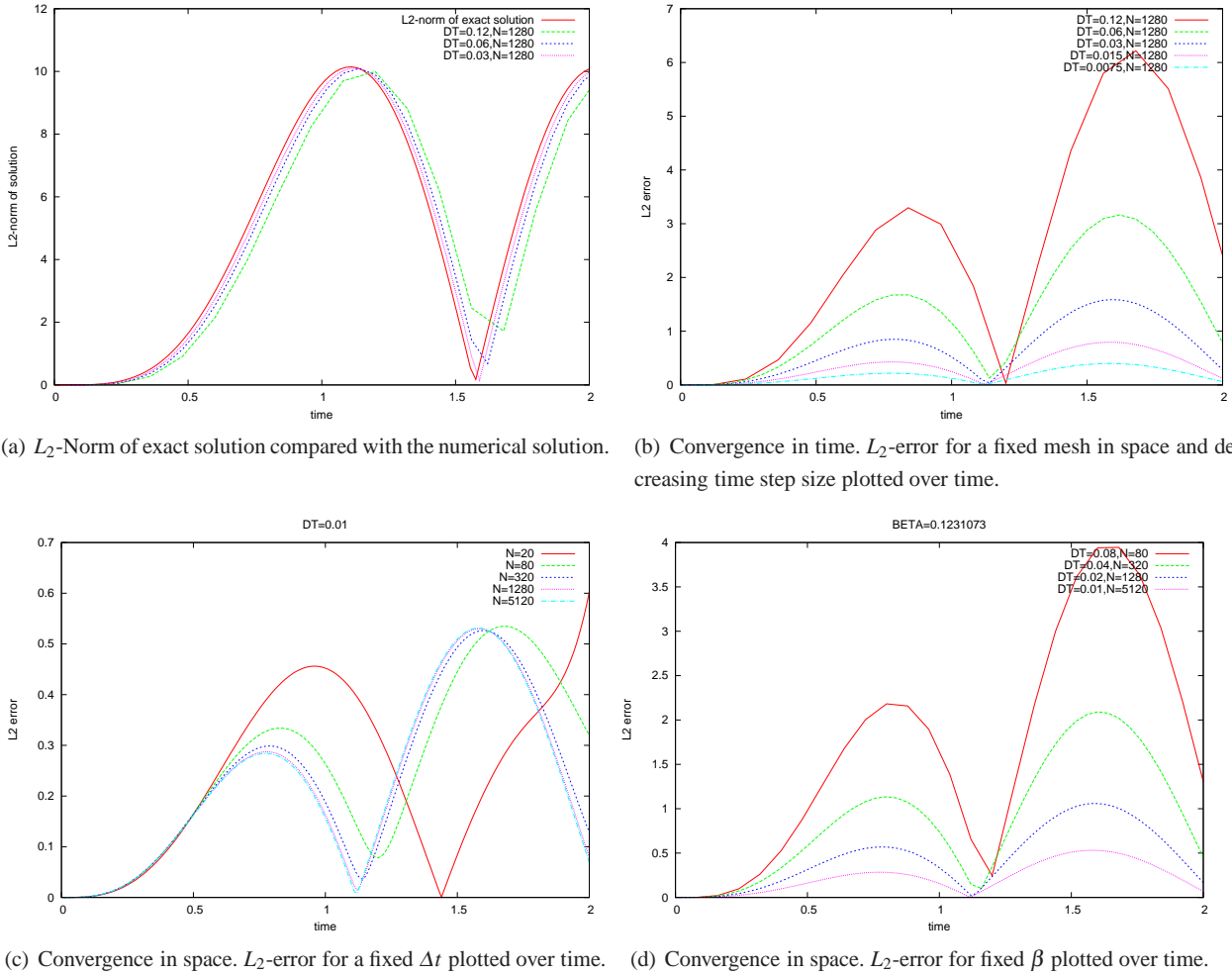


Fig. 5.2 Numerical results for benchmark of Sauter and Banjai

In Fig. 5.2 we compare the L^2 -error in each time step for different space and time discretizations. In Fig. 5.2(a) the L^2 -norm of the approximate solution converges towards the L^2 -norm of the exact solution for a fixed space mesh and a decreasing time step Δt . This is reflected by the behavior of the L^2 -error in Fig. 5.2(b), where the error halves if Δt halves. In Fig. 5.2(c) we fix $\Delta t = 0.01$ but observe, that the error in time is dominant. One a certain resolution a time is reached, the error is no longer significantly decreasing. But as the solution is constant in each time step this is not rather surprising. In Fig. 5.2(d) we fix $\beta \approx 0.12$ and observe almost the same behavior as in Fig. 5.2(a). Using the space-time L^2 -norm defined via

$$\|\varphi\|_{L^2([0,T],L^2(\Gamma))}^2 := \int_0^T \|\varphi(t,\cdot)\|_{L^2(\Gamma)}^2 dt,$$

we obtain for fixed values of β the convergence results presented in Fig. 5.3. Namely a convergence rate of approximately $1/3$ in space and 1 in time. Note that, as the error in time seems to be unrelated to the value of β , the error in space is smaller if β decreases, although the rate of convergence is the same.

In order to eliminate the influence of the error in space we choose a good approximation in space and vary Δt . here we again observe the order of convergence 1 . For the analysis unpolluted by the temporal error, we choose a high resolution in time and decrease h . Here we choose 500 and 1000 time steps corresponding to $\Delta t = 0.004$ and $\Delta t = 0.002$, respectively. The results are not very satisfactory as the temporal error is big compared to the spacial error, but a further reduction of the time step is not easily possible because the intersection of the discrete light cone integration domain with the mesh becomes very small.

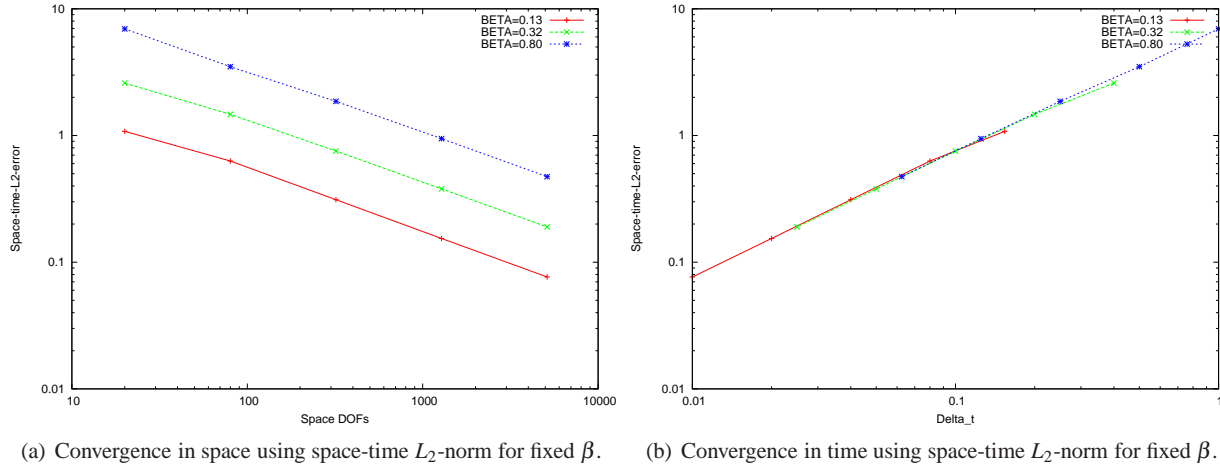


Fig. 5.3 Convergence results for fixed β .

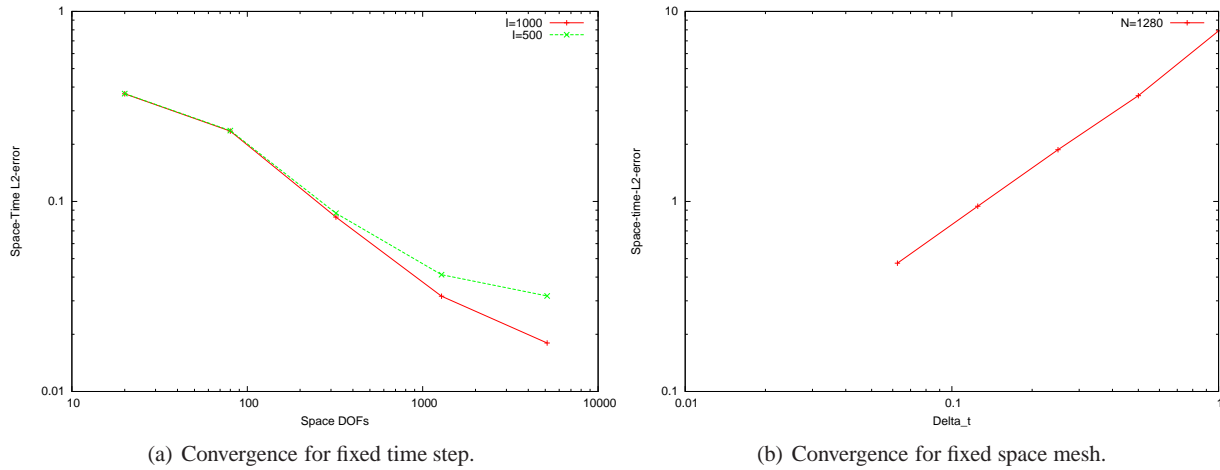


Fig. 5.4 Convergence results for fixed space and time resolutions.

5.2 Direct Problem using the Single Layer Potential

In this section we consider the direct formulation of the Dirichlet problem as discussed in 2.18. We use a benchmark given in [12]. Let $\Omega^- := B_R(0)$ and $\Gamma := \partial B_R(0)$, such that $\Omega = \mathbb{R}^3 \setminus \overline{B_R(0)}$. Then for $r = |x|$ and a wave velocity $c > 0$ there holds

$$u(t, r) = \frac{1}{r} \left(\frac{3}{4} - \cos \left(\frac{\pi(r - ct + 3R)}{2R} \right) + \frac{1}{4} \cos \left(\frac{\pi(r - ct + 3R)}{R} \right) \right) (H(r - ct + 3R) - H(r - ct - R)).$$

One easily verifies, that $\square u = 0$ for $(t, x) \in \mathbb{R}^+ \Omega$ and $\dot{u}(0, r) = u(0, r) = 0$ in $\overline{\Omega}$. In the following we fix $c = 1$. The Cauchy data on the surface of the sphere are

$$u(t, 1) = \left(\frac{3}{4} - \cos \left(\frac{\pi}{2}(4 - t) \right) + \frac{1}{4} \cos(\pi(4 - t)) \right) (H(4 - t) - H(-t)),$$

$$\frac{\partial u}{\partial n}(t, 1) = \left(-\frac{3}{4} + \cos \left(\frac{\pi}{2}(4 - t) \right) + \frac{\pi}{2} \sin \left(\frac{\pi}{2}(4 - t) \right) - \frac{1}{4} (\cos(\pi(4 - t)) + \pi \sin(\pi(4 - t))) \right) (H(4 - t) - H(-t)).$$

Thus the sphere is radiating a signal for $t \in (0, 4)$, compare Fig. 5.5.

For this problem we can study the long time behavior of our method. In Fig. 5.6 the error reduces if Δt reduces. Here we use a mesh with 320 elements, but for finer triangulation of the sphere we observed the same behavior. Two perturbing

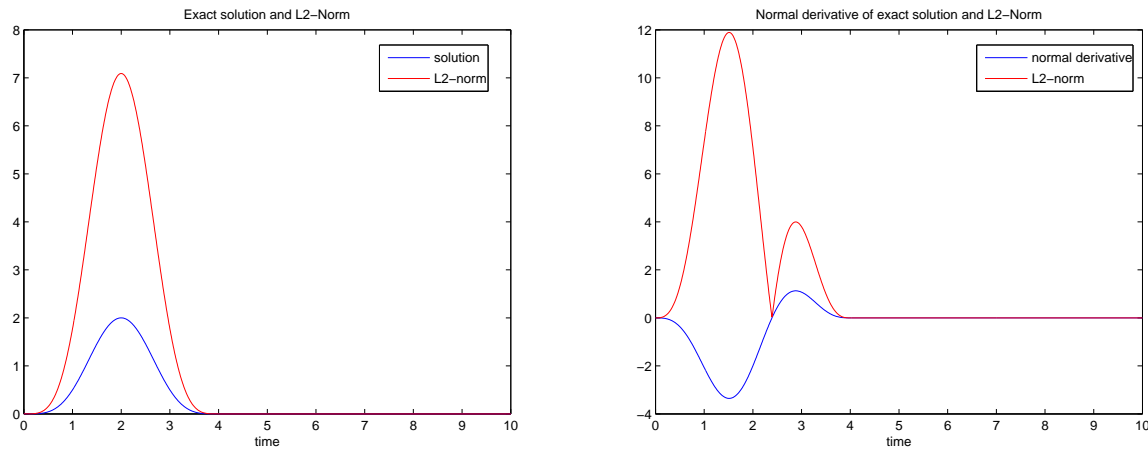
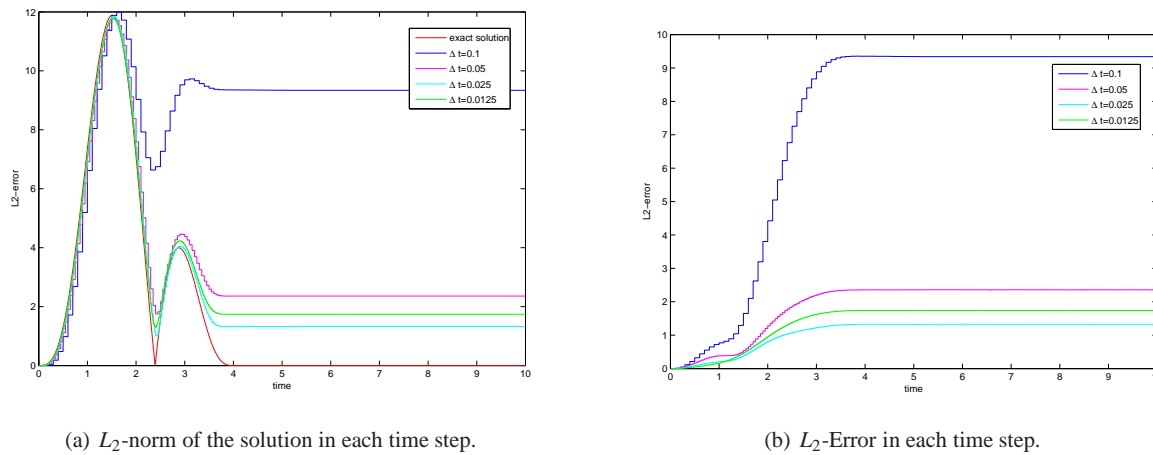


Fig. 5.5 Exact solution of direct problem.

facts remain. Once the signal vanishes, the error sticks a very high level and for a very high resolution in time the error increases again. One explanation might be, that the error in the retarded double layer potential pollutes the solution stronger than expected. Nevertheless, the method itself behaves very stable.



(a) L_2 -norm of the solution in each time step.

(b) L_2 -Error in each time step.

Fig. 5.6 Numerical solution of Dirichlet problem.

5.3 Computation Times, Memory Requirement and Performance

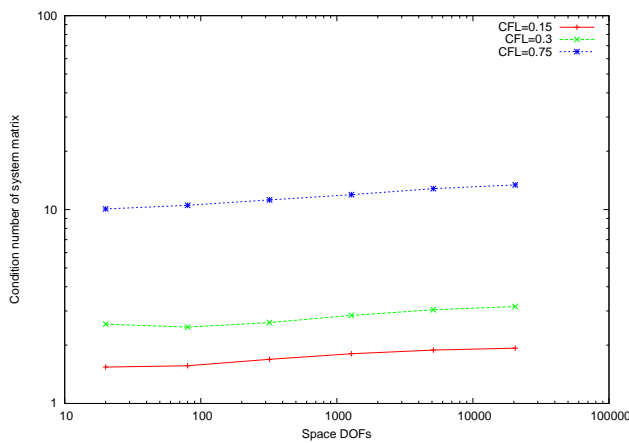
The computation of the matrices is by far the most expensive part in the computations. Only the use of the parallel computation of the matrix entries with OpenMP [11] provided in Maiprog resulted in acceptable computation times. In Table 5.1 we compare the computation time and memory requirements for a triangulation of the unit sphere into 5120 elements for the retarded single layer matrix. A higher resolution in time results in more non-vanishing matrices and thus the demand of memory and computation time increases, although each matrix becomes sparser as the light cone integration domain reduces if the time step size decreases.

Once the complete set of non-vanishing matrices is computed, the algorithm is very fast and the computation on arbitrarily long time intervals is no problem, as the MOT-scheme reduces to a plain matrix vector multiplication. First we assemble the right hand side as described in Section 2.3 and then we solve the linear equation system. Here the conjugate gradient method worked well, but as the system matrix is the in each time step a LR-decomposition could

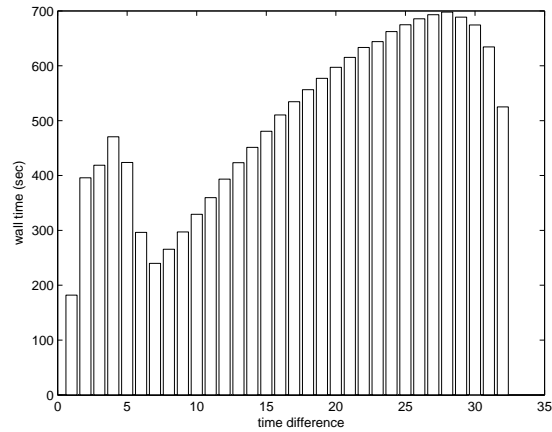
No. of matrices	Δt	Memory(MByte)	total Wall-time(Sec)
1	2.0	314.6	7.8266e+03
2	1.0	406.2	7.9025e+03
4	0.5	546.0	8.3621e+03
8	0.25	698.0	9.5144e+03
16	0.125	911.3	1.1621e+04
32	0.0625	1284.7	1.6032e+04
64	0.03125	1998.8	2.4803e+04

Table 5.1 Memory requirement for different resolution in time on the mesh of a unit sphere approximation with 5120 elements.

also be applied. Although the condition number of the system matrix is not bounded it is increasing very slowly as plotted in Fig. 5.7(a).



(a) Condition number of the system matrix.



(b) Computation time for the matrices per time difference.

Fig. 5.7

In Fig. 5.7(b) we compare the wall time needed for the computation of the different matrices. The first matrices are quite expensive, which is due to the grading strategy in the outer quadrature used for the singularities on the boundary of each element. If the near field is left the computation times increase as the light cone integration domain illuminates more elements due to the shape of the domain.

The approximate performance for the computation of one matrix is 15.25 for 64 matrices and 15.37 for 32 matrices on the computing system used for the numerical experiments. This coincides also with the overall performance of the method.

Chapter 6

Conclusions

There exist many possible continuations and extensions of the presented work. Compared to the time independent boundary integral method the theory of the retarded potential boundary integral method is still in its infancy. As pointed out in [15] the analysis in the weighted space-time Sobolev spaces is incomplete and the a priori error estimates are still not optimal. Although it is quite difficult to gain a complete overview of the state of the art, as many results are published in PhD thesis, which are not all available to the public, a further research in this area is definitely needful. Moreover, so far only the h-version was investigated although there is no obvious reason to restrict the computations in such a way. Higher polynomial degrees in space and time should lead to better convergence rates and might as well be able to tackle non-smooth input data.

Another logical step would be to study adaptive schemes in space and time. There are many works [58, 10] investigating residual and hierarchical error estimators, which aim to locally reduce the error by refining the mesh. Such a scheme should also be applicable for retarded boundary integral equations, where additional difficulties are expected. One question is how does a locally strongly refined mesh influence the condition number of the Galerkin matrix. But also a non-uniform time mesh can be applicable, when one e.g. deals with strongly changing input data in time. The implementation of adaptive meshes in space most probably requires the extension of the analysis presented in Chapter 3 on triangles to quadrilaterals, which should be straight forward as Lemma 3.2 is easily generalized.

FEM-BEM coupling approaches were presented in [3, 17], but here as well as in many other problems concerned with retarded potential integral equations the convergence analysis is still incomplete.

Finally let us discuss a possible realization of the outer quadrature presented in Section 4.2. Step by step one should include the different singularities and the cut-off behavior of the discrete retarded potential. Besides the classical singularities on the boundary of the element the planar geometrical light cone singularities have the strongest impact on the quadrature error. An appropriate decomposition and a possible grading towards this one-sided singularities should be taken into account. The next step would then be the implementation of the cylindrical light cone singularities and finally a decomposition with respect to the spheres around the vertices of the regarded element. Thus the computation of the desired decomposition involves the intersection with up to four planes, six cylinders and six spheres. The question is, if such a complex intersection problem, which is probably easily polluted by numerical instabilities can still result in a fast method. Therefore, one has to find a compromise between the needed accuracy and the efficiency of the computational implementation. Here the introduction of relative coordinates as used for the time independent potentials [49] might be an option.

First attempts on a fast evaluation of retarded potentials were made in [56].

Appendix A

Functional Framework and Notation

In this chapter, we give the functional framework and some basic notations. The indicator function $\chi_A(x)$ for a set A is defined by

$$\chi_A(x) = \begin{cases} 1 & x \in A \\ 0 & x \notin A \end{cases}.$$

In the following, $H(x)$ denotes the Heavyside function and $\delta(x)$ the delta distribution. Denote by $\langle \cdot, \cdot \rangle$ a possibly hermitian inner product defined via

$$\langle u, v \rangle := \int_{\Gamma} u \bar{v} ds_x.$$

Countably Normed Spaces

In this section we give the definition of the countably normed spaces which are extensively used throughout this thesis in order to describe the regularity of the discrete retarded potentials, cf. Chapter 3. The countably normed spaces $B_{\beta}^m(\Omega)$ where introduced in [2, 20]. Let Ω denote a bounded domain, then we first define the weighted Sobolev spaces $H_{\beta}^{m,l}(\Omega)$.

Definition A.1 (Weighted Sobolev space $H_{\beta}^{m,l}(\Omega)$). Let β be a real number with $\beta \in (0, 1)$ if not specified otherwise. The weight function $\Phi_{\beta,\alpha,l}(x)$ for $\alpha = (\alpha_1, \alpha_2, \alpha_3)$ and $l \in \mathbb{N}$ is defined throughout this work in several ways and is defined when needed. Moreover, denote

$$D^{\alpha} := \frac{\partial^{|\alpha|}}{\partial x_1^{\alpha_1} \partial x_2^{\alpha_2} \partial x_3^{\alpha_3}} = \partial_1^{\alpha_1} \partial_2^{\alpha_2} \partial_3^{\alpha_3}.$$

Then the **weighted Sobolev spaces** are defined for $m \in \mathbb{N}$ and $m \geq l \geq 1$ on some domain Ω by

$$H_{\beta}^{m,l}(\Omega) = \left\{ u : u \in H^{l-1}(\Omega) \text{ for } l > 0, \|\Phi_{\beta,\alpha,l} D^{\alpha} u\|_{L^2(\Omega)} < \infty \text{ for } l \leq |\alpha| \leq m \right\}$$

with the norm

$$\|u\|_{H_{\beta}^{m,l}(\Omega)}^2 = \|u\|_{H^{l-1}(\Omega)}^2 + \sum_{k=l}^m \sum_{|\alpha|=k} \int_{\Omega} |D^{\alpha} u(x)|^2 \Phi_{\beta,\alpha,l}^2(x) dx,$$

and a semi norm

$$|u|_{H_{\beta}^{m,l}(\Omega)}^2 = \sum_{k=l}^m \sum_{|\alpha|=k} \int_{\Omega} |D^{\alpha} u(x)|^2 \Phi_{\beta,\alpha,l}^2(x) dx.$$

These spaces are needed in order to define the countably normed spaces

Definition A.2 (Countably normed space $B_\beta^l(\Omega)$). $u \in B_\beta^l(\Omega)$ if $u \in H_\beta^{k,l}(\Omega)$ for all $k \geq l$ and if there holds

$$\|\Phi_{\beta,\alpha,l} D^\alpha u\|_{L^2(\Omega)} \leq C d^{k-l} (k-l)!$$

for $|\alpha| = k = l, l+1, \dots$ and with constants $C > 0$ and $d \geq 1$ independent of k . We refer to $B_\beta^l(\Omega)$ as countably normed space.

Indexed Sobolev Spaces in Space

In this section we define the indexed norms as used in the analysis of retarded potential integral equation. In [35, 36] the classical definition of Sobolev spaces in space and space-time is given. In the following $\|\cdot\|_{H^m(\Omega)}$ denotes the usual norm of the corresponding Sobolev spaces as defined in [35]. For $\omega \in \mathbb{C}$ and $m \in \mathbb{N}$ we define the indexed norms recursively by

$$\begin{aligned} \|u\|_{0,\omega,\Omega}^2 &:= \|u\|_{L^2(\Omega)}^2, \\ \|u\|_{m,\omega,\Omega}^2 &:= \|u\|_{m-1,\omega,\Omega}^2 + \frac{1}{|\omega|^2} \|\nabla u\|_{m-1,\omega,\Omega}^2. \end{aligned}$$

As pointed out in [23] this norm is equivalent to the common $H^1(\Omega)$ -Norm for $|\omega| \neq 0$. In [3] we the following definition is given, that extends the definition to real valued indices $r \in \mathbb{R}$.

Definition A.3. Let $u \in \mathcal{D}'(\Omega)$. u^ω is called the distribution, extended by ω in \mathbb{C} and for all $y \in |\omega|\Omega$ defined by

$$u^\omega := \frac{1}{|\omega|} u\left(\frac{y}{|\omega|}\right).$$

Then we define for all $\omega \in \mathbb{C}$, all $r \in \mathbb{R}$ and for all $u \in H^r(\Omega)$ a norm on $H^r(\Omega)$ by

$$\|u\|_{r,\omega,\Omega}^2 := \frac{1}{|\omega|} \|u^\omega\|_{H^r(|\omega|\Omega)}^2.$$

Due to Proposition 2.21 in [57] the indexed norms $\|\cdot\|_{s,\omega,\Omega}$ are equivalent to the classical Sobolev norms as e. g. given in [35].

Remark A.4. One has to be very careful while defining the above indexed norm. Using the same notation Ha-Duong [22] and Terrasse [57] define it differently, namely

$$\begin{aligned} \|u\|_{m,\omega,\Omega}^2 &:= |\omega|^2 \|u\|_{m-1,\omega,\Omega}^2 + \|\nabla u\|_{m-1,\omega,\Omega}^2 \quad (\text{Ha-Duong}) \\ \|u\|_{m,\omega,\Omega}^2 &:= \|u\|_{m-1,\omega,\Omega}^2 + \frac{1}{|\omega|^2} \|\nabla u\|_{m-1,\omega,\Omega}^2 \quad (\text{Terrasse}) \end{aligned}$$

This fact also been pointed out by Ha-Duong in his overview paper [23]. Both norms only differ by a factor $|\omega|$.

Weighted Functional Spaces in Space-Time

Based on these indexed norms, one defines weighted functional spaces in space-time [3, 17, 21]. Let X be an inner product space and denote by $\mathcal{D}'_+(X)$ the space of causal distributions over \mathbb{R} with values in X , i. e. with zero values for negative times. Moreover, let $\mathcal{S}'_+(X)$ be the union of all tempered distributions or distributions of slow growth in $\mathcal{D}'_+(X)$. For all $\sigma_0 \in \mathbb{R}$ define

$$\mathcal{L}(\sigma_0, X) = \{f \in \mathcal{D}'_+(X), e^{-\sigma_0 t} f \in \mathcal{S}'_+(X)\},$$

and the space of Laplace transformable distributions over \mathbb{R} with values in X

$$\mathcal{L}(X) = \{f \in \mathcal{D}'_+(X), \exists \sigma_0 : f \in \mathcal{L}(\sigma_0, X)\}.$$

One property of these spaces is

$$\forall \sigma \geq \sigma_0 \text{ and } f \in \mathcal{L}(\sigma_0, X) \text{ it holds } f \in \mathcal{L}(\sigma, X)$$

thus we denote by $\sigma(f) = \min_{\sigma \in \mathbb{R}} \{f \in \mathcal{L}(\sigma, X)\}$.

Definition A.5. Let $f \in \mathcal{L}(X)$. The *Fourier-Laplace transform* of f in the half plane $\{\omega \in \mathbb{C} : \text{Im } \omega \geq \sigma(f)\}$ denoted by \hat{f} is given by

$$\hat{f}(\omega) = \mathfrak{F}(e^{-\sigma t} f)(\eta) = \int_{-\infty}^{+\infty} e^{i\omega t} f(t) dt$$

if $e^{-\sigma t} f \in L^1(\mathbb{R}^+, X)$ where $\omega = \eta + i\sigma \in \mathbb{C}$ and $\text{Im } \omega \geq \sigma(f)$. \mathfrak{F} denotes the Fourier transform in time without normalization.

The Fourier-Laplace transform \mathfrak{L} may be defined for all Laplace transformable functions defined as above. In order to specify the inverse Fourier-Laplace transform \mathfrak{L}^{-1} , we need the theorem of Paley-Wiener.

Theorem A.6 ([23]).

1. (*Paley-Wiener theorem*). An X -valued function $\hat{f}(\omega)$ is the Fourier-Laplace transform of $f \in \mathcal{L}(X)$ if and only if it is homomorphic in some half plane $C_{\sigma_0} = \{\omega \in \mathbb{C}; \text{Im } \omega > \sigma_0\}$ and of temperate growth in some closed half plane of C_{σ_0} . This last condition means that there exists $\sigma_1 > \sigma_0$ and $k \in \mathbb{N}$ such that

$$\|\hat{f}(\omega)\|_X \leq C(1 + |\omega|)^k \quad \text{for all } \omega \text{ s.t. } \text{Im } \omega \geq \sigma_1 \quad (\text{A.1})$$

2. Moreover, the support of $f \in \mathcal{L}(X)$ is in $[T, \infty)$ if and only if the inequality (A.1) is replaced by

$$\|\hat{f}(\omega)\|_X \leq C(1 + |\omega|)^k e^{-(\text{Im } \omega)T} \quad \text{for all } \omega \text{ s.t. } \text{Im } \omega \geq \sigma_1$$

3. (*Parseval's formula*). On the other hand, if $f, g \in L^1_{loc}(\mathbb{R}, X) \cap \mathcal{L}(X)$, there holds

$$\frac{1}{2\pi} \int_{-\infty+i\sigma}^{+\infty+i\sigma} (\hat{f}(\omega), \hat{g}(\omega))_X d\omega = \int_{-\infty}^{+\infty} e^{-2\sigma t} (f(t), g(t))_X dt$$

where $(\cdot, \cdot)_X$ is the hermitian product of X and $\sigma > \max(\sigma(f), \sigma(g))$.

We need this formula, in order to transfer the results in frequency domain into time domain.

We define the operator $\Lambda^s : \mathcal{L}(X) \rightarrow \mathcal{L}(X)$ by

$$\Lambda^s u = \mathfrak{L}^{-1}((-i\omega)^s \hat{u}) \quad \forall s \in \mathbb{R},$$

where \mathfrak{L}^{-1} is the inverse Fourier-Laplace transform (FL-transform) as given in Def. A.5. For $s \in \mathbb{N}$ the operator Λ^s is the derivative of order s .

Let X denote an inner product space and $s, \sigma \in \mathbb{R}$ with $\sigma > 0$ then

$$\mathcal{H}^s_\sigma(\mathbb{R}^+, X) := \{u \in \mathcal{L}(\sigma, X) : e^{-\sigma t} \Lambda^s u \in L^2(\mathbb{R}^+, X)\}$$

where this Hilbert spaces are equipped with the natural norm

$$\begin{aligned} \|u\|_{\mathcal{H}^s_\sigma(\mathbb{R}^+, X)}^2 &:= \int_{-\infty}^{+\infty} e^{-2\sigma t} \|\Lambda^s u(t)\|_X^2 dt \\ &= \frac{1}{2\pi} \int_{-\infty+i\sigma}^{+\infty+i\sigma} |\omega|^{2s} \|\hat{u}(\omega)\|_X^2 d\omega \quad (\text{Parseval's formula}) \end{aligned}$$

Now, for $m \in \mathbb{N}$ and $s \in \mathbb{R}$ we define following [3]

$$\begin{aligned} H_\sigma^s(\mathbb{R}^+, H^m(\Omega)) &= \mathcal{H}_\sigma^s(\mathbb{R}^+, L^2(\Omega)) \\ H_\sigma^s(\mathbb{R}^+, H^m(\Omega)) &= \{u \in H_\sigma^s(\mathbb{R}^+, H^{m-1}(\Omega)), \nabla u \in H_\sigma^{s-1}(\mathbb{R}^+, H^{m-1}(\Omega)^3)\}. \end{aligned}$$

These Hilbert spaces are equipped with a norm

$$\|u\|_{H_\sigma^s(\mathbb{R}^+, L^2(\Omega))}^2 = \frac{1}{2\pi} \int_{-\infty+i\sigma}^{+\infty+i\sigma} |\omega|^{2s} \|\hat{u}\|_{m,\omega,\Omega}^2 d\omega.$$

One can extend the definition also to real valued Sobolev spaces. Let $r \in \mathbb{R}$, then

$$H_\sigma^s(\mathbb{R}^+, H^r(\Omega)) = \left\{ u \in \mathcal{L}(\sigma, H^r(\Omega)), \int_{-\infty+i\sigma}^{+\infty+i\sigma} |\omega|^{2s} \|\hat{u}\|_{r,\omega,\Omega}^2 d\omega < \infty \right\},$$

this space is again a Hilbert space and has the norm

$$\|u\|_{H_\sigma^s(\mathbb{R}^+, H^r(\Omega))}^2 = \|u\|_{s,\sigma,H^r(\Omega)}^2 = \frac{1}{2\pi} \int_{-\infty+i\sigma}^{+\infty+i\sigma} |\omega|^{2s} \|\hat{u}\|_{r,\omega,\Omega}^2 d\omega.$$

The theorem of Paley-Wiener in a slightly modified version gives us the equivalence result of the common norms and the indexed norms introduced above.

All above definitions can also be applied to the boundary $\partial\Omega$ of Ω .

Remark A.7. Note that, in [3, 23] the norms are abbreviated by $\|u\|_{s,\sigma,X} = \|u\|_{H_\sigma^s(\mathbb{R}^+, X)}$.

In [23] it is shown, that V is a bounded operator mapping from $H_{\sigma,\Gamma}^{1,-1/2,-1/2} := \{p : \dot{p} \in H_\sigma^{-1/2}(\mathbb{R}^+, H^{-1/2}(\Gamma))\}$ into $H_\sigma^{1/2}(\mathbb{R}^+, H^{1/2}(\Gamma))$. Moreover the coercivity estimate

$$\int_0^\infty S\dot{p}(t,x)p(t,x) d_\sigma t \geq C \|p\|_{H_\sigma^{-1/2}(\mathbb{R}^+, H^{-1/2}(\Gamma))}^2$$

is given.

Similar results hold for the other retarded potential boundary integral operators, compare [23] and the references therein.

Appendix B

Regularity of Discrete Retarded Potentials in \mathbb{R}^3

In this chapter we want to extend the analysis presented in Chapter 4 in order to describe the regularity of the discrete retarded potential on its three-dimensional elements of the decomposition $\Theta_{t_{\min}}^{t_{\max}}(T)$.

As we have seen in the proof of Lemma 3.8 the gradient of $(I_e^V \varphi)$ involves a function which is the derivative of

$$g(x) := (R^2 - x_1^2 - x_3^2)^{1/2}.$$

In the following lemma, we will give the regularity of g in terms of countably normed spaces in three dimensions, compare Lemma 3.9 for its reduction to a plane.

Lemma B.1. *Given a function $g(x) := (R^2 - x_1^2 - x_3^2)^{1/2}$.*

In S_4 the singularity is located on the cylinder wall and we define local cylindrical coordinates with the origin m_1 . ξ_1 denotes the radial variable, ξ_2 the angular variables and ξ_3 the variable parallel to the reference edge e . Then $g \in B_{\beta}^2(S_4)$ for $\beta \in (\frac{3}{4}, 1)$. In S_1 and S_2 the singularity is located on the equator of the spheres. we define local spherical coordinates with origins m_1 and m_2 respectively. ξ_1 denotes the radial variable and ξ_2 and ξ_3 the two angular variables. Then $g \in B_{\beta}^2(S_i)$ for $\beta \in (\frac{3}{4}, 1)$ with $i = 1, 2$. The countably normed space is defined via

$$B_{\beta}^l(S_i) := \left\{ u \in H^{l-1}(S_i) : \left\| (R^2 - \xi_1^2)^{\alpha_1 - l + \beta} \partial_{\xi_1}^{\alpha_1} \partial_{\xi_2}^{\alpha_2} \partial_{\xi_3}^{\alpha_3} u \right\|_{L^2(S_i)} \leq C d^{k-l} (k-l)! \text{ for } |\alpha| = k \geq l, C \geq 0, d \geq 1 \right\}.$$

Proof. Let us first regard the situation in S_4 . Here $g(\xi) = (R^2 - \xi_1^2)^{1/2}$. First we verify, that $g \in H^1(S_4)$.

$$\begin{aligned} \|\partial_{\xi_1} g\|_{L^2(S_4)}^2 &= \int_0^R \int_0^{2\pi} \int_0^1 (R^2 - \xi_1^2)^{-1} \xi_1^2 d\xi_1 d\xi_2 d\xi_3 \\ &= 2\pi \int_0^R (R^2 - \xi_1^2)^{-1} \xi_1^2 d\xi_1 \leq C \end{aligned}$$

In order to show, that $g \in H_{\beta}^{m,2}(S_4)$ for $m \geq 2$, we need to estimate the weighted norms of the higher derivatives of g for $2 \leq k \leq m$. The argumentation is exactly the same as in the proof of Lemma 3.9 for S_1 and we obtain $g \in B_{\beta}^2(S_4)$ with $\beta \in (\frac{3}{4}, 1)$. Similarly, we obtain, that $g \in B_{\beta}^2(S_i)$ for $i = 1, 2$ and $\beta \in (\frac{3}{4}, 1)$. \square

Lemma B.2 (Regularity of $I_e^V \varphi$ on a decomposition of \mathbb{R}^3). *Given the disjoint elements S_i ($i = 1, \dots, 5$) as defined in (3.11) of the decomposition of $C_R(e)$.*

- *For a cylindrical singularity w.r.t. edge e there holds in a local cylindrical coordinate system defined according to Lemma 3.9*

$$I_e^V \varphi(x) \in B_{\beta}^2(S_i \cap \mathcal{E})$$

with a weight function located on the cylinder wall of $C_R(e)$ and $\beta \in (0, 1)$.

- If on S_i a classically known kernel singularity w.r.t. edge e is observed, we can describe the regularity as follows.

$$I_e^v \varphi(x) \in B_\beta^{l_{ker}-1}(S_i \cap \mathcal{E})$$

with a weight function located on the edge e and $\beta \in (0, 1)$.

Proof. Here we follow the argumentation of Lemma 3.12 using Lemma B.1. \square

Lemma B.3. Denote by Q a bounded subset of \mathcal{E}_{ref} and define $Q_R := \{x : |x_3| < R \text{ and } (x_1, x_2, 0) \in Q\}$. We define a local cartesian coordinate system defined by the direction vectors of the plane \mathcal{E}_T and the plane normal n_T with variables ξ_2, ξ_3 and ξ_1 respectively. Then $I_{\mathcal{E}_{ref}}(x) \in B_\beta^2(Q_R)$ with

$$B_\beta^l(Q_R) := \left\{ u \in H^{l-1}(Q_R \cap \mathcal{E}) : \left\| (R^2 - \xi_1^2)^{\alpha_1 - l + \beta} \partial_{\xi_1}^{\alpha_1} \partial_{\xi_2}^{\alpha_2} \partial_{\xi_3}^{\alpha_3} u \right\|_{L^2(Q_R)} \leq C d^{k-l} (k-l)! \text{ for } |\alpha| = k \geq l, C \geq 0, d \geq 1 \right\}$$

Proof. We have show, that given a function $\tilde{g}(x) = (R^2 - \xi_1^2)^{1/2}$ and $\beta \in (0, 1)$, it holds $g \in B_\beta^1(Q_R)$ with a weight function. The proof follows the argumentation of the proof of Lemma 3.9. Note, that it is necessary to bound the integration domain to Q_R , but it is no loss of generality as we seek to study the integral $I_T \varphi$ on its naturally bounded support. \square

Again we delay the analysis of the integral $I_T \varphi$ until we regard the complete potential as pointed out in Section 3.2.2 the integral possesses next to the facial singularity parallel to the triangle the same kind of cylindrical singularities as observed for the edge-based integrals $I_{e_i} \varphi$. Thus we have to apply the same kind of partition as we will apply for the complete integral $P_R \varphi$.

Before we formulate the regularity of the whole decomposition of $E_R(T)$, we regard some characteristic elements. We start with the subdomain, if present, on which the regularity is only restricted by the regularity of the kernel, but not influenced by the geometrical light cone singularities. Namely, the common intersection of all three spheres. Note that this case occurs only, if $R > 0.5 \max_i |e_i|$. Here we observe a regularity comparable to the situation of the classical time independent boundary integrals and no influence of the classical singularities.

Let us now formulate the regularity of the whole retarded potential (3.2). Compare Theorem 3.22 for the formulation restricted to a plane.

Theorem B.4. Given a triangle T . On each $A \in \Theta_R(T)$ there exists only one type of singularity.

- For a cylindrical singularity w.r.t. edge e_i there holds in a local coordinate system (ξ_1, ξ_2, ξ_3) defined according to Lemma B.1

$$P_R \varphi \in B_\beta^3(A),$$

where $\beta \in (0, 1)$ and the weight function is located on the cylinder wall of $C_R(e_i)$.

- For a planar singularity there holds in a local cartesian coordinate system (ξ_1, ξ_2, ξ_3) defined according to Lemma B.3

$$P_R \varphi \in B_\beta^3(A),$$

where $\beta \in (0, 1)$ and the weight function is located in the planes parallelly shifted to the triangle plane \mathcal{E}_T by R .

- For a classically known kernel singularity w.r.t. edge e_i in a local coordinate system (ξ_1, ξ_2, ξ_3) with

$$P_R \varphi \in B_\beta^{l_{ker}}(A),$$

where $\beta \in (0, 1)$ and the weight function is located on the edge e_i .

Proof. Here we can follow the argumentation of Theorem 3.22 using Lemma B.2 and B.3. \square

For the complete potential $P\varphi$ there thus follows similar to Theorem 3.26

Theorem B.5. *Given a triangle T . On each $A \in \Theta_{r_{\min}}^{r_{\max}}(T)$ there exists only one type of singularity.*

- *For a cylindrical singularity w.r.t. edge e_i and radius R there holds in a local coordinate system (ξ_1, ξ_2, ξ_3) defined according to Lemma B.1*

$$P\varphi \in B_{\beta}^3(A),$$

where $\beta \in (0, 1)$ and the weight function is located on the cylinder wall of $C_R(e_i)$, where $R = r_{\min}$ or $R = r_{\max}$.

- *For a planar singularity there holds in a local cartesian coordinate system (ξ_1, ξ_2) defined according to Lemma B.3*

$$P\varphi \in B_{\beta}^3(A),$$

where $\beta \in (0, 1)$ and the weight function is located in the planes parallelly shifted to the triangle plane \mathcal{E}_T by R . The singularities if present are located on line segments and either $R = r_{\min}$ or $R = r_{\max}$.

- *For a classically known kernel singularity w.r.t. edge e_i in a local coordinate system (ξ_1, ξ_2, ξ_3) with*

$$P\varphi \in B_{\beta}^{l_{ker}}(A),$$

where $\beta \in (0, 1)$ and the weight function is located on the edge e_i .

Appendix C

Implementation Issues

In this chapter we will comment on the implementation of the retarded integrals and the realization of the MOT-scheme for retarded boundary integral equations as discussed in Chapter 2 and give some details on the analytical evaluation of the retarded time integrals.

Storage Allocation for Retarded Matrices

Given two triangles T_i and T_j in \mathbb{R}^3 and radii $0 \leq r_{\min} < r_{\max}$, we derive a rough superset of the interaction domain of these triangles is given by $E(T_i, T_j) = \{(x, y) \in (T_i, T_j) : r_{\min} \leq |x - y| \leq r_{\max}\}$ as introduced in Chapter 4. In order to allocate the matrix storage and to keep the computational cost as low as possible, we are interested in an a priori check, whether $E(T_i, T_j) = \emptyset$, as these elements do not contribute to a possible matrix entry.

In the following lemma, we give an easy computable superset of $E(T_i, T_j)$.

Lemma C.1. *Let $B_{r_k}(m_k)$ denote the circumsphere of triangle T_k for $k = i, j$. There exists a superset $\mathcal{S}_{E(T_i, T_j)}$ of the domain of influence $E(T_i, T_j)$ of two triangles T_i and T_j defined by*

$$\mathcal{S}_{E(T_i, T_j)} := \left(T_i \cap (B_{r_j+r_{\max}}(m_j) \setminus B_{(r_{\min}-r_j)_+}(m_j)) \right) \times \left((B_{r_i+r_{\max}}(m_i) \setminus B_{(r_{\min}-r_i)_+}(m_i)) \cap T_j \right)$$

Proof. The elements illuminate each other through their domain of influence $E(T_k)$, such that element T_i can maximally illuminate in $E(T_j)$ and vice versa. Thus it holds

$$E(T_i, T_j) \subset (T_i \cap E(T_j)) \times (E(T_i) \cap T_j).$$

Let $B_r(m)$ denote the circumsphere of triangle T . Now $E_{r_{\max}}(T) \subset B_{r+r_{\max}}(m)$ and $B_{(r_{\min}-r)_+}(m) \subset \bigcap_{i=1}^3 B_{r_{\min}}(p_i)$, such that with Lemma 3.23 it follows

$$E(T) \subset B_{r+r_{\max}}(m) \setminus B_{(r_{\min}-r)_+}(m).$$

□

Remark C.2. For the computation of the outer quadrature for the Galerkin elements it is necessary to decompose the test element in the domain of influence of the trial element. As $E(T)$ might possess a hole, we have to differ between its outer boundary $\Gamma_{E(T)}^+$ and its inner boundary $\Gamma_{E(T)}^-$. Applying Lemma 3.23, it immediately follows that

$$\Gamma_{E(T)}^+ = \partial E_{r_{\max}}(T) \quad \text{and} \quad \Gamma_{E(T)}^- = \partial \bigcap_{i=1}^3 B_{r_{\min}}(p_i).$$

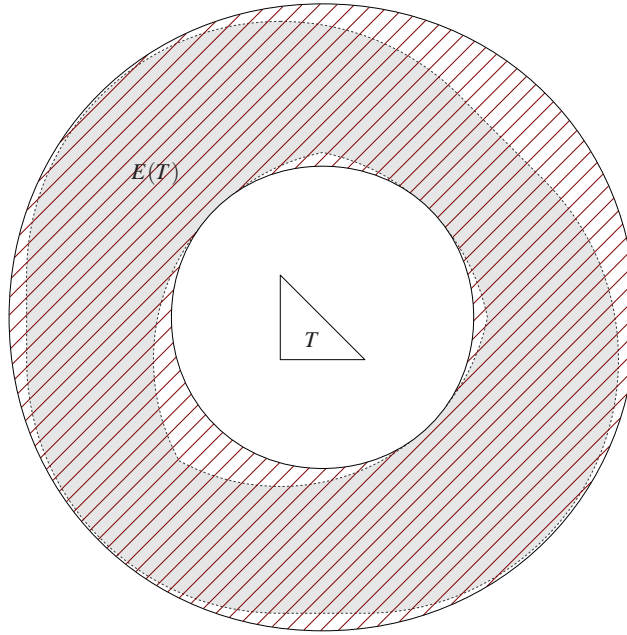


Fig. C.1 Sketch of superset of $E(T)$ in triangle plane \mathcal{E}_T .

Storage allocation scheme

Let us briefly describe the storage allocation scheme for a retarded matrix corresponding to a discrete light cone with radii r_{\min} and r_{\max} . Given a triangulation of Γ into n elements, then for each pair of elements T_i and T_j with $i, j = 1, \dots, n$ we have to check

- Step 1 Compute the circumspheres of T_i and T_j denoted by $B_{r_i}(m_i)$ and $B_{r_j}(m_j)$, resp.
 Step 2 Compute the distance of each element to its circumcenters:

$$d_i^{\min} = \text{dist}(m_j, T_i) \quad \text{and} \quad d_j^{\min} = \text{dist}(m_i, T_j)$$

Note: Here we used an algorithm proposed in [50]/Chapter 10.3.2

- Step 3 Compute maximal distance of each element to its circumcenters:

$$d_i^{\max} = \max_{x \in T_j} \|m_j - x\| \quad \text{and} \quad d_j^{\max} = \max_{x \in T_i} \|m_i - x\|$$

- Step 4 Allocate matrix entry (i, j) and (j, i) if $(d_i^{\min} \leq r_j + r_{\max}$ and $d_i^{\max} \geq (r_{\min} - r_j)_+$) and $(d_j^{\min} \leq r_i + r_{\max}$ and $d_j^{\max} \geq (r_{\min} - r_i)_+)$

We use a sparse row storage format for our matrices as e. g. introduced in [45]. In Fig. C.2 the allocated matrix entries and the actually non-vanishing matrix entries are compared for a mesh on a unit ball with 5120 elements and a time step of $\Delta t = 0.03125$.

Moreover, the computation of a matrix A^l corresponding to a retarded potential is the sum of basic Galerkin matrices $G^{\hat{l}}(k_A)$ which are used in different time steps, compare Section 2.3. Thus it is sensible to compute these matrices only once and to reuse them later. In (2.26) it is displayed, that especially for higher polynomial degrees in time, we compute basic Galerkin matrices on the same discrete light cone integration domain $E_{\hat{l}}$ but with a different kernel. It is only logical to allocate the storage once and to decompose the different integration domains only once. We then compute the different integral on the discrete light cone integration domain and store the solution in one matrix, where each matrix entry is an array of entries each corresponding to one kernel function. MaiProgs provides a subroutine, that enables the assembly of the matrix A^l based on the above described data structure.

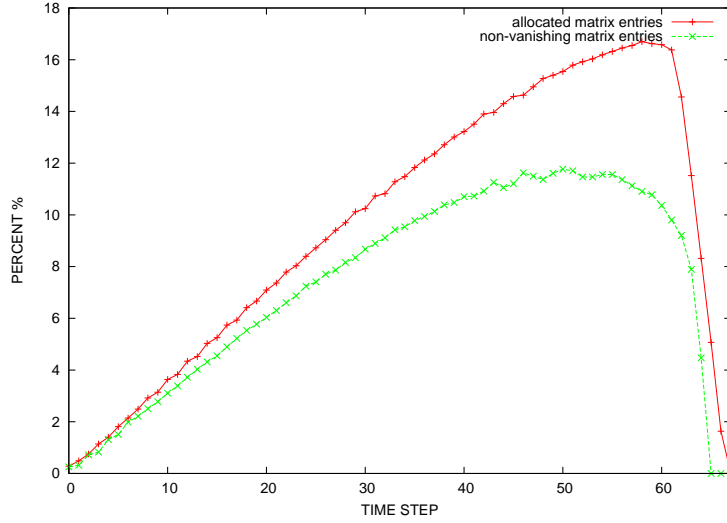


Fig. C.2 Allocated matrix entries (red) and actually non vanishing matrix entries (green).

Analytical evaluation of time integrals

In this section we compute some basic time integrals used in Section 2.3.2.

Basic time integrals

Let $n > m$ and $v, n, m \in \mathbb{N}$. In the following we will regard

$$\Upsilon_{p_1, p_2, v}^{n-m}(x, y) := \begin{cases} \int_0^\infty (t - |x - y| - t_{m+v})^{p_1} \chi_{I_m}(t - |x - y|) \dot{\chi}_{I_n}(t) dt & p_2 = -1 \\ \int_0^\infty (t - |x - y| - t_{m+v})^{p_1} \chi_{I_m}(t - |x - y|) \chi_{I_n}(t) dt & p_2 = 0 \end{cases}$$

Their evaluation is summarized in the next lemma.

Lemma C.3. *The integrals depend only on the difference $l = n - m$ and there holds*

$$\Upsilon_{p_1, p_2, v}^l(x, y) = \sum_{p=0}^1 \sum_{q=0}^{p_1+p_2+1} \Upsilon_{pq}^{p_1, p_2, l, v} |x - y|^q \chi_{E_{l-p}}(x, y)$$

and

$$\begin{aligned} \Upsilon^{0, -1, l, 0} &= \begin{pmatrix} -1 \\ 1 \end{pmatrix} & \Upsilon^{0, 0, l, 0} &= \begin{pmatrix} t_{l+1} & -1 \\ -t_{l-1} & 1 \end{pmatrix} \\ \Upsilon^{1, -1, l, v} &= \begin{pmatrix} -t_{l-v} & 1 \\ t_{l-1-v} & -1 \end{pmatrix} & \Upsilon^{1, 0, l, v} &= \frac{1}{2} \begin{pmatrix} t_{l-v}^2 - t_{v+1}^2 & -2t_{l-v} & 1 \\ t_{l-1-v}^2 - t_v^2 & 2t_{l-1-v} & -1 \end{pmatrix} \end{aligned}$$

Proof. The computation for $p_1 = 0$ and $p_2 = -1$ was already discussed in some detail in Chapter 2.3.2. For $p_1 = 0$ and $p_2 = 0$ it follows

$$\begin{aligned}
\Upsilon_{0,0}^{n-m}(x,y) &:= \int_0^{\Delta t} [H(t - |x-y| + t_{n-m}) - H(t - |x-y| + t_{n-m-1})] dt \\
&= t [H(t - |x-y| + t_{n-m}) - H(t - |x-y| + t_{n-m-1})] \Big|_{t=0}^{\Delta t} \\
&\quad - \int_0^{\infty} t [\delta(t - |x-y| + t_{n-m}) - \delta(t - |x-y| + t_{n-m-1})] [H(t) - H(t - \Delta t)] dt \\
&= \Delta t \chi_{E_{n-m}}(x,y) + (t_{n-m} - |x-y|) \chi_{E_{n-m}}(x,y) + (|x-y| - t_{n-m-1}) \chi_{E_{n-m-1}}(x,y)
\end{aligned}$$

For $p_1 = 1$ with $p_2 = -1$ the desired result follows immediately and for $(p_1, p_2) = (1, 0)$ we compute

$$\begin{aligned}
\Upsilon_{1,0,v}^{n-m}(x,y) &:= \int_0^{\infty} (t - |x-y| - t_{m+v}) \chi_{I_m}(t - |x-y|) \chi_{I_n}(t) dt \\
&= \int_0^{\Delta t} (t - |x-y| + t_{n-m-v-1}) [H(t - |x-y| + t_{n-m}) - H(t - |x-y| + t_{n-m-1})] dt \\
&= \frac{(t - |x-y| + t_{n-m-v-1})^2}{2} [H(t - |x-y| + t_{n-m}) - H(t - |x-y| + t_{n-m-1})] \Big|_{t=0}^{\Delta t} \\
&\quad - \int_0^{\Delta t} \frac{(t - |x-y| + t_{n-m-v-1})^2}{2} [\delta(t - |x-y| + t_{n-m}) - \delta(t - |x-y| + t_{n-m-1})] dt
\end{aligned}$$

Here we shifted the domain of integration and used partial integration. In the following we will use that $H(-x) = 1 - H(x)$ and as before, we can write

$$\begin{aligned}
\Upsilon_{1,0,v}^{n-m}(x,y) &= \frac{(t_{n-m-v} - |x-y|)^2}{2} \chi_{E_{n-m}}(x,y) - \frac{(t_{n-m-v-1} - |x-y|)^2}{2} \chi_{E_{n-m-1}}(x,y) \\
&\quad - \int_0^{\infty} \frac{(t - |x-y| + t_{n-m-v-1})^2}{2} [\delta(t - |x-y| + t_{n-m}) - \delta(t - |x-y| + t_{n-m-1})] [H(t) - H(t - \Delta t)] dt \\
&= \frac{(t_{n-m-v} - |x-y|)^2}{2} \chi_{E_{n-m}}(x,y) - \frac{(t_{n-m-v-1} - |x-y|)^2}{2} \chi_{E_{n-m-1}}(x,y) - \frac{t_{v+1}^2}{2} \chi_{E_{n-m}}(x,y) + \frac{t_v^2}{2} \chi_{E_{n-m-1}}(x,y) \\
&= \frac{1}{2} \left(|x-y|^2 - 2t_{n-m-v} |x-y| + (t_{n-m-v}^2 - t_{v+1}^2) \right) \chi_{E_{n-m}}(x,y) \\
&\quad - \frac{1}{2} \left(|x-y|^2 - 2t_{n-m-v-1} |x-y| + (t_{n-m-v-1}^2 - t_v^2) \right) \chi_{E_{n-m-1}}(x,y).
\end{aligned}$$

□

Discontinuous and Continuous Time Basis

For it holds $\Upsilon_0^l(x,y) = \Upsilon_{0,-1}^l(x,y)$. As we have seen in Chapter 2.3.2, the computation of the discrete hypersingular operator involves a more connected type of time integral. We use piecewise continuous linear trial functions in space $\beta^m(t) = \frac{t-t_{m-1}}{\Delta t} \chi_{I_m} - \frac{t-t_{m+1}}{\Delta t} \chi_{I_{m+1}}$ and piecewise constant test functions $\gamma_m(t) = \chi_{I_m}(t)$. Then

$$\begin{aligned}
\Upsilon_1^{n-m}(x,y) &= \int_0^{\infty} \dot{\beta}_m(t - |x-y|) \dot{\gamma}_n(t) dt \\
&= (\Delta t)^{-1} \int_0^{\infty} (\chi_{I_m}(t - |x-y|) - \chi_{I_{m+1}}(t - |x-y|)) \left(\frac{d}{dt} \chi_{I_n}(t) \right) dt \\
&= (\Delta t)^{-1} \left(\Upsilon_{0,-1,0}^{n-m}(x,y) - \Upsilon_{0,-1,0}^{n-m-1}(x,y) \right) \\
&= -(\Delta t)^{-1} (\chi_{E_{n-m}}(x,y) - 2\chi_{E_{n-m-1}}(x,y) + \chi_{E_{n-m-2}}(x,y))
\end{aligned}$$

where the second term of the derivative of $\beta^m(t)$ vanishes as it involves the delta distribution. Here we basically use Lemma C.3. The same works for

$$\begin{aligned}\Upsilon_2^{n-m}(x,y) &= \int_0^\infty \beta_m(t-|x-y|)\gamma_n(t) dt \\ &= (\Delta t)^{-1} \left(\Upsilon_{1,0,-1}^{n-m}(x,y) - \Upsilon_{1,0,0}^{n-m-1}(x,y) \right),\end{aligned}$$

Such that we finally obtain

$$\begin{aligned}\Upsilon_2^{n-m}(x,y) &= (2\Delta t)^{-1} \left(|x-y|^2 - 2t_{n-m+1}|x-y| + t_{n-m+1}^2 \right) \chi_{E_{n-m}}(x,y) \\ &\quad - (\Delta t)^{-1} \left(|x-y|^2 - (t_{n-m} + t_{n-m-1})|x-y| + \frac{1}{2}(t_{n-m}^2 + t_{n-m-1}^2) - \Delta t^2 \right) \chi_{E_{n-m-1}}(x,y) \\ &\quad + (2\Delta t)^{-1} \left(|x-y|^2 - 2t_{n-m-2}|x-y| + t_{n-m-2}^2 \right) \chi_{E_{n-m-2}}(x,y)\end{aligned}$$

Now,

$$\begin{aligned}\Upsilon_3^{n-m}(x,y) &= \int_0^\infty \beta_m(t-|x-y|)\dot{\gamma}_n(t) dt \\ &= (\Delta t)^{-1} \left(\Upsilon_{1,-1,-1}^{n-m}(x,y) - \Upsilon_{1,-1,0}^{n-m-1}(x,y) \right) \\ &= (\Delta t)^{-1} \left[(|x-y| - t_{n-m+1})\chi_{E_{n-m}}(x,y) + ((t_{n-m} + t_{n-m-1}) - 2|x-y|)\chi_{E_{n-m-1}}(x,y) \right. \\ &\quad \left. + (|x-y| - t_{n-m-2})\chi_{E_{n-m-2}}(x,y) \right]\end{aligned}$$

References

1. Andreas Atle. *Approximation of Integral Equations for Wave Scattering*. PhD thesis, Department of Numerical Analysis and Computer Science, Stockholm University, 2006.
2. I. Babuška and B. Q. Guo. Regularity of the solution of elliptic problems with piecewise analytic data. I. Boundary value problems for linear elliptic equation of second order. *SIAM J. Math. Anal.*, 19(1):172–203, 1988.
3. Alain Bachelot, Laurent Bounhoure, and Agnès Pujols. Couplage éléments finis–potentiels retardés pour la diffraction électromagnétique par un obstacle hétérogène. *Numer. Math.*, 89(2):257–306, 2001.
4. A. Bamberger and T. Ha Duong. Formulation variationnelle espace-temps pour le calcul par potentiel retardé de la diffraction d’une onde acoustique. I. *Math. Methods Appl. Sci.*, 8(3):405–435, 1986.
5. A. Bamberger and T. Ha Duong. Formulation variationnelle pour le calcul de la diffraction d’une onde acoustique par une surface rigide. *Math. Methods Appl. Sci.*, 8(4):598–608, 1986.
6. L. Banjai and S. Sauter. Rapid solution of the wave equation in unbounded domains: Abridged version. In *Proceedings of Waves 2007, University of Reading*, pages 38–40.
7. L. Banjai and S. Sauter. Rapid solution of the wave equation in unbounded domains. *SIAM J. Numer. Anal.*, 47(1):227–249, 2008/09.
8. Jules Bloomenthal and Ken Shoemake. Convolution Surfaces. *Computer Graphics*, 25(4):251–256, 1991.
9. Amir Boag, Vitaliy Lomakin, and Eric Michielssen. Nonuniform grid time domain (NGTD) algorithm for fast evaluation of transient wave fields. *IEEE Trans. Antennas and Propagation*, 54(7):1943–1951, 2006.
10. E.P. Stephan C. Carstensen. Adaptive coupling of boundary elements and finite elements. *Math. Modelling Numer. Anal.*, 29:779–817, 1995.
11. Barbara Chapman, Gabriele Jost, and Rudd van der Pas. *Using OpenMP*. The MIT Press, 2008.
12. D. J. Chappell, P. J. Harris, D. Henwood, and R. Chakrabarti. A stable boundary element method for modeling transient acoustic radiation. *The Journal of the Acoustical Society of America*, 120(1):74–80, 2006.
13. Alexey Chernov, Tobias von Petersdorff, and Christoph Schwab. Exponential convergence of hp quadrature for integral operators with gevrey kernels. *M2AN*, 2009. (submitted).
14. G. M. Constantine and T. H. Savits. A multivariate Faà di Bruno formula with applications. *Trans. Amer. Math. Soc.*, 348(2):503–520, 1996.
15. Martin Costabel. Time-dependent problems with the boundary integral equation method. *Encyclopedia of Computational Mechanics*, pages 1–28, 2004.
16. Penny J. Davies and Dugald B. Duncan. Stability and convergence of collocation schemes for retarded potential integral equations. *SIAM J. Numer. Anal.*, 42(3):1167–1188 (electronic), 2004.
17. Joseph el Gharib. *Méthode des Potentiels retardés pour l’acoustique*. PhD thesis, Ecole Polytechnique, 1999.
18. A. A. Ergin, B. Shanker, and E. Michielssen. Fast analysis of transient acoustic wave scattering from rigid bodies using the multilevel plane wave time domain algorithm. *J. Acoust. Soc. Am.*, (107 (3)):1168–1178, 2000.
19. A. A. Ergin, Balasubramaniam Shanker, and Eric Michielssen. Analysis of transient wave scattering from rigid bodies using a Burton-Miller approach. *The Journal of the Acoustical Society of America*, 106(5):2396–2404, 1999.
20. B. Guo and I. Babuška. The h, p version of the finite element method. Part I. The basic approximation results. *Comp. Mech.*, 1(1):21–41, 1986.
21. T. Ha-Duong, B. Ludwig, and I. Terrasse. A Galerkin BEM for transient acoustic scattering by an absorbing obstacle. *Internat. J. Numer. Methods Engrg.*, 57(13):1845–1882, 2003.
22. Tuong Ha-Duong. *Equations intégrales pour la résolution numérique de problèmes de diffraction d’ondes acoustiques dans \mathbb{R}* . PhD thesis, Université Pierre et Marie Curie, 1987.
23. Tuong Ha-Duong. On retarded potential boundary integral equations and their discretisation. In *Topics in computational wave propagation*, volume 31 of *Lect. Notes Comput. Sci. Eng.*, pages 301–336. Springer, Berlin, 2003.
24. Wolfgang Hackbusch. *Hierarchische Matrizen*. Springer, 2009.
25. Wolfgang Hackbusch, Wendy Kress, and Stefan A. Sauter. Sparse convolution quadrature for time domain boundary integral formulations of the wave equation by cutoff and panel-clustering. In *Boundary element analysis*, volume 29 of *Lect. Notes Appl. Comput. Mech.*, pages 113–134. Springer, Berlin, 2007.
26. N. Heuer and E. P. Stephan. The hp -version of the boundary element method on polygons. *J. Integral Equations Appl.*, 8(2):173–212, 1996.
27. Norbert Heuer, Matthias Maischak, and Ernst P. Stephan. Exponential convergence of the hp -version for the boundary element method on open surfaces. *Numer. Math.*, 83(4):641–666, 1999.
28. H. Holm, M. Maischak, and E. P. Stephan. Exponential convergence of the h - p version BEM for mixed boundary value problems on polyhedrons. *Math. Methods Appl. Sci.*, 31(17):2069–2093, 2008.

29. George C. Hsiao and Wolfgang L. Wendland. *Boundary Integral Equations*. Springer, 2008.
30. Stratton JA. *Electromagnetic Theory*. McGraw-Hill: New York, 1941.
31. Monika Jäger. *Entwicklung eines effizienten Randelementverfahrens für bewegte Schallquellen*. PhD thesis, Technische Universität Braunschweig, 1994.
32. Wendy Kress and Stefan Sauter. Numerical treatment of retarded boundary integral equations by sparse panel clustering. *IMA J. Numer. Anal.*, 28(1):162–185, 2008.
33. Prem K. Kytte and Michael R. Schäferkötter. *Handbook of Computational Methods for Integration*. Chapman and Hall CRC, 2000.
34. Antonio R. Laliena and Francisco-Javier Sayas. Theoretical aspects of the application of convolution quadrature to scattering of acoustic waves. *Numer. Math.*, 112(4):637–678, 2009.
35. J.-L. Lions and E. Magenes. *Non-homogeneous boundary value problems and applications. Vol. I*. Springer-Verlag, New York, 1972. Translated from the French by P. Kenneth, Die Grundlehren der mathematischen Wissenschaften, Band 181.
36. J.-L. Lions and E. Magenes. *Non-homogeneous boundary value problems and applications. Vol. II*. Springer-Verlag, New York, 1972. Translated from the French by P. Kenneth, Die Grundlehren der mathematischen Wissenschaften, Band 182.
37. Matthias Maischak. Webpage of the software package MaiProgs. <http://www.ifam.uni-hannover.de/~maiprogs>.
38. Matthias Maischak. *hp-Methoden für Randintegralgleichungen bei 3D-Problemen, Theorie und Implementierung*. PhD thesis, Universität Hannover, 1996.
39. Matthias Maischak, Elke Ostermann, and Ernst P. Stephan. TD-BEM for sound radiation in three dimensions and the numerical evaluation of retarded potentials. In *NAG/DAGA 2009 – Rotterdam*, pages 633–636.
40. Matthias Maischak, Elke Ostermann, and Ernst P. Stephan. Efficient quadrature of retarded potentials. In Martin Costabel and Ernst P. Stephan, editors, *Oberwolfach Report*, volume 19/2008, pages 975–978, 2008.
41. Thomas Meise. Randelementverfahren zur Berechnung der Ausbreitung skalarer Wellen im 3d-Zeit- und Frequenzbereich. Technical report, Institut für konstruktiven Ingenieurbau, Ruhr-Universität Bochum, 1990.
42. E. Michielssen. personal communication.
43. Patrick Mund. On the implementation of the h - p boundary element method on curved surfaces. In *Boundary elements: implementation and analysis of advanced algorithms (Kiel, 1996)*, volume 54 of *Notes Numer. Fluid Mech.*, pages 182–193. Vieweg, Braunschweig, 1996.
44. Georgios Natsiopoulos. *Time Domain Boundary Element Methods for Acoustic Scattering*. PhD thesis, Division of Applied Acoustics, Chalmers University, 2008.
45. Sergio Pissanetzky. *Sparse matrix technology*. Academic Press Inc. [Harcourt Brace Jovanovich Publishers], London, 1984.
46. D. C. Rizos and S. Zhou. An advanced direct time domain BEM for 3-D wave propagation in acoustic media. *J. Sound Vibration*, 293(1-2):196–212, 2006.
47. Stefan Sauter. *Über die effiziente Verwendung des Galerkinverfahrens zur Lösung Fredholmscher Integralgleichungen*. PhD thesis, Christian-Albrechts-Universität zu Kiel, 1992.
48. Stefan Sauter and Christoph Schwab. *Randelementmethoden: Analyse, Numerik und Implementierung schneller Algorithmen*. Vieweg+Teubner, 2004.
49. Stefan A. Sauter and Christoph Schwab. Quadrature for hp -Galerkin BEM in \mathbf{R}^3 . *Numer. Math.*, 78(2):211–258, 1997.
50. Phillip J. Schneider and David H. Eberly. *Geometric tools for computer graphics*. Morgan Kaufmann Publishers, 2003.
51. C. Schwab. Variable order composite quadrature of singular and nearly singular integrals. *Computing*, 53(2):173–194, 1994.
52. Christoph Schwab. *p - and hp -Finite Element Methods — Theory and Applications in Solid and Fluid Mechanics*. Oxford Science Publications, 1998.
53. B Shanker, Mingyu Lu, Jun Yuan, and E. Michielssen. Time domain integral equation analysis of scattering from composite bodies via exact evaluation of radiation fields. *IEEE Transactions on Antennas and Propagation*, 57(5):1506 – 1520, 2009.
54. Ernst P. Stephan, Matthias Maischak, and Elke Ostermann. Transient boundary element method and numerical evaluation of retarded potentials. In Marian Bubak, Geert Dick van Albada, Jack Dongarra, and Peter M.A. Sloot, editors, *Computational Science – ICCS 2008*, volume 5102 of *LNCS*, pages 321–330. Springer, 2008.
55. Daniel S.Weile, Greeshma Pisharody, Nan-Wei Chen, Balasubramaniam Shanker, and Eric Michielssen. A novel scheme for the solution of the time-domain integral equations of electromagnetics. *IEEE transactions on antennas and propagation*, 52(1):283–295, 2004.
56. Guillaume Sylvand. Équation des Ondes en Acoustique: Accélération des Potentiels Retardés par la Méthode Multipôle Temporelle. Technical report, Rapport de recherche de l’INRIA - Sophia Antipolis, Equipe: CAIMAN, <http://www.inria.fr/rrrt/rr-5017.html>, 2003.
57. I. Terrasse. *Résolution mathématique et numérique des équations de Maxwell stationnaires par une méthode de potentiels retardés*. PhD thesis, Ecole Polytechnique, 1993.
58. Rüdiger Verfürth. *A Review of A Posteriori Error Estimation and Adaptive Mesh- Refinement Techniques*. Teubner Verlag, 1996.
59. Ali E. Yilmaz, Jian-Ming Jin, and Eric Michielssen. Time domain adaptive integral method for surface integral equations. *IEEE Trans. Antennas and Propagation*, 52(10):2692–2708, 2004.
60. Éliane Bécache. *Resolution par une methode d’équations integrales d’un probleme de diffraction d’ondes elastiques transitoires par une fissure*. PhD thesis, École Polytechnique, 1991.

Curriculum Vitae

02.12.1980	Born in Barßel, Germany
2000	Abitur at the Albertus Magnus Gymnasium, Friesoythe
10/2000 – 03/2006	study of mathematics with minor subject Physics, Leibniz Universität Hannover
10/2002	Intermediate diploma in Mathematics
09/2003 – 09/2004	Master Course in <i>Computational mathematics with modeling</i> , Brunel University, West London, UK Thesis: <i>Elliptic variational inequalities: A viscoelastic obstacle problem</i>
03/2006	Diploma in Mathematics, Diploma thesis: <i>Discretization of viscoelastic contact problems with friction</i>
since 04/2006	Research assistant and Ph.D. student at the Institute of Applied Mathematics (IfAM), Leibniz Universität Hannover